Dissertation

submitted to the
Combined Faculties for the Natural Sciences and Mathematics
of the Ruperto-Carola University of Heidelberg, Germany

for the degree of
Doctor of Natural Science

presented by
M.Sc. Dominik Kato
born in Mannheim, Germany
Oral examination: 19.12.2025

The Role of the Transcription Factor REVERBα in Immunotherapy of Macrophages in Colorectal Cancer

Referees: Prof. Dr. Viktor Umansky
Prof. Dr. Elke Burgermeister

„Cunoașterea de sine este începutul oricărei înțelepciuni.”

Self-knowledge is the beginning of all wisdom.

— Romanian proverb

„Aki a tudást keresi, az a végtelent keresi.”

He who seeks knowledge, seeks the infinite.

— Hungarian proverb

Contents

1. Introduction 1
1.1 Colorectal cancer and its global burden 1
1.2 Development of polyps, genetic alterations and colorectal cancer 3
1.3 Treatment strategies of colorectal cancer 4
1.4 Molecular subtypes and characteristics of colorectal cancer 7
1.5 Circadian rhythm in colorectal cancer 10
1.6 Macrophage diversity and subtype classification 12
1.7 Targeting circadian rhythm components in colorectal cancer therapy 13
1.8 TIGIT and the poliovirus receptor as novel immune checkpoint 14
1.9 Inhibitory mechanisms of the PVR and TIGIT system within immune cells 16
1.10 The role of TIGIT/PVR in cancer therapy 18
1.11 Transcriptional regulation of immune checkpoint targets by nuclear receptors 19
1.12 Tumor organoids as a model system for colorectal cancer 20
1.13 Experimental approaches to study macrophage-tumor cell cross talk 21
1.14 Goal and outlook 22

2. Materials and Methods 25
2.1 Materials 25
2.1.1 Companies 25
2.1.2 Reagents 27
2.1.3 Devices & Equipment 31
2.1.4 Cell culture 32
2.1.5 Cell lines and bacterial strains 33
2.1.6 Antibodies 34
2.1.7 Enzymes 35
2.1.8 Plasmids 35
2.1.9 Oligonucleotides 36
2.1.10 Kits 38
2.1.11 Plastic consumables 39
2.1.12 Buffers 40
2.1.13 Software and Statistics 41

2.2 Methods 42
2.2.1 Golden-Gate molecular cloning of sgRNA 42
2.2.1.1 Oligonucleotide design 42
2.2.1.2 Oligo Annealing 43
2.2.1.3 Golden-Gate reaction 43
2.2.2 Design of luciferase vector 44
2.2.2.1 Amplification of human *PVR* gene promoter 44
2.2.2.2 Analysis and isolation of PCR product for cloning 45
2.2.2.3 Cloning of amplified *PVR* promoter into TOPO® vector 46
2.2.3 Transformation of competent E. coli 46
2.2.4 Colony selection with antibiotics 47
2.2.5 Plasmid isolation via miniprep 47
2.2.6 Quantification of DNA and RNA 48
2.2.7 Liquid cultures for plasmid multiplication and purification 48
2.2.8 Generation of CRISPR/Cas9-sgRNA knockdown cell clones 48
2.2.8.1 Transfection of THP1 cells via electroporation 48
2.2.8.2 Transfection of HEK293T, HT29 and THP1 cells with plasmid vectors 50
2.2.8.3 Picking and cultivation of adherent single clone colonies selected via puromycin treatment 51
2.2.9 Cell culture and in vitro assays 51
2.2.9.1 Thawing of frozen cells 52
2.2.9.2 Freezing of cells 53
2.2.9.3 Splitting of adherent cells 53
2.2.9.4 Splitting of suspension cells 53
2.2.9.5 Isolation of primary derived Monocytes from healthy donor blood 54
2.2.9.6 Monocyte isolation from PBMCs 54
2.2.9.7 Isolation of Patient-Derived Organoids 55
2.2.9.8 Splitting of Patient-Derived Organoids 56
2.2.10 Co-Culture of human CRC cell lines or PDOs with macrophages 57
2.2.10.1 Handling of parental THP1 and CRISPR modified THP1 cells 57
2.2.10.2 Handling of PBMC derived macrophages 57

2.2.10.3 Co-Culture assay with colorectal cancer cells 58
2.2.10.4 Co-Culture assay with PDOs 58
2.2.10.5 Treatment of Co-Cultures with antibodies 59
2.2.10.6 Treatment of co-cultures with REVERBα ligands 59
2.2.11 Isolation and analysis of RNA, protein and DNA 59
2.2.11.1 Isolation and purification of RNA 59
2.2.11.2 Isolation of protein samples with SDS-lysis and RIPA-lysis buffer 60
2.2.11.3 Determination of protein concentration 60
2.2.11.4 Isolation of genomic DNA 61
2.2.12 Immunoblotting of protein samples 61
2.2.13 cDNA synthesis and PCR 62
2.2.14 Quantitative PCR 64
2.2.15 Colorimetric MTT cell viability assay 65
2.2.16 Preparation of living cells for flow cytometry analysis 65
2.2.16.1 Intracellular flow cytometry staining 66
2.2.16.2 Live/Dead flow cytometry analysis 66
2.2.17 Immunofluorescence staining and microscopy 69
2.2.18 Chromatin Immunoprecipitation 69
2.2.18.1 Crosslinking and cell pellet isolation 70
2.2.18.2 Lysis and MNase digestion 71
2.2.18.3 Immunoprecipitation and pre-clearing 71
2.2.18.4 Elution and DNA recovery 72
2.2.19 Luciferase assay 73
2.2.20 Phagocytosis assay 73
2.2.21 Efferocytosis assay 73
2.2.22 Live cell imaging 74

3. Results 75

3.1 Characterization of REVERBα expression and function 75
3.1.1 REVERBα expression in THP1 and PBMC-derived macrophages 75
3.1.2 Binding of REVERBα to the human *PVR* Promoter 77
3.2 Detection of REVERBα in parental and CRISPR/Cas9-modified THP1-derived macrophages 78

3.3 Modulation of REVERBα expression and function 83
3.4 Validation of monocyte differentiation and macrophage subset markers 89
3.5 Effects of genetic and pharmacological REVERBα modification in macrophages on effero- and phagocytosis 91
3.6 Macrophages in co-culture with CRC cells and PDOs 93
3.6.1 Effects of REVERBα ligands on the viability of HT29 cancer cells in co-cultures with CRISPR/Cas9-modified THP1-derived macrophages 94
3.6.2 Effects of PVR blocking Ab and REVERBα ligands on CRC cell viability in co-cultures with PBMC-derived primary macrophages 96
3.6.3 Effects of PVR blocking Ab and REVERBα ligands on PDO viability in cell co-culture with macrophages 100
3.6.3.1 Cancer cell viability and death types of co-cultures with macrophages and PDOs from patient no. P022 101
3.6.3.2 Cancer cell viability and death types of co-cultures with macrophages and PDOs from patient no. P007 106
4. Discussion 108
4.1 Functional characterization of REVERBα 111
4.2 Regulatory interaction of REVERBα and the human *PVR* promoter 114
4.3 Ligand-mediated modulation of REVERBα activity 115
4.4 Impact of REVERBα modulation and immune checkpoint blockade on macrophage-tumor cell interactions 120
4.5 Conclusion and future perspectives 126
5. References 129
6. Supplementary Data 156
7. Acknowledgment 180

Summary

Colorectal cancer (CRC) is the second leading cause of cancer-related death, and responses to immune checkpoint therapies remain limited due to the immuno-suppressive tumor microenvironment. Tumor-associated macrophages (TAMs) are playing a crucial role in shaping this environment, with the poliovirus receptor (PVR/CD155)-TIGIT axis representing an immune checkpoint system which suppresses T/NK cell activities. However, the transcriptional mechanisms regulating PVR expression in macrophages still remains poorly understood.

This thesis investigates the role of the circadian nuclear receptor REVERBα (NR1D1) and its regulatory function in macrophage-mediated anti-tumor responses in CRC. Using human CRISPR/Cas9-modified THP1-derived macrophages, PBMC-derived primary macrophages with HT29 cells or patient-derived tumor organoids (PDOs) from patients with CRC in co-culture, we characterized REVERBα expression and its functional impact on macrophage-tumor interactions. Chromatin-immunoprecipitation revealed that REVERBα directly binds to the human *PVR* gene promoter. Furthermore, pharmacological modulation showed that REVERBα SR9009 agonist reduced *PVR* expression and promoter binding, whereas SR8278 antagonist increased both, highlighting REVERBα as a fine-tunable repressor of immune checkpoint regulation. Notably, CRISPR/Cas9-modification of the human *REVERBα* gene disrupted ligand responsiveness, suggesting an altered or misfolded protein conformation and loss of function. Functional assays further demonstrated that REVERBα modulation by gene editing or ligands altered macrophage efferocytosis, phagocytosis as well as cytokine expression. Importantly, combining PVR blocking with macrophages enhanced tumor cell killing in both HT29 and PDO co-cultures, underscoring the translational relevance of these findings.

Altogether, these findings identify REVERBα as a novel regulator of PVR expression and macrophage function in CRC. By linking circadian biology, transcriptional repression and immune checkpoint regulation, this work highlights REVERBα as a potential target, supporting future investigations of its modulation in combination with immune checkpoint blockade as a macrophage-focused immunotherapeutic strategy against CRC.

Zusammenfassung

Das kolorektale Karzinom (CRC) stellt die zweithäufigste krebsbedingte Todesursache global dar. Die Wirksamkeit von Immuncheckpoint-Therapien ist jedoch durch das immunsuppressive Tumormikromilieu stark eingeschränkt. Es ist bekannt, dass tumorassoziierte Makrophagen (TAMs) wesentlich zu diesem immunsuppressiven Milieu beitragen, wobei die PVR/CD155-TIGIT-Achse eine zentrale inhibitorische Schnittstelle bildet. Die genauen regulatorischen Mechanismen, die die PVR-Expression in Makrophagen steuern, sind jedoch bislang weitgehend ungeklärt.

Diese Arbeit untersucht die Rolle des zirkadianen Kernrezeptors REVERBα (NR1D1) und dessen regulatorische Funktion in der Makrophagen vermittelten Anti-Tumor-Antwort in CRC. Die Verwendung von CRISPR/Cas9-modifizierten THP1-Zellen Makrophagen sowie Makrophagen aus differenzierten isolierten primären Monozyten (PBMCs) in Ko-Kulturen zusammen mit HT29 CRC Zellen oder Tumor Organoiden aus CRC-Patienten (PDOs), wurden die REVERBα-Expression sowie dessen Einfluss auf die Makrophagen-Tumor-Interaktionen charakterisiert. Chromatin-Immunpräzipitations-Experimente zeigten, dass REVERBα direkt an den Promotor des humanen *PVR*-Gens bindet. Pharmakologische Experimente belegten zudem, dass der REVERBα-Agonist SR9009 die PVR-Expression und Promotorbindung reduzierte, während der Antagonist SR8278 beides erhöhte. Dies unterstreicht die Funktion von REVERBα als modulierbaren Repressor der Immuncheckpoint-Regulation. Bemerkenswerterweise führte die CRISPR/Cas9-Modifikation des *REVERBα*-Gens zu einem Verlust der Liganden-Sensitivität, was auf eine veränderte oder fehlgefaltete Proteinkonformation und Funktionsverlust hindeutet. Funktionelle Analysen zeigten ferner, dass die Modulation von REVERBα durch Geneditierung oder Liganden Efferozytose, Phagozytose sowie Zytokinexpression von Makrophagen beeinflusst. Einen besonderen Effekt zeigte die Kombination von PVR blockierenden Antikörpern mit Makrophagen, die den Tumorzelltod sowohl in HT29- als auch in PDO-Ko-Kulturen verstärkte, was die translationale Bedeutung dieser Erkenntnisse unterstreicht.

Zusammenfassend identifizieren diese Ergebnisse REVERBα als neuartigen Regulator der *PVR*-Expression und der Makrophagenfunktion in CRC. Durch Zusammenführen der zirkadianen Biologie, transkriptioneller Repression und

Immuncheckpoint-Regulation wird REVERBα als potenzielles therapeutisches Ziel zur Entwicklung neuer Makrophagen basierter Immuntherapien vorgeschlagen. Diese Arbeit legt nahe, REVERBα in Kombination mit Immuncheckpoint-Blockaden weiter zukünftig zu untersuchen.

Abbreviations

Abbreviation	Full name
AHR	Aryl-hydrocarbon receptor
ADCC	Antibody-dependent cellular cytotoxicity
ADAR	Adenosine deaminase RNA specific
APC	Antigen-presenting cell
APC (mutation)	Adenomatous polyposis coli
BB	Backbone (empty vector control)
BCA	Bicinchoninic acid
BMAL1	Brain and muscle Arnt-like protein-1
BMP	Bone morphogenic protein
BSA	Bovine serum albumin
CAPOX	Capecitabine+oxaliplatin
ctDNA	Circulating Tumor DNA
CCG	Circadian cycle of clock-controlled genes
CCL2	Chemokine ligand 2
CIMP	CpG island methylator phenotype
CLOCK	Circadian locomotor output cycles kaput
CMS	Consensus molecular subtype
CRC	Colorectal cancer
CRISPR/Cas9	Clustered regularly interspaced short palindromic repeat/ CRISPR-associated protein 9
CRY 1/2	Cryptochrome 1/2
CTLA-4	Cytotoxic-T-lymphocyte-associated-protein 4
DC	Dendritic cells
Dgat2	Diacylglycerol O-acyltransferase 2
DMEM	Dulbecco´s modified eagle medium
DNAM-1 (CD226)	DNAX Accessory Molecule-1
DTT	Dithiothreitol
EGFR	Epidermal growth factor receptor
FACS	Fluorescence-activated cell sorting
FC	Flow Cytometry
Fap2	Fibroblast activation protein 2

FCS	Fetal calf serum
FGF-1	Fibroblast growth factor 1
FOLFIRI	Folinic acid+fluorouracil+irinotecan
FOLFOX	Folinic acid+fluorouracil+oxaliplatin
GCK	Glucokinase
GM-CSF	Granulocyte-macrophage colony stimulating factor
GSK3b	Glycogensynthase-kinase 3
HDI	Human development index
HDAC3	Histone deacetylase 3
HEPES	4-(2-hydroxyethyl)-1-piperazineethanesulfonic acid
HER2	Human Epidermal growth factor receptor 2
HGF	Hepatocyte growth factor
HLADRB	HLA class II histocompatibility antigen
HRAS	Harvey rat sarcoma viral oncogene homologe
HRP	Horse radish peroxidase
HSP90	Heat shock protein 90
IRS1	Insulin receptor substrate 1
IFN-γ	Interferon γ
IL	Interleukin
ISG15	Interferon stimulated gene 15
ITTFL	Interlocked transcription/translation feedback loops
ITIM	Immunoreceptor tyrosine-based inhibitory motif
KRAS	Kirsten rat sarcoma virus
LAK	Lymphokine-activated killer (NK/T) cells
LBD	Ligand Binding Domain
LBP	Ligand Binding Pocket
LFA1	Lymphocyte function-associated antigen 1
LIPA	Lipase A, lysosomal acid type
LPIN2	Lipid phosphate phosphatase 2
LPS	Lipopolysaccharide
LRR	Leucine rich repeat
M-CSF	Macrophage-colony stimulating factor
MLH1	MutL Homolog 1

MMR	Mismatch repair
MSH2	MutS Protein Homolog 2
MSI	Microsatellite instability
MSS	Microsatellite stability
MTT	(4,5-dimethylthiazol-2-yl)-2,5-diphenyltetrazolium bromide
NCoR	Nuclear receptor co-repressor
NK	Natural killer cell
NLRP3	NOD-, LRR- and pyrin domain-containing protein 3
NOD	Nucleotide-binding and oligomerization domain
NO	Nitric oxide
NSAID	Nonsteroidal anti-inflammatory drugs
NY-ESO	New York esophageal squamous cell carcinoma
PBMC	Peripheral blood mononuclear cells
PDGF	Platelet-derived growth factor
PDL1	Programmed death ligand 1
PDO	Patient-derived tumor organoid
PER 1/2/3	Period 1/2/3
PGE2	Prostaglandin E2
PI3K	Phosphatidylinositol 3-kinase
PIK3CA	Phosphatidylinositol-4,5-bisphosphate 3-kinase catalytic subunit alpha
PAM	Protospacer adjacent motif
PMA	Phorbol 12-myristate-13-acetate
PMS2	PMS1 Homolog 2, Mismatch Repair Protein
PPAR	Peroxisome-proliferator-activated receptor
PVR (CD155)	Poliovirus receptor
PVRIG	PVR-related immune globulin domain
PVRL2	Poliovirus receptor related 2
PVSRIPO	Polio-rhinovirus chimera
eRNA	Enhancer RNA
REVERBα	Reverse c-ErbAα
RevRE	REVERBα responsive element

ROR α/β	Retinoic acid receptor-related orphan receptor α/β
RORE	ROR responsive element
RPMI	Roswell Park Memorial Institute
SCN	Suprachiasmatic nucleus
SCNA	Somatic Copy Number Alteration
SIRPα	Signal regulatory protein α
SNP	Single nucleotide polymorphism
SSP	Sessile serrated polyps
STAT	Signal transducer and activator of transcription
TGF-β	Transforming growth factor β
TME	Tumor microenvironment
TNF-α	Tumor necrosis factor α
TNM	Tumor/Nodes/Metastasis
TIGIT	T cell immunoreceptor with Ig and ITIM domains
TAM	Tumor-associated macrophage
UTR	Untranslated region
VEGF	Vascular endothelial growth factor

1. Introduction

1.1 Colorectal cancer and its global burden

The annual number of cancer diagnoses is evidently increasing as the population ages, influenced by demographic shifts, industrialization, and the adoption of a “Western” lifestyle. Colorectal cancer (CRC) ranks among the most frequently diagnosed cancers and is the fourth leading cause of cancer-related deaths worldwide, following breast, lung, and prostate cancers (Balata and Azzam, 2025). According to the GLOBOCAN database over 1.9 million new CRC cases and 930000 deaths were recorded globally in 2020 (Morgan et. al., 2023). It is a general fact that the growth in economy together with rapid industrialization of countries go hand in hand. The adoption of fast-food dietary habits, obesity, physical inactivity, alcohol consumption, and smoking are all risk factors contributing to the increase in CRC incidence (Caceres-Matos et. al., 2024), (Shaw et. al., 2018), (McNabb et. al., 2019), (Li et. al., 2024). Additionally, this rising trend of CRC in economically advanced nations can be observed by the Human Development Index (HDI), a measure of life expectancy, income, and education. Although CRC incidence is rising in high-HDI countries, CRC mortality rates have declined in some nations, like Slovenia and Italy, due to enhanced screening allowing early disease detection and treatment (Zorzi and Urso, 2023). Conversely, mortality rates are climbing in countries with limited healthcare resources, such as Russia and Brazil (Lu et. al., 2021). Furthermore, recent studies indicate that the CRC burden is shifting towards low- and middle-income developing nations. Moreover, the CRC incidence in individuals under 50 is showing a rising trend attributed to dietary habits, lifestyle factors, and screening practices (Keum and Giovannucci, 2019), (Chen et. al., 2025), (Sung et. al., 2025).

As CRC is a cancer, it is a disease of aging. The incidence rates are increasing beyond 50 years of age, 90% of global cases and deaths are occurring after this age in both male and female as indicated in Fig.1.

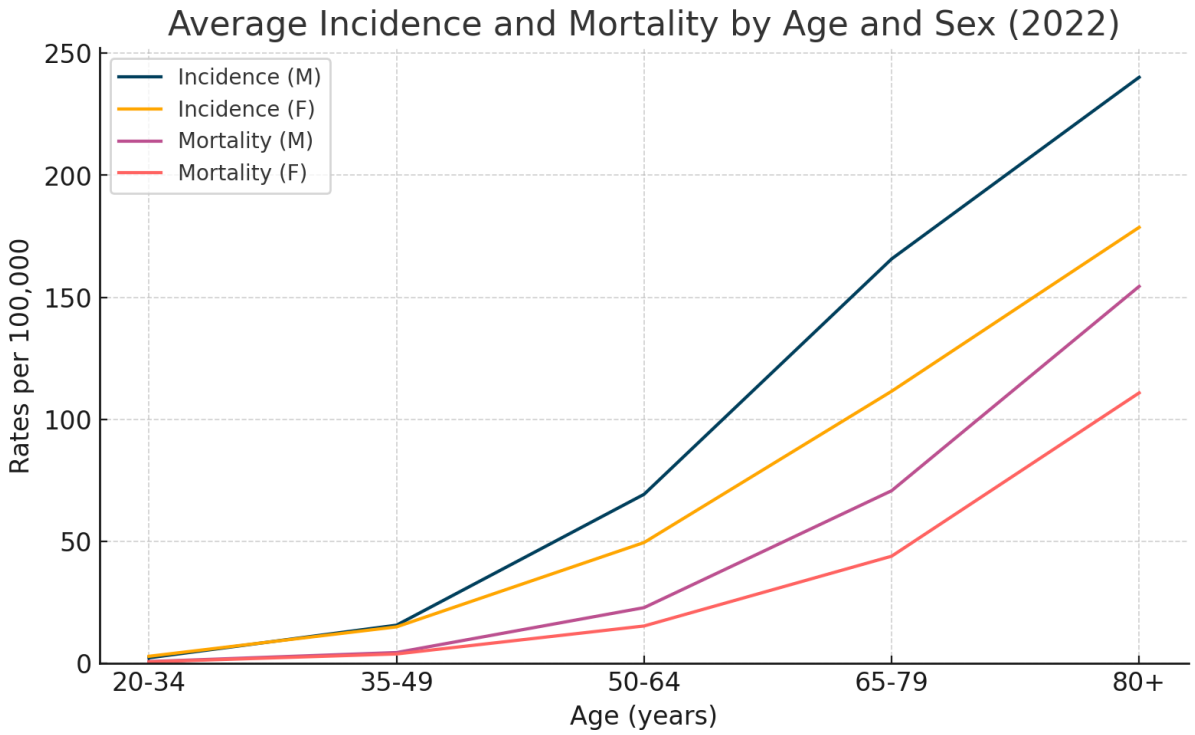

Fig. 1: Worldwide incidence and mortality of CRC by age in male and female Line graph depicting age-specific incidence and mortality rates per 100.000 population, divided by sex. The Incidence (blue = men, orange = women) and mortality (purple = men, red = women) rise steeply with age, showing consistently higher rates in men compared to women across all age groups. Source: Cancer TODAY | IARC – https://gco.iarc.whi.int, Data version: Globocan 2022 (v1.1) – 08.02.2024

As showed in Fig.1, the incidence of CRC as well as the mortality are 30-40% higher in men than in women. Furthermore, the elevated incidence rate of CRC in men might be related to a combination of multiple factors like environmental and genetic factors. These high rates are influenced by increased screening procedures and the fact that CRC is often diagnosed in advanced stages. Moreover, the heritability of CRC in men is estimated to be 28% and 45% for women (Graff et. al., 2017). Generally speaking, evidence indicates higher heritability in woman than in men (Samadder and Curtin, 2017). Additionally, twin studies showed that CRC has a hereditary component which is estimated to be 35-40% (dos Santos et. al., 2025). Approximately 25% of CRC cases are showing a family history which are not tied to a specific genetic cancer syndrome. In addition, only 5% of CRC cases are associated to hereditary cancer syndromes like familial adenomatous polyposis or hereditary nonpolyposis colorectal cancer (Jasperson et. al., 2010). It is known that low penetrance genetic variations, like single nucleotide polymorphisms (SNPs) are associated with CRC risk. However, only a small

proportion of identified CRC SNPs are providing some clarification of its heritability (Jiao et. al., 2014).

1.2 Development of polyps, genetic alterations and colorectal cancer

The development and progression of CRCs generally occurs very slowly without evoking any symptoms until reaching a prominent size, in most cases several centimetres (Simon, 2016). It is a known fact that the development of CRC includes various genetic alterations like mutations and epigenetic modifications which basically transform normal glandular epithelial cells into a benign neoplasia (Mundade et. al., 2014). Most of the colon tumors are developing via a multistep process accumulating several changes in morphology and histology over time, ultimately transforming the benign neoplasia (Markowitz et. al., 2009), (Brenner et. al., 2014). As noted previously, typical risk factors such as nutrition and lifestyle increase the risk of developing CRC. Those risk factors are all modifiable risk factors. Additionally, the consumption of green leafy vegetables, calcium, dietary fiber and folate has shown protective effects against CRC development (Simon, 2016). In contrast, hereditary conditions like the Lynch syndrome or familial history of colorectal tumors and intestinal bowel disease as well as diabetes mellitus type 2 are non-modifiable risk factors (Decker et. al., 2019).

Colorectal cancer usually originates from benign polyps undergoing genetic changes. These are typically clusters of abnormal cells growing within the intestinal mucosa, protruding into the lumen of the colon. As genetic mutations accumulate, polyps become more dysplastic and begin to invade the colon and rectal wall if not removed (Levine & Ahnen 2006), (Decker et. al., 2019). This malignant growth can develop new blood vessels by neovascularization, providing a pathway for tumor cells to enter the circulatory and lymph systems, finally causing metastasis in distant organs (Nagy et. al., 2009). Only a small fraction of these altered polyps acquire enough mutational changes to develop malignant features. Moreover, it usually takes years or decades to complete the progression from polyps to intestinal cancer (Stracci et. al., 2014).

There are two types of DNA alterations relevant for CRC. Those that are acquired and those that are inherited. The latter ones consist mutations in genes like *MLH1, PMS2, MSH2* and *APC* which are associated with CRC but relatively uncommon. Only about 5% of CRCs are attributed to such inherited alterations (Kinzler & Vogelstein, 1996). As mentioned previously, malignant colorectal cancers arise from serrated or tubulo-villous adenomas following two genetic pathways (Mezzapesa et. al., 2022). One

pathway is associated with adenomas usually showing its character via chromosomal instability due to a cascade of accumulated mutations which can be observed in 65-70% all sporadic cancer types (Simon, 2016). The cascade of genetic alterations begins within the *APC* gene affecting the process of chromosomal segregation during cell division. In about 80% of sporadic colon cancer cases a mutation of *APC* gene was detected (Kwong & Dove, 2009). This mutation can also be found in dysplastic epithelium and small benign adenomas (Fearon & Vogelstein, 1990). Furthermore, mutations are also occurring in the *KRAS* gene, a typical oncogene which stimulates cell growth, motility, survival and differentiation. Finally, adenomas may eventually loose the function of the p53 tumor suppressor gene due to further mutations impairing apoptosis, transcription and other cellular functions such as DNA-repair mechanisms, ultimately leading to carcinogenesis (Pino & Chung, 2010). In contrary, serrated polyps often begin with mutations in the *BRAF* gene, disrupting apoptosis and altering growth signaling (Yamane et. alt., 2014). Additionally, mutations in the *KRAS* gene are less frequent in serrated polyps than in tubular adenomas. Furthermore, abnormal hypermethylation in promoter regions represent an epigenetic alteration which is common in serrated type CRC. This hypermethylation inhibits gene transcription keeping the affected genes in an inactive state which has a great impact on other regulatory genes promoting cell growth (Mezzapesa et. al., 2022). Finally, another mechanism which enhances the genetic diversity in CRC, occurs in both serrated and tubular adenomatous polyps is microsatellite instability (MSI). Microsatellite instability is caused by mutations in DNA-repair genes causing the disruption of the DNA-repair system. In addition, MSI also occurs in non-coding regions due to uneven replication of short, repetitive DNA-sequences. MSI cancers can rapidly acquire additional mutations and express numerous neoantigens (Ganesh et. al., 2019).

1.3 Treatment strategies of colorectal cancer

Current treatment strategies utilized in CRC treatment are depicted in Fig. 2. The choice of the respective treatment strategy depends on the tumor stage as indicated. The primary and ideal treatment option is the complete surgical resection of the primary tumor and any metastasis, which serves as the cornerstone for treating stages I-III (Benson et. al., 2021). However, most CRC tumors are diagnosed at an advanced stage with metastasis, including about 20% that have metachronous metastasis which brings up great challenges for surgical tumor removal and therefore treatment by

operation (Decker et. al., 2019). Consequently, for patients with unresectable malignancies or those ineligible for surgery, the main goal is to reduce tumor size, inhibit tumor growth and spread, which is typically achieved through chemotherapy or radiotherapy for rectal cancer. In addition, both chemo- and radiotherapy can be used as adjuvant or neoadjuvant treatment before and after surgery (Messersmith, 2019). For example, chemotherapy can be given as a single-agent therapy or in a combined approach, such as the combination with 5-Fluorouracil (5-FU) / Folinic acid and Irinotecan (FOLFIRI). Other drug combinations include 5-FU / Folinic acid + Oxaliplatin (FOLFOX) (McQuade et. al., 2017), (Buikhuisen et. al., 2020). The cornerstone for stage III colorectal cancer therapy continues to be oxaliplatin-based therapies such as FOLFOX or CAPOX (capecitabine/oxaliplatin) which is administered for up to six months, remaining as the historical standard of care for MSS tumors where immunotherapy has not yet become standard (Taieb, 2020). However, treatment strategies are increasingly shifting towards biomarker-driven personalization. For example, retrospective and randomized trials are evaluating whether circulating tumor DNA-guided (ctDNA) therapeutic strategies can optimize therapy increasing chemotherapy efficacy for ctDNA-positive patients or sparing toxicity in ctDNA-negative patients (Cha, 2025). Moreover, recently published data suggests targeted agents like celecoxib, which improves the outcomes in ctDNA-positive patients. This underlines ctDNA not only as a prognostic marker, but also as a predictive biomarker giving information about adjuvant therapy decicions (Sanderson et. al., 2025).

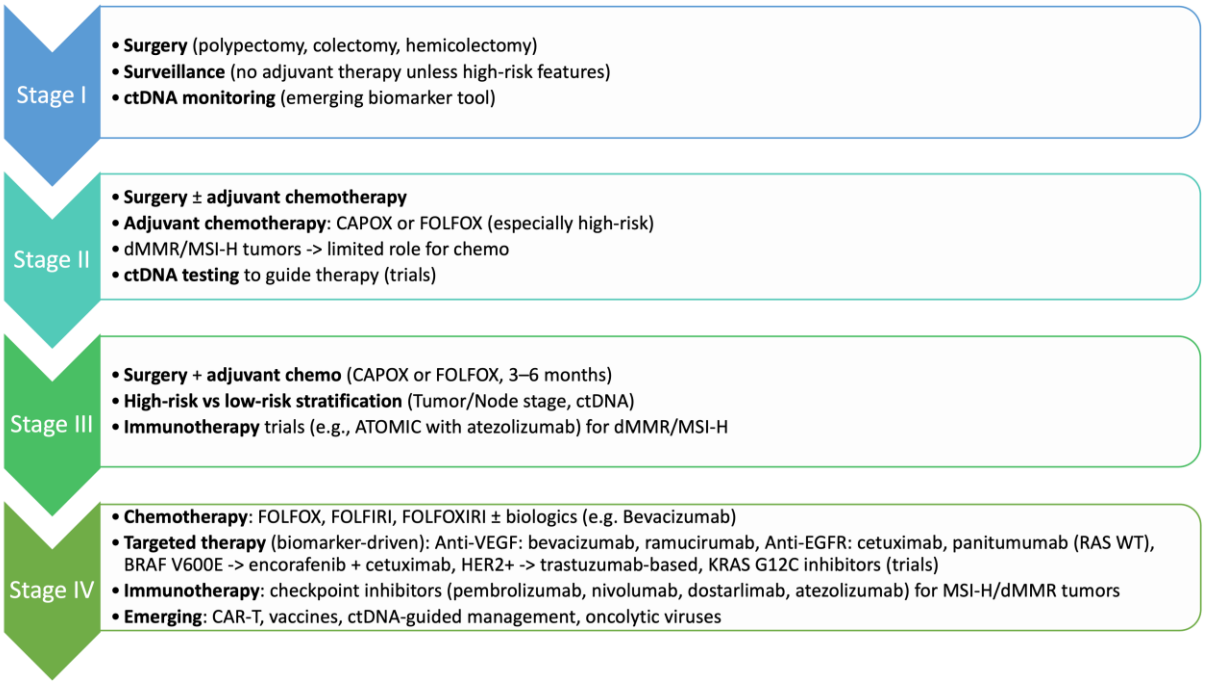

Fig. 2: CRC treatment strategies and specifications. Overview of standard and emerging therapeutic methods across stages I-IV. Surgery is conducted in early stages, with adjuvant chemotherapy (CAPOX/FOLFOX) applied at high-risk stages II-III. Further stage IV treatments include systemic chemotherapy, targeted therapy, immunotherapy for MSI-H/dMMR tumors and novel approaches such as CAR-T, vaccines, ctDNA-guided management and oncolytic viruses. Source: (McQuade et. al., 2017), (Xie et. al., 2020), (Taieb, 2020), (Sanderson et. al., 2025)

However, another common treatment strategy besides surgery and chemotherapy is immunotherapy, which marks a crucial and important approach in anti-cancer therapy (André et al., 2020). In general, immunotherapy is considered when all other therapy options proved to be insufficient, making it the last-line therapeutic strategy to manage tumors and metastasis. Moreover, cancer cells possess the ability to hide and evade detection from the immune system (evasion/escape) by activating negative immune checkpoints, which inhibit the immunologic responses of various cells like NK cells, T-cells and macrophages (Sultan et. al, 2017). Current targeted therapies focus on inhibition of tumor growth factors such as VEGFA and EGFR, as well as addressing immune checkpoint ligand-receptor systems. Additionally, oncolytic viruses and anti-cancer vaccines, including peptide and DNA vaccines, are also used in cancer immunotherapy (Galassi et. al., 2024). For instance, a genetically engineered Poliovirus (PVSRIPO) tested in clinical trials showed high efficacy in killing malignant cells (Peruzzi & Chiocca, 2018). Moreover, the most common immune checkpoints, PD1, PDL1 and CTLA4, are targeted by various monoclonal blocking antibodies like

Nivolumab, Atezolizumab and Ipilimumab, respectively (André et al., 2025), (Kciuk et. al., 2025). These immune checkpoints, expressed on activated T cells, have been approved as effective targets for treating different cancer types and advanced stages. However, targeting just a single immune checkpoint has shown that over 50% of the patients failed to respond treatment. Therefore, a combined approach of PD1 and CTLA4 checkpoint inhibitors such as Nivolumab (anti-PD1) and Ipilimumab (anti-CTLA4), has significantly increased the response rates of renal cell carcinoma, metastatic melanoma and metastatic colorectal carcinoma with high microsatellite instability (MSI-H) and DNA mismatch repair (MMR) alterations (Rotte 2019). Lastly, the optimization of drug delivery through chronotherapy can increase the patients tolerance to high doses of anti-cancer drugs, improving anti-tumor and anti-metastatic effects in colorectal cancer patients (Giacchetti, 2002).

1.4 Molecular subtypes and characteristics of colorectal cancer

The current treatment strategies available for CRC patients which are sharing similar pathological conditions are widely following the model of ‘one drug fits all’. Due to the fact that colorectal cancer is a very heterogenous type of disease and not all patients are sharing the same genetic and pathological conditions, molecular subtypes of CRC were designated to characterize patients’ tumors by genetic and pathological signatures (Singh et. al., 2021). This characterization allows a better clinical decision making by choosing the therapy which is fitting the best regarding specific molecular and pathological aspects to finally improve the patient’s clinical outcome. This approach is also known as personalised precision medicine. Currently, prognosis prediction, therapy selection and tumor classification rely on histological, respectively pathological features (Nagtegaal et. al., 2019). This standard treatment and staging protocols (TNM, UICC) have major issues in identifying all the colon cancer patients with poor prognosis which should receive their adjuvant therapy as well as failing to predict patients benefiting from this therapy option. Some patients are overtreated while others are inadequately treated with chemotherapeutics due to insufficient categorization (Punt et. al., 2017).

Fig. 3 depicts the four different consensus molecular subtypes (CMS) of CRC whose main goal is to improve the diagnosis and prognosis of CRC at different stages. It may

help to specify the patient's personalized therapy which is expected to achieve the best outcome (Singh et. al., 2021).

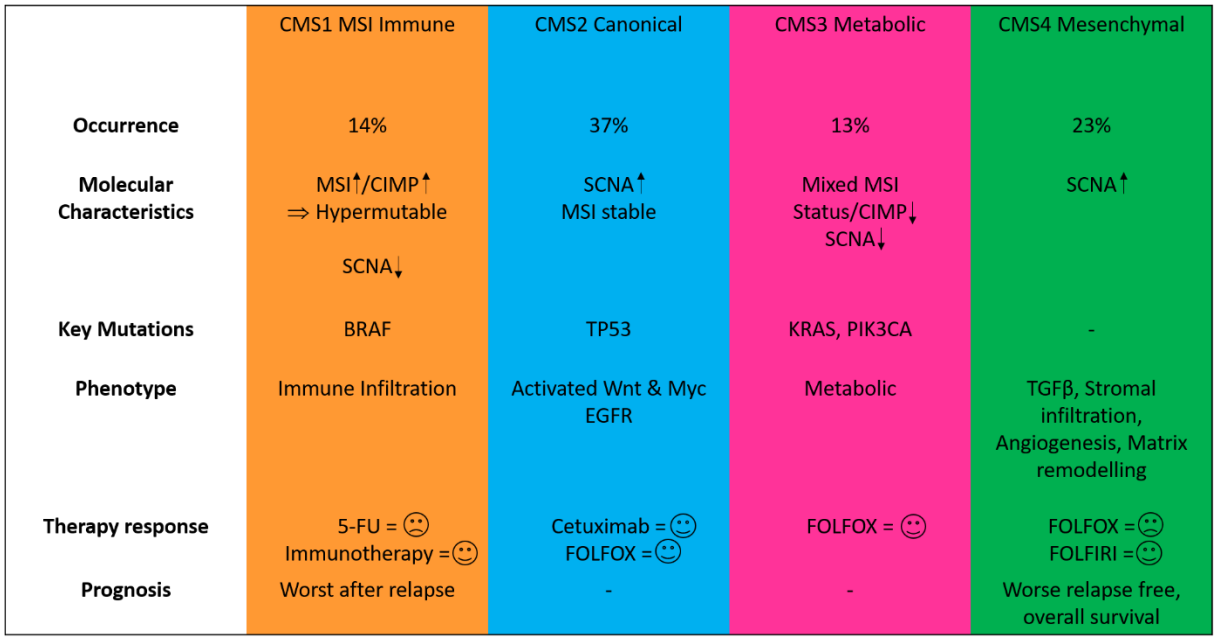

Fig. 3: Key Characteristics of CMS subtypes in CRC (Modified from Buikhuisen, J.Y., Torang, A., and Medema, J.P. (2020). Exploring and modelling colon cancer inter-tumour heterogeneity: opportunities and challenges. Oncogenesis 9, 66.) The defined features and subtypes of colorectal cancer are summarized in the respective illustration. MSI = Microsatellite instability, CIMP = CpG island methylator phenotype, SCNA = Somatic Copy Number Alteration, 5-FU = 5-Fluorouracil, FOLFOX = Folinic acid (Leucovorin), 5-FU or capecitabine (5-FU prodrug) and oxaliplatin, FOLFIRI = Folinic acid (Leucovorin), 5-FU or capecitabine (5-FU prodrug) and irinotecan.

Recent transcriptomic analyses revealed two major intrinsic epithelial subtypes of CRC iCMS2 and iCMS3 (Dunne and Arends, 2024). An important finding concerning MSS tumors with iCMS3 epithelium (iCMS3_MSS) phenotype showed strong features in genomic, transcriptomic and biological pathway displaying higher similarity to classical CMS1 MSI-H tumors than to iCMS2_MSS. As commonly known, the CMS4 subtype is characterised by fibrotic cancer types. According to the refined classification, iCMS2 and iCMS3 are classified in either fibrotic or non-fibrotic tumor states, suggesting that fibrosis is an essential factor for subdividing CRC tumors. Importantly, CMS4 tumors, as stated in Fig.3, show the worst relapse-free overall survival. Recent studies revealed that the CMS4 subgroup with identified iCMS3 epithelial cells is found in patients with the worst prognosis compared to other CRC types. The integration of epithelial subtypes into the CMS classification system revealed a novel spectrum of CRC classification, categorizing the epithelial cells of CRC tumors into first epithelial

statis (i), second microsatellite instability status (M) and third fibrotic status (F) (Joanito et. al., 2022). Fig.4 depicts the refined categorization of the classical CRC CMS subtype classification.

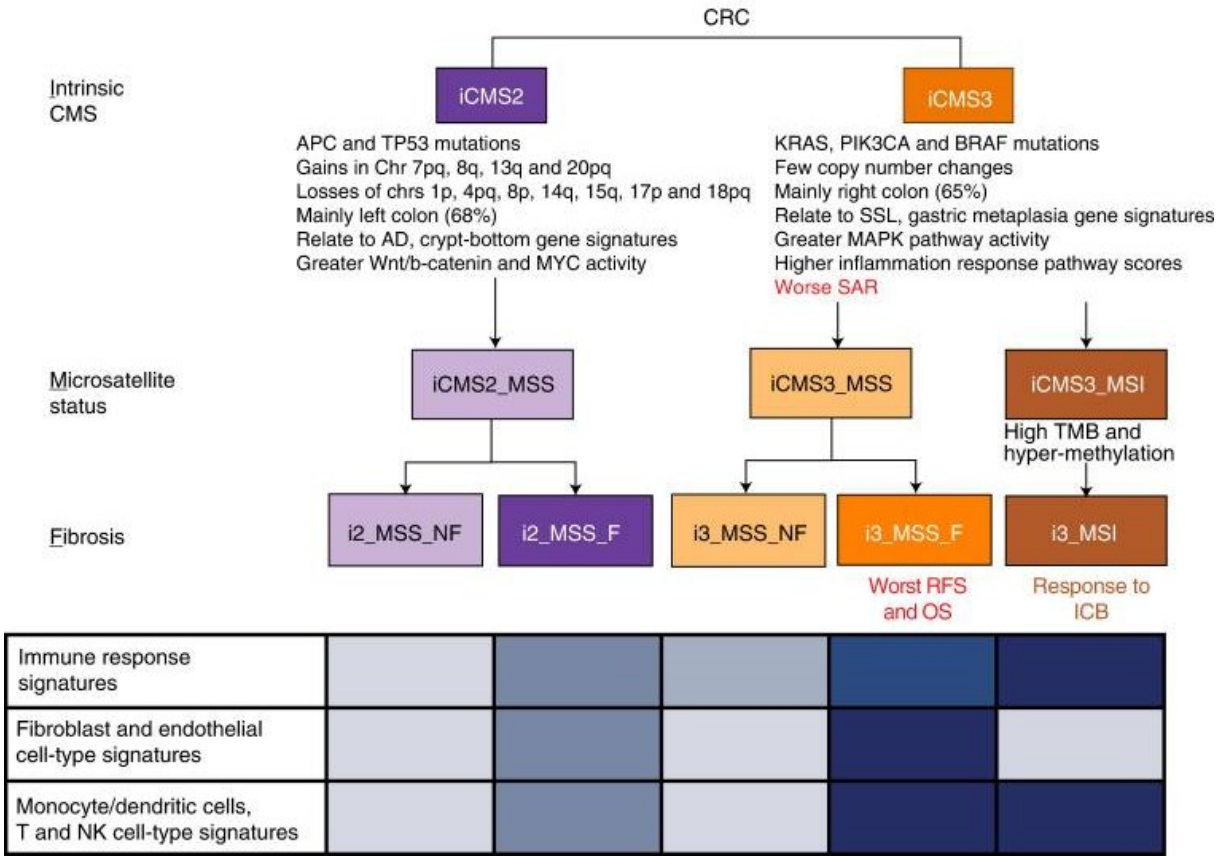

Fig. 4 Refined CMS classification system (Modified: Joanito et. al., Single-cell and bulk transcriptome sequencing identifies two epithelial tumor cell states and refines the consensus molecular classification of colorectal cancer. Nat Genet. 2022 Jul;54(7):963-975. doi: 10.1038/s41588-022-01100-4. Epub 2022 Jun 30. PMID: 35773407; PMCID: PMC9279158.) Refined CMS subtype classification depicting a layered classification fundated on intrisic CMS subtypes, MSI and fibrotic status, showing clinical features as key mutations, immune infiltration and response as well as single cell and cell type specific signatures from e.g. fibroblast, endothelial and various immune cell types. The color coded table represents the intensity of signature expression, the darkest color represents the highest or strongest expression.

1.5 Circadian rhythm in colorectal cancer

The circadian clock is a highly specialized pacemaker and timed machinery crucial for the regulation and maintenance of physiological rhythms in organisms (Verlande & Masri 2019). This circadian system in mammals is composed of two tiers, a master clock which is located in the suprachiasmatic nucleus (SCN) of the brain and peripheral clocks residing in peripheral tissues and organs. Light for instance is transmitted via the retina to the SCN, which converts and integrates this information from the brain to peripheral tissues resulting in the regulation and maintenance of circadian oscillations in cells (Zhang et. al., 2021). Not only is light an important external stimulus, but also environmental factors, the intake of food and hormones from the body influences and controls the SCN and therefore the circadian rhythm in cells. On the molecular level, this machinery consists of two main autoregulatory interlocked transcription/translation feedback loops (ITTFL) counter modulating each other by the expression of output genes. “Circadian locomotor output cycles kaput” (CLOCK) and “brain and muscle Arnt-like protein-1” (BMAL1) for instance are activators of the feedback loops, whereas period (PER-1/2/3) and cryptochrome (CRY-1/2) are inhibitors of these feedback loops. In addition, the activators CLOCK and BMAL1 are part of the first (activatory) loop, forming both a transcriptional activator complex driving the cyclical expression of their own repressors PER and CRY. The periodic expression of BMAL1 is regulated by the activator “retinoic acid receptor-related orphan receptor” (ROR) a/β and REVERBa/β playing the role as repressor (Lee, 2021). The name of REVERBα is derived from “reverse c-ErbAα“ as the encoding gene resides on the antisense strand relative to the human “thyroid hormone receptor alpha” (THRA/c-ErbAα) (Gomatou et. al., 2023). This complex machinery of feedback loops and periodically expressed circadian genes depicted in Fig.5 are forming the circadian rhythm in every eukaryotic cell, regulating the expression or circadian cycle of clock-controlled genes (CCGs). The disruption of the circadian machinery by nightshift, chronic jetlag or change in nutrition increases the risk for the development of common cancer types like lung, breast, prostate or colorectal cancer among others (Lee, 2021). Moreover, it was shown that a lower BMAL1 expression resulted in a shorter overall survival rate at five years in patients (Mazzoccoli et. al., 2011). In addition, BMAL1 is involved in the regulation of the cell cycle, tumor metastasis and metabolism. A disturbance in its expression can shift physiological patterns and cellular activities, driving the progression of CRC (Rao et. al., 2022). Furthermore, CLOCK expression has been

associated to tumor cell migration and metastasis in CRC by modulating HIF1α/β and VEGFα pathways within the tumor microenvironment (TME) (Wang et. al., 2017). As the major negative feedback loop circadian rhythm factor, REVERBα plays a crucial role in cancer development and progression. An increased REVERBα expression was associated with poor prognosis in CRC patients (Aroca-Siendones et. al., 2021). Additionally, it was shown that REVERBα supports CRC metastasis and growth by driving the expression of VEGFα (Burgermeister et. al., 2019).

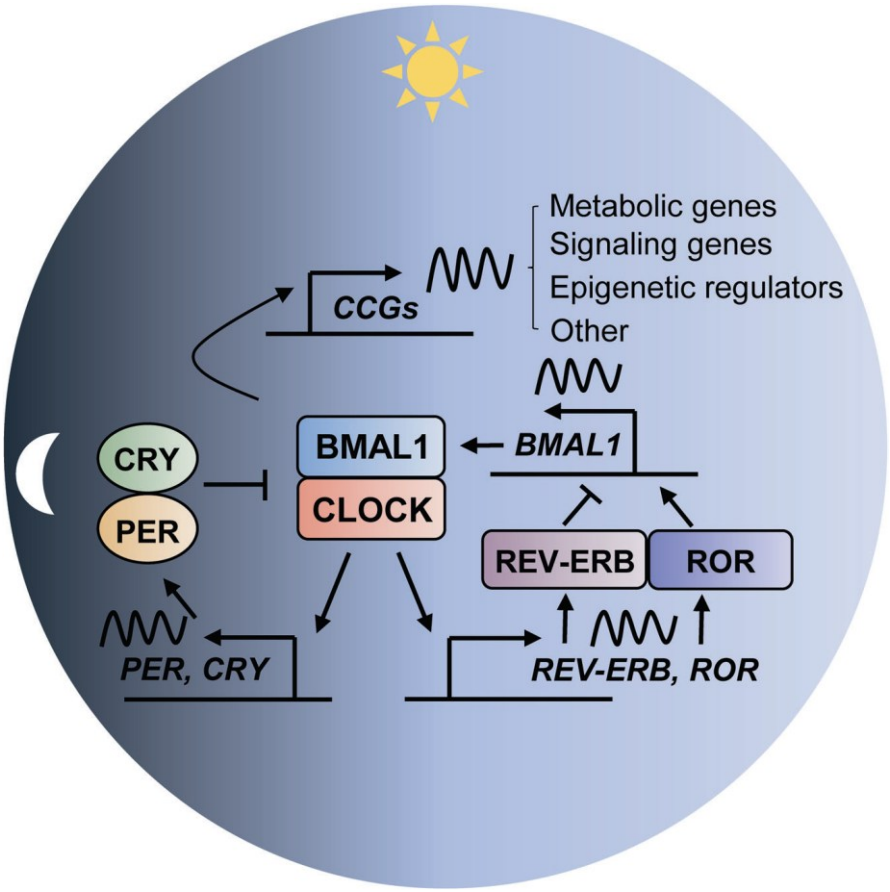

Fig. 5 Molecular mechanisms of the mammalian circadian clock (Lee, 2021). Interlocked autoregulatory transcription/translation feedback loops of core circadian rhythm factors depicting the loop cycling between the transcriptional activator complex CLOCK/BMAL1 and its repressors (CRY/PER & REVERBα) or activators (RORα/β). These loops are regulating the cyclic or oscillative expression of several CCGs like epigenetic factor and regulators, metabolic as well as signaling genes.

1.6 Macrophage diversity and subtype classification

For decades, macrophages were classified into two major classes, M1 “classically” and M2 “alternatively” activated macrophages. The M1-like phenotype typically resembles proinflammatory macrophages which are induced via toll-like receptors (TLR) by bacterial LPS or cytokines like IFNγ or TNFα. On the other hand, M2-like macrophages which are have been polarised by IL4 and IL13 are exerting anti-inflammatory properties by production of pro-fibrotic factors like TGFβ (Mills et. al., 2000). Due to the fact that the surrounding tissue microenvironment has a great impact on macrophage differentiation, polarisation and activity, the landscape of macrophage subtypes has been recently evinced (Mulder et. al., 2021) to be highly diverse as depicted in Fig.6. This functional diversity of tumor-associated macrophages (TAMs) is not only regulated by the spatial proximity to organs, cancer types and microenvironment, but also to its ontogeny (Casetta and Pollard, 2018).

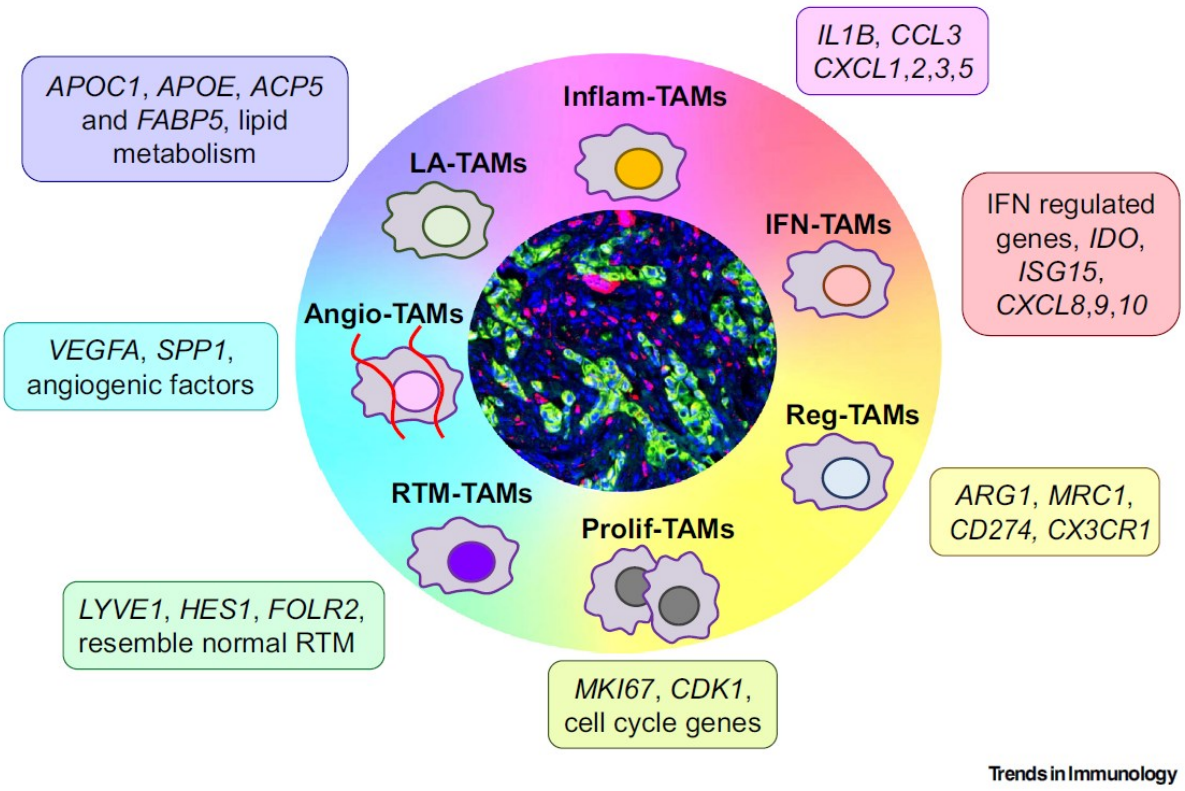

Fig. 6 Macrophage TAM subset types with distinctive molecular features (Ma et. al., 2022) The subsets shown include interferon-primed TAMs (IFN-TAMs), immune regulatory TAMs (Reg-TAMs), inflammatory cytokine-enriched TAMs (Inflam-TAMs), lipid-associated TAMs (LA-TAMs), pro-angiogenic TAMs (Angio-TAMs), RTM-like TAMs (RTM-TAMs), and proliferating TAMs (Prolif-TAMs).

Over the past decade, the identification of this functional diversity of TAMs has been subject to current research. Advancements in single cell analysis of omics data revealed the multidimensional complexity of macrophage diversity during the past years, so that the old terminology become now obsolete (Mulder et. al., 2021). Nowadays, macrophages are classified according to specific signature markers they are expressing. These markers are indicators of macrophage behaviour and function. For example, the expression markers ISG15, TNFα and IL1β are indicators of macrophages exerting pro-inflammatory properties (Xue et. al., 2014), (Murray, 2017), (Zhao et. al., 2025). On the other hand, macrophages with anti-inflammatory characteristics can be identified by their expression of HALDRB, IL1β and LIPA (Rakina et. al., 2024), (Xie et. a., 2025), (Martinez & Gordon, 2014).

1.7 Targeting circadian rhythm components in colorectal cancer therapy

Several strategies can be exploited to target the circadian rhythm. First the circadian clock can be targeted by intervening in its rhythm to enhance or keep up a robust circadian rhythm. Fasting, a change in sleep-wake or dark-light cycles can affect the circadian rhythm. Secondly, the circadian clock can be directly targeted by drugging it with small molecules. Finally, the accurate timing of drugs to reduce side effects and improve its efficacy can be used to manipulate the circadian clock as well (Sulli et. al., 2019). All these mentioned methods are part of the so called chronotherapeutic approach in anti-cancer therapy. Circadian desynchrony and CRC development are closely linked together (Masri and Sassone Corsi, 2018). Moreover, almost every stage of CRC like progression, metastasis, invasion, resistance etc. involves circadian disorder (Zhu et. al., 2023). Immune checkpoints like the programmed cell death ligand 1 (PDL1) for instance have a daily oscillation. This rhythmic expression of PDL1 has a great influence on the efficacy of immune checkpoint inhibitors (ICIs) in tumor-associated macrophages (TAMs) during anti-cancer therapy. Thus, the timing of PDL1 inhibitors or ICIs in general might benefit an improved outcome for CRC (Fortin et. al., 2024). In addition, another currently used approach incorporating circadian related treatments in colorectal cancer is the inhibition of VEGFa via monoclonal antibodies like Bevacizumab. Bevacizumab and chemotherapeutics like FOLFOX of FOLFIRI are used in combination to increase CRC treatment efficacy. The circadian clock transcription factor BMAL1 was shown to drive the expression of VEGFa in CRC.

Therefore, BMAL1 can be seen as both potential druggable target preventing VEGFa therapy resistance, and biomarker due to its frequent expression in CRC patients (Burgermeister et. al., 2019). Furthermore, combining the hormone melatonin which regulates the sleep-wake cycle with FOLFOX reduced 5-FU resistance in CRC cells. However, the response to circadian therapy differs between patients (Sakatani et. al., 2019). As mentioned above REVERBs and other circadian genes play a crucial role in the development and growth of CRCs. BMAL1 and REVERBα are both contributing to VEGFa expression in CRC (Burgermeister et. al., 2019). Moreover, it was shown that REVERBα inhibition caused an effective reduction in CRC cell proliferation *in vitro* (Della-Morte, 2019). Therefore, REVERBα might be suitable as a therapeutic target in CRC. Finally, the exploration of the functional roles of the circadian genes within the immune landscape of the tumor microenvironment marks an important aspect in cancer research residing still in its infancy.

1.8 TIGIT and the poliovirus receptor as novel immune checkpoint

The immune system protects our bodies from invading pathogens and infections. Over a century ago, it was discovered that immune cells could also identify and eliminate neoplastic cells (Vesely et. al., 2011), (Ehrlich, 1899). Nowadays, we understand that tumor cells have developed mechanisms to escape, evade or hide from the detection by the immune system. They achieve this by down-regulating their antigenicity, making it harder for immune cells to recognize them as threats. Tumor cells which have lowered their immunogenicity often show an upregulation of immunoinhibitory molecules like PDL1, triggered by IFN-γ released from tumor infiltrating lymphocytes (Guo et. al., 2022). Blocking this immune checkpoint with monoclonal antibodies such as Nivolumab can restore immune cell functions, enabling the elimination of malignant cells (André et. al., 2020). Furthermore, the TIGIT-PVR/PVRL2 axis serves as an alternative immune checkpoint system which has emerged as a promising target in cancer therapy (Murakami and Ganguly, 2024). The TIGIT receptor, short for “T – Cell – Immunoreceptor – with – Ig – and – Immunoreceptor – Tyrosine – Based - Inhibition (ITIM) - domains”, is part of the Ig superfamily playing a pivotal role in regulating both innate and adaptive immunity (Chiang et. al., 2022). TIGIT interacts within a complex immune regulatory network, binding various ligands and competing with co-stimulatory receptors like DNAM-1/CD226. In general, TIGIT itself is expressed on multiple

immune cell types, including memory and activated T cells, cytotoxic, regulatory, and helper T cells, NK and NKT cells as well as on monocytes and macrophages. In addition, the physiologically low TIGIT expression on naive T- and NK cells is upregulated upon activation (Yu et al., 2009), (Kurtulus et al., 2015). As illustrated in Fig.7, TIGIT binds to several ligands on antigen-presenting or tumor cells, including the poliovirus receptor (PVR/CD155), poliovirus receptor-related proteins 2 (PVRL2/CD112) and 3 (PVRL3/CD113), and Fap2, a protein secreted by *Fusobacterium nucleatum*, a gut bacterium (Chauvin & Zarour, 2020) (Gur et al., 2015). Among these ligands, PVR/CD155 shows the highest affinity for TIGIT, while CD112 and CD113 display lower binding affinities (Yu et al., 2009). Additionally, PVR is part of the nectin family (including CD155/PVR, CD112/PVRL2, and CD113/PVRL3), which are cell adhesion molecules (Wu et al., 2024). Although PVRs are normally expressed by tissues and contribute to antiviral immunity, they are also able to establish an anergic microenvironmental niche in solid tumors, preventing NK and T cells from effectively attacking tumor cells (Whelan et al., 2019). When PVR+ tumor cells and macrophages bind TIGIT, they reduce the effector functions of NK and T cells, such as cytotoxicity, phagocytosis, and cytokine production (Stamm et al., 2018). Moreover, studies in human and mice have shown that TIGIT expression is elevated on tumor-infiltrating lymphocytes within the tumor microenvironment of several cancers, including breast, gastric, and colon cancers, non-small cell lung carcinoma, melanoma, multiple myeloma, and acute myeloid leukemia (Johnston et. al., 2014), (Inozume et. al., 2016). Furthermore, the accumulation of PVR/TIGIT in CRC and other tumors was shown to be associated with mutation and activation of oncogenic pathways, including EGFR/Ras, Wnt/GSK3b and Sonic Hedgehog, which promote metastasis and are linked to poor survival outcomes (Murakami and Ganguly, 2024). Collectively, this immune checkpoint axis opens up new targets and strategies to be developed as novel anti-cancer therapy. Fig.7 depicts the interactions of PVR/CD155 on tumor and immune cells with its different ligands.

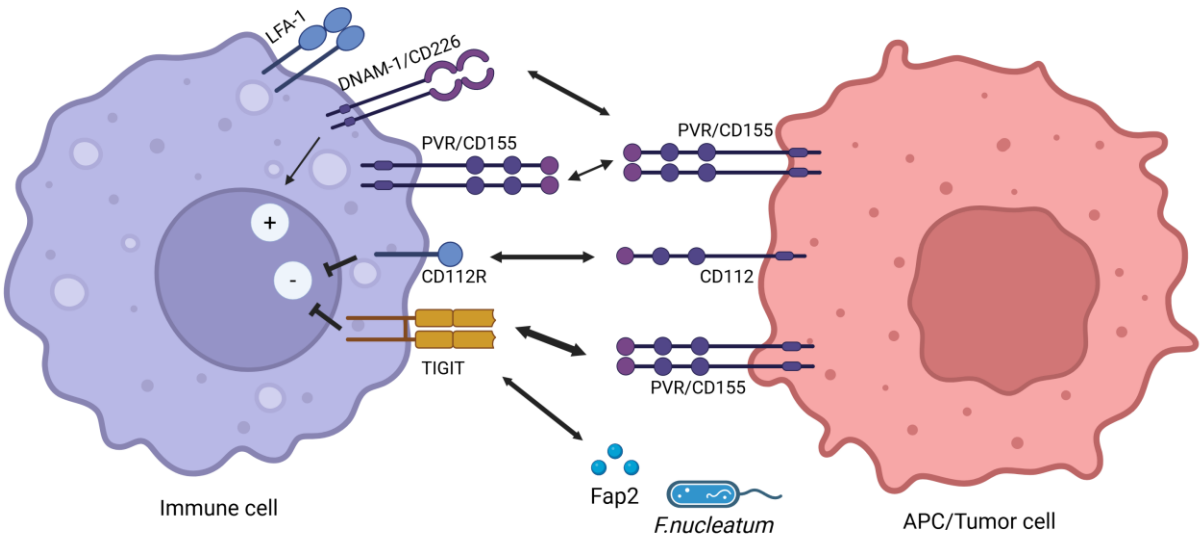

Fig. 7 PVR-TIGIT immune checkpoint axis and interactions PVR(CD155)-TIGIT immune checkpoint axis and interactions. CD155 is expressed on tumor and antigen-presenting cells and binds to a variety of ligands like TIGIT and DNAM1 forming heterotypic interactions as well as homotypic interactions with other CD155 molecules. The interaction of CD155 with TIGIT on immune cells such as macrophages inhibits their anti-tumoral effector functions. In contrary, the binding of CD155 to DNAM1 and CD155-CD155 homodimerization triggers cell adhesion and an activatory signal within the effector cell. The arrow thickness depicts the strength of interaction which increases with thickness. APC = Antigen presenting cell, LFA-1 = Lymphocyte function associated antigen 1.

1.9 Inhibitory mechanisms of the PVR and TIGIT system within immune cells

As previously discussed, TIGIT, PVR and other immune checkpoints play crucial roles in regulating immune responses, particularly within cancer. Furthermore, several inhibitory mechanisms of the PVR/TIGIT interaction suppressing both adaptive and innate immunity are known, as depicted in Fig. 8. The first inhibitory mechanism is cell-intrinsic, where TIGIT directly interacts with PVR/CD155 on tumor cells generating an inhibitory signal within effector cells such as NK and T-cells, which dampens their activity (Harjunpää and Guillery et. al., 2020). The second mechanism is cell-extrinsic, involving indirect inhibition via dendritic cells (DCs). In this case, TIGIT binds to PVR on DCs, initiating a signaling cascade which reduces the production of the pro-inflammatory cytokine IL-12 while increasing IL-10 levels.

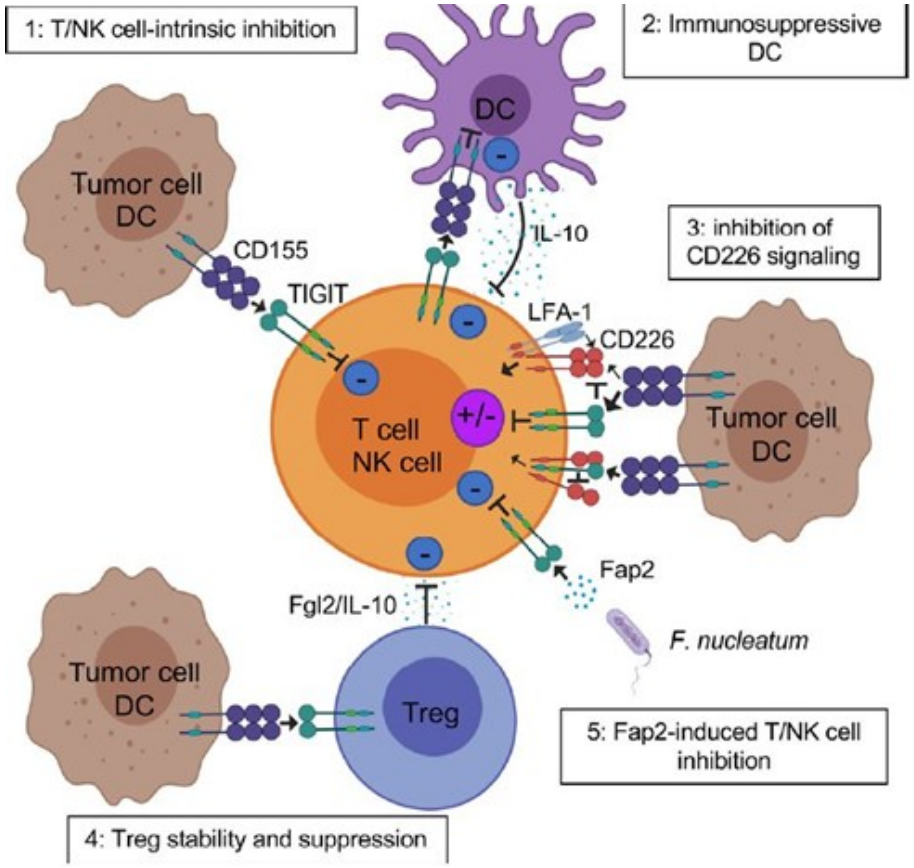

Fig. 8 Interaction and mechanisms of TIGIT inhibition on T-Cells (Chauvin and Zarour, 2020) Mechanism of different inhibitory pathways of TIGIT within the tumor microenvironment (TME). There are several pathways in which TIGIT triggers inhibition of immune cell function, like 1. The direct contact of CD155/PVR with TIGIT on immune cells. 2. TIGIT binds to CD155/PVR on dendritic cells (DC) to trigger IL10 secretion resulting in inhibition of immune cell function. In contrast to CD155/PVR, TIGIT also binds to CD226/DNAM1 which exerts an activatory signal. 3. Inhibition of CD226/DNAM1 signaling, occurs due to higher affinity of CD155/PVR to TIGIT and disruption of CD226/DNAM1 homodimerization. Additionally, TIGIT-PVR interaction impairs immune functions due to an indirect way of 4. Stabilization of T-reg cell activity and suppression through IL10 secretion. Finally, TIGIT can also bind to bacterial proteins like 5. Fap2 from *F. nucleatum* inducing inhibition of immune cells via TIGIT activation.

IL-10 exerts an inhibitory effect on a variety of surrounding immune cells (Yu et al., 2009). Third, studies indicate that TIGIT interferes with the interaction between PVR (CD155) and DNAM-1 (CD226). DNAM-1 is a co-stimulatory receptor found on several immune cells, including monocytes, platelets, NK cells, and T cells. Upon activation, this receptor associates with LFA-1, initiating a stimulatory signal within the effector cell (Dougall et. al., 2017), (Stanietsky et. al., 2009). The inhibitory effect here results from the higher affinity of TIGIT for PVR compared to DNAM-1, effectively limiting

effector cell activation via DNAM-1 (Yu et al., 2009). Additionally, TIGIT disrupts DNAM-1 homodimerization as well as its binding to PVR (Johnston et al., 2014). Fourth, the interaction of PVR with TIGIT on regulatory T cells (Tregs) enhances their immunosuppressive properties, leading to further inhibition of various immune cells (Joller et al., 2014). Finally, gut bacteria such as *Fusobacterium nucleatum* secrete Fap2, which binds to TIGIT and inhibits effector cell function (Gur et al., 2015).

1.10 The role of TIGIT/PVR in cancer therapy

As mentioned earlier, TIGIT is an inhibitory immune checkpoint expressed by various immune cells. Blocking the PVR/TIGIT interaction within the tumor microenvironment shows promising therapeutic potential, as it can restore immune cell function. Studies have demonstrated that TIGIT blockade in cancer patients reactivates T cell activity (Harjunpää & Guillerey, 2020). Additionally, in AML patients, siRNA-mediated knockdown of TIGIT resulted in increased IFN-γ and TNFα expression, along with reduced T cell apoptosis (Kong et al., 2016). Furthermore, enhanced CD8+ T cell proliferation and elevated cytokine expression were also observed in melanoma patients upon stimulation with tumor antigens, such as New York esophageal squamous cell carcinoma (NY-ESO), following TIGIT blockade. The combination of anti-PD-L1 and anti-TIGIT antibodies further intensified this effect through dual checkpoint inhibition (Chauvin et al., 2015). Compared to single-agent therapy, this co-blockade of TIGIT and PD-L1 has demonstrated significant clinical benefits while maintaining comparable toxicity levels (Rodriguez-Abreu et al., 2020). Moreover, PVR/TIGIT accumulation in CRC and other cancer types is often triggered by mutations in oncogenic pathways, such as EGFR/Ras, Wnt/GSK3b, and Sonic Hedgehog, which contribute to metastasis and thus worsen patient survival rates (Hirota et al., 2005). Inhibiting these oncogenic drivers in CRC, using targeted signaling inhibitors (e.g., EGFR inhibitors) alongside immune checkpoint inhibitors, may down-regulate PVR expression on tumor cells. This down-regulation would, in turn, allow lymphokine-activated killer cells (LAKs), including NK/T cells and cytotoxic macrophages, to effectively target and destroy tumor cells.

1.11 Transcriptional regulation of immune checkpoint targets by nuclear receptors

As outline above, inactivation (anergy/dysfunction) of immune cells within the tumor microenvironment after PVR-TIGIT interaction is of clinical potential due to the availability of therapeutic blocking antibodies (Abs). Consistently, TIGIT blockage in cancer patients has been shown to restore T-cell activity (Harjunpaa & Guillerey, 2020). Moreover, the human *PVR* gene is regulated by ligand-driven transcription factors including the AhR which stimulates and PPARγ which inhibits the expression of *PVR* in macrophages (Burgermeister et. al., 2019), (McKay et. al. 2021). These intracellular receptors can be influenced by various chemical agents and physiological (metabolic) cues as showcased in figure 9.

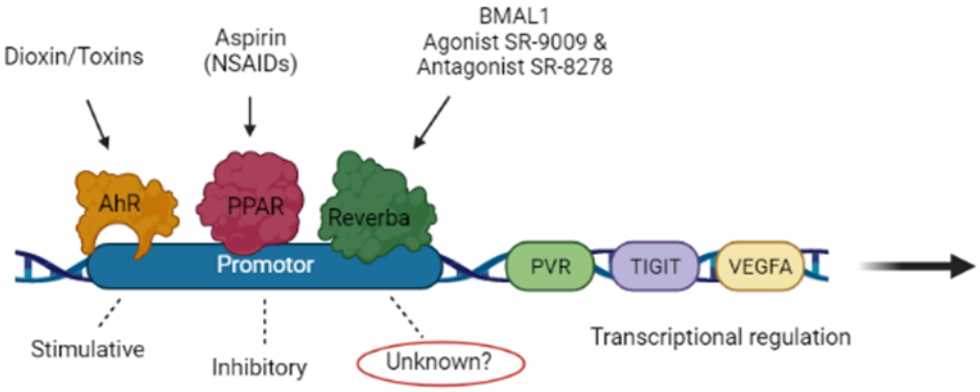

Fig. 9 Transcriptional regulation of immune checkpoint targets by intracellular nuclear receptors and transcription factors. The activity of intracellular receptors like AhR and PPARs are regulated by various chemical compounds. Dioxins or other toxins interact with AhR, whereas NSAIDs (such as aspirin) and fatty acid derivatives interact with PPARs and alter the transcriptional activity of target genes like *PVR e.a.*. It is currently unknown which regulatory function REVERBα and its synthetic drug- or physiological ligands (such as Fe2+ or Fe3+ Heme) exert on these designated target genes.

The transcriptional regulator REVERBα, a member of the nuclear receptor superfamily (NR1D1) acts as a repressor on target genes and coordinates circadian rhythms, immunity and metabolism (Yin et. al., 2007). REVERBα is a key component of the circadian machinery by forming the negative feed-back loop of the circadian clock through repression of the core pacemaker components CLOCK, BMAL1, PER1/2 and CRY1/2 (Lee, 2021). Furthermore, REVERBα also regulates genes which are involved in metabolic functions including gluconeogenesis, lipid and bile acid metabolism as well as genes involved in the inflammatory response of macrophages such as IL6 (Cho

et. al., 2012). However, its impact on macrophage checkpoints in CRC remains unknown.

1.12 Tumor organoids as a model system for colorectal cancer

Tumors are complex and heterogenous assemblies of malignant cells, whose growth and spread are influenced by a large network of surrounding components. The tumor microenvironment (TME), shaped by the developing malignancy itself, is infiltrated by various inflammatory cells, including lymphocytes and innate immune cells (Whiteside, 1993). This broad diversity of NK, T cells, monocytes and macrophages are not only inhibited by tumor-derived signals preventing anti-tumor response, but they play an important role in the promotion of tumor growth (Whiteside, 2006). To study this complexity, researchers have traditionally relied on *in vitro* 2D cell cultures and genetically modified animal models. However, a more advanced approach involves the use of *in vitro* human tissue-derived organoid cultures, allowing the investigation of tumor immunobiology. These organoids are 3D cultures derived from tumor tissues or pluripotent/stem cell lineages and are utilized to model cancers and their microenvironments (Fuji et. al., 2019). Moreover, patient-derived organoids (PDOs) can be cultivated *in vitro* which are isolated from tumor patients' biopsies. In addition, their scalability allows the establishment of comprehensive tumor biobanks documenting the mutational diversity and histological features of various human cancer subtypes (Drost and Clevers, 2018), (Betge et. al., 2022). Furthermore, to generate these organoids, cancer stem cells isolated from patient tissues are dissociated and embedded in Matrigel® droplets, providing a 3D scaffold for the stem cells mimicking the extracellular matrix of tissues. This setup, combined with exact conditions tailored to the tumor histology and type, requires the addition of specific factors like R-Spondin, epidermal growth factor (EGF), Wnt3a, and the bone morphogenetic protein (BMP) inhibitor Noggin. These components are essential for promoting differentiation and self-renewal of tumor stem cells (Sato et al., 2008). To conclude, the reconstitution of tumor organoids or PDOs with single or multiple immune cell types in co-culture systems offers a valuable platform to replicate and study the tumor microenvironment. This approach enhances the understanding of the intricate interactions within tumors and enables the testing of various immunotherapeutic strategies. Ultimately, it opens up new avenues for advanced personalized medicine (Yuki et. al., 2020).

1.13 Experimental approaches to study macrophage-tumor cell cross talk

In this PhD thesis, the human CRC MSS+ cell line HT29, the monocytic leukemia cell line THP1, PBMC-derived macrophages and PDOs were used to elucidate the cross-talk between macrophages and tumor cells with a focus on the PVR/TIGIT checkpoint and its regulation by REVERBα. Human THP1 cells were transfected with CRISPR/Cas9 constructs to knock-down the expression of REVERBα. Thus, THP1 cells were differentiated into adherent M0 macrophages with phorbol ester (PMA) and polarised into proinflammatory M(LPS/IFNy) *vs.* anti-inflammatory M(IL4/IL13) macrophages. HT29 cancer cells and PDOs were co-cultured with macrophages derived from either THP1 or PBMCs which were isolated from the blood of healthy donors. In this setting, direct cell-cell-contact co-cultures were used to study cell-intrinsic and non-cell-autonomous response mechanisms. The analysis of the co-cultured cells was done by live-cell imaging or immune-fluorescence microscopy to observe morphology. Colorimetric assays were used for viability, proliferation and cell death (apoptosis/necrosis) were analyzed via flow cytometry (FC). Furthermore, phagocytosis and efferocytosis were tested by labeling HT29 cells with CFSE and co-culturing them with macrophages to investigate differential effects of co-culture conditions like REVERBα ligand and functional antibody treatment PVR affecting macrophage function. These assays were analyzed via FC as well. Furthermore, the expression of main target REVERBα was analyzed via immunoblot. Finally, the impact of small molecule drugs on REVERBα and its regulation of PVR marks the main goal of this project.

1.14 Goal and outlook

It is well known, that colorectal cancer (CRC) belongs to one of the most common cancer types world-wide (Keum & Giovannucci, 2019). Although current therapy options range from surgery to chemotherapy, immunotherapy plays a fundamental role as last line strategy of anti-cancer treatment. Recent studies have demonstrated that targeting of immune checkpoints is an effective approach to enhance the anti-tumor response. Herein, the checkpoints PD1/PDL1 and CTLA4 expressed by activated T cells are effective targets which have been approved for the treatment of different cancer types and advanced stages. Nonetheless, targeting just a single immune checkpoint showed that more than 50% of the patients receiving a treatment failed to respond. Therefore, a combined approach of checkpoint inhibitors can drastically increase the response rate in tumor patients in general (Rotte 2019). However, the observed gain in PVR/TIGIT expression in tumors results in a poor survival rate due to the up-regulation of oncogenic and immune evasion/escape pathways.

REVERBα marks a key component of the circadian machinery. It also regulates genes involved in metabolic functions including gluconeogenesis, lipid and bile acid metabolism as well as genes involved in the inflammatory response of macrophages (Cho et. al., 2012). Studies in macrophages revealed, that REVERBs tend to regulate target gene expression by inhibiting the distal enhancers. These distal enhancers are selected by macrophage linage-determination factors, activating a specific program of repression (Lam et. al., 2013). Moreover, this nuclear receptor REVERBα acts as a repressor on target genes coordinating circadian rhythms, immunity and metabolism (Yin et. al., 2007). However, its impact on macrophage checkpoints remains unknown. Therefore, the general idea lies in the utilization of REVERBα to target the PVR-TIGIT immune checkpoint system, which might be an auspicious strategy to enhance the responsiveness of CRC patients to macrophages within the tumor microenvironment. Ultimately, the leading goal of this PhD thesis is to elucidate the role of REVERBα on the PVR-TIGIT immune checkpoint system, to enforce the anti-tumor efficacy of macrophages against CRC cells.

The following aims were addressed in this project:

1. Aim: Investigation of REVERBα expression in macrophages, target interaction and checkpoint Ab response in macrophage-tumor cell cross-talk in CRC

We aim to CRISPR/Cas9 knock-out (KO) REVERBα in monocytic leukemia-derived THP1 macrophages and conduct co-cultivation with human CRC lines. Results shall be compared to 3D co-cultures of primary macrophages and PDOs from CRC patients in Aim 3. Morphology and viability will be analyzed via live cell imaging and flow cytometry (FC). Furthermore, expression of REVERBα in CRISPR/Cas9 modified THP1- and PBMC-derived primary macrophages shall also be investigated.

2. Aim: Unravelling the molecular mechanisms of REVERBα in macrophages and malignant cell phenotypes

The impact of overexpression and CRISPR/Cas9 modification of REVERBα as well as the modulation of REVERBα target genes by synthetic drug agonist (SR9009) and antagonist (SR8278) will be analyzed via immunoblot, RT-qPCR, ChIP and luciferase reporter gene assays. Moreover, essential macrophage functions are planned to be investigated in CRISPR-modified THP1- and PBMC-derived primary macrophages upon treatment with REVERB modulating synthetic ligands. Phagocytosis of fluorescent beads and tumor cell efferocytosis assays are the methods for examining these functions.

Additional *ex vivo* experiments with mouse macrophages are planned to study the mechanism how REVERBα interferes with the Type-I IFN/JAK/STAT signal transduction pathway (based on a cooperation with Prof. M. Müller, Vienna).

3. Aim: Integration of outcomes on drugged REVERBα function in CRC cell co-culture models

Primary PBMC-derived macrophages isolated from healthy donor blood are co-cultivated with CRC cell line HT29 and patient-derived organoids (PDOs) from patients with CRC. The supplementation of co-cultures with synthetic drug agonist (SR9009) and antagonist (SR8278) targeting REVERBα, together with PVR blocking antibodies, is planned to enhance macrophage-mediated tumor cell killing. This approach aims to unravel novel therapeutic strategies leveraging macrophage functionality for more effective CRC treatment.

The main project hypothesis states that the knockout or pharmacological modulation of REVERBα in macrophages is expected to reactivate or increase their anti-tumor efficacy against CRC cells e.g. patient-derived tumor organoids (PDOs). Thus, the overall aim of this PhD thesis is to elucidate the role of REVERBα on the PVR-TIGIT immune checkpoint system, to enforce the anti-tumor efficacy of macrophages against CRC cells.

2. Materials and Methods

2.1 Materials

2.1.1 Companies

Company	Headquaters	Abbreviation
Abcam	Cambridge, UK	Abcam
Addgene	Watertown Massachusetts, USA	Addgene
American Type Culture Collection	Manassas, Virginia, USA	ATCC
Applied Biosystems	Waltham, Massachusetts, USA	AB
Becton Dickinson	Franklin Lakes, New Jersey, USA	BD
Biozym	Hessisch Oldendorf, Germany	Biozym
BioLegend	SanDiego, California, USA	BL
Bio-Rad Laboratories, Inc.	Herkules, California, USA	BioRad
BINDER GmbH	Tuttlingen, Germany	Binder
Bethyl Laboratories	Montgomery, Texas, USA	Bethyl
Bemis	Neenah, Wisconsin, USA	Bemis
B. Braun Melsungen	Melsungen, Germany	Braun
Carl Zeiss AG	Oberkochen, Germany	Zeiss
Carl Roth GmbH + Co. KG	Karlsruhe, Germany	Roth
Cayman Chemical	Ann Arbor, Michigan, USA	Cayman
Cell Signaling Technology	Danvers, Massachusetts, USA	Cell Signaling
Consort BVBA	Turnhout, Belgium	Consort
Corning	New York, USA	Corning
Cryoport Systems	Brentwood, Tenessee, USA	MVE

Cytiva	Little Chalfont, UK	Cytiva
Emerson Electric Company	St. Louis, Missouri, USA	Emerson
Eppendorf AG	Hamburg, Germany	Eppendorf
Eurofins Scientific	Luxemburg	Eurofins
Greiner Bio-One GmbH	Frickenhausen, Germany	Greiner
HETTICH | Andreas Hettich GmbH & Co. KG	Tuttlingen, Germany	Hettich
Heraeus Holding GmbH	Hanau, Germany	Heraeus
Heidolph Instruments GmbH & Co. KG	Schwabach, Germany	Heidolph
Invitrogen AG	Carlsbad, USA	Invitrogen
IKA®-Werke GmbH & CO. KG	Staufen, Germany	Ika
Intas Science Imaging Instruments GmbH	Göttingen, Germany	Intas
JULABO GmbH	Seelbach, Germany	Julabo
Knick Elektronische Messgeräte GmbH & Co. KG	Berlin, Germany	Knick
Leica Microsystems	Wetzlar, Germany	Leica
Life Technologies	Carlsbad, California, USA	LifeTech
Merk Millipore	Burlington, Massachusetts, USA	Millipore
Menzel GmbH	Braunschweig, Germany	Epredia
neoLab Migge GmbH	Heidelberg, Germany	neoLab
New England BioLabs Inc.	Ipswich, Massachusetts, USA	NEB
Novus Biologicals	Littleton, Colorado, USA	Novus
PeproTech Inc.	Rocky Hill, New Jersey, USA	Pepro
PEQLAB Biotechnologie GmbH	Erlangen, Germany	peqLab

Phoenix Instrument GmbH	Grabsen, Germany	Phoenix Instruments
Promega GmbH	Walldorf, Germany	Promega
QIAGEN GmbH	Venlo, Netherlands	Qiagen
Sartorius AG	Göttingen, Germany	Sartorius
SARSTEDT AG & Co. KG	Nümbrecht, Germany	Sarstedt
Sigma-Aldrich	St. Louis, Missouri, USA	Sigma
Sigma Laborzentrifugen GmbH	Osterode am Harz, Germany	SigmaCentrifuge
STARLAB INTERNATIONAL GmbH	Hamburg, Germany	Starlab
Tecan Trading AG	Männedorf, Swizerland	Tecan
Thermo Fisher Scientific	Waltham, Massachusetts, USA	Thermo
Techno Plastic Products AG	Trasadingen, Swizerland	TPP

2.1.2 Reagents

Name	**Manufacturer**	**Catalogue No.**
ROTIPHORESE®NF-Acrylamid/Bis-Lösung 30	Roth	A124.1
Acetic Acid	Sigma	45726
Ammoniumpersulfat ≥ 98%	Sigma	248614
Amersham Protran 0.45 NC nitrocellulose	Cytiva	4675.1
Ampicillin 100 mg/ml	Sigma	A5354
Aqua Spüllösung 1000ml steril	Braun	-
β-Mercaptoethanol ≥ 99%	Sigma	M6250
Biozyme LE Agarose	Biozym	840001
Bromphenolblau	Sigma	B5525
BSA	Millipore	810033

Complete™ Proteasehemmer-Cocktail	Roche	04693116001
DMSO	Sigma	D2438
DTT 1,4-Ditrhiotreitol 1	Sigma	11474
EDTA	Sigma	E6134 500g
Ethidiumbromid	Sigma	E1510
Ethanol absolut analysis EMSURE® ACS,ISO,Reag.	Sigma	Ph Eur 1.00983
FacsClean	BD	340345
FacsFlow	BD	342003
FacsRinse	BD	340346
GeneRuler 100 bp DNA Ladder 50µg, 0,5µg/µL	Thermo	SM0241
Glycin Pufferan® ≥ 99%	Roth	3908.2
Glycerol ≥ 99%	Sigma	G5516
HCl 37%	Sigma	258148 500 ml
HCl 1M	Merck	1.09057
Hydrogenperoxid Solution 30 % (w/w) in H_2O, contains stabilizer	Sigma	H1009
2-Propanol	Roth	1HPK.1
iTaq Universal SYBR Green Supermix	BioRad	-
JumpStart REDTaq Ready Mix	Sigma	P0982
LB-Agar (Lennox) 500 g X965.1	Roth	
LB-Medium (Lennox) 500 g	Roth	X964.1
Lipofectamine™ 2000	Invitrogen	11668019
Lipofectamine™ RNAiMAX	Invitrogen	13778150
Methanol ROTISOLV® ≥ 99% UV/IR Grade	Roth	AE71.1
Milkpowder blotting grade, low fat	Roth	T145.2

MS Columns	Miltenyi	130-042-201
Na^+orthovanadate ≥ 90%	Sigma	S6508
Nicotinamide	Sigma	N0636 100g
p-Coumaric acid	Sigma	C9008
PageRuler™ Prestained Protein Ladder, 10 to 180 kDa	Thermo	26616
PageRuler™ Plus Prestained Protein Ladder, 10 to 250 kDa		26619
PMA	Sigma	182230
Poncau S Solution	Sigma	P7170 1L
2-Propanol ROTISOLV® Pestilyse® ≥ 99,8%	Roth	T902.1
ProLong™ Gold anti fade reagent with DAPI	Invitrogen	P36935
Puromycin-Dihydrochlorid	Gibco	12122530
Pierce RIPA Buffer	Thermo	89900
REV-ERBα Antagonist, SR8278 -	Sigma	CAS 101910-24-1 - Calbiochem
REV-ERB Agonist II, SR9009 - Calbiochem	Sigma	554726
ROTI®Mark TRICOLOR 250 µL	Roth	8271.2
pHrodo™ Green STP ester	Thermo	P35369
Protease Inhibitor Cocktail I	Sigma	539131
Protease Inhibitor Cocktail II	Sigma	539132
SuperSignal™ West Pico PLUS	Thermo	34580
SDS ≥ 99% UltraPure	Roth	2326.1
SOC Broth Fluka Analytical 10ml	Sigma	SU-85469
TEMED 99% 25ml	Roth	2367.3
Tris Pufferan® ≥ 99% Ultra	Roth	5429.1
Trypaneblue 0,4% solution	GIbco	15250061

TurboFect Transfection Reagent	Thermo	R0533
Y-27632 (hydrochloride)	Cayman	10005583
Zeba Spin Desalting Columns 7K MWCO	Thermo	89882

2.1.3 Devices & Equipment

Name	Manufacturer	Catalogue No.
BD FACSCanto™ II Flow Cytometry System	BD	338962
BD Model 56 Incubator	Binder	9010-0323
Branson Sonifier 250	Emerson	101-063-965R
CERTOMAT IS	Sartorius	85030-520-53
Duomax 1030 balance shaker	Heidolph	444-1330
Electrophoresis Power Supply GPS 200/400	Pharmacia	SKU 09299-11-R
Eppendorf® Centrifuge 5804/5804R	Eppendorf	022625080
Eppendorf® Thermomixer Comfort 5355	Eppendorf	5355
Eppendorf® Microcentrifuge 5424R	Eppendorf	05401203
Eppendorf® Microcentrifuge 5415C	Eppendorf	Z365998
GeneAmp PCR System 9700	AB	4339386
Fusion FX	Vilber	SKU 1511-0-1
Heracell 150	Heraeus	51026538
Heidolph Hei End magnetic stirrer	Heidolph	P/N 505-50000-00-0
IKA RCT	Ikamag	0025005927
Gel iX Imager	Intas	GEL-IX-2023
Julabo TW20 Waterbath	Julabo	9550120
Labor-pH-Meter 766	Knick	766
Leica DMIRB Inverted Modulation Contrast Microscope	Leica	800-6834
MiniMACS™ and OctoMACS™ Separators	Miltenyi Biotec	130-042-109 130-042-102
Mini power supply, EV245	Consort	EV245

MIKRO 200 | 200 R centrifuge	Hettich	2400
Nanodrop ND-1000 Spectrophotometer	peQLab	26337
RSM-10HS	Phoenix Instruments	6.280 200
Sartorius 1204 MP Digital Scale	Sartorius	2903999
Sartorius MC1 Laboratory LC 4800 P	Sartorius	W--5026-e02112
Sigma 3k12 centrifuge	Braun	017447
Tecan Infinite M200	Tecan	30125944
PowerPac basic	BioRad	1640300
Promax 2001 shaker	Heidolph	P/N: 543-22332-00
Zeiss Axiovert 25 Inverted Microscope	Zeiss	451235
ZEISS Axio Observer	Zeiss	491916-0001-000
ZEISS ApoTome.2	Zeiss	423667-9100-000

2.1.4 Cell culture

Name	**Manufacturer**	**Catalogue No.**
Accutase	Sigma	A6964
Advanced DMEM/F-12	Gibco/Thermo	12634028
Cultrex Reduced Growth Factor Basement Membrane Extract, Type R1	R&D Systems	3433-005-R1
DMEM, high glucose, pyruvate	Gibco	41966
DPBS, no calcium, no magnesium	Gibco	14190
Fetal Bovine Serum, qualified	Gibco	10270106
GlutaMAX™ Supplement	Gibco	35050061
HEPES (1 M) 100ml	Gibco	15630-080

L-Glutamine (200 mM)	Gibco	25030081
LPS 1 mg/ml from Escherichia coli	Sigma	O111:B4
PBS, pH 7.4	Gibco	10010023
Penicillin-Streptomycin (10,000 U/mL)	Gibco	15140122
Recombinant Human IFN-γ	Pepro	300-02
Recombinant Human IL-13	Pepro	200-13
Recombinant Human IL-4	Pepro	200-04
Recombinant Human M-CSF	Pepro	300-25-500UG
Recombinant Human GM-CSF	Pepro	300-03-500UG
RPMI 1640 Medium	Gibco	21875034
Trypsin-EDTA (0.25%), phenol red	Gibco	25200056
TrypLE™ Express Enzyme (1X), no phenol red	Gibco	12604013
Invitrogen™ UltraPure™, DNase/RNase-free destilled water	LifeTech	10977049

2.1.5 Cell lines and bacterial strains

Name	**Manufacturer**	**Catalogue No.**
One Shot™ TOP10 Chemically Competent *E. coli*	Thermo	C404010
Stellar™ Competent Cells *E.coli*	Takara	636766
HT-29	ATCC	HTB-38
HEK293	ATCC	CRL-1573
SW480	ATCC	CCL-228
THP-1	ATCC	TIB-202

2.1.6 Antibodies

Name	Application	Manufacturer	Catalogue No.
APC anti-human CD11b	FACS	Biolegend	301310
Amersham ECL Mouse IgG, HRP-linked F(ab')$_2$ fragment (from sheep)	WB	Cytiva	NA9310-1ML
Anti-Poliovirus Receptor/PVR antibody C-terminal	WB	Abcam	ab229553
Anti-rabbit IgG, HRP-linked Antibody	WB	Cell Signaling	7074S
β-Actin Antibody (AC-15)	WB	Santa Cruz	sc-69879
BMAL1 (D2L7G) Rabbit mAb	WB	Cell Signaling	14020
CD47 Monoclonal Antibody (B6H12), Functional Grade, eBioscience™	*in vitro* assay	Invitrogen	16-0479-85
CLOCK (D45B19) Rabbit mAb	WB	Cell Signaling	5157
CD155 Monoclonal Antibody (2H7CD155), FITC, eBioscience	FACS	Thermo	11-1550-42
CD155 Monoclonal Antibody (D171)	*in vitro* assay	Thermo	MA5-13493
FITC Annexin V	FACS	Biolegend	640906
FITC Anti-NR1D1 + RVR antibody	FACS	Abcam	[EPR10376]
HSP90 alpha/beta (F-8)	WB	Santa Cruz	sc-13119

Mouse IgG1 kappa Isotype Control (P3.6.2.8.1), Functional Grade, eBioscience™	*in vitro* assay	Invitrogen	16-4714-85
NR1D1 Rabbit Polyclonal Antibody	WB	Proteintech	14506-1-AP
NR1D1 Polyclonal Antibody	IF	Invitrogen	PA5-29865
PerCP/Cyanine5.5 anti-human CD226 (DNAM-1) Antibody	FACS	BL	338314
PE-anti-human EpCAM	FACS	Biolegend	324206
Rev-Erbα (E1Y6D) Rabbit mAb	WB	Cell Signaling	#13418
SYTOX™ Blue Dead Cell Stain, for flow cytometry	FACS	Thermo	S34857

2.1.7 Enzymes

Name	Manufacturer	Catalogue No.
GoTaq® DNA Polymerase	Promega	M3001
KpnI-HF	NEB	R3142L
HindIII-HF	NEB	R3104L
T7 DNA Ligase	NEB	M0318S

2.1.8 Plasmids

Name	Manufacturer	Catalogue No.
pSpCas9(BB)-2A-Puro (PX459) V2.0 Plasmid	Addgene	#62988
pGL3 Basic Vector	Addgene	#212936
pCR™4-TOPO™ TA	Invitrogen	#K457501

2.1.9 Oligonucleotides

All sgRNA RNA sequences and Primers used were purchased and synthesized from Eurofins Genomics.

Oligonucleotide	Sequence 5´ -> 3	Product size (bp)
sgRNA Sequences		
C-terminal CD155/PVR knockdown sgRNA	GTTGGCAGACTAGAGTACAG	-
N-terminal CD155/PVR knockdown sgRNA	GCTCTCGTGCTCCACCTTGC	-
REVERBα CRISPR/Cas9 KO validation Primer		
5´-WTKO-REVERBα	CTGGCATGTCCTATGAACATG	299/156
3´-KO-REVERBα	GGTCATGCTGAGAAAGGTTCA	156
3´-WT-REVERBα	GTCTCCCATGCCCATGGCACC	299
5´-CT-REVERBα	GGTGCCATGGGCATGGGAGAC	320
3´-CT-REVERBα	TCACTGGGCGTCCACCCGGA	320
ChIP RT-PCR Primer		
5´-huPVR-CHIP	ACTCCTGGACCTCTGGTGATCC	180
3´-huPVR-CHIP	GTTAGAGGCTTCAGTGAGCTAC	180
RT-PCR and general PCR		
5´-huREVERBα/NR1D1	CTGGGAGGATTTCTCCATG	168
3´-huREVERBα/NR1D1	TTCACGTTGAACAACGAAGC	168
5´-huPVRC	AGTGAGCACTCAGGCATGTC	143
3´-huPVRC	GGACACAGATGACAGTGCCA	143
5´-huIL1B	GGACAAGCTGAGGAAGATGC	120
3´-huIL1B	TCGTTATCCCATGTGTCGAA	120
5´-huIL10	TTACCTGGAGGAGGTGATGC	151
3´-huIL10	GGCCTTGCTCTTGTTTTCAC	151
5´-huTLR4	TGAGCAGTCGTGCTGGTATC	166
3´-huTLR4	CAGGGCTTTTCTGAGTCGTC	166
5´-huTREM2	CACAACTTGTGGCTGCTGTC	127

3´-huTREM2	GGTAGAGACCCGCATCATGG	127
5´-huIDO1	GGCCAGCTTCGAGAAAGAGT	125
3´-huIDO1	TTGCCCCACACATATGCCAT	125
5´-huIL4I1	CTATCTCAGCTTCGCCGAGG	197
3´-huIL4I1	GAGAGGTCTCGATCTGCACG	197
5´-huISG15	ACCTGACGGTGAAGATGCTG	252
3´-huISG15	TCCTCACCAGGATGCTCAGA	252
5´-huFCGR3A	ATCTCCCAAAGGCTGTGGTG	222
3´-huFCGR3A	GGGTGGAGAGGTTTGTCTGG	222
5´-huLIPA	TCGCCTTCTGGTACTAGCCCT	312
3´-huLIPA	GCCTGGCTCCAGTGTAACAT	312
5´-huHLADRB1	ACTGCAGACACAACTACGGG	129
3´-huHLADRB1	CACTCACAGAGCAGACCAGG	129

2.1.10 Kits

Name	Manufacturer	Catalogue No.
CellTrace™ CFSE Cell Proliferation Kit, for flow cytometry	Invitrogen	C34570
Cell Meter™ Fluorimetric Phagocytosis Assay Kit *Red Fluorescence*	ATT Bioquest	21225
DNeasy Blood & Tissue Kit (50)	Qiagen	69504
Dual-Luciferase® Reporter Assay System	Promega	E1910
HiSpeed Plasmid Midi Kit (25)	Qiagen	12643
Neon™ Transfektionssystem 100 µl-Kit	Invitrogen	MPK10025
Pan Monocyte Isolation Kit, human	Miltenyi	130-096-537
Pierce™ BCA Protein Assay Kit	Thermo	23225
Pierce™ Agarose ChIP Kit	Thermo	26156
Pure Yield™ Plasmid Miniprep System	Promega	A1223
Qtracker™ 655 Cell Labeling Kit	Life Technologies	Q25021MP
QIAquick Gel Extraction Kit	Qiagen	28704
RNA Isolation, Total RNA Kit, peqGOLD	peqLab	13-6834-02
RNase-Free DNase Set (50)	Qiagen	79254
Topo™ TA Cloning™ Kit	Invitrogen	450641
Verso cDNA Synthesis Kit	Thermo	AB1453A

2.1.11 Plastic consumables

Name	Manufacturer	Catalogue No.
Aspiration pipet 2 ml	Greiner	710183
Cellstar® Cell Culture flask, 250 ml, 25 cm²	Greiner	690170
Cellstar® Supension Cell Culture flask, 250 ml, 25 cm²	Greiner	690195
Cellstar® Cell Culture flask, 250 ml, 75 cm²	Greiner	658170
Cellstar® Supension Cell Culture flask, 250 ml, 75 cm²	Greiner	658190/658195
Cellstar® Cell Culture flask, 550 ml, 175 cm²	Greiner	660160/660175
Cellstar® Supension Cell Culture flask, 550 ml/650 ml, 175 cm²	Greiner	660190/661195
Cellstar® Cell Culture Multiwell Plate 12 Well	Greiner	665180
Cellstar® Cell Culture Multiwell Plate 24 Well	Greiner	662160
Cellstar® Cell Culture Multiwell Plate 48 Well	Greiner	677165
Cellstar® Cell Culture Multiwell Plate 96 Well	Greiner	650160
Cellstar® Suspension Cell Culture Multiwell Plate 6 Well	Greiner	657185
Cellstar® Cell Culture Dish 100/20 mm	Greiner	664160
TubeSpin® Bioreaktor 15	TPP	TPP87017
Eppendorf Safe-Lock Tubes 0,5 ml	Eppendorf	0030121023
Eppendorf Safe-Lock Tubes 1,5 ml	Eppendorf	0030120086
Eppendorf Safe-Lock Tubes 2 ml	Eppendorf	0030120094
Falcon 15 ml Tubes	Greiner	188161
Falcon 50 ml Tubes	Greiner	227261
1000 µl Sarstedt® Filtertips (steril)	Sarstedt	70.3050.255

200 µl T Sarstedt ® Filtertips (steril)	Sarstedt	70.3031.255
10 µl Sarstedt ® Filtertips (steril)	Sarstedt	70.3010.255
1000 µl Sarstedt ® Pipette tips	Sarstedt	70.3050
200 µl Sarstedt ® Pipette tips	Sarstedt	70.3030
10 µl Sarstedt ® Pipette tips	Sarstedt	70.3010
Parafilm® M	Bemis	PM-999
Pipette, 50 ml	Greiner	768180
Pipette, 25 ml	Greiner	760180
Pipette, 10 ml	Greiner	607180
Pipette, 5 ml	Greiner	606180
PETRISCHALE, PS, 60/15 MM, MIT NOCKEN, 20 ST./BTL.	Greiner	628102

2.1.12 Buffers

Buffer	**Composition**
5x Alkaline SDS-Loading buffer	TrisBase (pH > 10) 62,5 mM, 10% SDS, β-MSH (5%), Glycerol (50%), Bromphenolblue
Antibody dilution buffer	1% FCS (v/v) in PBS
RBC lysis buffer (ELP buffer) 500 ml	44,95g NH_4Cl, 5g $KHCO_3$, 0,19g EDTA pH 8 in PBS
FACS buffer low BSA	1xPBS, 2 mM EDTA, 0,5% FCS, 0,4% BSA
IC Fixation Buffer	4% PFA (v/v) in PBS
Macs dilution buffer	0,5% BSA, 2 mM EDTA, pH 7,2 in PBS
10x PBS	9,55g PBS per L
Permeabilization Buffer	0,1% Triton X-100 (v/v) in PBS
10x Run/Transfer buffer 2L	288g Glycin, 6g TRIS
SDS Lysis buffer	50 mM Tris-HCl pH 7,6, 2% (w/v) SDS
Stacking buffer (SDS-PAGE)	0,5 M Tris-HCl pH 6,8
Separating buffer (SDS-PAGE)	1,5 M Tris-HCl pH 8,8
50x TAE buffer pH 8,5 1L	242g TRIS, 37,2 EDTA, 57,1 ml Acetic acid pH 8,5

10x TBS	88g NaCl, 200 ml 1M TRIS-HCl pH 7,4
Tris-HCl	1 M Tris-HCl pH 7,4

2.1.13 Software and Statistics

All data are displayed as mean ± S.E with at least N=3 independent experiments from different passages of cell lines or PDOs. Per co-culture set-up, PBMCs from one single healthy donor were used. As indicated in the legends, data were normalized to house-keeping genes or proteins and calculated as fold or % compared to control. Statistical analyses were performed following Graphpad Prism Version 9.1.0 guidelines for data distribution and appropriate comparisons between one or multiple groups. Unless stated otherwise, all tests were unpaired and two-tailed. A p-value of less than 0.05 was considered statistically significant (*). Sequence alignments for amino acids and genes were performed using BLAST (https://blast.ncbi.nlm.nih.gov), while three-dimensional (3D) structural modelling of proteins was conducted through the PHYRE2 Protein Fold Recognition Server (https://www.sbg.bio.ic.ac.uk). To identify potential transcription factor binding sites, the Alibaba tool (Transfac), version 2.1 (http://gene-regulation.com/pub/programs /alibaba2/), was used. Furthermore, to strengthen the literature base AI powered research-tool Consensus (2025) was employed to identify relevant peer-reviewed studies. Finally, the large language model ChatGPT-5 (OpenAI, 2025) was used for exploratory purposes, contributing to the refinement of the theoretical framework of this thesis.

2.2 Methods

2.2.1 Golden-Gate molecular cloning of sgRNA

All DNA plasmids and single stranded oligonucleotides (primers) were designed using the OligoPerfect® Primer Designer Software from Thermofisher. The DNA backbones were purchased from Addgene. All Primers were ordered at Eurofins Genomics and dissolved to 100 µM in sterile water.

2.2.1.1 Oligonucleotide design

In order to clone the sgRNA sequence into the vector pSpCas9(BB)-2A-Puro (PX459) V2.0 Plasmid #62988, the oligos should be designed, so that the forward and reverse strands pair with each other resulting in two overhangs that can be ligated into the vector.

Oligo 1 = Forward 5´-CACCGNNNNNNNNNNNNNNNNNN -3´
Oligo 2 = Reverse 3´- CNNNNNNNNNNNNNNNNNNNCAAA-5´

The PAM sequence is not included in this oligo design. Oligonucleotide sequences to generate the final sgRNA sequence cloned into the CRIPSR/Cas9 vector for REVERBα knockdown are listed in the following.

N-terminal REVERBα knockdown sgRNA Primer sequence:

Forward 5´-CACCGGGAGTGCCATACCTTCTCCC-3´
Reverse 5´-AAACGGGAGAAGGTATGGCACTCCC-3´

C-terminal REVERBα knockdown sgRNA Primer sequence:

Forward 5´-CACCGGGTCATGCTGAGAAAGGTCA-3´
Reverse 5´-AAACTGACCTTTCTCAGCATGACCC-3´

These two primer pairs were used in the following described oligo annealing and golden-gate reaction to create CRISPR/Cas9 vectors with sgRNA targeting the N-terminus and sgRNA targeting the C-terminus of REVERBα.

2.2.1.2 Oligo Annealing

For oligo annealing, the components as shown in Tab.1 were mixed and incubated in a PCR cycler with the following conditions: 37°C for 30 min, 95°C for 5 min followed by lowering the temperature in 5°C steps every 5 min until 25°C is reached and holded.

Tab. 1 Oligo annealing components

Component	**Amount [µl]**
Forward oligo (100 µM)	1
Reverse complement oligo (100 µM)	1
10x T4 ligase buffer (NEB)	1
T4 PNK (Polynucleotide Kinase) (NEB)	0.5
H_2O	6.5
Total volume	**10**

2.2.1.3 Golden-Gate reaction

In the following the finished annealed oligos from the previous step are diluted 1:10 by adding 90 µl of H_2O. The components for the following Golden gate reaction are displayed in the following Tab.2.

Tab.2 Components of Golden-Gate reaction

Component	**Amount [µl]**
2x T7 ligase buffer (NEB)	12,5
BSA [20mg/ml] (NEB)	0,125
EcoRI 20,000 units/ml (NEB)	1
T7 ligase (NEB)	0,125
Annealed oligo (1:10)	1
Vector [1 µg/µL]	1
H_2O	4,25
Total volume	**20**

After mixing the components for the Golden-Gate reaction as shown in Tab.2 the mix was incubated in a PCR cycler with the following settings displayed in Tab.3.

Tab.3: Golden Gate PCR reaction settings

Temperature [°C]	Time [min]	Cycles
37	5	15
20	5	15
4	∞	1

The ligation was first diluted 1:10 to finally analyze the ligated product by gel electrophoresis. To this end, 10 µl of the diluted product were pipetted into one pocket of a 2% agarose gel with ethidium bromide. The gel was run in 1xTAE buffer for 45-60 min at 120 V. Then the gel was finally analyzed by an Intas Gel iX imager.

2.2.2 Design of luciferase vector

2.2.2.1 Amplification of human *PVR* gene promoter

The following specific primers with restriction enzyme cloning sites were used for PVR promoter amplification.

Oligo1 = Forward KpnI-5´-ATGGTACCGTGATTTTCCTGTCTTAGCCTC-3´

Oligo 2 = Reverse HindIII-3´-ATAAGCTTCATGCCAGTTGCTCCGAGCAGC-5´

Genomic DNA from Parental THP1 cells was isolated and used as template DNA. For the PCR reaction 500 ng template DNA were used for one reaction. Tab.4 displays the PCR reaction components in detail.

Tab.4: PCR reaction components for one reaction

Component	Volume [µl]
DNA-Template	6
5x PCR Buffer	12
dNTP-Mix	3
5´-Forward Primer (1:10 dill.)	3
3´-Reverse Primer (1:10 dill.)	3
$MgCl_2$	3
GoTaq® DNA-Polymerase	0,75
Add H_2O to Total volume	**50**

For PCR product amplification the following reaction was performed using a Thermocycler with settings as shown in the following Tab.5.

Tab.5: PCR cycling parameters for *PVR* Promoter Amplification

Step	Temperature [°C]	Time [min]	Cycles
Initial denaturation	94	2	1
Denaturation	94	1	45
Annealing	60	1	45
Elongation	72	1	45
Final extension	72	5	1
Hold	4	∞	1

2.2.2.2 Analysis and isolation of PCR product for cloning

First, the amplified PCR product was evaluated by loading the complete reaction on an 2% agarose gel stained with ethidium bromide. The gel was run in 1xTAE buffer for 1,5-2h at 120 V. At the end, the gel was analyzed by an Intas Gel iX imager. After detecting the correct signal, the desired band was excised from the gel with a sterile scalpel and transferred into a 2 ml Eppendorf tube. The Eppendorf tube containing the excised DNA fragment was weighed. 3 volumes of Buffer QG were added to 1 volume of gel (e.g. 100 mg gel ~ 100 µl). After adding the calculated amount of Buffer QG, the tube was incubated at 50°C for 10 min until the gel slice has been completely dissolved. During incubation the tube was vortexed every 2 to 3 min to assist dissolution of gel. 1 volume of isopropanol was added to the sample mix after dissolution of the gel fragment. For DNA isolation the sample was load onto a QIAquick column and centrifuged for 1 min at 13000 rpm at RT. To wash, 750 µl of Buffer PE were added to the QIAquick column and centrifuged with the same settings as before. The flow through was discarded and the column was spinned again 1 min for drying. Finally, for elution the column was placed into a new 1,5 ml Eppendorf tube. 20 µl of 55°C pre-warmed ddH_2O were applied to the column membrane, incubated for 1 to 5 min before finally centrifuging for 1 min. Concentration of isolated DNA fragment was measured with the NanoDrop 1000 spectrophotometer described in section 2.2.6.

2.2.2.3 Cloning of amplified *PVR* promoter into TOPO® vector

For the reaction everything as listed in Table 6 was mixed gently and incubated for 30 min at room temperature. After incubation the reaction was placed on ice and transformation into competent bacteria was continued as described in the following section.

Tab.6: Setup of the TOPO® cloning reaction

Component	Volume [µl]
Fresh PCR product	2
Salt solution	1
TOPO® Vector	1
Water	add to 6
Total volume	**6**

2.2.3 Transformation of competent *E. coli*

For the transformation of the ligated vector, One Shot® TOP10 Competent *E.coli* from Invitrogen were used. The transformation was carried out according to the manufacturer's protocol as followed. First, the vial with the ligation mix was spinned down and placed on ice. One vial of 50 µl One Shot® TOP10 cells was thawed 1h on ice for each ligation/transformation. Then, 1-5 µl of ligation mix were directly pipetted into the vial with competent cells and gently mixed by tapping. The remaining ligation mix was stored at -20°C. The vial was incubated on ice for 30 min followed by an additional incubation in a 42°C water bath or thermo block for exactly 30 seconds with no mixing and shaking. After the incubation in the at 42°C, the vial was placed on ice, and 250 µl of pre-warmed S.O.C medium was added to each vial. The vial was then shaken at 225 rpm for 1 h at 37°C in a thermomixer device. Finally, 15 to 30 µl from each transformation vial were plated out separately on pre-warmed LB agar plates with ampicillin. The agar plates were inverted and incubated over night at 37°C.

2.2.4 Colony selection with antibiotics

After overnight incubation at 37°C of the agar plates, 5 to 8 single colonies were picked from the agar plate with a 200µl pipet tip. Each colony was transferred via the pipet tip under semi-sterile conditions into a culture tube containing 2-10 ml of LB media with ampicillin 100 µg/ml. All culture tubes were incubated at 37°C and 280 rpm 8-10 h.

2.2.5 Plasmid isolation via miniprep

For plasmid purification from *E. coli,* the PureYield Plasmid Miniprep Kit from Promega was used. First, 1000 µl of each bacterial culture were transferred to 1.5 ml Eppendorf tubes and centrifuged at maximum speed. The supernatant was discarded, and another 1000 µl were transferred to the tubes and centrifuged as before. Thereafter, the pellet was resuspended in 300 µL of PBS, and 100 µl of cell lysis buffer were added to each tube, and the solution mixed by inverting the tube 6 times. After the solution changed from opaque to clear blue indicating complete lysis, 350 µl of cold neutralization buffer were added to each tube and mixed by inverting 3-4 times until the sample turned yellow. Then, the neutralized samples were centrifuged at maximum speed for 3 min. The supernatant of each tube was transferred to PureYield Mini-columns for each sample. All columns were centrifuged at maximum speed for 15 seconds. The flow through was discarded, and 200 µl of Endotoxin Removal Wash were added onto each column, and the tubes centrifuged at maximum speed for 15 seconds. Then, 400 µl of Column Wash Solution were pipetted to each column and centrifuged at maximum speed for 30 seconds. All columns were transferred to 1.5 ml Eppendorf tubes. For the elution step, 30 µl of 38°C pre-warmed DNAse/RNAse free water was directly added onto each mini-column matrix and incubated at room temperature for 5 min. Finally, all columns were centrifuged at maximum speed for 15 seconds to elute the plasmid. Further analysis of the plasmid concentration was performed as indicated in the following section 2.2.6. The purified plasmids were stored at -20°C. Five microliters of isolated plasmid were mixed with 5 µl of appropriate sequencing primers (1:10 diluted) and send to Eurofins for sequencing.

2.2.6 Quantification of DNA and RNA

Nucleic acids were measured by a NanoDrop 1000 spectrophotometer. Before each measurement, a 1 µl blank measure was performed with the solution the DNA, RNA or plasmid to be measured was eluted in. The concentration of every sample was determined by applying 1 µl of it onto the lower measurement pedestal. Between each measurement, the pedestal was cleaned with a paper towel.

2.2.7 Liquid cultures for plasmid multiplication and purification

After analyzing the results of plasmid sequencing, the appropriate clones were selected for liquid culture. To this end, 200 ml of LB media supplemented with 100 µg/ml Ampicillin were inoculated with 2 ml of the pre-culture and incubated at 37°C at 280 rpm 8-10 h. The next day, the multiplied plasmids were isolated according to the protocol of the MIDI prep kit from Qiagen, following the same principle as described in section 2.2.5. Finally, the plasmid concentration was measured using the NanoDrop 1000 spectrophotometer as described in the previous section.

2.2.8 Generation of CRISPR/Cas9-sgRNA knockdown cell clones

2.2.8.1 Transfection of THP1 cells via electroporation

For the generation CRISPR/Cas9 knockdown cell clones of *REVERBα* gene, the following sgRNA primer sequences were used.

sgRNA sequences cloned into the CRIPSR/Cas9 vector:

N-terminal REVERBα knockdown sgRNA Primer:
Forward 5´-CACCGGGAGTGCCATACCTTCTCCC-3´
Reverse 5´-AAACGGGAGAAGGTATGGCACTCCC-3´

C-terminal REVERBα knockdown sgRNA Primer:
Forward 5´-CACCGGGTCATGCTGAGAAAGGTCA-3´
Reverse 5´-AAACTGACCTTTCTCAGCATGACCC-3´

The transfection of cultured THP1 cells with a CRISPR/Cas9 plasmid containing a specifically designed sgRNA sequence was performed by using the Neon™ transfection system from Invitrogen. Three days prior electroporation 0.2x10^6 THP1 cells/ml were seeded. On the day of electroporation, the cell density was around 0.8-1x10^6 cells/ml. 2x10^6 THP1 cells were used per transfection. Before transfection, cells were washed once with PBS. Then the cells were spinned down at 400g for 5 min at RT and resuspended in R-Buffer (100 µl per 2x10^6 cells) after discarding the supernatant. The cells were then transferred into a sterile 1.5 ml Eppendorf tube. Before electroporation a 6 well plate with 1 ml pre-warmed RPMI medium without P/S per well was prepared. For electroporation, the Neon™ tube was filled with 3ml electrolytic buffer (Buffer E) and inserted into the Neon™ pipette station. After that 1 µg of plasmid DNA per transfection was transferred into the tube containing the cells and mixed gently. The cell-DNA mixture was taken up with the Neon™ pipette holding a Neon™ tip by slowly pushing to the first stop and releasing the push-button very carefully to aspirate the mixture into the Neon™ tip. Further, the Neon™ Pipette was vertically set into the Neon™ pipette station until a click sound appeared. Each electroporation was performed with the following parameters.

Voltage (V): 1400

pulse width (ms): 20

pulse number: 2, cells/ml: 2x10^7

tip type: 10µl

After entering the parameters for electroporation, the start button was pressed to deliver the electric pulse. The notification “complete” appeared after successful completion of the electroporation. Furthermore, the Neon™ pipette was immediately removed from the Neon™ station and the sample was transferred into one well of the prepared 6 well plate. The plate was gently rocked to assure even distribution of transfected cells and incubated at 37°C with 5% CO_2. The next day post-transfection, 20% FCS was added to each well containing transfected THP1 cells. Finally, 0.25 µg/ml puromycin were added into each well to start clonal selection.

2.2.8.2 Transfection of HEK293T, HT29 and THP1 cells with plasmid vectors

The transfection of cultured HEK293T, HT29 and THP1 cells with CRISPR/Cas9, *PVR*-promoter Luciferase or REVERBα overexpression vector was performed by using TurboFect™ or Lipofectamine 2000 Transfection Reagent from Thermofisher. One day before transfection, 250.000 cells/well are seeded into a 6-well plate. For each well, 2 µg of vector DNA were diluted in 100 µl of serum-free DMEM or RPMI media. Furthermore, 6 µl of the transfection reagent were diluted in 100 µl of serum-free DMEM or RPMI media and vortexed. The diluted DNA and transfection reagent were combined and mixed by pipetting. This transfection/DNA mix was incubated for 15-20 min at room temperature. Then, 200 µl of the transfection/DNA mix were added dropwise into each well of the 6-well plate prepared with seeded cells. The plate was then gently tilted and swirled to achieve an even distribution of the transfection mix. Finally, 24 h upon transfection a medium change was performed.

For CRISPR/Cas9 clones the clone selection was started by adding 0,5-1 µg/ml of puromycin into each well 48 h post-transfection. A medium change with DMEM or RPMI complete plus 0,5-1 µg/ml puromycin was carried out every two days.

The number of seeded cells for different *in vitro* setups is depicted by Tab. 7.

Tab.7 Number of seeded cells for different experimental setups

Cell Line	12 Well [cells/well]	6 Well [cells/well]	48 Well [cells/well]	10 cm dish [cells/well]
HEK293T	-	350.000	-	6.000.000
HT29 Parental	15.000	250.000	3333.33	6.000.000
THP1 Parental	150.000	500.000	50.000	6.000.000
PBMCs	150.000	1.000.000	50.000	-

2.2.8.3 Picking and cultivation of adherent single clone colonies selected via puromycin treatment

After visible colonies of cells had grown on the plate, 3 to 5 colonies were picked or scratched off separately using a 200 µl pipet tip. Each colony was picked and collected. After picking, the colony was gently washed with 2 ml DMEM complete media in the well and transferred into a 15 ml falcon tube. This process was repeated 3 to 5 times until the desired number of single clones were picked. Thereafter, the colonies were centrifuged at 400 g for 10 min at room temperature. The supernatant was discarded, and the pellet resuspended in 0.5-1 ml trypsin followed by 10 min incubation in a water bath at 37°C. During incubation the tubes were shaken and tapped every few minutes so that the cells separated well. The trypsin reaction was stopped by adding 5 ml DMEM complete media to each tube. Further separation of cells was performed by pipetting up and down using a blue pipet tip attached to a 10 ml serological pipet. Then, the cells were centrifuged as before, and the pellet resuspended in 500 µl DMEM complete media supplemented with 0.5 µg/ml puromycin. Depending on the clone's size, the resuspended cells were seeded in one or two wells either into a 96-well plate for small to medium sized clones and intro a 48 well plate for large clonal colonies. Once the density was high enough in the wells, the clones were passaged and transferred to the next larger volume until they were cultivated in a 6 well plate. From here on, the clones were seeded and cultivated in 10 cm dishes to finally freeze backup tubes. Four 10 cm dishes of one clone were trypsinized and pooled. The number of cells was enumerated by using a Neubauer-Improved counting chamber, and 1.5 ml of the pooled clone were reseeded into a 25 cm^2 or a 75 cm^2 cell culture flask, depending on the previous cell density. Clonal cells were frozen and stored in liquid N_2.

2.2.9 Cell culture and *in vitro* assays

All cell culture experiments were carried out with human adherent (CRC: HT29, HEK293T) cancer cell or suspension (monocytic leukemia: THP1) cell lines. HT29, HEK293T and THP1 cells were provided by ATCC. All patient derived organoids (PDOs) were provided by the Dept. of Internal Medicine II (Prof. M. Ebert). Human ethics approvals regarding work on patient samples (PDO, blood, tissue) have been granted to the Dept. of Internal Medicine II. Adherent cell lines were cultivated in 25 cm^2, 75 cm^2 and 175 cm^2 culture flasks with DMEM complete (5 ml for 25 cm^2/10 ml

for 75 cm^2 flasks). Suspension cells were cultivated in 25 cm^2, 75 cm^2 and 175 cm^2 culture flasks with RPMI complete. All cell lines and organoids were cultivated at standard conditions at 37°C with 5% CO_2 in a humidified atmosphere (incubator) Tab.8 lists media and their components.

Tab.8: Cell culture media compositions

Media	Components
DMEM complete	10% FCS, 5ml Glutamine and 10 µg/ml Pen/Strep
RPMI complete	10% FCS, 5 mM GlutaMAX, 5 mM HEPES and 10 µg/ml Pen/Strep
Advanced DMEM complete	0,5 mM HEPES, 1xGlutaMAX and 10 µg/ml Pen/Strep
ENA+Y (Y only after splitting with trypsin-LE)	1,23 mM NAC, 50 ng/ml EGF, 500 nM A-83-01, 2% B27, 10% Noggin,10 µM Y-27365,10 mM nicotinamide, 10mM PGE2, 20 nM Gastrin, 100 µg/ml primocin
PBS Biopsy washing	5 ml Pen/Strep, 5 mM HEPES, 1x GlutaMAX and 100 µg/ml Primocin

2.2.9.1 Thawing of frozen cells

Frozen cell lines were thawed according to the following protocol. First, the frozen vial was incubated for 2 min in a water bath at 37°C. After thawing the vial, the cells were transferred to a 15 ml falcon tube with 9 ml of DMEM and 2 ml of FCS. The tube was centrifuged at 400 g for 10 min at room temperature. Afterwards, the cell pellet was resuspended in 5 ml of DMEM complete media with 20% FCS. The cells were then seeded into a pre-warmed 25 cm^2 cell culture flask. A change of media containing 20% FCS was performed the following day.

2.2.9.2 Freezing of cells

First, the cells were washed once with 2 ml PBS. Then, the cells were detached by adding Trypsin-EDTA 0,25% (1 ml in 25 cm^2/2ml in 75 cm^2 culture flasks) followed by a 5-10 min incubation at 37°C. Trypsinization was neutralized with pre-warmed DMEM complete (5 ml for 25 cm^2/8 ml for 75 cm^2 flasks), and cells transferred into a 15 ml falcon tube. The cells were centrifuged at 400 g for 10 min at room temperature. Then, the pellet was resuspended in 10 ml pre-warmed DMEM complete, and cells were counted via Neubauer-Improved counting chamber. Thereafter, the cells were centrifuged as before and resuspended in FCS supplemented with 10% DMSO. Finally, $5*10^6$ cells per ml were aliquoted in cryotubes (1 ml per tube) and immediately frozen at -80°C. The next day the frozen cells were transferred into liquid N_2 for long-term storage.

2.2.9.3 Splitting of adherent cells

All cells were passaged when reaching a confluence of 80-90%. For cell passaging, the medium was aspirated, and cells were washed once with 2 ml PBS. After removal of PBS, Trypsin-EDTA 0,25% (1 ml in 25 cm^2/2ml in 75 cm^2 culture flasks) was added followed by 5-10 min incubation at 37°C. The detached cells were taken up with pre-warmed DMEM complete (5 ml for 25 cm^2/8 ml for 75 cm^2 flasks) and transferred into a 15 ml falcon tube. After that, the cells were centrifuged at 400 g for 10 min at room temperature. Finally, the cells were resuspended in 10 ml DMEM complete and seeded 1:10 into new culture flasks.

2.2.9.4 Splitting of suspension cells

The suspension cell lines were passaged once a week after reaching a high density of $1*10^6$ cells/ml. First, the cells were transferred into a 50 ml falcon tube and centrifuged at 400 g for 10 min at room temperature. After removing the supernatant, the cells were washed once with 10-15 ml PBS by repetitive pipetting and centrifugation as before. Then, the cells were resuspended in 30 ml RPMI complete and counted within the Neubauer-Improved counting chamber. Finally, 300.000 cells/ml to 500.000 cells/ml were seeded in a new 75 cm^2 or 175 cm^2 flask in 10 or 20 ml RPMI complete media.

2.2.9.5 Isolation of primary derived Monocytes from healthy donor blood

For the isolation of primary derived blood monocytes (PBMCs) the Pan monocyte isolation kit from Miltenyi was used together with MS columns and MiniMACS™ separator. First of all, 13 ml RT warm Ficoll-Plaque was added into each 50 ml falcon. The falcons where centrifuged at 400g for 2 min to remove any Ficoll sticked to the falcon sides. Furthermore, the patient blood bags upper hose was cut with a sterilized scissor and blood was poured into an empty 50 ml falcon tube. After opening the blood bag, the patient blood was diluted 1:10 with sterile PBS and mixed vigorously. 35 ml of blood-PBS mixture was pipetted slowly to the falcons containing the Ficoll to create a clear gradient. Thereafter, the tubes were centrifuged at 930g at 21°C for 17 min with an acceleration of 3 and disabled break (very important!). Following this, a white layer was visible containing the PBMCs. This layer of PBMCs was slowly taken up with a 10 ml serological pipette and transferred into a new 50 ml falcon tube. All falcon tubes containing PBMCs were filled completely with PBS and centrifuged at 350g at 21° for 5 min with an acceleration of 9 and deacceleration of 8. A white cell pellet was visible and the supernatant was discarded before washing every pellet with 25 ml PBS. The resuspended cells of two falcon tubes were combined and centrifuged at 350g at 21° for 5 min as before. This process of washing and pooling was repeated until four falcon tubes containing PBMCs remained. Next, each pellet of the four falcons was resuspended in 12,5 ml RBC lysis buffer (diluted 1:10 with ddH_2O) and incubated at room temperature for 10 min. The suspension was mixed every 2 min to ensure proper lysis. Afterwards, the tubes were filled up with PBS and centrifuged at 350g at 21° for 5 min as before. Following this, the supernatant was discarded and the pellets resuspended in 25 ml PBS, each combined and centrifuged as before. This washing was repeated until one falcon tube containing PBMCs remained. As next step, the cells were calculated using a improved Neubauer cell counting chamber (1:1 dilution with trypan blue).

2.2.9.6 Monocyte isolation from PBMCs

For the initial monocyte isolation 200.000.000 cells were used. The following numbers of the kit components were calculated for isolating monocytes from 200.000.000 PBMCs. The calculated number of PBMCs was transferred into a new falcon tube and centrifuged at 350g at 21° for 5 min. Then, after discarding the supernatant the pellet was resuspended in 800 µl of Macs dilution buffer, 200 µl of FcR block and 200 µl of

Biotin-Antibody cocktail. This suspension was mixed and incubated at 4°C for 5 min. Following this incubation, 600 µl of Macs dilution buffer and 400 µl of Anti-Biotin Microbeads were added, the suspension mixed and incubated again at 4°C for 10 min. During this incubation four MS columns were equilibrated with 500 µl of Macs dilution buffer. In the next step, the cell suspension was equally distributed to all four columns and the flow through was collected. The columns were washed 3 times with 500 µl Macs dilution buffer. After that, all the flow through was pooled into one 15 ml falcon tube and centrifuged at 400 g for 10 min at RT. Subsequently, the pellet of isolated monocytes was resuspended in 10 ml RPMI complete media and cells were counted with a Neubauer cell counting chamber. Finally, the desired number of cells were seeded with 100 ng/ml M-CSF and left 5 to 7 days for differentiation.

2.2.9.7 Isolation of Patient-Derived Organoids

First, the fresh biopsy was washed with 10-15 ml PBS supplemented with (5 ml Pen/Strep, 5 mM HEPES, 1x GlutaMAX and 100 µg/ml Primocin). The biopsy was then transferred into a 15 ml tube with an FCS-coated pipette. After the biopsy formed a pellet in the bottom of the tube, the PBS was changed with 10-15 ml of new PBS and the tube was inverted three times. This procedure was repeated three times for washing of the biopsy. Two pieces of the biopsy were frozen for genetic screening. Then, the rest of the biopsy was cut into smaller pieces for enzymatic digestion. In 1.5 ml Eppendorf tubes, 500 µl of collagenase and 500 µl of hyaluronidase were mixed together with the biopsy pieces. The mixture was then incubated at 37°C in a water bath with light swiveling for 15 min. After that, the biopsies were again cut into smaller pieces and incubated for 15 min at 37°C with a new prepared enzyme mix. The healthy tissue was washed the same as explained before and frozen. Then, the supernatant with dissolved cancer cells was transferred into a 15 ml tube and the digestion was stopped with 9 ml of Advanced complete medium. The remaining tissue was trypsinized with 1 ml Trypsin EDTA 0,25% for 20 min at 37°C in water bath and mixed every 10 min. Following that, all contents were transferred and filtered through a 100 µm filter into a 15 ml tube. The supernatant from before and the new filtrate were both filtered again and centrifuged at 400g for 10 min at room temperature. After discarding the supernatant, the pellet was resuspended in Advanced complete medium and centrifuged as before. Finally, the pellet was resuspended in 250 µl Matrigel® or Culturex BME (amount is dependent on the cell density), and the isolated cancer cells

were plated out onto 6-well plates dropwise with 100 µl per well, and the plates were incubated upside-down for 1 h at 37°C to solidify the matrix. Thereafter, the appropriate organoid media ENA+Y was added to the wells with 2 ml per well. The next day, the medium was changed to ENA+Y.

2.2.9.8 Splitting of Patient-Derived Organoids

In general, one well of growing organoids was splitted to three wells, which were cultured in 6-well suspension culture plates. All work steps with organoids were performed on ice. First, before splitting, the Matrigel®/BME was thawn on ice. DPBS and FCS were aliquoted 10 ml-wise into 15 ml tubes and pre-cooled on ice, one tube DPBS for each patient. 1 ml/well of pre-cooled DPBS was added onto to the organoid droplets. Following that, the droplets were scrapped, transferred into a 15 ml tube and dissolved by up/down pipetting with an FCS-coated pipette on ice until no Matrigel®/BME was visible anymore. The dissolved organoid rings were centrifuged at 400 g for 10 min at 4°C. After removing the supernatant and Matrigel®/BME debris, the pellet was resuspended in 10 ml ice-cold DPBS and centrifuged a second time for washing with the same conditions as before to get rid of all Matrigel®/BME remnants. Finally, 1 ml Trypsin-LE express was added onto each pellet. The tubes were then incubated at 37°C in the water bath with shaking every 2 min. Trypsinization was stopped with addition of cold 2 ml FCS plus 7 ml Advanced complete media and followed by centrifugation as before. After discarding the supernatant, the pellet was resuspended in Matrigel®/BME (dependent on pellet size), and the single cells were seeded as small drops into wells of 6-well suspension culture plates with 100 µl per well. The plate was then incubated upside-down for 1 h at 37°C to provide the polymerization of the extracellular matrix and to prevent the attachment of the organoids to the plastic surface. Finally, 2 ml of appropriate media e.g., ENA+Y was added. The next day, medium was changed with ENA+Y. Further culturing of organoids was conducted with ENA medium w/o Y until splitting.

2.2.10 Co-Culture of human CRC cell lines or PDOs with macrophages

All co-culture experiments were carried out in 12-well, 48-well or 6-well plates and 10 cm cell culture dishes with the appropriate number of cells as displayed in Tab. 7. The experiments were performed with human colorectal cancer cell line HT29, HEK293T cells, THP1 cells and THP1 CRISPR/Cas9 knockdown clones as well as with PDOs.

2.2.10.1 Handling of parental THP1 and CRISPR modified THP1 cells

First, THP1 cells were seeded on 12-well, 48-well, 6-well plate or 10 cm cell culture dish (Tab.7). For differentiation, THP1 cells were mixed with 8 nM of PMA and incubated for 72 h at 37°C. The attached THP1 cells, herewith termed M0 macrophages, were washed once with PBS, differentiated and polarized for additional 48 h into either pro-inflammatory M(IFNγ/LPS) or anti-inflammatory M(IL4/IL13) macrophages using RPMI complete media supplemented with cytokines as indicated in Tab.9.

Tab.9: Polarization media for THP1 differentiation

Media	Components
pro-inflammatory M(IFNγ/LPS)	10 pg/ml LPS, 20 ng/ml IFN-γ
anti-inflammatory M(IL4/IL13)	20 ng/ml IL-4, 20 ng/ml IL-13

2.2.10.2 Handling of PBMC derived macrophages

PBMCs were isolated from healthy volunteers (DRK, Blood Donation Center, Mannheim) using Ficoll®-based density gradient centrifugation as described in section 2.2.9.5. For differentiation, isolated monocytes were treated with 100 ng/ml M-CSF for 5 to 7 days at 37°C before starting polarization into pro-inflammatory M(IFNγ/LPS) or anti-inflammatory M(IL4/IL13) macrophages. Furthermore, the stimulated monocytes were washed once with PBS and polarized for additional 48 h into either pro-inflammatory M(IFNγ/LPS) or anti-inflammatory M(IL4/IL13) macrophages with 100 ng/ml GM-CSF for M(IFNγ/LPS) and 100 ng/ml M-CSF for M(IL4/IL13) as indicated in Tab.10. M0 were left untreated as control.

Tab.10: Polarization media for PBMC differentiation

Media	Components
M1	100 ng/ml GM-CSF, 10 pg/ml LPS, 20 ng/ml IFN-γ
M2	100 ng/ml M-CSF, 20 ng/ml IL-4, 20 ng/ml IL-13

2.2.10.3 Co-Culture assay with colorectal cancer cells

CRC cell lines were trypsinized and added to an adherent monolayer of macrophages (in 6-, 12- or 48-well plates) in an effector-to-target (E:T) ratio of 3 macrophages : 1 cancer cell or 10:1 to enhance efficacy. A 50:50 mixture of DMEM/RPMI complete media was used and the plate was then incubated at 37°C for 1 to 5 days dependent on the assay. After incubating for the specified amount of time, co-cultures were analyzed by colorimetric MTT assays, phagocytosis/efferocytosis assay, IF, FACS or extraction of RNA and protein lysates for Western blot.

2.2.10.4 Co-Culture assay with PDOs

First of all, all steps with organoids were performed on ice. PDOs were separated to single intact organoid rings three days before starting the co-culture by passaging them without trypsinization. After 48 h of incubation at 37°C for differentiation and polarization of monocytes to macrophages, intact organoid rings were counted and resuspended in liquid Matrigel®/BME (1:100 dilution with media) and added to the adherent monolayer of differentiated macrophages with an effector-to-target (E:T) ratio of 50 macrophages : 1 organoid ring using a 50:50 media mix composed of DMEM/ENA (dependent on the patient). Furthermore, co-cultures were treated either with functional antibodies or small molecule drugs as described in the following section. Finally, after 3 to 5 days of incubation, FACS analysis or colorimetric MTT cell viability assay was performed with the PDO co-culture.

2.2.10.5 Treatment of Co-Cultures with antibodies

For co-cultures which were supplemented with blocking antibodies, the DMEM/RPMI complete 50:50 media mix was used together with functional blocking antibodies and isotype controls diluted. Respective concentrations are displayed in Table 11. The anti-CD155/PVR antibody was purified using Zeba™ spin desalting columns to remove any sodium azide.

Tab.11 Functional antibody concentrations

Antibody	Concentration [µg/ml]
Anti-CD155/PVR	5
Anti-CD47	10
Anti-TIGIT	5
IgG1 Isotype control	5
IgG1 kappa isotype control	10

2.2.10.6 Treatment of co-cultures with REVERBα ligands

For certain assays co-culture and single culture setups were treated with REVERBα small molecule drugs SR9009 Agonist and SR8278 Antagonist. For each experimental setup, DMSO was used as respective control. The concentrations used are listed in the Table 12 below.

Tab.12 REVERBα small molecule drug concentrations

Compound	Concentration [µM per ml]
SR9009 Agonist	1 or 10
SR8278 Antagonist	0,67 or 6,7

2.2.11 Isolation and analysis of RNA, protein and DNA

For all following sections, $1*10^6$ cells per well were seeded into 6-well plates (two wells per condition).

2.2.11.1 Isolation and purification of RNA

For RNA isolation, 350 µl TRK lysis buffer were pipetted onto cells of one well of a 6-well plate after aspirating the media. Then, the cells were scrapped off the well and

transferred into the second well sharing the same condition where the process was repeated. Following that, the RNA lysate was then transferred into 1.5 ml Eppendorf tube. Subsequently, the RNA purification was performed according to the protocol of the peqGOLD Total RNA Isolation Kit. After purification, the RNA concentration was measured by a NanoDrop 1000 spectrophotometer as described in section 2.2.6. All RNA samples were stored at -80°C.

2.2.11.2 Isolation of protein samples with SDS-lysis and RIPA-lysis buffer

The protein isolation resembles the previous isolation of the RNA with slight modifications. First, for protein isolation with SDS lysis buffer, 250 µl of SDS lysis buffer (1% SDS (w/v), 50 mM Tris HCl pH 7.4) supplemented with ¼ of a protease inhibitor tablet, 100 mM DTT and 100 mM sodium orthovanadate were used. The cells were scrapped off, and the lysate was transferred into the second well sharing the same condition and the process was repeated. Then, the protein lysates were transferred into a 1.5 ml Eppendorf tube and incubated for 15 min at room temperature. Further lysis was supported by sonification of the lysates 20x times and 2 repeats at 20% power before the samples were cooled on ice and prepared for western blot. Moreover, for protein isolation with the RIPA lysis buffer, 150 µl of RIPA lysis buffer containing protease inhibitor tablet, protease inhibitor cocktail I and II diluted 1:10 were used. The cells were scrapped off, and the lysate was transferred into the second well as before. After transferring the lysate into a 1.5 ml Eppendorf tube, the lysate was incubated at 4°C and 1500 rpm on a thermoshaker for 45 min. Following this, the lysate was spinned down at 13.000g for 15 min at 4°C. Finally, the lysate was transferred into a new 1.5 ml Eppendorf tube and protein measurement was continued from this point on.

2.2.11.3 Determination of protein concentration

The protein concentration was determined using the Pierce™ BCA Protein Assay Kit. To this end, 20 µl of each standard (provided by the Kit) was pipetted into two wells of a 96-well plate. The protein lysate was diluted 1:5 with ddH_2O or PBS, and 20 µl of this dilution were pipetted into two wells of the plate. Following that, the working solution was prepared by mixing solution A with solution B 1:50. Then, 200 µl of the prepared working solution were pipetted into each well containing either standard or sample. The plate was then incubated at 37°C for 30 min. Thereafter, the plate was cooled to room temperature, and the absorbance was measured at 562 nm with a Tecan Infinite

M200 multiplate reader. The final protein concentration was calculated using the standard curve.

2.2.11.4 Isolation of genomic DNA

All isolations of genomic DNA were carried out using the DNeasy Blood & Tissue Kit from Qiagen. Before staring, the desired cells were detached (if needed) 5*10^6 in total, washed and centrifuged at 300g for 5 min at RT. The pellet was resuspended in 200µl PBS and 20µl proteinase K were added together with 4µl RNase A (100mg/ml). Following that, 200µl Buffer AL without ethanol were added, mixed and incubated at 56°C for 10 min. Furthermore, 200µl ethanol (96-100%) were added to the sample, mixed and pipetted onto a DNeasy Mini spin column which was placed into a 2 ml collection tube. Each column was centrifuged at >6000g for 1 min at RT and the flowthrough was discarded. 500µl Buffer AW1 were added to each column and centrifuged again as before. After discarding the flowthrough, 500µl Buffer AW2 were added and columns were centrifuged as before. Finally, all columns were placed into a new 1,5 ml Eppendorf tube and genomic DNA was eluted wit 50µl prewarmed RNAse/DNAse free water. DNA concentration was measured as described in section 2.2.6.

2.2.12 Immunoblotting of protein samples

All Western blots were performed by using prepared 10% SDS-PAGE Gels. For each lane or pocket, 40 µg of protein were loaded. First, the calculated amount of 40 µg protein per sample was mixed and diluted with H_2O and 5xSDS loading buffer. All samples were then incubated at 99°C for 10 min in a thermomixer device. After loading the samples on the gel (15 µl per pocket), the separation was started first with 80 V for 10-15 min until forming an even frontline. Then the voltage was changed to 100-130 V until the running front reached the end of the gel. Following that, the transfer was done at 100 V for 1 h in prepared transfer buffer. After the transfer was done, the blot was stained with Ponceau S solution to verify the transfer to the nitrocellulose membrane. Following the destaining of the membrane with ddH_2O, the membrane was blocked with 5% powdered milk or BSA in PBST (PBS plus 0,1% TWEEN) for 1 h. The first antibody was diluted in 5% blocking solution (10 ml per blot) and incubated over night at 4°C on a rocking platform with gentle move. The next day, the membrane was washed with PBST three times á 5 min. Then, the blot was incubated with the second

antibody (linked to HRP) diluted in blocking solution for 30 min at room temperature on a rocking platform. Furthermore, the blot was washed again three times with PBST before starting the detection. For detection, SuperSignal™ West Pico PLUS substrate solution was mixed with reaction solution 1:1 and added to the membrane. The blot was incubated for 1 min at room temperature before detection of chemiluminescence signals using a Fusion FX-imager device. As a loading control, the expression of HSP90 or GAPDH was observed.

2.2.13 cDNA synthesis and PCR

To analyze the isolated and purified RNA, cDNA synthesis was performed. To this end, the Verso cDNA synthesis kit from Thermofisher was used. Each sample was prepared as indicated in Tab.13.

Tab.13 cDNA synthesis reaction mix components

Component	**Volume [µl]**	**Final Conc.**
5x cDNA synthesis buffer	4	1x
dNTP mix	2	500 µM each
Random Hexamer Primer	1	-
RT Enhancer	0,5	-
Verso Enzyme mix	0,5	-
PCR grade H_2O	variable	-
RNA sample	1-5 µl	1 µg
Total volume	**20**	

The following cDNA synthesis was carried out by using a Thermocycler with the following settings as displayed in Tab.14.

Tab.14 Reverse transcription program for cDNA synthesis

Step	Temperature [°C]	Time [min]	Cycles
cDNA synthesis	42	30	1
Inactivation	95	2	1
Hold	4	∞	1

After reverse transcription, the cDNA was stored at -20°C. For further analysis of the cDNA, PCR were carried out. The cDNA as well as the primers were first diluted 1:10 in DNAse/RNAse free water. Every PCR was set up according to Tab.15.

Tab.15 PCR mix set up

Component	Volume [µl]
cDNA	2
Forward Primer (1:10 dill.)	1
Reverse Primer (1:10 dill.)	1
REDTaq® ReadyMix™ MM	10
H_2O	6
Total volume	**20**

The following PCR reaction was performed using a Thermocycler with the following parameters as shown in Tab.16.

Tab.16 PCR cycling parameters

Step	Temperature [°C]	Time [min]	Cycles
Initial denaturation	94	2	1
Denaturation	94	1	30
Annealing	60	1	30
Elongation	72	2	30
Final extension	72	5	30
Hold	4	∞	1

All amplified DNA products were evaluated by loading 10 µl of the PCR reaction on an 2% agarose gel stained with ethidium bromide. The gel runed in 1xTAE buffer for 45-60 min at 120 V. At the end, the gel was analyzed by an Intas Gel iX imager.

2.2.14 Quantitative PCR

For quantitative PCR analysis, 2µl of template DNA was pipetted into each well of a 96 well plate. 8µl of Mastermix was added afterwards to each well. The composition of the Mastermix is listed in Table 17. Following that, the plate was spinned down at 3700g for 10 sec and put into the qPCR machine. The qPCR was carried out by StepOne Plus Realtime PCR System from Applied Biosciences.

Tab.17 qPCR mix set up

Component	**Volume [µl]**
cDNA	2
Forward Primer (1:10 dill.)	1
Reverse Primer (1:10 dill.)	1
iTaq Universal SYBR Green Supermix	10
H_2O	6
Total volume	**20**

Table 18 lists the cycling parameters used for each qPCR.

Tab.18 qPCR cycling parameters

Step	**Temperature [°C]**	**Time [min]**	**Cycles**
Initial denaturation	94	2	1
Denaturation	94	1	40
Annealing	60	1	40
Elongation	72	2	40
Final extension	72	5	40
Hold	4	∞	1

2.2.15 Colorimetric MTT cell viability assay

MTT assays were performed on co-culture experiments in 48-well plates. First, 50 µl (in 500 µl total. Vol.) of the MTT reagent (thiazoyl blue tetrazolium bromide) were added to each well of a co-culture experiment as well as to each single culture controls. The plate was then incubated for 4 h at 37°C until brown blue/violet precipitation was visible. Then 500 µl (in 500 µl total. Vol.) of MTT lysis buffer was added to each well to stop the reaction. Following that, the plate was incubated over night at 37°C. On the next day, the plate was incubated on a linear shaker with 140 rpm at room temperature for 30 min. The content of each well was resuspended with a 1000 µl pipette until every precipitate was dissolved. Finally, the plate was measured at a wave length of 565 nm in a Tecan M200 multiplate reader.

2.2.16 Preparation of living cells for flow cytometry analysis

All cells used for FACS analysis were seeded on 6- or 12-well plates to provide a sufficient number of cells for staining. First, all cells were washed 2-3 times with PBS (only monocultures). For all co-culture setups, the media was transferred into a 15 ml falcon tube with pre-warmed appropriate media (DMEM/RPMI complete). Then the cells were detached by using 0,5-0,7 ml Accutase® dissociation enzyme reagent per well and incubated at 37°C for 10-15 min. The reaction was neutralized by transferring the detached cells into the prepared 15 ml falcon tubes from above. Then the cells were centrifuged at 400 g for 5-10 min at room temperature. Further, the cells were washed 2-3 times by resuspending the cell pellet with 1 ml PBS. As last washing step, the cells were resuspended in 1 ml FACS buffer and transferred into 1.5 ml Eppendorf tubes. Furthermore, the cells were centrifuged as before and resuspended in 200 µl FACS buffer. From this point on the cells were blocked with 5 µl FcR block for 10 min at 4°C. Afterwards, further staining with labelled FACS antibodies was carried out. Before staining, 100 µl of unstained sample of each condition was transferred into an additional 1.5 ml Eppendorf tube. Then, 5 µl of fluorescence-labelled antibody was pipetted into each sample for staining except for the unstained controls. The tubes were incubated at 4°C for 30 min in the dark. After staining, all samples were washed 2 times with 500µl PBS and once with 500µl FACS buffer. Finally, the pellet was resuspended in 200 µl of FACS buffer, transferred into a FACS tube and analyzed by a FACS Canto II device. For every sample 20000 events were recorded.

2.2.16.1 Intracellular flow cytometry staining

All cells used for FACS analysis were seeded on 6-well plates to provide a high number of cells for staining. First, all cells were washed 2-3 times with PBS. Then, they were detached using 0,5-0,7 ml Accutase® dissociation enzyme reagent per well and incubation at 37°C for 10-15 min. The reaction was neutralized by transferring the cells from the well into 10 ml of the appropriate media (DMEM/RPMI complete). After transferring, the cells were centrifuged at 400 g for 10 min at room temperature. Then, the cells were again washed 2-3 times with 1 ml PBS and were finally resuspended in 1 ml FACS buffer and transferred into a 1.5 ml Eppendorf tube. Furthermore, the cells were centrifuged as before and resuspended in 180 µl FACS buffer. An equal volume of IC fixation buffer was added and cells were vortexed. The samples were incubated for 10-60 min at RT. Following that, the cells were centrifuged at 400 g for 10 min at room temperature and the supernatant was discarded. Then the cells were resuspended in 1 ml ice cold 90-100% methanol vortexed and incubated for 30 min at 4°C. The cells were centrifuged at 400 g for 10 min at room temperature and the supernatant was discarded. 180 µl FACS buffer was used to resuspend the cells and 90 µl were transferred into separate tubes for unstained control. 5 µl per sample FcR block were added and cells were incubated at 4°C for 10 min. Following blocking, 5 µl directly conjugated intracellular antibodies were pipetted into each sample for staining except for the unstained controls. The tubes were incubated at 4°C for 30 min in the dark. 1 ml FACS buffer was added and cells were centrifuged at 400 g for 10 min at room temperature. Finally, the pellet was resuspended in 200 µl of FACS buffer, transferred to a FACS tube and analyzed by a FACS Canto II device. For every sample 10000 events were recorded.

2.2.16.2 Live/Dead flow cytometry analysis

The FACS sample preparation was carried out as described in section 2.2.16. Following the blocking with FcR block for 10 min at 4°C, the samples were staining with labelled FACS antibodies. Before staining, 100 µl of unstained sample of each condition was transferred into an additional 1.5 ml Eppendorf tube. For co-culture labeling, anti-EpCAM antibody was used against CRC cells, while anti-CD11b antibody was used to detect macrophage like cells. 2,5µl of EpCAM/CD11b antibody was used for staining 10^6 cells. Each sample was stained except for the unstained controls. The tubes were incubated at 4°C for 30 min in the dark. After staining, all samples were

washed 2 times with 500µl PBS and once with 500µl FACS buffer. Then the pellet was resuspended in 500 µl of FACS buffer. Following that, the samples were transferred into FACS tubes and washed two times with Cell Wash and centrifuged at 400g for 5 min at RT. The cells were resuspended in 100µl Annexin Binding Buffer together with 2,5µl Annexin V per sample. For live/dead staining, all samples were incubated for 15 min in the dark at RT. Following the incubation, the cells were washed once with cell wash, centrifuged again as before and resuspended in Annexin Binding Buffer with SytoxBlue (1:2000) for necrosis staining. Dead cell exclusion was achieved by addition of SytoxBlue 7-AAD dye. Finally, all samples were analyzed by a FACS Canto II device. For every sample 20000 events were recorded and analysis was done using FACS Diva and FlowJo® softwares. Figure 10 depicts the gating which was used for analyzing co-culture setups.

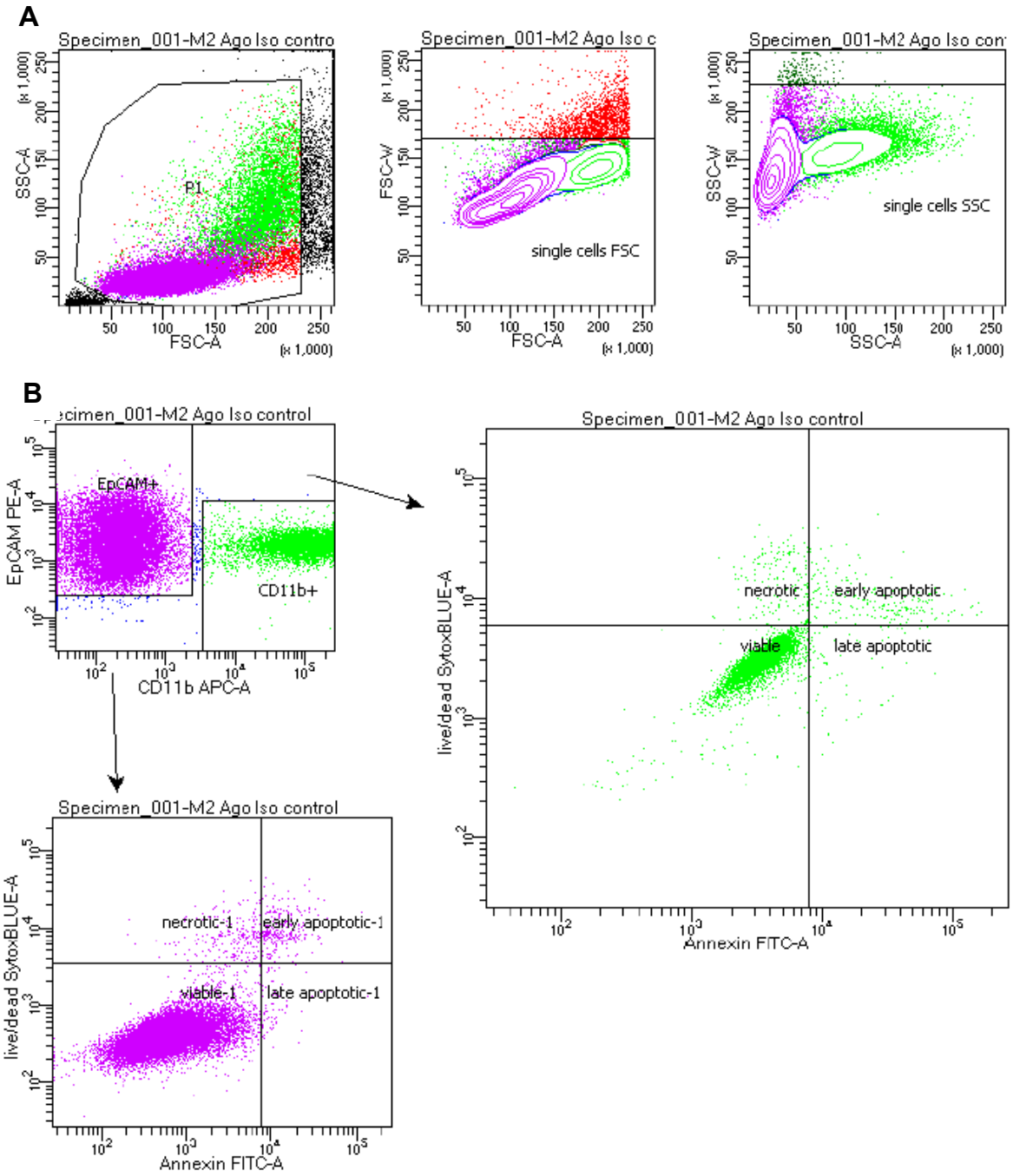

Fig.10 Gating strategy example for live/dead FACS analysis of co-cultures
The gate of the co-culture main population was set in order to analyze single cell events (A). Furthermore, all single cell events were analyzed by separating EpCAM positive cells from CD11b positive cells which was conducted by staining with specifically labeled antibodies for tumor cells (EpCAM) and macrophages (CD11b). To quantify apoptosis, necrosis and viability, each population of EpCAM and CD11b positive gated cells were analyzed via quadrant statistic analysis (B).

2.2.17 Immunofluorescence staining and microscopy

For immunofluorescence, cells were seeded on sterile glass cover slips which were prepared in 6-well plates. After cells attached to the glass plate, the media was aspirated and cells were washed once with PBS before adding 1 ml 4% PFA (diluted with PBS) and left 20 min at RT for fixation. After fixation, the cells were washed with once with PBS for 5 min. Following that, cells were permeabilized for 10 min at RT by adding 0,5-1 ml permeabilization buffer. After permeabilization, the cells were washed three times with PBS each time for 5 min. Furthermore, blocking with 100% FCS was performed for 60 min at RT. Post blocking, 1-2 ml primary antibody (1:1000) diluted in antibody dilution buffer was added to the cells and incubated over night at 4°C in a humid chamber box. All following steps were carried out in the dark. The next day, the cells were washed three times with PBS + 0,1% TWEEN. Following that, fluorescently labeled secondary antibody (1:1000) was diluted in antibody dilution buffer and added to the cells which were then incubated for 1h at RT in the humid chamber. After secondary antibody incubation, the cells were washed three times with PBS + 0,1% TWEEN + phalloidin dye (1:1000) for 5 min. Then, the cells were washed again three times with PBS + 0,1% TWEEN and cover slips were removed with forceps, dryed carefully on clean paper tissue and placed upside down with one drop of ProLong™ Gold anti fade reagent with DAPI on a microscopy glass slide. Finally, the samples were stored at 4°C in the dark until fluorescence microscopy analysis.

2.2.18 Chromatin Immunoprecipitation

For chromatin isolation and immunoprecipitation, the Pierce Agarose ChIP Kit was used with slight modifications. Firstly, 6*10^6 cells were seeded on a 10 cm petri dish. The cells were treated with the REVERBα Agonist or Antagonist or left untreated to check for REVERBα binding to the *PVR*-promotor. Table 19 lists the prepared buffers for this ChIP kit.

Tab. 19 Pierce agarose ChIP Kit buffers for one reaction

ChIP Buffer	Components
Lysis Buffer 1	1 µl HALT Cocktail, 100 µl Membrane Extraction Buffer
Lysis Buffer 2	0.5 µl HALT Cocktail, 50 µl Nuclear Extraction Buffer
MNase Digestion Buffer Working Solution	0.1 µl of 1 M DTT, 100 µl MNase Digestion Buffer, (Micrococcal dependent on number of reactions processed!)
1x IP Dilution Buffer	100 µl IP Dilution/Wash Buffer (5x), 5 µl HALT Cocktail, 395 µl nuclease-free water
IP Wash Buffer 1	0.1 ml IP Dilution Buffer/Wash Buffer (5x), 0.4 ml nuclease-free water
IP Wash Buffer 2	0.2 ml IP Dilution Buffer/Wash Buffer (5x), 70 µl Sodium Chloride (5 M), 730 µl nuclease-free water
IP Wash Buffer 3	0.1 ml IP Wash Buffer 3 (5x), 0.4 ml nuclease-free water
1x IP Elution BUffer	75 µl pre-warmed IP Elution Buffer (2x), 75 µl nuclease-free water

2.2.18.1 Crosslinking and cell pellet isolation

For higher yield, three plates with the same condition were pooled. To each petri dish 1,6ml 16% of formaldehyde was added to get a final concentration of 1%. The dish was mixed well by gently swirling the dish and incubating for 10 min at RT. After the incubation to stop the process of fixation 1,16 ml 10x glycerine solution was added to the dish, gently swirled and incubated for 5 min at RT. Following that, the media was discarded and the cells were washed two times with one media volume (10 ml) ice-cold PBS. Furthermore, 100µl HALT Cocktail were diluted to 10 ml of ice-cold PBS and 1 ml was pipetted to the cells. Then, the cells were detached by scraping off and transferring them into a 1.5 ml Eppendorf tube. Finally, the cells were then centrifuged

at 3000 g for 5 min at RT and the supernatant was removed. Each sample was further processed immediately after crosslinking.

2.2.18.2 Lysis and MNase digestion

If cells were frozen before, they were thawn on ice which was never done due to lower quality of crosslinked chromatin. To continue, 100µl Lysis Buffer 1 containing protease inhibitors were added to the cell pellet and pipetted up and down to break up the cell pellet. The tube was vortexed for 15 sec. and incubated for 10 min on ice. After incubation, the tube was centrifuged at 9000 g for 3 min and the supernatant was discarded. Following that, the pellet was resuspended in 330µl MNase Digestion Buffer Working Solution and 0,75µl Micrococcal Nuclease (ChIP Grade) (10 U/µl) were added. This mixture was incubated on ice for 5 min and centrifuged at 9000 g for 5 min afterwards to recover the nuclei. After removing the supernatant, the nuclei were resuspended in 150µl Lysis Buffer 2 containing protease/phosphatase inhibitors and incubated on ice for 15 min. Each tube was vortexed every 5 min for 15 sec.. Finally, the samples were centrifuged at 9000 g for 5 min and the supernatant containing the digested chromatin was transferred to a new 1.5 ml Eppendorf tube. 5µl of the supernatant was transferred to extra tubes as 10% total input sample and stored at -80°C. The samples were frozen at -80°C and processed the next day.

2.2.18.3 Immunoprecipitation and pre-clearing

For each sample the DNA concentration was described in section 2.2.6. To each 45µl of supernatant 450µl of 1x IP Dilution Buffer were added. For pre-clearing 20µl of Agarose Beads were added to each sample and incubated overnight on a rotator at 4°C. After pre-clearing, the samples were centrifuged at 3000g for 2 min and the supernatant was transferred into a new 1.5 ml Eppendorf tube. Following that, for each IP the sample with highest DNA concentration was used as positive control, and a random sample was chosen as negative control. 7.5 µg antibody were used for target specific IPs. Every IP was pipetted on a plugged spin column and incubated over night at 4°C on a rotator. The next day, 20 ml of ChIP Grade Protein A/G Plus Agarose Beads were added to each sample and incubated for 1 h at 4°C on the rotator. After incubation, the columns were centrifuged at 3000 g for 1 min and the flow through was discarded. 500µl of IP Wash Buffer 1 was added to each column and incubated for 5 min at 4°C on the rotator. The tubes were again centrifuged as before and washed with

IP Wash Buffer 2. This process was repeated twice before finally washing once with IP Wash Buffer 3. Finally, the residual Wash Buffer was removed by centrifuging at 3000 g for 1 min.

2.2.18.4 Elution and DNA recovery

150µl 1x IP Elution Buffer were added to the washed resin and incubated at 65°C for 30 min at 500 rpm on a thermomixer. Every 10 min the columns were flicked to ensure re-suspension. During incubation, 1.5 ml Eppendorf tubes were prepared for each IP containing 6µl of 5M NaCl and 2µl of 20mg/ml Proteinase K. Following that, the total input sample was thawn, mixed with 150 µl of Elution Buffer and transferred into the prepared tubes with NaCl and Protease K. Furthermore, after 30 min incubation the columns were put into the prepared Eppendorf tubes containing NaCl and Proteinase K and centrifuged at 6000 g for 1 min. The columns were discarded and all IP and total Input samples were incubated at 65°C for 1,5h on a heating block.

For DNA Recovery 600 µl of DNA Binding Buffer was added to each eluted IP and total Input sample. After that, 500 µl of each sample was pipetted directly onto a DNA clean-up column. All samples were centrifuged at 10000 g for 1 min, discarding the flow through afterwards. The remaining sample was load onto the column and again centrifuged as before. Following that, the DNA was washed by adding 600 µl DNA Column Wash Buffer to each column. Each column was then centrifuged as above with discarding the flow through afterwards. A follow up centrifugation step of 2 min at 10000 g was performed to dry the column membrane. For DNA Elution each column was transferred into a new 1.5 ml Eppendorf tube. 50 µl of DNA Column Elution Solution were pipetted to the center of each column. Finally, after centrifugation at 10000 g for 1 min, DNA concentration was measured by spectrophotometer as described in section 2.2.6. Following DNA Recovery qPCR was performed for final results.

2.2.19 Luciferase assay

For luciferase assays, luciferase dual-luciferase reporter assay kit was used. Firstly, cells were seeded in 6-well plates. After stimulation, the media was removed and cells were washed three times with PBS. 150µl passive lysis buffer was added into each well and the plate was shaken at 365 rpm for 10 min RT. Following that, the cells were scrapped, transferred into a 1.5 ml Eppendorf tube and centrifuged at full speed in a microcentrifuge for 15 min at 4°C. The supernatant was then transferred into a new 1.5 ml Eppendorf tube and protein concentration was measured as described in section 2.2.6. Furthermore, luciferase activity was measured separately by transferring 10µl of sample into a well of a 96 well plate (white chimney). 35 µl of luciferase substrate reagent was added to each well before measuring with a multiplate reader at 550 nm. Finally, the ratio of luciferase counts and protein concentration was calculated.

2.2.20 Phagocytosis assay

For phagocytosis assay the fluorometric phagocytosis assay kit from ATT Bioquest® was used. The cells were seeded into 6 well plates and stimulated or treated with small molecule drugs. Following the stimulation or treatment, 12.5µl Protonex™ 600 Red-Latex beads conjugate solution (12x) were added into each well of the 6 well plate. The plate was then incubated for 4h at 37°C. After incubation, 12.5µl CytoTrace™ Green working solution (12x) was added into each well and again incubated at 37°C for a minimum time of 30 min. Following the last incubation, the cells were washed once with PBS and the cells were observed with the ZEISS Axio Observer microscope. For detecting phagocytosis Texas Red filter (Ex/Em = 570/600 nm) was used, while detecting the CytoTrace™ green in cells with the FITC filter (Ex/Em = 490/525 nm).

2.2.21 Efferocytosis assay

For the efferocytosis assay experiments, HT29 cancer cells were firstly labeled with cell tracing dye (CFSE). To start HT29 cancer cells labeling, 1µl of CellTrace™ stock solution diluted in DMSO was added to each ml of cells in suspension in PBS (10^6 cells/ml). The solution was incubated for 20 min at 37°C protected from light. Following that, to stop the reaction, five times of the original staining volume were added to cells, mixed and incubated before centrifuging at 400g for 5 min at RT. The pellet was resuspended into fresh pre-warmed complete media and cells were counted for seeding. Following that, the desired number of cells were seeded for e.g. co-culture

experiments with macrophages. Finally, the co-culture assay was analyzed via FACS. Sample preparation was carried out as described in section 2.2.16.

2.2.22 Live cell imaging

First, all bright field images from organoids, cells and co-cultures were documented by a Leica DMIRB Inverted Contrast Microscope or by a Zeiss AXIO Observer Z1. All Fluorescence images were taken with the Zeiss AXIO Observer Z1. In general, all images were taken from living cells and PDOs at room temperature under sterile conditions.

3. Results

3.1 Characterization of REVERBα expression and function

3.1.1 REVERBα expression in THP1 and PBMC-derived macrophages

The first step to understand the role of REVERBα in CRC was to characterize its expression and function in THP1- and PBMC-derived human macrophages. RT-qPCR analysis of RNA which was collected from THP1- and PBMC-derived macrophages differentiated and polarized into M(IFNγ/LPS) pro- and M(IL4/IL13) anti-inflammatory macrophages revealed the cyclic expression of *REVERBα* and *PVR-C* over 24h as depicted in Fig.11. Both cell types exhibited low expression of *REVERBα* during day time and high expression at night time, in accordance with (Cho et. al., 2012).

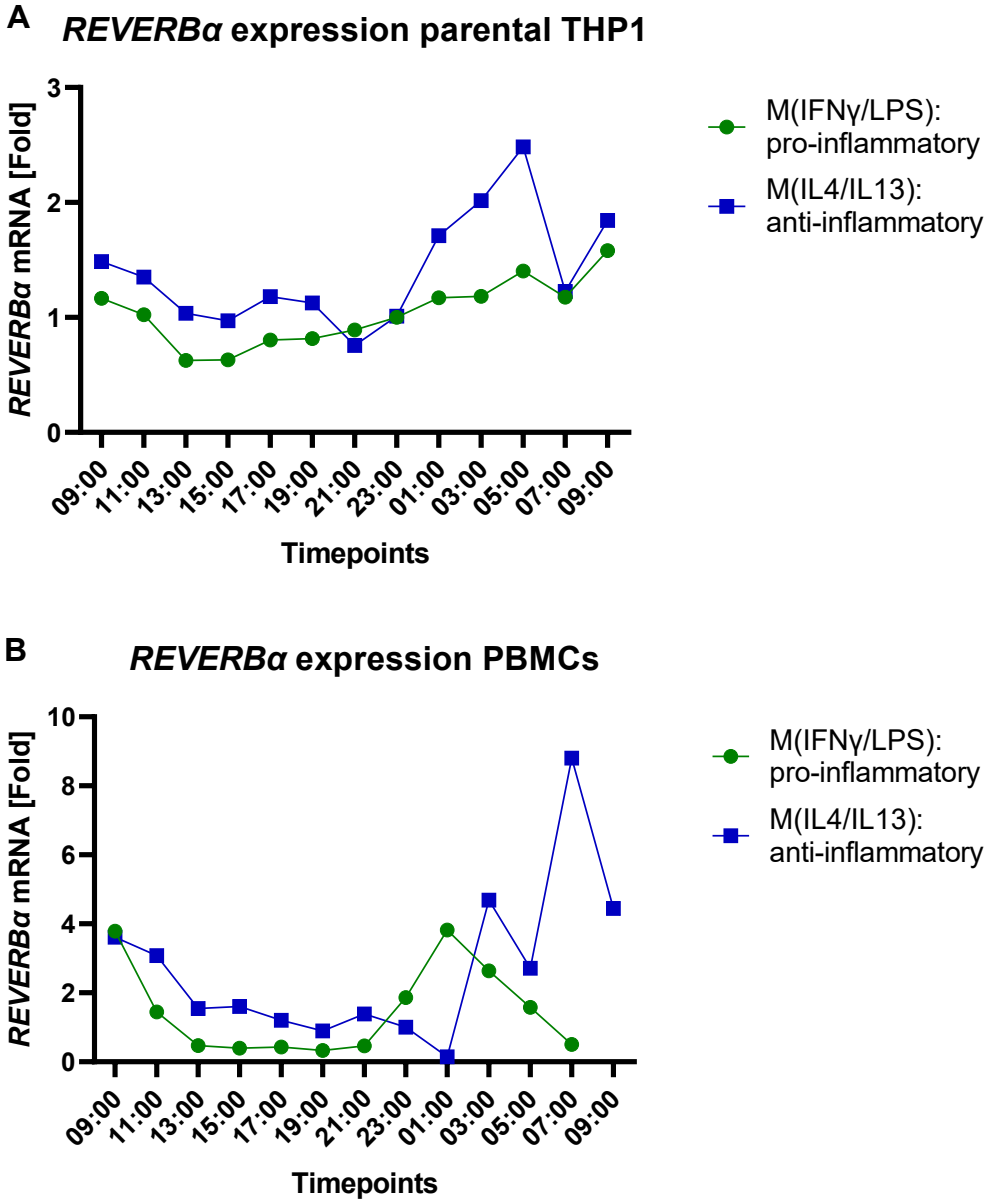

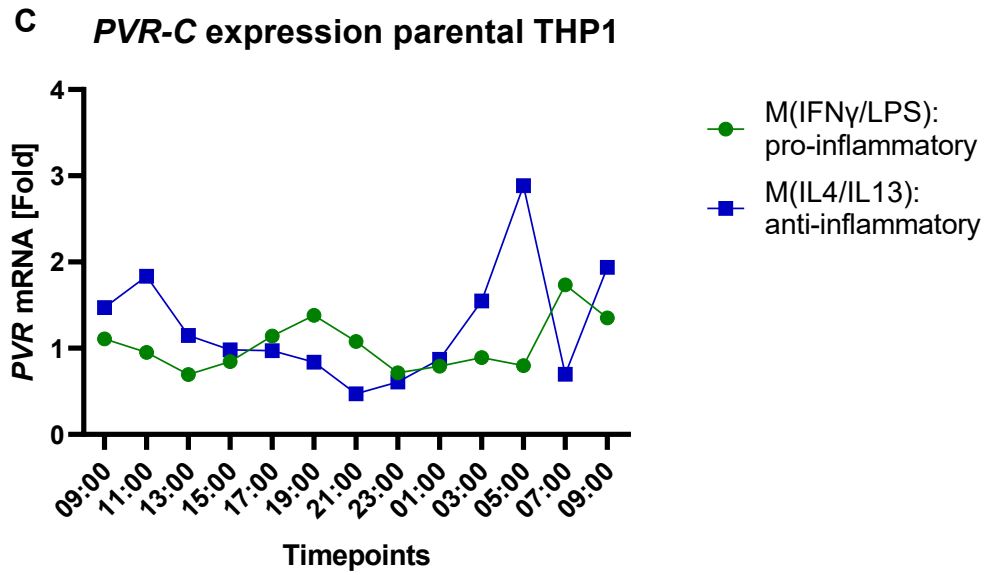

Fig.11 Expression of *REVERBα* & *PVR-C* mRNA in THP1- and PBMC-derived macrophages (RT-qPCR). RT-PCR analysis of RNA isolated from polarized THP1- and PBMC-derived macrophages was performed with 40x cycles, 92°C melting temp., 60°C annealing temp. and 75°C extending temp. (A) *REVERBα* is cyclically expressed in M(IFNγ/LPS) pro- and M(IL4/IL13) anti-inflammatory THP1- and (B) PBMC-derived macrophages over a time period of 24h. (C) *PVR-C* is cyclically expressed in M(IFNγ/LPS) pro- and M(IL4/IL13) anti-inflammatory THP1-derived macrophages. Monocytes were isolated via MACS from PBMCs originating from healthy donor blood. A representative experiment is shown (N=1 per cell type).

The expression of the *PVR* and *REVERBα* genes in PBMC-derived primary macrophages is depicted in the following Fig.12. Each macrophage type expressed a comparable amount of *PVR* and *REVERBα* mRNA.

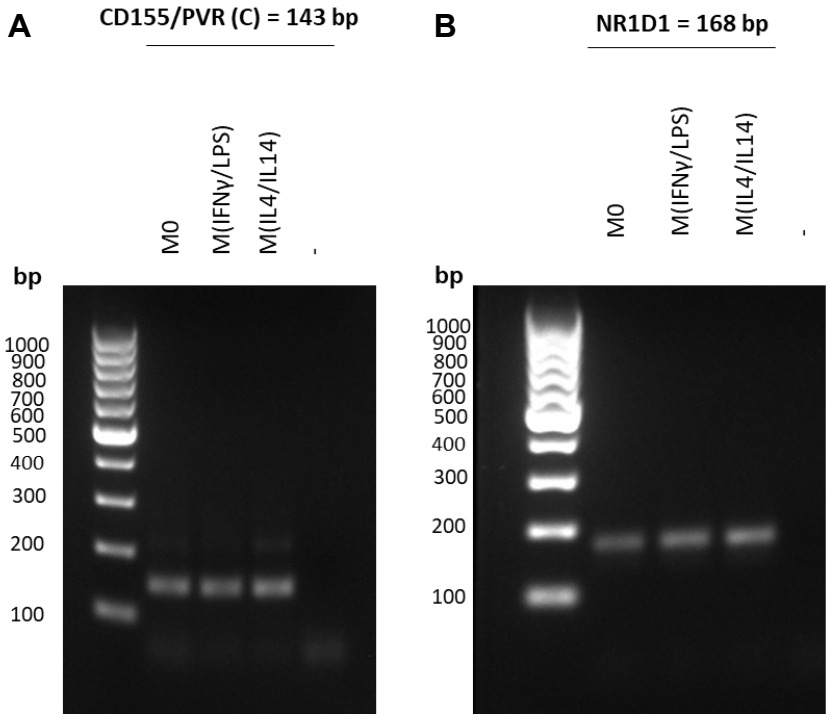

Fig.12 Expression of *PVR-C* and *REVERBα* mRNAs in PBMC-derived primary macrophages. (A) Amplicons of *PVR-C* with a length of 143 bp and (B) *REVERBα* (*NR1D1*) with a length of 168 bp. RT-PCR analysis of RNA isolated from polarized PBMC-derived macrophages was performed with 40x cycles, 92°C melting temp., 60°C annealing temp. and 75°C extending temp. Monocytes were isolated via MACS from PBMCs originating from healthy donor blood. As DNA amplicon size reference, the GeneRuler 100 bp DNA Ladder 50µg was used. A representative experiment is shown (N=2 per cell type).

3.1.2 Binding of REVERBα to the human *PVR* Promoter

To investigate the interaction of REVERBα with the human *PVR* gene promotor chromatin immunoprecipitation (ChIP) was conducted. Consistently, ChIP experiments, as shown in Fig.13, demonstrated the binding of REVERBα protein to the promotor of the human *PVR* gene, indicating the interaction of REVERBα with upstream gene elements of the *PVR* gene.

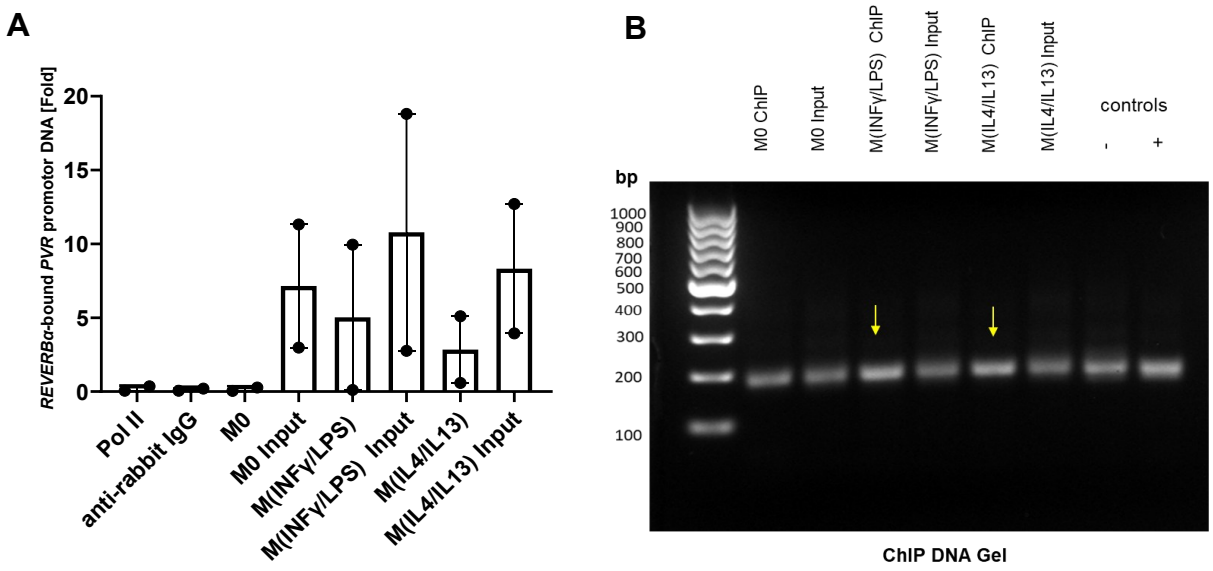

Fig.13 Interaction of REVERBα protein with the human *PVR* gene promotor in THP1-derived macrophages detected by ChIP. qPCR with genomic DNA samples, enriched by ChIP with REVERBα Ab (polyclonal 14506-1-AP), was performed with 40x cycles, 92°C melting temp., 60°C annealing temp. and 75°C extending temp. (A) Genomic qPCR results of DNA from M(IFNγ/LPS) pro- and M(IL4/IL13) anti-inflammatory macrophages. (n.s., N=2 independent experiments, mean ± SEM). (B) Agarose gel analysis of genomic qPCR ChIP samples revealing intensities of amplicon expression. The yellow arrows indicate the bands with highest intensity. As DNA size reference the GeneRuler 100 bp DNA Ladder 50µg was used. A representative gel is shown.

3.2 Detection of REVERBα in parental and CRISPR/Cas9-modified THP1-derived macrophages

To detect REVERBα in CRISPR/Cas9-modified THP1 cell clones, Western blot and immunofluorescence microscopy was performed. Ab staining of CRISPR/Cas9-modified THP1 macrophages revealed the presence of REVERBα in clones transfected with sgRNA targeting the C-terminal side of the REVERBα coding sequence (CDS) or the empty vector control (backbone, BB). The clone which received the sgRNA against the N-terminus of the CDS exhibited lower expression of REVERBα as compared to the other two clones (Fig.14 (A)). Western blot analysis, as shown in Fig.15, confirmed expression of REVERBα protein in THP1-derived macrophages (Fig.15 (A)), in HEK293T cells (Fig.15 (B)) as well as in PBMC-derived primary macrophages (Fig. 15 (C)). Overexpression of REVERBα in HEK293T cells, as shown in Fig.15 (B), served as control, depicting a strong expression.

N-terminal and the C-terminal CRISPR/Cas9 modifications, as shown in Western blots in Fig.16, revealed the absence of isoforms with post-translational modifications compared to the BB control with stronger total band intensities, quantified by optical densitometry.

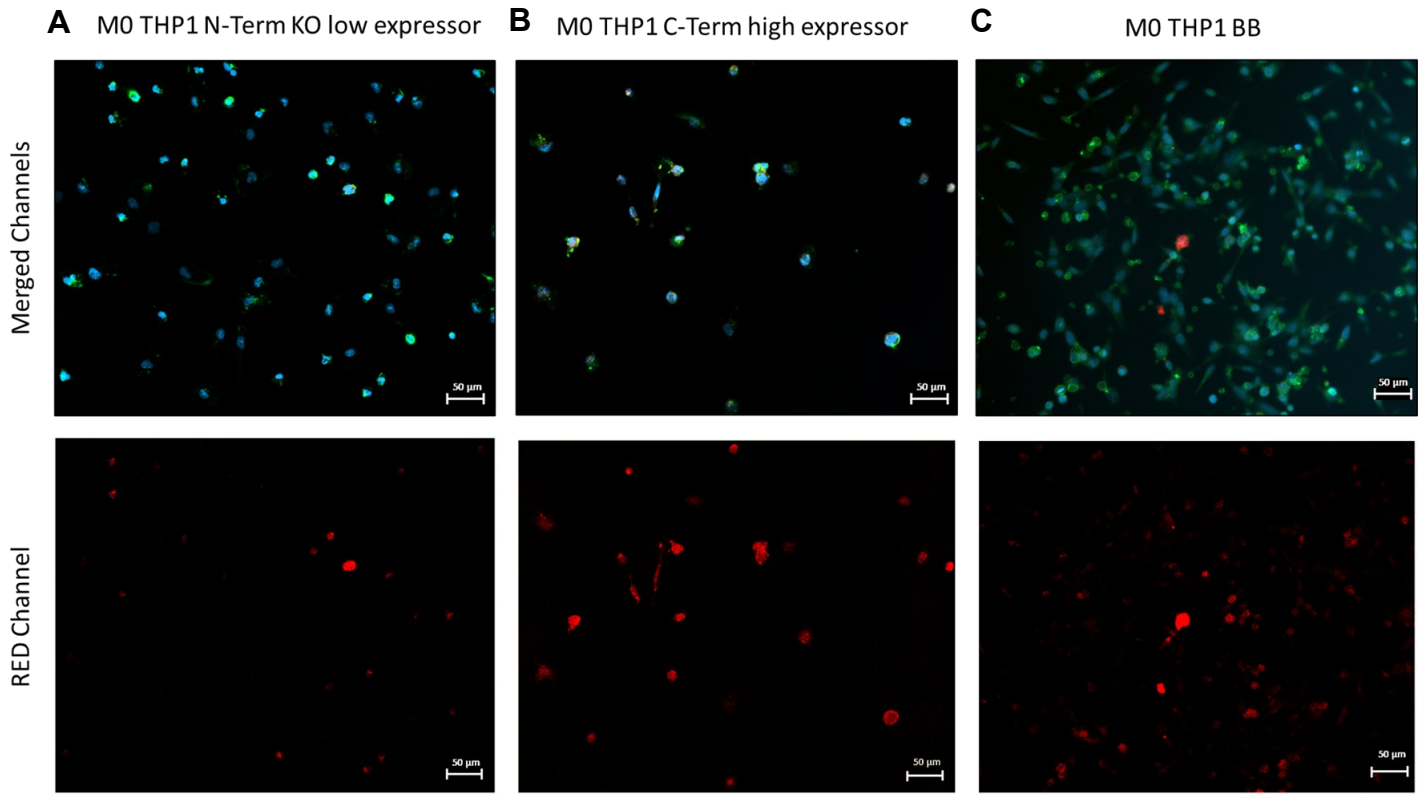

Fig.14 Immunofluorescence imaging of REVERBα in M0 CRISPR/Cas9-modified THP1-derived macrophages. PMA-differentiated, unpolarized (M0) THP1-derived macrophage clones with: (A) N-Terminal sgRNA "low expressor", (B) C-Terminal sgRNA "high expressor" and (C) BB (backbone, empty vector control) were stained with REVERBα Ab (PA5-29865) (red channel). Cell nuclei were stained with DAPI (blue channel), and the actin cytoskeleton was stained with phalloidin (green channel). Images were acquired at a 40x magnification, scale bar = 50 µm.

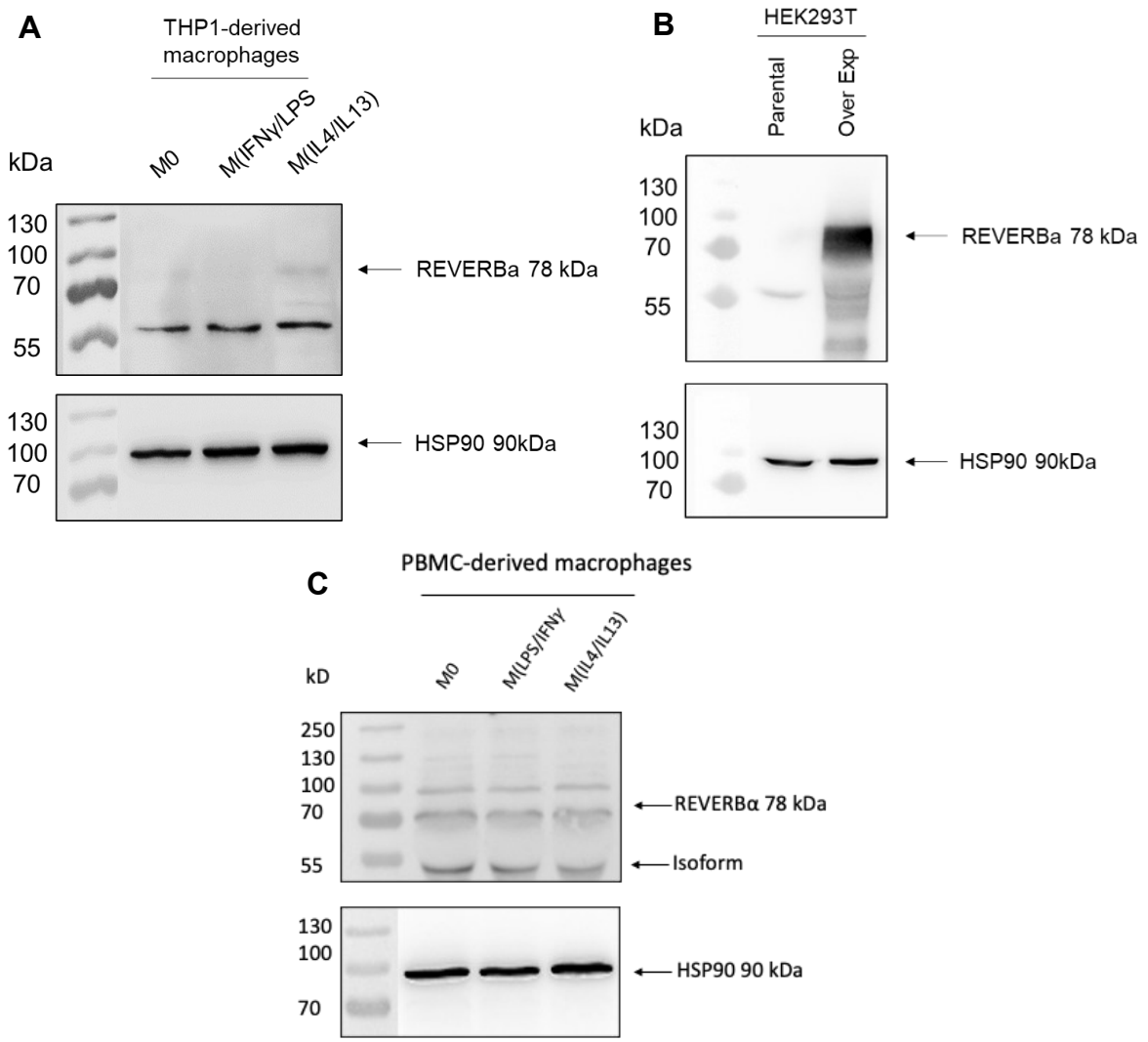

Fig.15 Detection of REVERBα in THP1-derived macrophages and HEK293T (non-cancer control) cells. Western blot analysis of REVERBα (expected size 78 kDa) with Ab ((A)/(B) REVERBα (E1Y6D) mAb #13418 (cross-reaction with unidentified protein at 60 kDa), (C) REVERBα (polyclonal 14506-1-AP) was done with total cell protein lysates from (A) THP1-derived macrophages, (B) parental HEK293T cells transfected with a REVERBα expression plasmid as well as (C) PBMC-derived primary macrophages. 40 µg of protein were loaded per lane on a 10% gel for SDS-PAGE, HSP90 (90 kDa) served as control. As a protein marker the Roti Mark Tricolor 10-245 kDa was used.

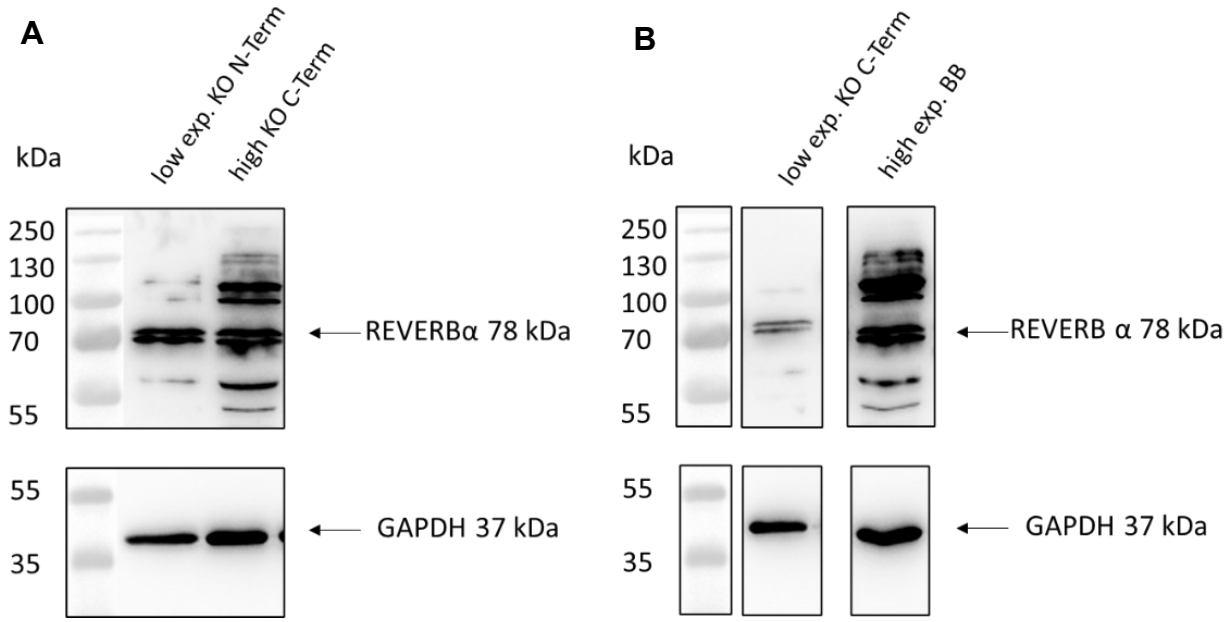

Fig.16 Detection of REVERBα in CRISPR/Cas9-modified THP1-derived macrophages. Western blot analysis of REVERBα (78 kDa, REVERBα polyclonal 14506-1-AP) was done with total cell protein lysates from THP1-derived CRISPR/Cas9 cell clones with modified *REVERBα* gene. Parental THP1 cells were transfected via electroporation with CRISPR/Cas9 vectors each carrying a different sgRNA. (A) sgRNA targeting the N-terminus (low expressor) and sgRNA targeting the C-terminus (high expressor) of the *REVERBα* gene. (B) An empty vector (BB, backbone) was used as control. 40 µg of protein were loaded per sample on a 10% gel for SDS-PAGE. HSP90 (90 kDa) served as control. As a protein marker the Roti Mark Tricolor 10-245 kDa was used.

In addition to the detection of REVERBα via Western blot, intracellular flow cytometry (FC) analysis was utilized to investigate the intracellular expression of REVERBα in parental and CRISPR/Cas9-modified THP1-derived macrophages. As depicted in Fig.17 and Fig.18, REVERBα was shown to be present in both parental and CRISPR/Cas9-modified PMA-differentiated (M0) THP1-derived macrophages.

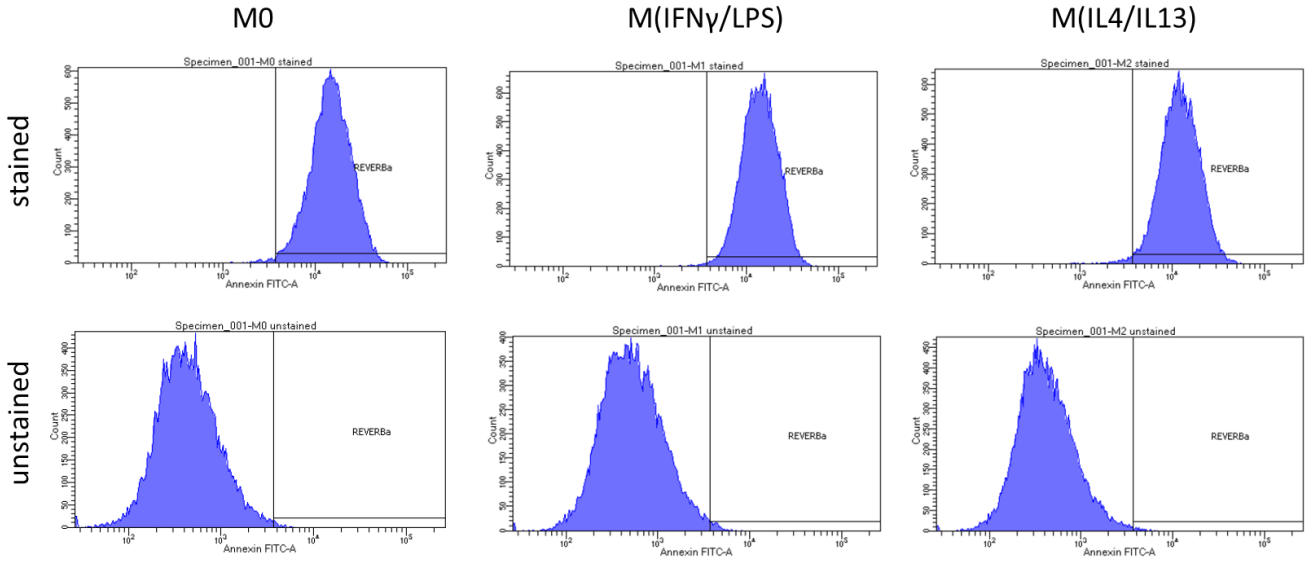

Fig.17 Intracellular flow cytometry (FC) detection of REVERBα in parental THP1 macrophages THP1 cells were differentiated with PMA to M0 macrophages followed by polarisation to M(INFγ/LPS) pro- and M(IL4/IL13) anti-inflammatory macrophages, followed by fixation and staining for intracellular REVERBα (Ab, EPR10376). The confidence interval was set to 0.5%, 10000 events were recorded in total. The percentage of positive cells is shown in the histograms compared to the background signal from unstained control cells (vertical gate line). Representative data are shown (n=1). Cells were analyzed on a BD Canto FACS device (Flow Core UMM).

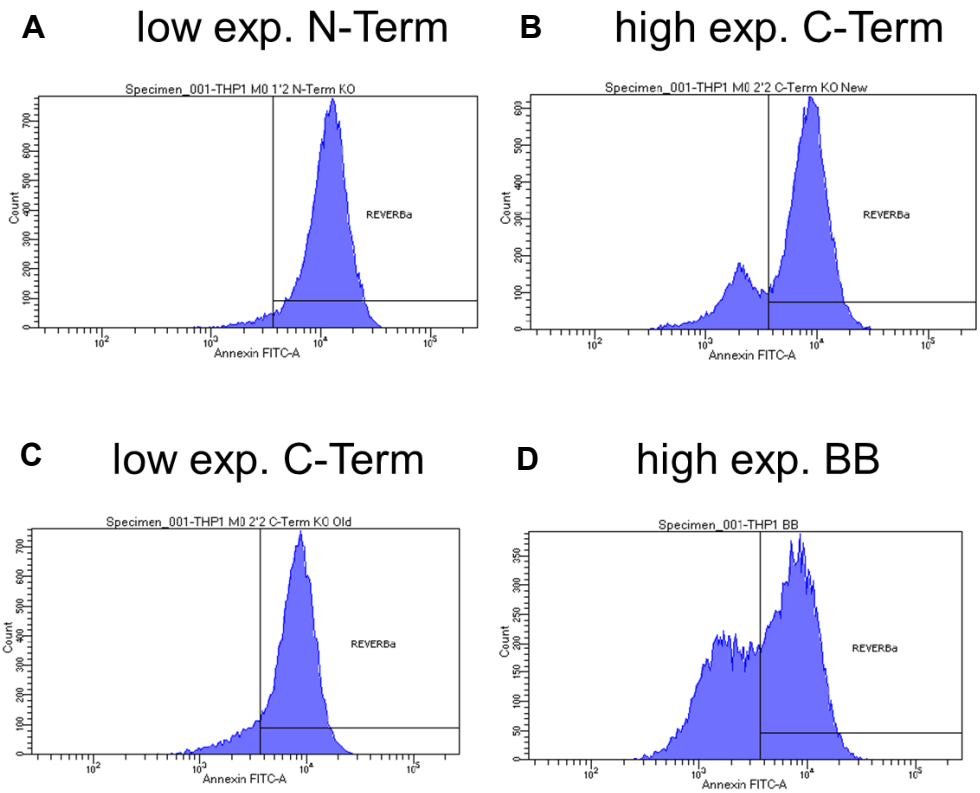

Fig.18 Intracellular FC detection of REVERBα in CRISPR/Cas9-modified M0 THP1-derived macrophages THP1 cells were differentiated with PMA to M0 macrophages followed by fixation and staining for intracellular REVERBα (Ab, EPR10376). Results from FC are showing the presence of REVERBα protein in the nucleus in (A) N-Terminal modified THP1 cells, (B) C-Terminal modified THP1 cells with high REVERBα expression, (C) C-Terminal modification of REVERBα gene with low expression and (D) the empty vector (BB, backbone) control. The confidence interval was set to 0.5%, 10000 events were recorded in total. The percentage of positive cells is shown in the histograms compared to the background signal from unstained control cells (vertical gate line). Representative data are shown (n=2 independent experiments). Cells were analyzed on a BD Canto FACS device (Flow Core UMM).

3.3 Modulation of REVERBα expression and function

To understand the functional role of REVERBα, ChIP experiments were conducted as before, to investigate the binding of the transcription factor to the *PVR* promotor. The binding of REVERBα to the *PVR* promoter was predicted *in-silico* by using Alibaba (Transfac) version 2.1. Consistently, the ChIP experiments confirmed the binding of REVERBα protein to the human *PVR* promotor in M0 THP1-derived macrophages as shown previously. Notably, the treatment of cells with SR9009 agonist caused a reduction of REVERBα binding to the *PVR* promotor, whereas the treatment with

SR8278 antagonist resulted in the opposite effect, an increased binding, as depicted in Fig.19. These experiments revealed a significant difference in REVERBα-binding to the human *PVR* gene promotor after treating THP1 cells with REVERBα-ligands. The here observed efficacy of REVERBα-ligands underscores the drugability and potential therapeutic modulation of REVERBα function, as described by Uriz-Huarte et. al., 2020.

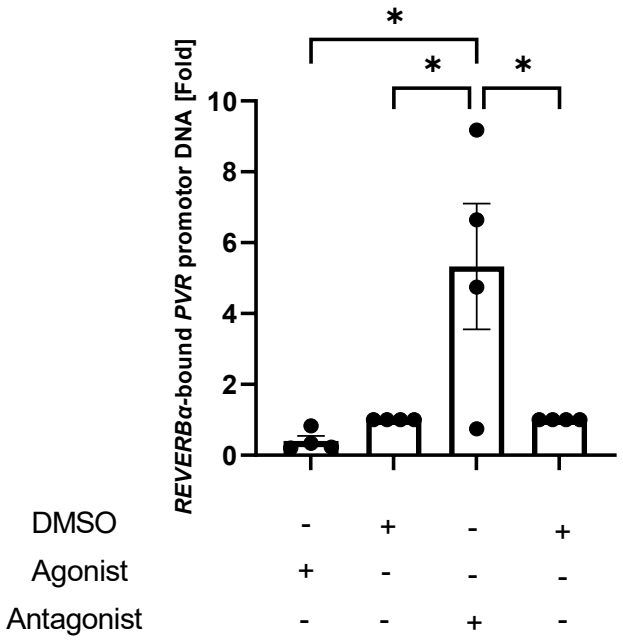

Fig.19 Detection of REVERBα binding to the human *PVR* gene promotor in M0 THP1-derived macrophages after REVERBα ligand treatment by ChIP. Parental THP1 cells were differentiated with PMA to M0 macrophages and treated with vehicle (DMSO), REVERBα SR9009 agonist (1 µM) or SR8278 antagonist (0,67 µM) for 3 days. RT-qPCR results of DNA immunoprecipitated by REVERBα Ab (polyclonal 14506-1-AP). Ct-values were calculated according to the ΔΔCT method, -fold changes normalized to DMSO (= set to 1) as reference and expressed as the ratio fold bound/input. Significances were calculated using two-way ANOVA with Tukey´s multiple comparisons test (*p<0.05, N=4 independent experiments, mean ± SEM).

To further investigate the effect of REVERBα ligands on the *PVR* gene expression, THP1-derived macrophages (M0, M(IFNγ/LPS), M(IL4/IL13)) were treated with REVERBα SR9009 agonist or SR8278 antagonist, respectively. A significant difference of *PVR* mRNA expression (Fig.20) was evident in M0 and M(IL4/IL13) macrophages upon treating with REVERBα agonist and antagonist.

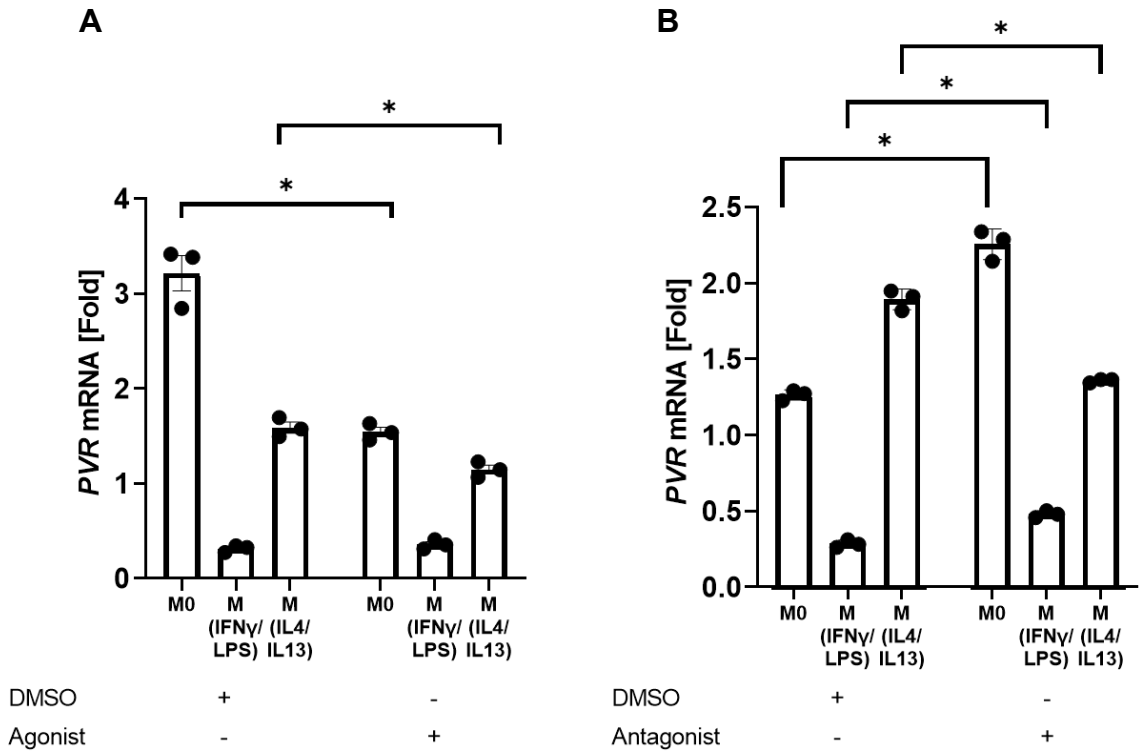

Fig.20 Reciproal expression of *PVR* mRNA in THP1-derived macrophages by REVERBα ligands. Cells were treated with vehicle (DMSO), REVERBα agonist (1 µM) (A) or antagonist (0,67 µM) (B) for 24 h. RT-qPCR analysis of RNA isolated from treated M0, M(IFNγ/LPS) pro- and M(IL4/IL13) anti-inflammatory THP1-derived macrophages was performed with 40x cycles, 92°C melting temp., 60°C annealing temp. and 75°C extension temp. Significances were calculated using two-way ANOVA with Tukey´s multiple comparisons test (*p<0.05, N=3 independent experiments, mean ± SEM).

Similar effects of reciprocal *PVR* gene regulation after treatment with REVERBα agonist and antagonist were recorded in cancer cell lines using *PVR*-promoter driven luciferase reporter gene activity assays as depicted in Fig.21.

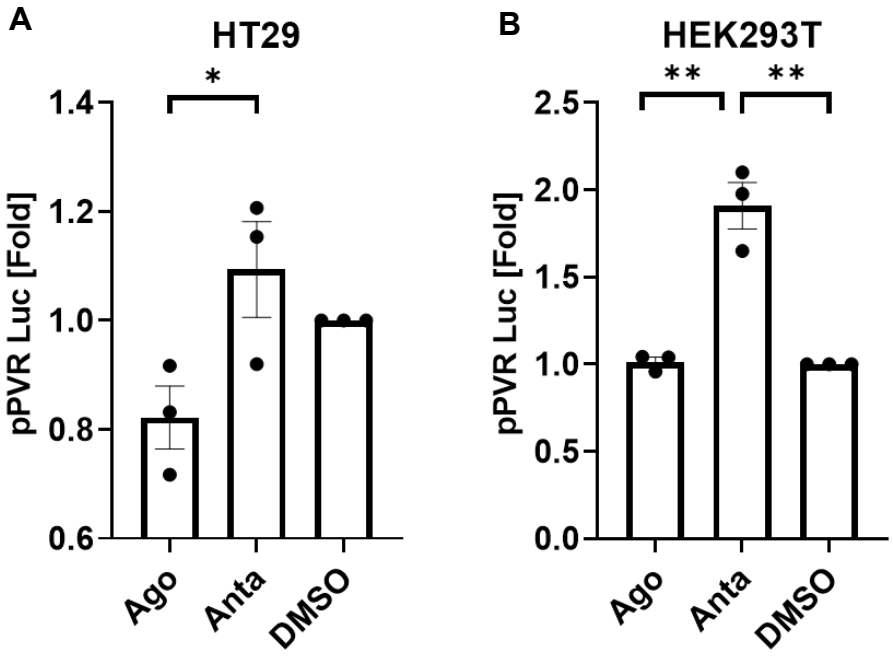

Fig.21 *PVR* promotor activity in parental HT29 and HEK293T cells upon treatment with REVERBα ligand. Human CRC cell line HT29 and non-cancer control (HEK293T) were transfected with luciferase reporter gene plasmids harboring the human *PVR* promoter. Transfected cells were then treated with vehicle (DMSO), REVERBα agonist (1 µM) or antagonist (0,67 µM) for 48h. Analysis of luciferase activity in transfected (A) parental HT29 and (B) parental HEK293T cells was conducted by measuring the emitted wavelength at 550 nm after adding luciferase substrate. (A) and (B) Significances were calculated using two-way ANOVA with Tukey´s multiple comparisons test (*p<0.05, N=3 independent experiments, mean ± SEM).

In addition to its role as a regulator of immune checkpoint genes like *PVR*, REVERBα impacts other immune-relevant genes in macrophages. Fig.22 shows the expression of selected cytokines and immune-relevant factors including IL1b, IL10 and TLR4 in CRISPR/Cas9-modified THP1-derived macrophages. Elevated expression of IL10 and IL1b upon CRISPR/Cas9-modification of REVERBα was stated.

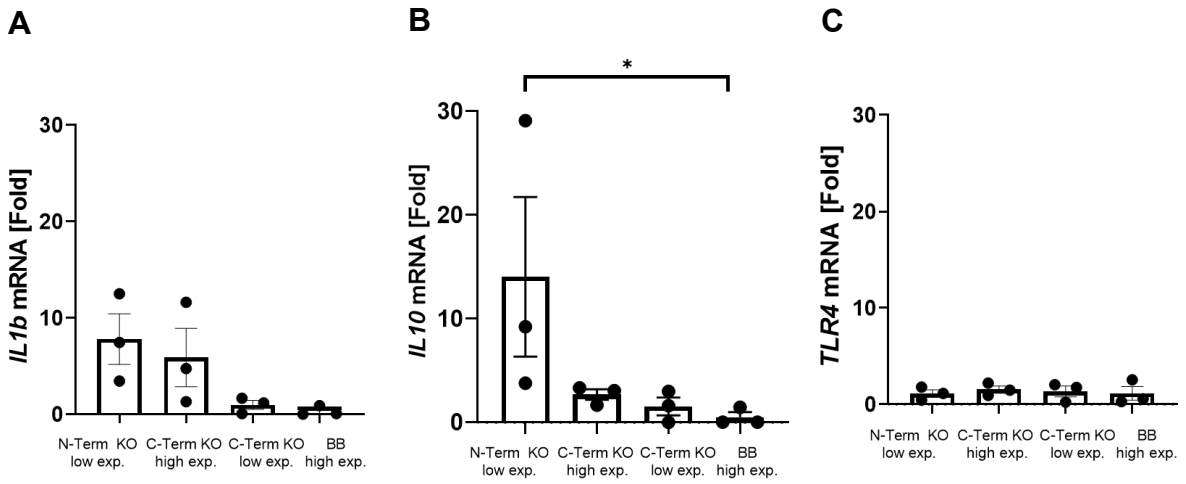

Fig.22 Expression of *IL1b*, *IL10* and *TLR4* mRNA in THP1-derived M0 macrophages with CRISPR/Cas9-modified REVERBα. RT-qPCR analysis of total mRNA was performed with 40x cycles, 92°C melting temp., 60°C annealing temp. and 75°C extension temp. (A and C) Significances were calculated using two-way ANOVA with Tukey´s multiple comparisons test (*p<0.05, N=3 independent experiments, mean ± SEM). (B) Significances were calculated using Kruskal-Wallis test (*p<0.05, N=3 independent experiments, mean ± SEM in duplicates).

To critically test, if the CRISPR/Cas9-modification leads to a potential “loss-of-function” (LOF) of the REVERBα protein, *PVR* promoter luciferase assays were repeated in the THP1 clones (Fig.23). Notably, none of the three CRISPR/Cas9-modified THP1 clonal cell lines exerted an effect on the *PVR* promoter upon treatment with SR9009 agonist or SR8278 antagonist. In contrast, the REVERBα-proficient empty vector (BB) control repressed the *PVR* promoter activity after treatment with SR9009 agonist (Fig.23 (D)), indicating a potential LOF of REVERBα protein in the CRISPR/Cas9-modified clones.

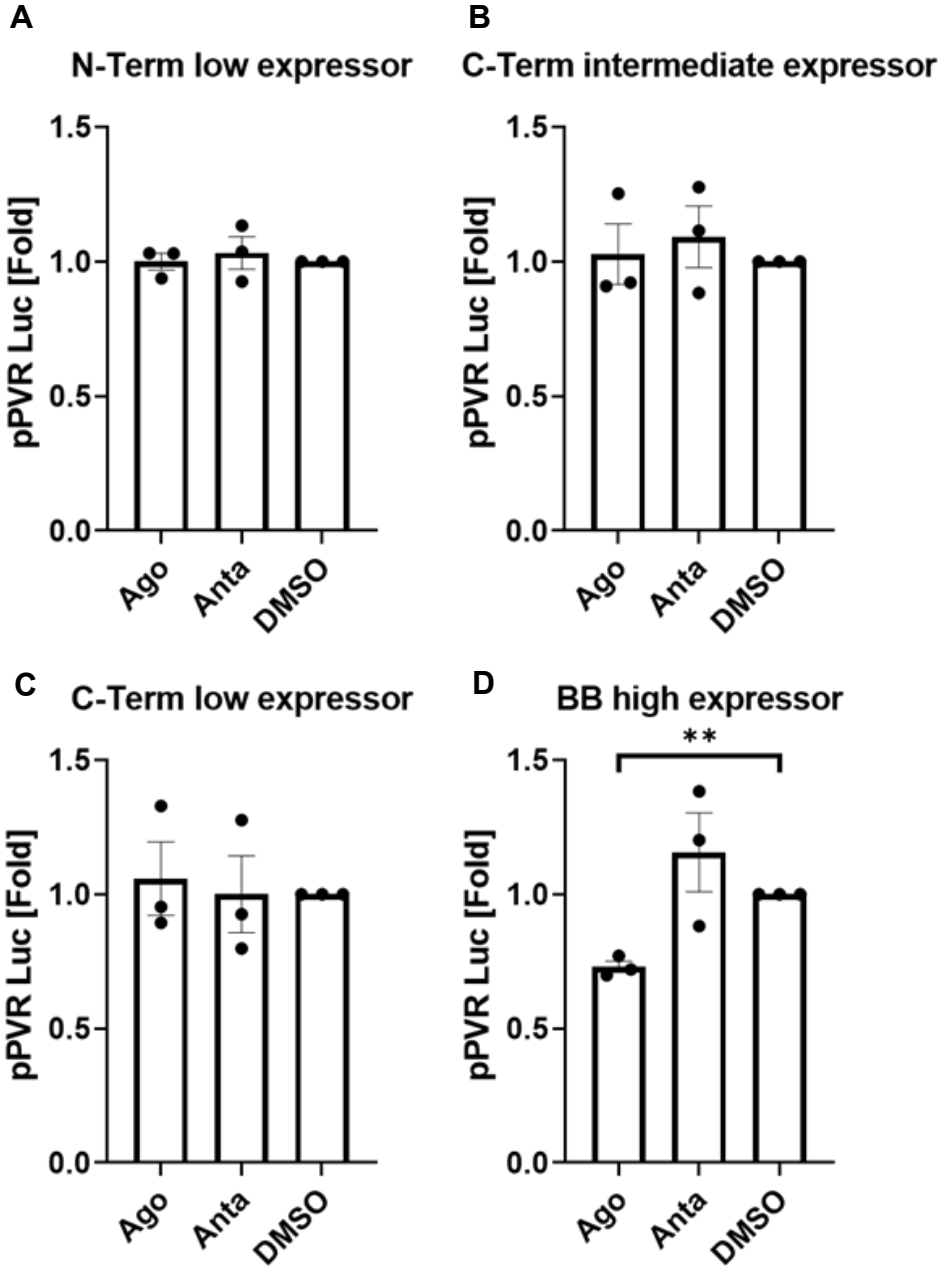

Fig.23 *PVR* promotor activity in CRISPR/Cas9-modified THP1-derived macrophages. M0 macrophages were transfected with luciferase reporter gene plasmid harboring the human *PVR* promoter and were treated for 48h with vehicle (DMSO), REVERBα agonist (1 µM) or antagonist (0,67 µM). Analysis of luciferase activity was conducted by measuring the emitted wavelength at 550 nm after adding luciferase substrate. (A) N-Terminal "low expressor, (B) C-Terminal high expressor, (C) C-Terminal "low expressor" CRISPR/Cas9-modified THP1 and (D) empty vector control ("BB"). (A), (B), (C) and (D) Significances were calculated using two-way ANOVA with Tukey´s multiple comparisons test (*p<0,05, N=3 independent experiments, mean ± SEM in duplicates).

3.4 Validation of monocyte differentiation and macrophage subset markers

The widely used dichotomic terminology for macrophage classification into M1 and M2 has been gone obsolete nowadays. Tumor-associated macrophages (TAMs) are now characterized into at least seven different subsets, each with distinctive molecular features (Ma et. al., 2022). Therefore, the investigation of this subset markers is important to validate the polarization status of the macrophages used in the current experimental setting. As such, the polarization of PBMC-derived primary macrophages with IFNγ, LPS and GM-CSF revealed higher expression of *IDO1, IL4I1* and *ISG15* as depicted in Fig.24. These subset markers were used for confirming the differentiation and polarization of PBMC-derived primary macrophages.

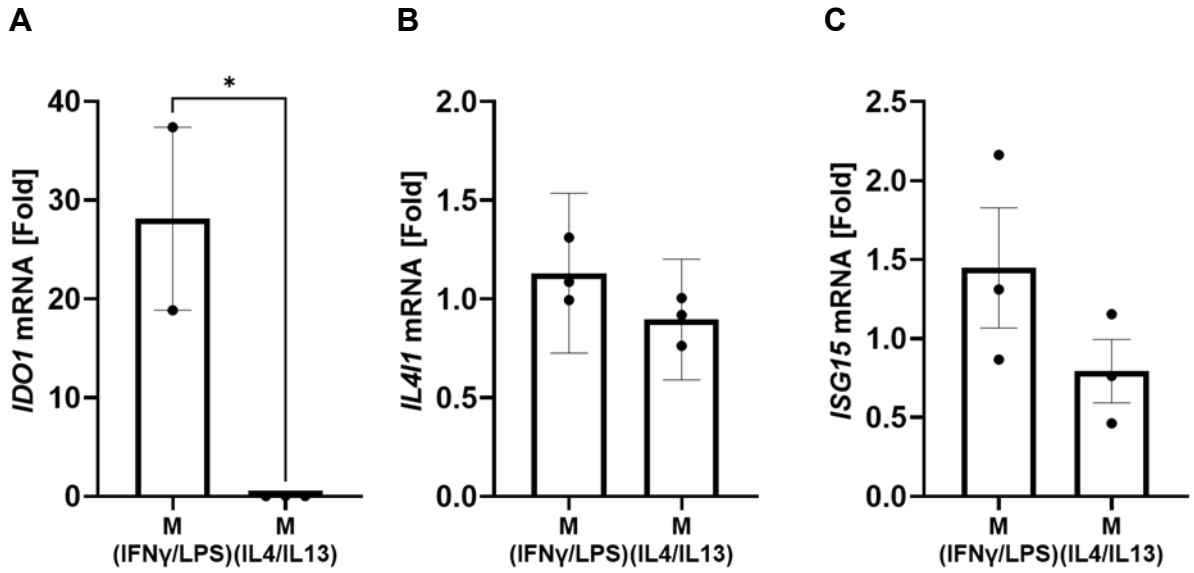

Fig.24 Expression of M(IFNγ/LPS) pro-inflammatory macrophage subset marker in PBMC-derived primary macrophages. Expression of (A) *IDO1*, (B) *IL4I1* and (C) *ISG15* genes in PBMC-derived primary macrophages. RT-qPCR analysis of mRNA isolated from M(IFNγ/LPS) pro-inflammatory and M(IL4/IL13) anti-inflammatory primary macrophages was performed with 40x cycles, 92°C melting temp., 60°C annealing temp. and 75°C extension temp. Significances were calculated using unpaired t-test (*p<0.05, N=3 independent experiments, mean ± SEM in duplicates).

Further, PBMC-derived primary macrophages polarized with IL4, IL13 and M-CSF showed higher expression in genes like *TREM2*, *FCGR3A*, *LIPA* and *HLADRB* as shown in Fig.25.

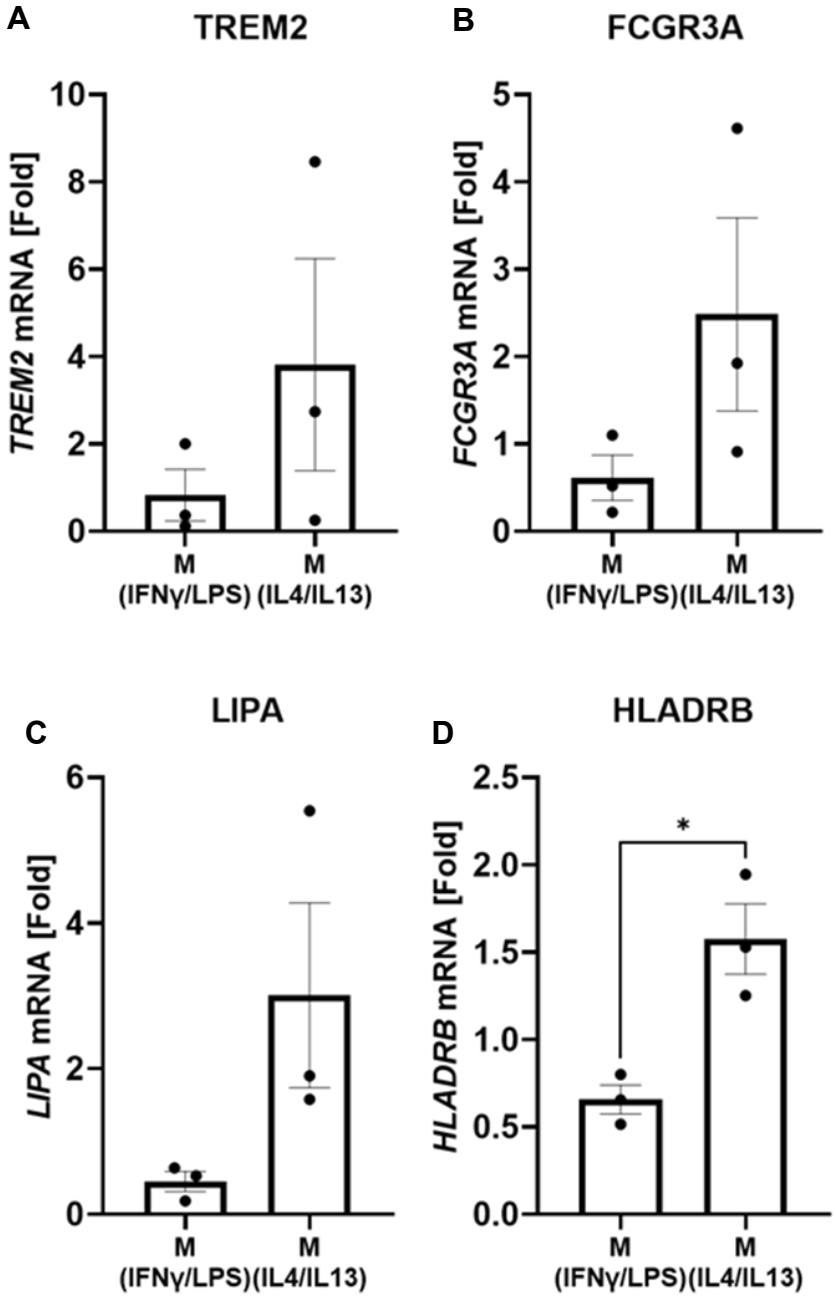

Fig.25 Expression of M(IL4/IL13) anti-inflammatory macrophage subset marker in primary PBMC-derived macrophages. Expression of (A) *TREM2*, (B) *FCGR3A*, (C) *LIPA* and (D) *HLADRB* genes in PBMC-derived primary macrophages. RT-qPCR analysis of mRNA isolated from M(IFNγ/LPS) pro-inflammatory and M(IL4/IL13) anti-inflammatory primary macrophages was performed with 40x cycles, 92°C melting temp., 60°C annealing temp. and 75°C extension temp. Significances were calculated using unpaired t-test (*$p<0.05$, N=3 independent experiments, mean ± SEM in duplicates).

3.5 Effects of genetic and pharmacological REVERBα modification in macrophages on effero- and phagocytosis

To investigate the impact of CRISPR/Cas9 modification on macrophage function, phagocytosis and efferocytosis assays were performed. First, *in vitro* phagocytosis assays, visualizing the uptake of fluorescent beads as a surrogate for tumor cell efferocytosis or pathogen clearance, revealed a trend of higher phagocytotic activity in CRISPR/Cas9-modified THP1-derived pro-inflammatory M(IFNγ/LPS) macrophages compared to the empty vector control (BB, backbone) as shown in Fig.26.

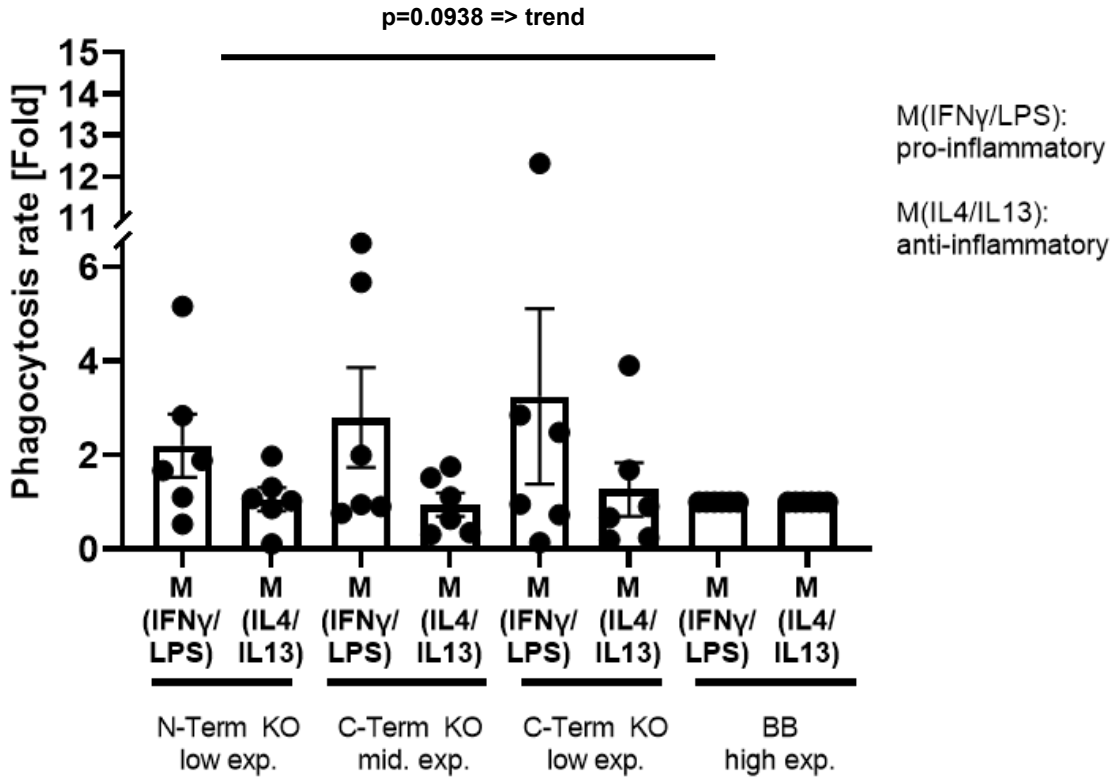

Fig.26 Phagocytosis of fluorescent beads by CRISPR/Cas9-modified THP1-derived macrophages. CRISPR/Cas9-modification of *REVERBα* trends to elevate phagocytosis in M(IFNγ/LPS) pro-inflammatory macrophages. FITC-labelled Protonex™ 600 Red-Latex beads were incubated with THP1 CRISPR/Cas9-modified cell clones for 4 h before staining of the cytoskeleton with CytoTrace. The bead uptake was measured with immunofluorescence (IF) microscopy after 4 h of incubation. Significances were calculated relative to M0 macrophages and were normalized to the respective backbone (BB) controls (set to =1) using Wilcoxon-Signed-Rank Test (*p<0.05, N=6 independent experiments, mean ± SEM).

Furthermore, to unravel the impact of CRISPR/Cas9 modification of the *REVERBα* gene on efferocytosis, an elevated intake rate of CFSE-labelled HT29 cells by C-Terminally CRISPR-modified THP1-derived pro-inflammatory M(IFNγ/LPS) macrophages was observed. Additionally, a general trend of higher efferocytosis in all pro-inflammatory M(IFNγ/LPS) macrophage CRISPR/Cas9-modified THP1 cell clones could be shown as depicted in Fig.27. The rate of ingested CFSE positive HT29 cells by macrophages was measured via flow cytometry (FC).

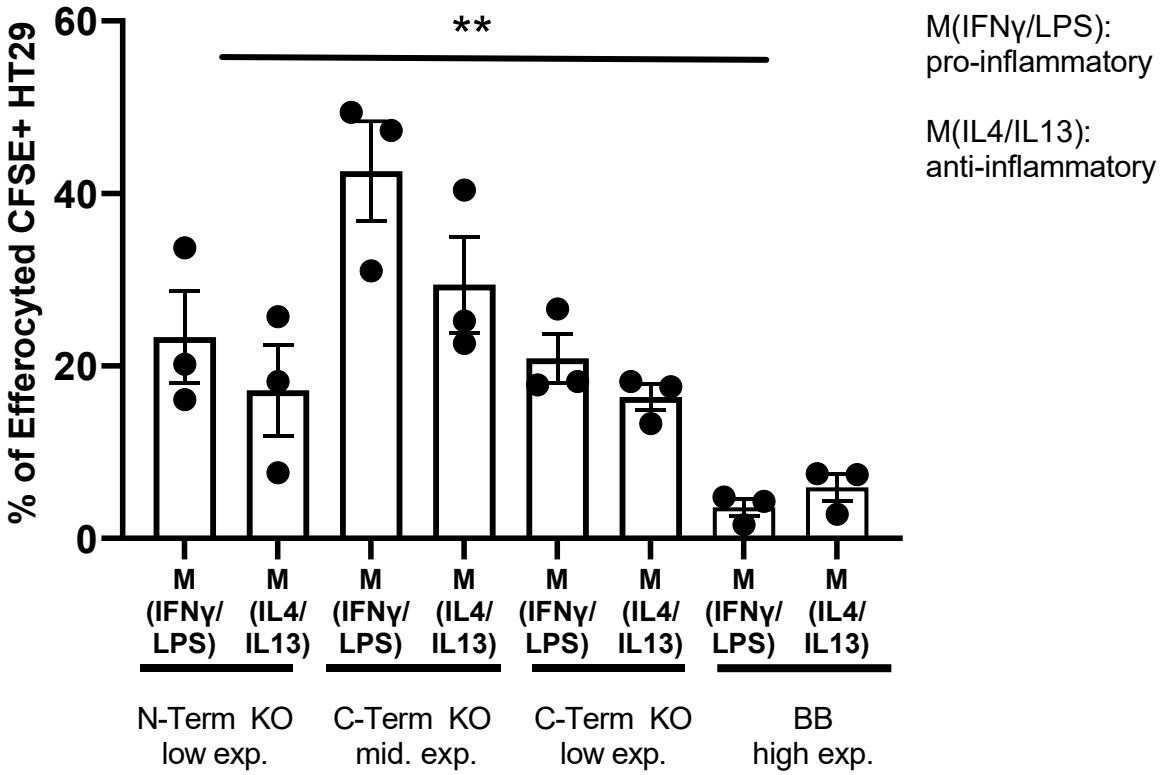

Fig.27 Efferocytosis of HT29 CRC cells by CRISPR/Cas9-modified THP1-derived macrophages. CRISPR/Cas9 modification of *REVERBα* in M(IFNγ/LPS) pro-inflammatory and M(IL4/IL13) anti-inflammatory THP1-derived macrophages trends to elevate efferocytosis. The uptake of CFSE-labelled HT29 was measured via flow cytometry (FC) after 24h of co-culture. Significances were calculated using Kruskal-Wallis test (*p<0.05, N=3 independent experiments, mean ± SEM).

Likewise, treatment of CFSE-labelled HT29 and PBMC-derived primary macrophages with REVERBα ligands showed an elevation in efferocytosis of CFSE-labeled HT29 by M(IFNγ/LPS) pro-inflammatory macrophages compared to its M(IL4/IL13) anti-inflammatory counterpart (Fig.28).

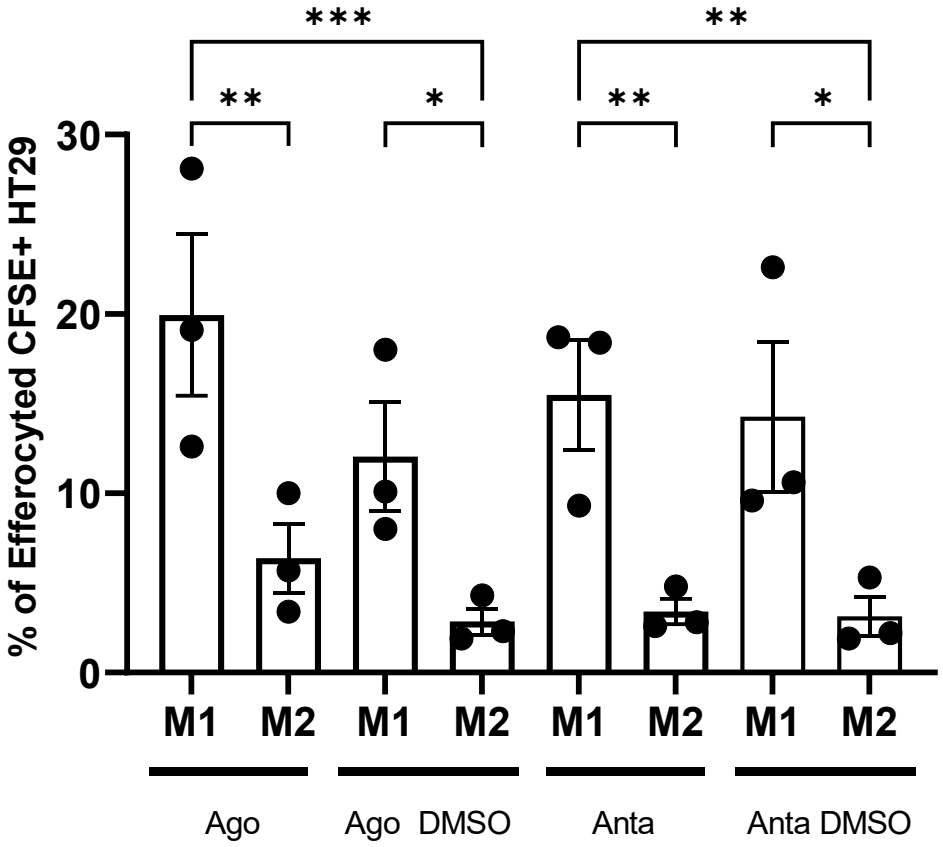

Fig.28 Efferocytosis Assay of HT29 tumor cells by PBMC-derived primary macrophages. Monocytes were isolated via MACS sorting for each experiment from PBMCs originating form healthy donor blood. Differentiated and polarized primary macrophages were treated with vehicle (DMSO), REVERBα SR9009 agonist (10 µM) or SR8278 antagonist (6,7 µM) before and during co-culture. For co-culture, HT29 cancer cells were labelled with CFSE cell tracing dye. Efferocytosis was measured via FC by detecting CFSE-labelled HT29 ingested by CD11b positive macrophages after 24h. Significances were calculated using two-way ANOVA with Tukey´s multiple comparisons test (*$p<0.05$, N=3 independent experiments, mean ± SEM).

3.6 Macrophages in co-culture with CRC cells and PDOs

There is ample evidence that the tumor microenvironment represents a conglomerate of malignant cells embedded in a network of fibroblasts, smooth muscle, endothelial and various immune cells. Within this environment, many immune cells, like tumor-associated macrophages (TAMs), remain in a dormant state of low or inactive function abrogating their tumoricidal potential. To investigate the impact of REVERBα, its regulation of *PVR* gene expression and the overall effect on macrophage effector functions against cancer cells, co-culture experiments were conducted with HT29 cancer cells and patient-derived organoids (PDOs). All co-cultures were subjected to REVERBα ligand and Ab treatment. Functional grade PVR blocking Abs were used to

disrupt the interaction of PVR with TIGIT, while blocking of the “do-not-eat-me” receptor CD47 was intended to reduce inhibition of phagocytosis.

3.6.1 Effects of REVERBα ligands on the viability of HT29 cancer cells in co-cultures with CRISPR/Cas9-modified THP1-derived macrophages

To investigate how CRISPR/Cas9-modification of the *REVERBα*-gene in THP1-derived macrophages impacts HT29 cancer cell viability, co-culture experiments were conducted. Colorimetric MTT assays were performed to investigate the overall viability of co-cultures. Treating co-cultures with REVERBα agonist resulted in no significant difference in the overall death rates between ligand and vehicle (DMSO) treated co-cultures. In contrary, a significant higher amount of overall cell death was observed in co-cultures with CRISPR/Cas9-modified THP1-derived macrophage clones as depicted in Fig.29 and Fig.30.

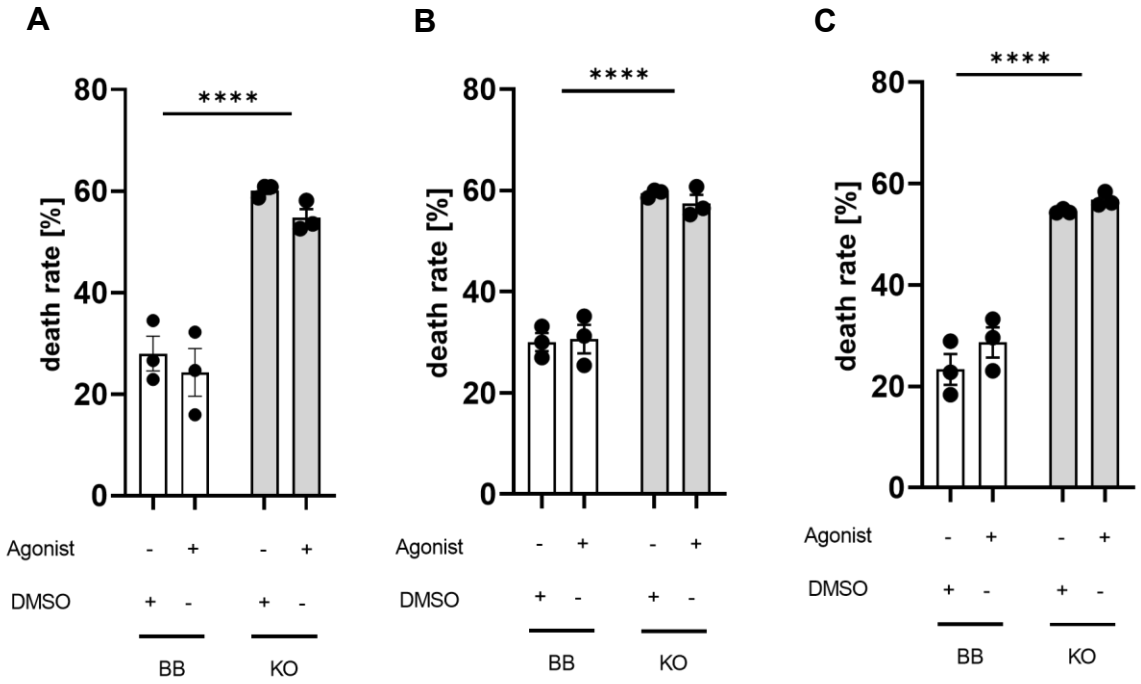

Fig.29 Death rates of co-cultures with HT29 cancer cells and differentiated, polarized CRISPR/Cas9-modified THP1-derived macrophages (A) M0, (B) pro-inflammatory M(IFNγ/LPS) & (C) anti-inflammatory M(IL4/IL13) treated with REVERBα agonist. Co-cultures were conducted with CRISPR/Cas9-modified REVERBα THP1-derived macrophages and its respective empty vector control (BB, backbone). The co-cultures were treated with vehicle (DMSO), 1 µM REVERBα agonist SR9009 for 48 h, and the death rates were calculated from the percentage of viable cells after optical density (OD) measurement of the colorimetric MTT assay. Significances were calculated relative to the vehicle (DMSO) control in M(IL4/IL13) co-cultures using two-way ANOVA and Tukey´s multiple comparisons test (*p<0.05, N=3 independent experiments, mean ± SEM).

Nonetheless, treating co-cultures with REVERBα antagonist, a minor reduction in the overall death rate was observed in M0 CRISPR/Cas9-modified THP1-derived macrophages relative to its DMSO control (Fig.30 (A)).

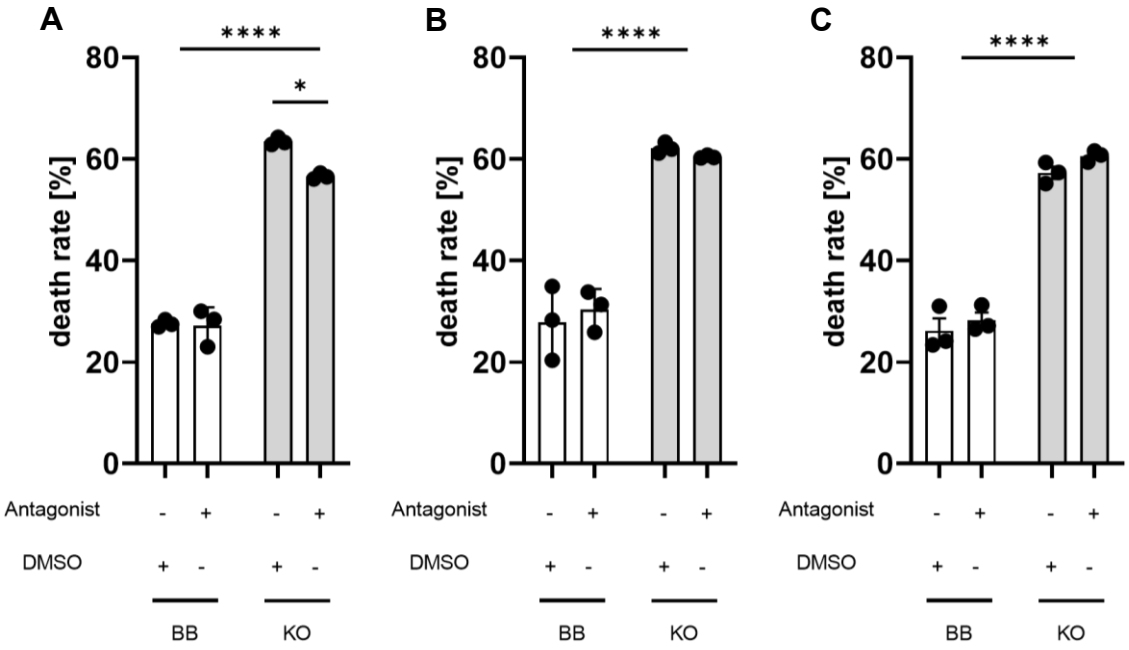

Fig.30 Death rates of co-cultures with HT29 cancer cells and differentiated, polarized CRISPR/Cas9-modified THP1-derived macrophages (A) M0, (B) pro-inflammatory M(IFNγ/LPS) & (C) anti-inflammatory M(IL4/IL13) treated with REVERBα antagonist. Co-cultures were conducted with CRISPR/Cas9-modified REVERBα THP1-derived macrophages and its respective empty vector (BB, backbone) control. The co-cultures were treated with vehicle (DMSO), 0.67 µM REVERBα antagonist SR8278 for 48 h, and the death rates were calculated from the percentage of viable cells after optical density (OD) measurement of the colorimetric MTT assay. Significances were calculated relative to the DMSO control of the M(IL4/IL13) co-culture using two-way ANOVA and Tukey´s multiple comparisons test (*p<0.05, N=3 independent experiments, mean ± SEM).

3.6.2 Effects of PVR blocking Ab and REVERBα ligands on CRC cell viability in co-cultures with PBMC-derived primary macrophages

To test whether inhibition of PVR and CD47 by blocking Abs as well as modulating REVERBα with synthetic ligands promote cancer cell death, primary PBMC-derived macrophages and HT29 CRC cells were co-cultured. Here, the co-culture setups were carried out in presence of functional grade PVR/CD155 (5 µg/ml) and CD47 (10 µg/ml) blocking Abs as well as SR9009 agonist (10 µM) or SR8278 antagonist (6.7 µM). Isotype-matched Abs and vehicle (DMSO) were used as respective controls. Flow cytometry (FC) was used to analyze the viability and death types of the co-culture. A reduction of EpCAM+ HT29 cancer cell viability was evident, as shown in Fig.31 (A) and (B), upon co-culture with the PVR/CD47 Ab combination and REVERBα ligand. Co-cultures with M(IL4/IL13) anti-inflammatory macrophages treated with isotype control Ab had higher levels of viable EpCAM+ tumor cells compared to M(IFNγ/LPS) pro-inflammatory macrophages as depicted in Fig.31. Notably, the viability of macrophages remained constant as depicted in Fig.32.

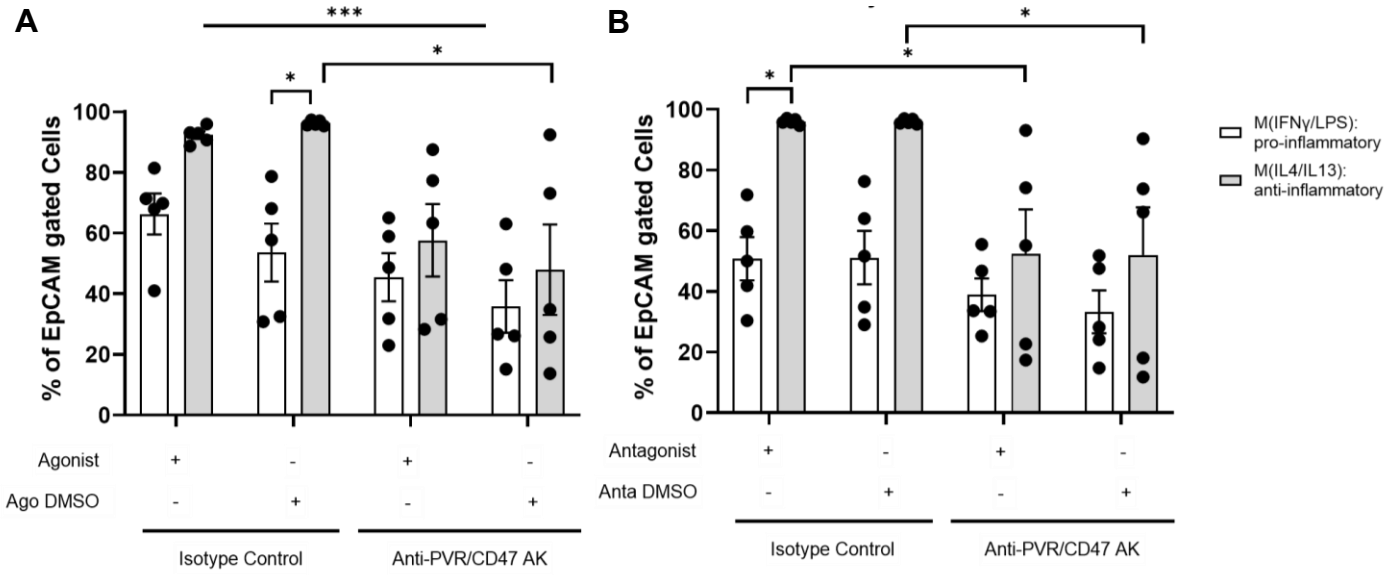

Fig.31 Viability of HT29 cancer cells after co-culture with differentiated, polarized PBMC-derived primary macrophages (M(IFNγ/LPS) & M(IL4/IL13)) The co-cultures were treated with vehicle (DMSO), REVERBα (A) 10 µM SR9009 Agonist or (B) 6.7 µM SR 8275 Antagonist together with 5 µg/ml PVR and 10 µg/ml CD47 blocking Abs vs. isotype control for 5 days. Flow cytometry (FC) was used to detect the viability and death types of EpCAM+ tumor cells and CD11b+ macrophage viability using annexin & SYTOX™ dye. Respective percentages of gated EpCAM+ cells are shown. HT29 viability after PVR Ab treatment is depicted in both (A) and (B). Significances were calculated using two-way ANOVA with Tukey´s multiple comparisons test (*p<0.05; N=5 independent experiments, mean ± SEM). Cells were analyzed on a BD Canto FC device (Flow Core UMM).

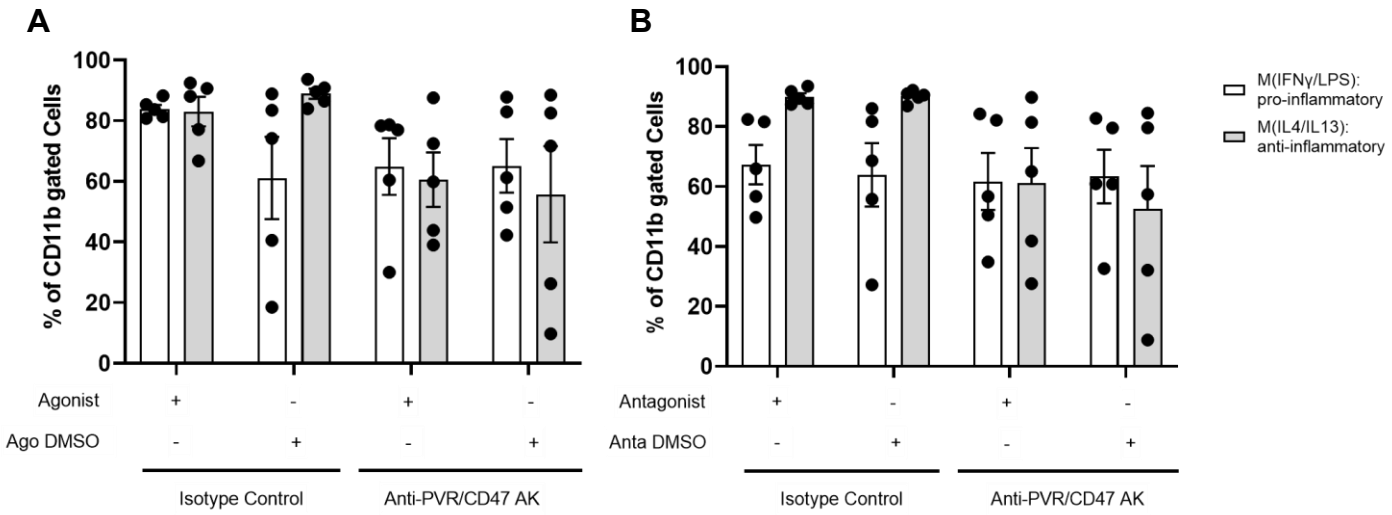

Fig.32 Viability of differentiated, polarized PBMC-derived primary macrophages (M(IFNγ/LPS) & M(IL4/IL13)) upon co-culture with HT29 cancer cells The co-cultures were treated with vehicle (DMSO), REVERBα (A) 10 µM SR9009 Agonist or (B) 6.7 µM SR 8275 Antagonist together with 5 µg/ml PVR and 10 µg/ml CD47 blocking Abs vs. isotype control for 5 days. Flow cytometry (FC) was used to detect the viability and death types of CD11b+ macrophages using annexin & SYTOX™ dye. Respective percentages of gated CD11b+ cells are shown. Both (A) and (B) are showing viability of CD11b+ macrophages in all conditions. Significances were calculated using two-way ANOVA with Tukey´s multiple comparisons test (n.s.; N=5 independent experiments, mean ± SEM). Cells were analyzed on a BD Canto FC device (Flow Core UMM).

Next to the viabilities of tumor and immune cells upon co-culture, the individual death types, like necrosis and apoptosis, were also subject of investigation. Fig. 33 depicts HT29 cancer cells undergoing necrosis in co-culture treated with PVR/CD47 Abs and REVERBα ligands. As depicted in Fig. 33 higher numbers of necrotic CRC cells were evident after treatment with PVR and CD47 blocking Abs. Additionally, necrosis in co-cultures with pro-inflammatory M(LPS/IFNγ) macrophages was observed to be higher than in co-cultures with anti-inflammatory M(IL4/IL13) macrophages as shown in Fig. 33 (A) and (B). Fig. 33 (B) outlines a higher amount of necrotic cancer cells in co-cultures with anti-inflammatory macrophages M(IL4/IL13) treated with PVR and CD47 blocking Abs as compared to the isotype control.

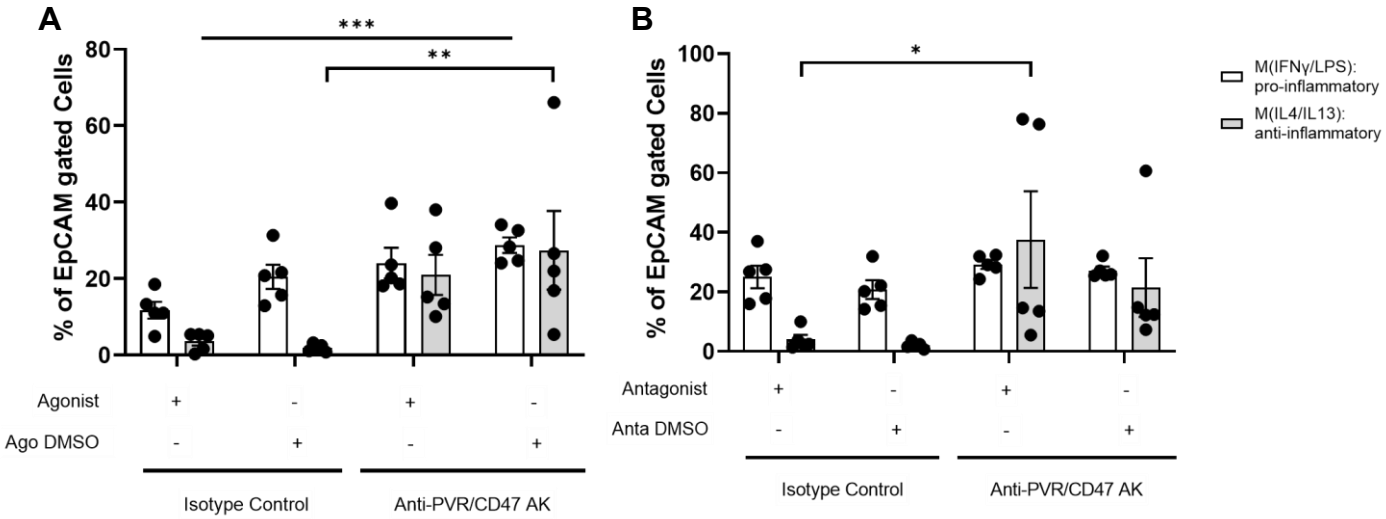

Fig.33 Necrotic HT29 cancer cells after co-culture with differentiated, polarized PBMC-derived primary macrophages (M(IFNγ/LPS) & M(IL4/IL13)) The co-cultures were treated with vehicle (DMSO), REVERBα (A) 10 µM SR9009 Agonist or (B) 6.7 µM SR 8275 Antagonist together with 5 µg/ml PVR and 10 µg/ml CD47 blocking Abs vs. isotype control for 5 days. Flow cytometry (FC) was used to detect the viability and death types of EpCAM+ tumor cells using annexin & SYTOX™ dye. Respective percentages of gated EpCAM+ tumor cells are shown. The amount of HT29 cells undergoing necrosis after PVR Ab treatment is depicted in both (A) and (B). Significances were calculated using two-way ANOVA with Tukey´s multiple comparisons test (*p<0.05; N=5 independent experiments, mean ± SEM). Cells were analyzed on a BD Canto FC device (Flow Core UMM).

Furthermore, FC assays with the same blocking Abs in single culture setups did not reveal a significant toxic effect on the viability of HT29 cancer cells or primary PBMC-derived macrophages compared to the untreated controls (UT) as depicted by Fig. 34, indicative of the need to cooperate at the physical synapse of tumor cells and macrophages to exert a tumoricidal effect in co-cultures.

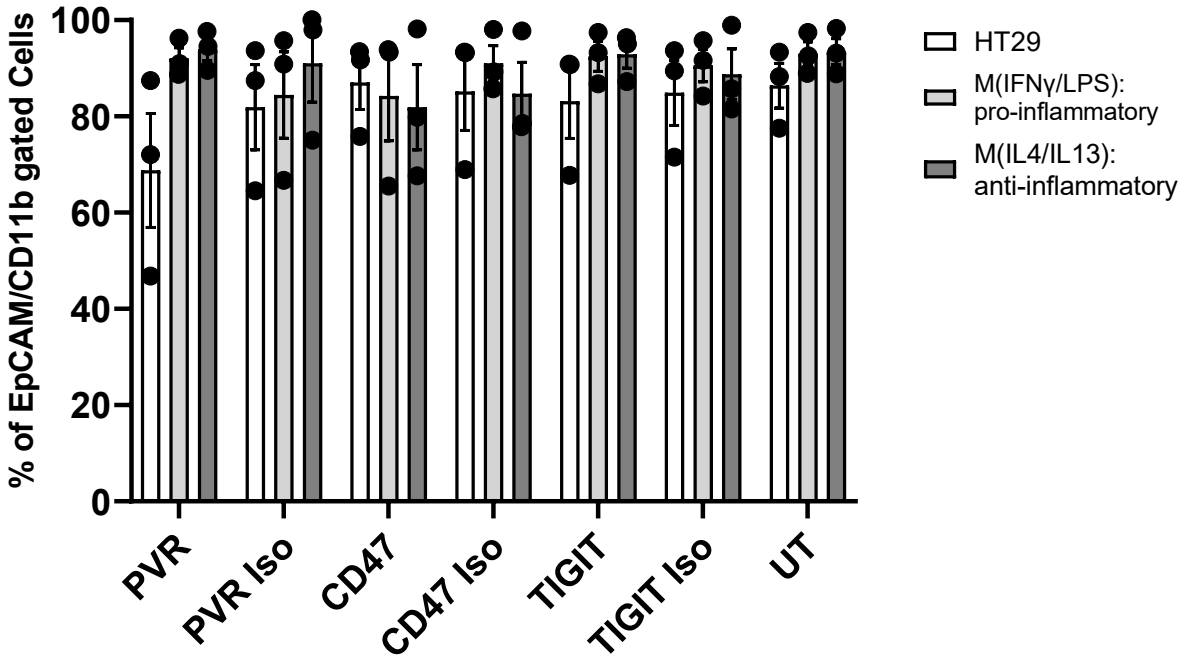

Fig.34 Viability of single cultures upon functional grade blocking Ab treatment in HT29 cancer cells and differentiated, polarized PBMC-derived primary macrophages (M(IFNγ/LPS) & M(IL4/IL13)) The single cultures were treated with 5 µg/ml PVR, 10 µg/ml CD47 or 5 µg/ml TIGIT blocking Abs vs. isotype controls for 3 days. Flow cytometry (FC) was used to detect the viability and death types of EpCAM+ tumor cells and CD11b+ macrophages using annexin & SYTOX™ dye. Respective percentages of gated cells are shown. Significances were calculated using two-way ANOVA with Tukey´s multiple comparisons test (n.s.; N=3 independent experiments, mean ± SEM). Cells were analyzed on a BD Canto FC device (Flow Core UMM).

3.6.3 Effects of PVR blocking Ab and REVERBα ligands on PDO viability in cell co-culture with macrophages

Aiming to translate our findings to patients´ tumors, the following data displays the results of tumor stem cell viability in co-cultures of macrophages with representative PDOs from patients with CRC. Each PDO originated from an individual patient and was taken from our clinical biobank (Betge et al 2022). The Human Ethics approvals (2014-633 N-MA; 2016-607 N-MA) have been granted to the II. Med. Klinik of the UMM to work on patient samples (PDO, blood, tissue). First of all, the co-culture experiments were carried out with PDOs generated from biopsies isolated from different patients. Written informed consent was obtained from all patients prior to biopsy or peripheral blood collection. All patients in this work have been screened by sequencing and clinical phenotyping which was performed by Betge et. al. in 2022. Each patient has its own characteristic, a set of mutated genes driving tumor growth and progression which are represented in Tab.20. For instance, one of the main features of patient no. 7 (P007) are high mutation rates in *KRAS* and *APC* genes, a missense variant for the *KRAS* mutation and a stop codon integration for *APC*. (Betge et. al, 2019). These particular patients were chosen due to their classification as CMS type 2 (Betge et al 2022) and similar key mutations. As stated in the introduction part, only patients with CMS1 classified tumors and MSI-H with high mutation rates (~ 14%) as well as immune infiltration are susceptible for immunotherapy with ICIs (e.g., PD1 Abs). Thus, we intended to develop novel strategies for the large subset of CMS2 (40%) non-MSI patients with CRC, currently not eligible for ICI therapy.

Tab.20 Key mutations of CMS2 classified PDOs from patients with CRC (Betge et. al., 2022)

Patient	Mutations with high frequency
P007	*KRAS, APC*
P022	*TP53, KRAS, APC*

To investigate macrophage-mediated anti-cancer effects in conjunction with REVERBα modulation and PVR blockage, co-culture setups with PDOs were employed to generate a more physiological environment of macrophage-tumor interaction. The following results in this section showcase the impact of modulating REVERBα via ligands and blocking PVR with Abs. To this end, all experimental setups were performed with 10 µM SR9009 REVERBα agonist, 6.7 µM SR8272 REVERBα antagonist and 5 µg/ml of PVR/CD155 blocking Ab. As before, the viability and death types were measured via FC.

3.6.3.1 Cancer cell viability and death types of co-cultures with macrophages and PDOs from patient no. P022

Blocking PVR in co-culture was shown to reduce the viability of EpCAM+ CRC cells in PDOs compared to its isotype control as depicted in Fig.34 (A) and (B). Additionally, low CRC cell viability was also evident in co-cultures with pro-inflammatory M(LPS/IFNγ) macrophages compared to its anti-inflammatory M(IL4/IL13) counterpart. REVERBα ligands had no effect on the viability of the PDOs (Fig.35 (A) and (B)).

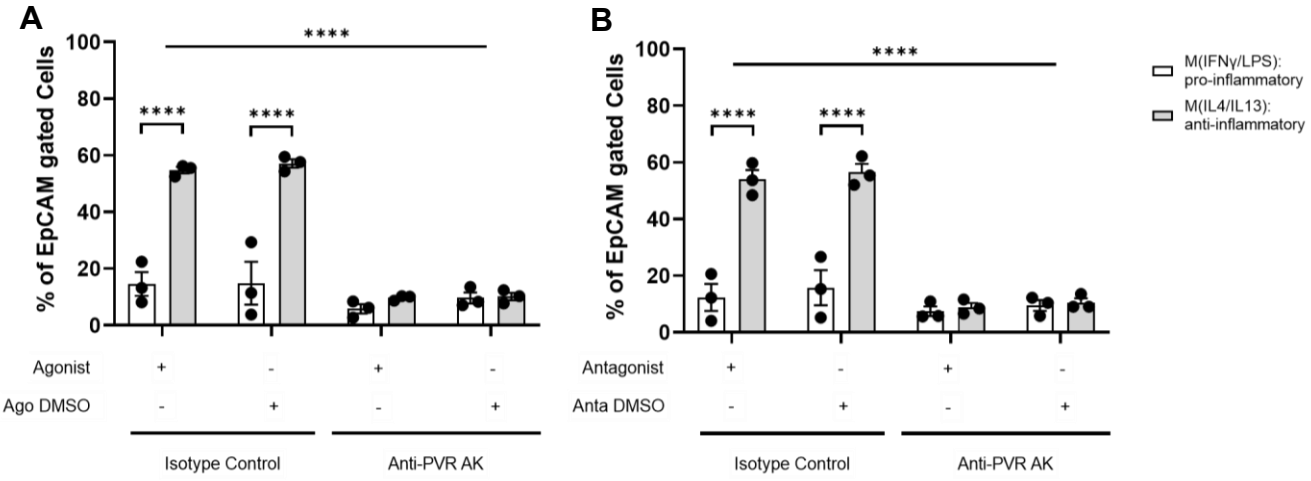

Fig.35 Viability of PDO P022 CRC cells after co-culture with differentiated, polarized PBMC-derived primary macrophages (M(IFNγ/LPS) & M(IL4/IL13)) The co-cultures were treated with vehicle (DMSO), REVERBα (A) 10 µM SR9009 Agonist or (B) 6.7 µM SR 8275 Antagonist together with 5 µg/ml PVR blocking Ab vs. isotype control for 5 days. Flow cytometry (FC) was used to investigate the viability and death types of EpCAM+ tumor cells using annexin & SYTOX™ dye. Respective percentages of gated EpCAM+ tumor cells are shown. Significances were calculated using two-way ANOVA with Tukey´s multiple comparisons test (*p<0.05; N=3 independent experiments, mean ± SEM). Cells were analyzed on a BD Canto FC device (Flow Core UMM).

Importantly, the macrophage viability remained stable under all treatment conditions and was neither reduced by PVR Ab nor by REVERBα ligand (Fig.36 (A) and (B)).

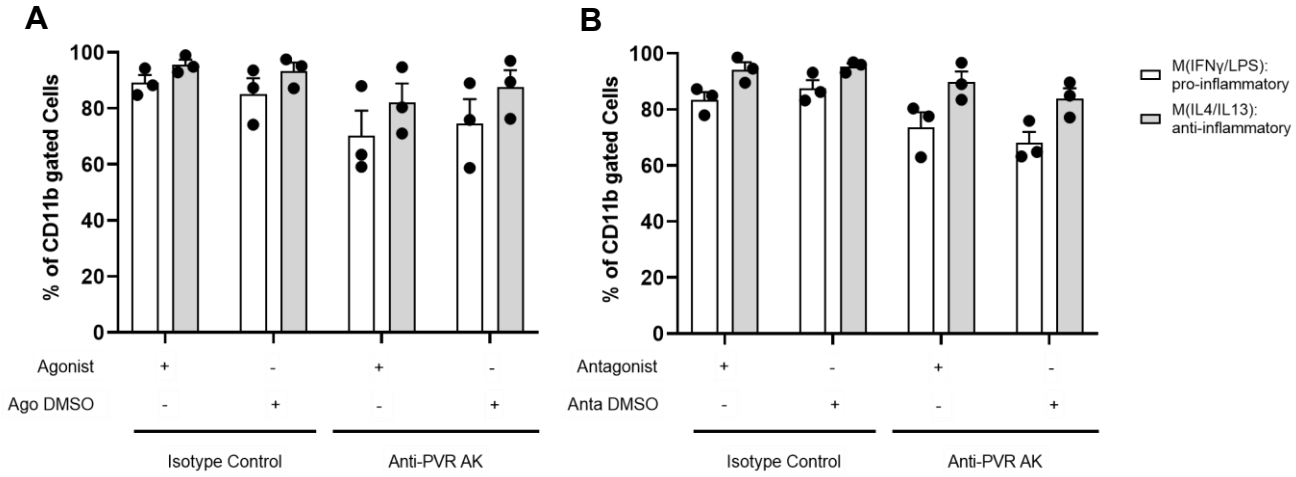

Fig.36 Viability of differentiated, polarized PBMC-derived primary macrophages (M(IFNγ/LPS) & M(IL4/IL13)) in co-culture with PDO P022 The co-cultures were treated with vehicle (DMSO), REVERBα (A) 10 µM SR9009 Agonist or (B) 6.7 µM SR 8275 Antagonist together with 5 µg/ml PVR blocking Ab vs. isotype control for 5 days. Flow cytometry (FC) was used to investigate the viability and death types of CD11b+ macrophages using annexin & SYTOX™ dye. Respective percentages of gated CD11b+ cells are shown. Significances were calculated using two-way ANOVA with Tukey´s multiple comparisons test (n.s.; N=3 independent experiments, mean ± SEM). Cells were analyzed on a BD Canto FC device (Flow Core UMM).

Quantitative analysis of the necrotic state of the cancer cells in co-cultures revealed increased levels of PDOs undergoing necrosis in both pro- and anti-inflammatory macrophage co-cultures following PVR blockade as shown in Fig.37.

Importantly, there was a significant increase in necrotic EpCAM+ tumor cells in presence of REVERBα antagonist and PVR blocking Ab as compared to the respective isotype controls, as given in Fig.37 (B) (right panel).

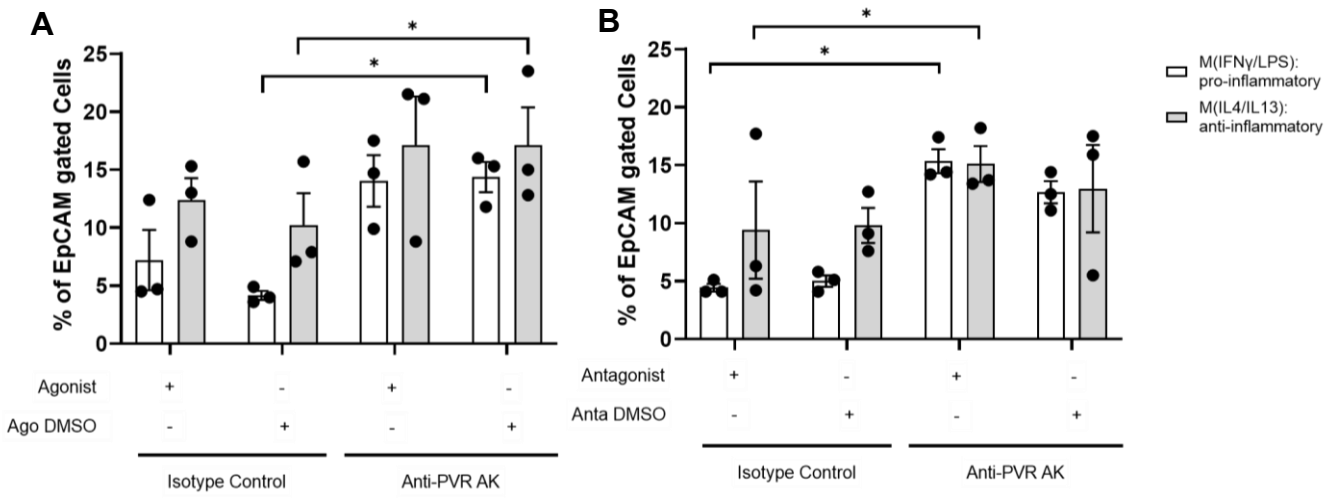

Fig.37 Necrotic PDO P022 CRC cells after co-culture with differentiated, polarized PBMC-derived primary macrophages (M(IFNγ/LPS) & M(IL4/IL13)) The co-cultures were treated with vehicle (DMSO), REVERBα (A) 10 µM SR9009 Agonist or (B) 6.7 µM SR 8275 Antagonist together with 5 µg/ml PVR blocking Ab vs. isotype control for 5 days. Flow cytometry (FC) was used to investigate the viability and death types of EpCAM+ tumor cells using annexin & SYTOX™ dye. Respective percentages of gated EpCAM+ tumor cells are shown. The amount of PDO cells undergoing necrosis after PVR Ab treatment is depicted in both (A) and (B). Significances were calculated using two-way ANOVA with Tukey´s multiple comparisons test (*p<0.05; N=3 independent experiments, mean ± SEM). Cells were analyzed on a BD Canto FC device (Flow Core UMM).

In addition to elevated necrosis, a higher number of PDO cancer stem cells undergoing early phase apoptosis was evident in all co-cultures under PVR Ab treatment as shown in Fig.38. Further on, co-cultures with pro-inflammatory M(LPS/IFNγ) macrophages without PVR Ab treatment revealed higher amounts of early apoptotic PDOs compared to co-cultures with anti-inflammatory M(IL4I/L13) macrophages as shown in Fig.38 (A) and (B).

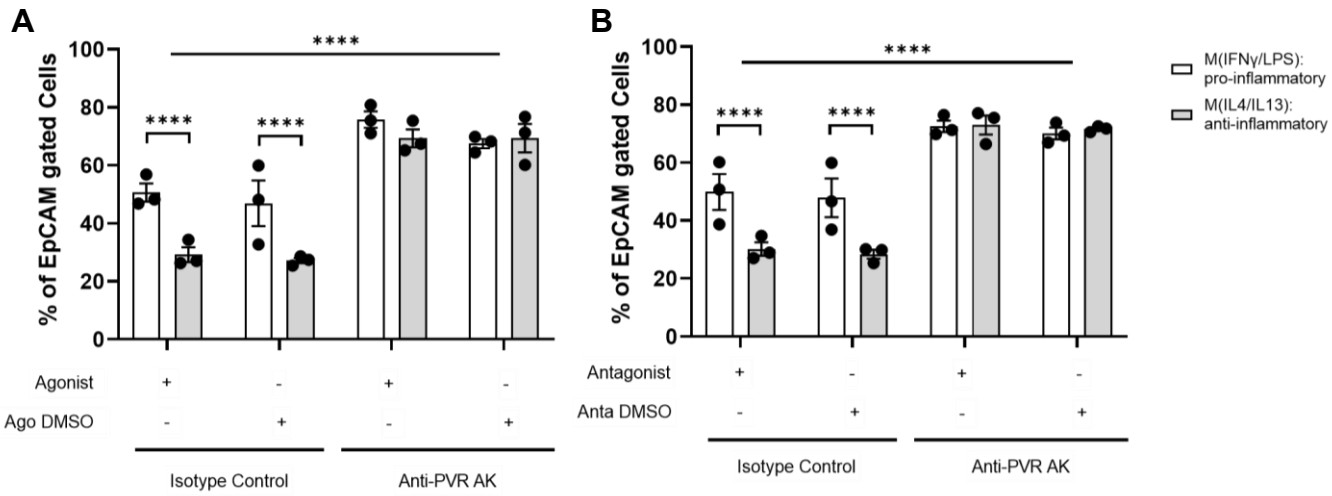

Fig.38 Early apoptotic PDO P022 CRC cells after co-culture with differentiated, polarized PBMC-derived primary macrophages (M(IFNγ/LPS) & M(IL4/IL13)). The co-cultures were treated with vehicle (DMSO), REVERBα (A) 10 µM SR9009 Agonist or (B) 6.7 µM SR 8275 Antagonist together with 5 µg/ml PVR blocking Ab vs. isotype control for 5 days. Flow cytometry (FC) was used to investigate the viability and death types of EpCAM+ tumor cells using annexin & SYTOX™ dye. Respective percentages of gated EpCAM+ tumor cells are shown. The amount of early apoptotic PDOs after PVR Ab treatment is depicted in both (A) and (B). Significances were calculated using two-way ANOVA with Tukey´s multiple comparisons test (*p<0.05; N=3 independent experiments, mean ± SEM). Cells were analyzed on a BD Canto FC device (Flow Core UMM).

Despite the high number of PDOs undergoing early apoptosis (Fig. 38), the number of PDOs in late apoptotic state was shown to be lower after PVR Ab treatment as shown in Fig.39. As depicted in both Fig.39 (A) and (B) a significant higher number of PDOs undergoing late apoptosis was evident in co-cultures with pro-inflammatory M(LPS/IFNγ) macrophages without PVR Ab treatment.

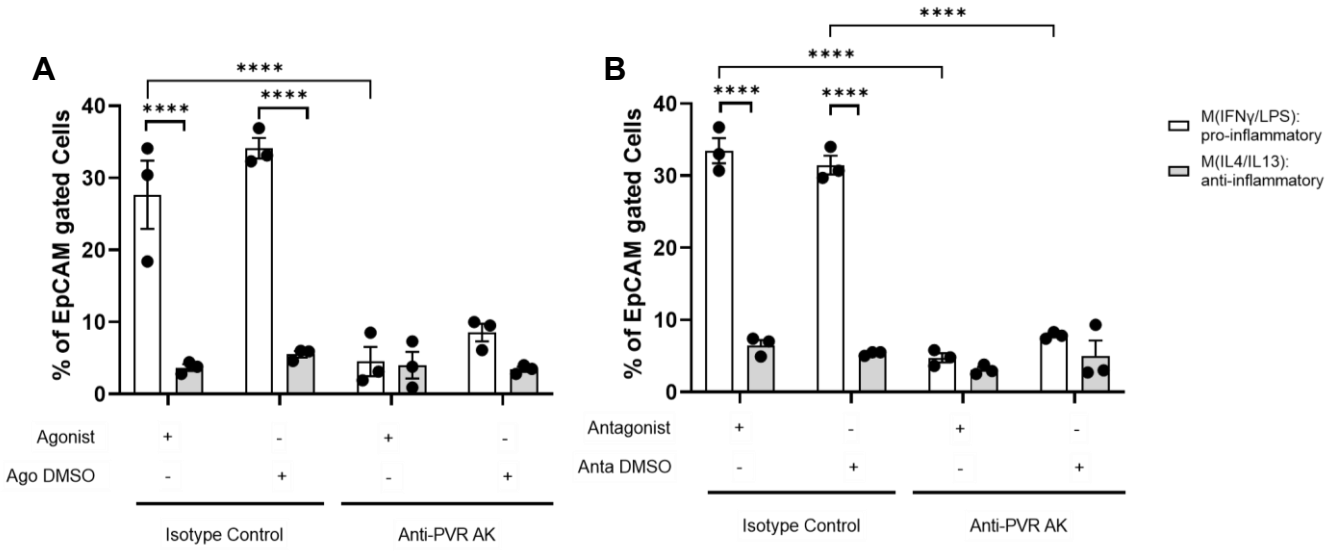

Fig.39 Late apoptotic PDO P022 CRC cells after co-culture with differentiated, polarized PBMC-derived primary macrophages (M(IFNγ/LPS) & M(IL4/IL13)). The co-cultures were treated with vehicle (DMSO), REVERBα (A) 10 µM SR9009 Agonist or (B) 6.7 µM SR 8275 Antagonist together with 5 µg/ml PVR blocking Ab vs. isotype control for 5 days. Flow cytometry (FC) was used to investigate the viability and death types of EpCAM+ tumor cells using annexin & SYTOX™ dye. Respective percentages of gated EpCAM+ tumor cells are shown. The amount of PDOs undergoing late apoptosis after PVR Ab treatment is depicted in both (A) and (B). Significances were calculated using two-way ANOVA with Tukey´s multiple comparisons test (*p<0.05; N=3 independent experiments, mean ± SEM). Cells were analyzed on a BD Canto FC device (Flow Core UMM).

In contrast to the observed antagonist-induced necrosis phenotype (Fig.37 B), neither the REVERBα agonist nor the antagonist significantly impacted the viability and apoptotic death types in co-cultures with PDO22.

3.6.3.2 Cancer cell viability and death types of co-cultures with macrophages and PDOs from patient no. P007

Blocking PVR in co-culture was shown to reduce the viability of CRC cells in PDOs compared to its isotype control as depicted in Fig.39 (A) and (B). Additionally, low viability of PDOs was evident in co-cultures with pro-inflammatory M(LPS/IFNγ) macrophages compared to its anti-inflammatory M(IL4/IL13) counterpart. REVERBα ligands had no effect on the PDO viability (Fig.40 (A) and (B)).

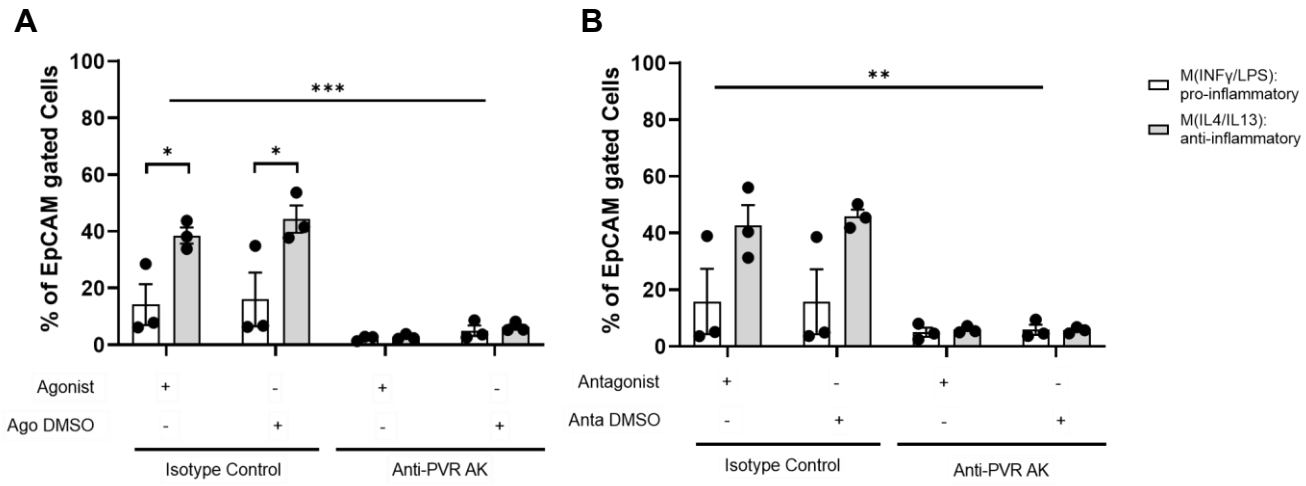

Fig.40 Viability of PDO P007 CRC cells after co-culture with differentiated, polarized PBMC-derived primary macrophages (M(IFNγ/LPS) & M(IL4/IL13)) The co-cultures were treated with vehicle (DMSO), REVERBα (A) 10 µM SR9009 Agonist or (B) 6.7 µM SR 8275 Antagonist together with 5 µg/ml PVR blocking Ab vs. isotype control for 5 days. Flow cytometry (FC) was used to investigate the viability and death types of EpCAM+ tumor cells using annexin & SYTOX™ dye. The amount of viable PDOs after PVR Ab treatment is depicted in both (A) and (B). Respective percentages of gated EpCAM+ tumor cells are shown. Significances were calculated using two-way ANOVA with Tukey´s multiple comparisons test (*p<0.05; N=3 independent experiments, mean ± SEM). Cells were analyzed on a BD Canto FC device (Flow Core UMM).

Finally, as depicted in Fig.41, the viability of CD11b+ macrophages in co-cultures with PDO P007 remained stable and high, except of co-cultures containing pro-inflammatory M(LPS/IFNγ) macrophages, whose viability was lower compared to the other co-culture conditions, however, without reaching statistical significance.

Conclusively, both patients were responsive to PVR Ab treatment, whereas the PDOs, consistent with other reports, exhibited a phenotype of ligand/drug resistance, suggesting that inter-patient variability may play a critical role as further addressed in the discussion.

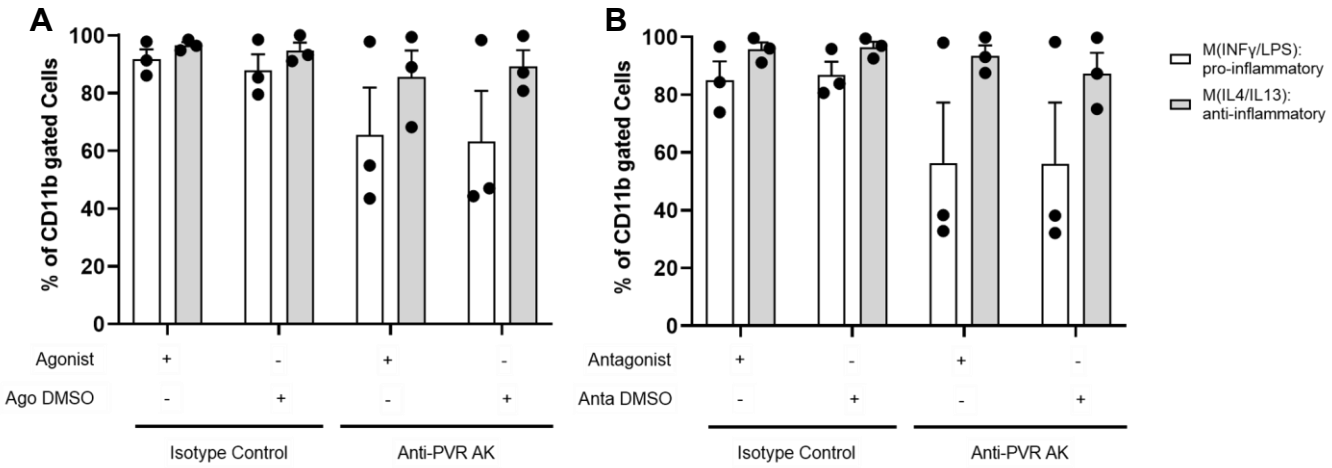

Fig.41 Viability of differentiated, polarized PBMC-derived primary macrophages (M(IFNγ/LPS) & M(IL4/IL13)) in co-culture with PDO P007 The co-cultures were treated with vehicle (DMSO), REVERBα (A) 10 µM SR9009 Agonist or (B) 6.7 µM SR 8275 Antagonist together with 5 µg/ml PVR blocking Ab vs. isotype control for 5 days. Flow cytometry (FC) was used to investigate the viability and death types of CD11b+ macrophage using annexin & SYTOX™ dye. Respective percentages of gated CD11b+ macrophages are shown. Significances were calculated using two-way ANOVA with Tukey´s multiple comparisons test (n.s.; N=3 independent experiments, mean ± SEM). Cells were analyzed on a BD Canto FC device (Flow Core UMM).

4. Discussion

The role of our immune system in combating colorectal cancer (CRC) and other common malignant cancer types has been a major area of investigation in both basic and clinical research. Despite recent technological advances and deeper understanding of immune-cancer interactions, multiple critical questions remain unanswered. One generally known key challenge in the immunotherapy of CRC is the immunosuppressive nature of the tumor microenvironment (TME), limiting the effectiveness of treatments based on immune cells (Wang et. al., 2025). Macrophages, however have emerged as powerful key regulators and effector cells of anti-tumor immune responses. In CRC, macrophages exist in a spectrum of dynamic subtypes influencing the tumor progression, treatment response and the overall clinical outcomes. Within our gastrointestinal tract, these immune cells are in constant contact and communication with the gut microbiota playing a crucial role in influencing cancer development as well as anti-cancer treatment efficacy. This highlights macrophages as a target for the development of novel therapeutic approaches against cancer (Mantovani et. al., 2017), (Mola et. al, 2020). In recent times, the focus has turned towards immune checkpoint molecules such as the poliovirus receptor (PVR/CD155) and TIGIT (T-cell immunoglobulin and immunoreceptor tyrosine-based inhibitory motif domain) which both have shown to be promising novel targets for therapy (Cui et. al., 2025). The PVR-TIGIT axis is known to dampen immune responses by modulating cytokine secretion from effector cells to reduce interferon-γ (IFNγ) and tumor-necrosis-factor-α (TNFα) levels (Zhang et. al., 2020). Additionally, another study showed that dendritic cells enhanced production of the immunosuppressive interleukin-10 (IL10) while reducing the production of proinflammatory IL12 upon PVR-TIGIT interaction. This concept can be expanded to macrophages, where TIGIT has been reported to inhibit macrophage activation, driving peritoneal macrophages to shift from a pro-inflammatory “M1-like” phenotype towards an anti-inflammatory more immune-suppressive “M2-like” macrophage phenotype (Chiang et. al., 2022). Likewise, *in vivo* studies with mouse CRC models revealed that the blockage of TIGIT enhanced CD8+ T-cell responses against the tumor. Together with the blocking of PD-1 and PD-L1 or TIM-3, synergistic anti-tumor effects were evident in this study (Archilla-Ortega et. al., 2022). Moreover, in hepatocellular carcinoma blocking PVR and TIGIT resulted in

restoration of CD8+ T-cell activity, highlighting the relevance of PVR and TIGIT as targets in multiple cancer types like CRC and melanoma (Zhang et. al., 2020).

Ample evidence has demonstrated the mechanistic link between the circadian clock and therapeutic resistance to bevacizumab (anti-VEGFA therapy). REVERBα was shown to bind a RORE motif in close proximity to the BMAL1 E-box within the VEGFA promoter, collaborating with BMAL1 to upregulate the expression of VEGFA in CRC. CRC patient tumors with elevated levels of BMAL1 revealed a poorer prognosis and survival, suggesting that this signaling axis is associated with bevacizumab resistance (Burgermeister et. al., 2019). These findings describe how REVERBα influence cancer-relevant pathways in a circadian manner, raising the question whether similar kinds of mechanisms may be extended to immune checkpoint regulation in CRC. Additionally, Burgermeister et. al., 2019 showed that targeting this axis with REVERBα antagonists caused a reduction in VEGFA expression and therefore tumor angiogenesis in mice.

Describing the role of REVERBα expression in cancer appears highly context dependent, with evidence supporting both tumor-promoting functions on the one hand and tumor suppressive on the other. Some reports which are based on immunohistochemistry suggested the upregulation REVERBα in CRC, especially in tumor epithelia when compared to normal mucosa. Furthermore, REVERBα expression may decrease in advanced CRC or metastasis, suggesting differentiated views on REVERBα expression based on tumor stages and the tissue compartment observed (Wu, 2021), (Burgermeister et. al., 2019). This raises the possibility, that REVERBα contributes to not only CRC, but also other malignancies, underscoring its potential as a therapeutic target.

Recent studies instead revealed that REVERBα switches from a transcriptional repressor to an activator of tumorigenic programs in cancer cells. For example, it was shown that REVERBα directly targets oncogenic signalling pathways like MAPK, PI3K-AKT and cell cycle genes (Yang et. al., 2024). Based on this, previous findings demonstrated that REVERBα expression is altered in gastric tumors, correlating with advanced TNM (Tumor/Nodes/Metastasis) stages and poor prognosis. Alongside this, REVERBα acts as a metabolic gatekeeper reducing glycolytic flux and in human gastric cancer cells. Tao et. al., 2019 showed that knocking down REVERBα highly increases the glycolytic flux in pentose phosphate pathway and tumor cell proliferation in human gastric cancer. The pharmacological activation of REVERBα via the

GSK4112 agonist was shown to reverse these effects (Tao et. al.,2019). Extending this, the perturbation of REVERBα with other agonists like SR9009 and SR9011 showed to affect a number of oncogenic drivers such as human BRAF, HRAS, PIK3CA and more (Sulli et. al., 2018).

In immune cells, REVERBα was shown to transcriptionally repress murine *IL1β*, *NLRP3*, and *IL18*, thereby regulating inflammasome activation and cytokine secretion in macrophages. Accordingly, REVERBs deficiency lead to exaggerated inflammatory responses, underscoring its role as a key modulator of innate immune homeostasis (Pourcet et. al., 2018), (Wang et. al., 2018). Additionally, REVERBα controls the rhythmic expression of genes in murine macrophages, influencing markers like *CCL2* and inflammatory cytokines. The loss of REVERBα disrupts these oscillations, leading to dysregulated immune activity (Sato et. al., 2014). Another aspect worth considering is that in acidic TME conditions, the circadian rhythms become altered in macrophages affecting their polarization states and innate immune functions. Therefore, REVERBα may contribute to tumor-associated macrophage (TAM) reprogramming (Knudsen-Clark et. al., 2024) and modulation of immune checkpoint genes, including the PVR-TIGIT axis. To date, no studies have directly elucidated the exact mechanistic link between REVERBα and PVR in context of colorectal cancer.

While REVERBα is well characterized as a regulator of the circadian rhythm, its role in modulating the expression of PVR in macrophages and CRC cells remains largely unexplored. Beyond circadian rhythm genes, the broader transcriptional targets of REVERBα in CRC are not well defined. In particular, its influence on TAM polarization and interaction with CRC cells within the TME remains poorly understood, despite its potential relevance for the development of novel therapeutic strategies. Moreover, while the rhythmic activity of REVERBα is known to affect metabolic and immune processes (Cho et. al., 2012), (Pariollaud et. al., 2018), its impact on TAM function, tumor growth and immune evasion in context of the circadian rhythm remains still unresolved. It is known that REVERBα controls metabolism in many cell types (Wang et. al., 2025), but its effect on the immune metabolic landscape of TAMs and CRC cells has not been uncovered yet. Notably, the majority of pharmacological studies investigating REVERBα have been conducted in non-CRC models (Gomatou et. al., 2023). As mentioned earlier, to date there is no experimental evidence confirming or denying whether REVERBα directly regulates the expression of the human or murine *PVR/Pvr* genes. Importantly, clinical data on REVERBα expression levels in human

CRC tissues, particularly in relation to immune infiltration and patient prognosis remain limited (Gomatou et. al., 2023). Therefore, this thesis aimed to elucidate the role of the transcription factor REVERBα in regulating macrophage-mediated anti-tumor responses in colorectal cancer, with a specific focus set on its modulation of the PVR-TIGIT immune checkpoint axis. Uncovering these regulatory mechanisms laid the groundwork for future studies aimed at the developing of novel therapeutic strategies to enhance immunotherapy efficacy and overcome immune evasion in colorectal cancer.

4.1 Functional characterization of REVERBα

As mentioned previously REVERBα (NR1D1) is a nuclear receptor and transcriptional repressor traditionally known for regulating circadian rhythm, metabolic homeostasis, cellular differentiation as well as inflammatory functions (Burris, 2008), (Ikeda et. al., 2019). However, emerging evidence revealed REVERBα´s involvement in immune modulation, particularly within macrophages (Angulo et. al., 2025). As already mentioned, REVERBα is known for its anti-inflammatory properties by modulating and controlling cytokine production in myeloid cells. Previous studies showed that pharmacological stimulation of REVERBα suppresses inflammatory responses and direct polarization of macrophages away from the pro-inflammatory “M1-like” phenotype towards the anti-inflammatory “M2-like” state (Sato et al., 2014), (Zhang et al., 2023). This capability to switch and reshape cellular phenotypes suggests that REVERBα may function as a checkpoint regulator linking circadian rhythm, metabolism and innate immunity.

While REVERBα has been extensively studied in context of circadian rhythm and metabolism (Everett and Lazar, 2014), its specific role and function in macrophages and colorectal cancer still remains widely unexplored. In the present thesis, one of the first key findings was the detection of REVERBα expression in macrophages. As shown by Western blot in Fig.15, REVERBα was expressed in both THP1-derived (Fig.15 A) and PBMC-derived primary macrophages (Fig.15 C). The manufacturer of the REVERBα (E1Y6D, #13418) monoclonal Ab proposed that it recognizes endogenous REVERBα protein at a range of 60-78 kDa in Fig.15 A and C. Likewise, the manufacturer of REVERBα polyclonal Ab (14506-1-AP) suggested a similar range of 55 and 78 kDa. To experimentally verify the Ab specificities, REVERBα was overexpressed from a commercial plasmid in HEK293T cells (Fig.15 B). Therein,

Western blotting revealed a band at exact 78 kDa size, confirming the specificity in detecting REVERBα.

Consequently, flow cytometry (FC) of THP1-derived macrophages confirmed the intracellular expression of REVERBα protein in all subsets of polarized pro-M(LPS/IFNγ) and anti-inflammatory M(IL4/IL13) macrophages (Fig.17). In addition, *REVERBα* gene expression in PBMC-derived primary macrophages was also proven at a genetic level (Fig.12). To further understand the function of REVERBα in macrophages, CRISPR/Cas9 modification of the *REVERBα* gene in THP1-derived macrophages was conducted. Accordingly, both Western blot and intracellular FC analysis revealed expression of REVERBα in CRISPR/Cas9-modified THP1-derived macrophages (Fig.16 and Fig.18). As shown in Fig.16, both N-terminal (Fig.16 A) and C-terminal (Fig.16 B) CRISPR/Cas9-modifications of the *REVERBα* gene resulted in the absence of protein isoforms when compared to the backbone (BB) empty vector control, which displayed the strongest band intensities. Although REVERBα was still expressed in CRISPR/Cas9-modified THP1-derived macrophages, the absence of these isoforms suggests that the CRISPR/Cas9 editing may caused alterations to the *REVERBα* gene or protein sequence, presumably changes in proteolytic stability and/or post-translational modifications (PTMs) (Smits et. al., 2019). This hypothesis was supported by the lack of bands above and below the expected size of REVERBα (78 kDa) (Fig.15 A). These findings are further underscored by immunofluorescence microscopy of REVERB*α* protein in THP1-derived macrophages with CRISPR/Cas9-modified *REVERBα* gene. As depicted in Fig.14, N-terminally modified THP1-derived macrophages (Fig.14 A) exhibited lower REVERBα expression compared to both C-terminally modified macrophages (Fig.14 B) and the BB empty vector control (Fig.14 C). Each CRISPR/Cas9-modified THP1-derived macrophage clone expressed REVERBα protein at different levels, indicating that the genetic modifications exerted distinct transcriptional or post-transcriptional effects on *REVERBα* gene expression. Nonetheless, residual REVERBα was still present in the CRISPR/Cas9-modified THP1 clones. Hence, it cannot be excluded that a “loss-of-function” in this protein occurred by frame shift or truncation mutations. Using the Phyre2 software (Powell et. al., 2025) , a 3D model of wildtype REVERBα was created, illustrating its structure which is depicted in S2 of the supplementary section. In addition, supplementary figure S3 depicts the 3D structure C-terminally CRISPR/Cas9-modified REVERBα protein, illustrating how the C-terminal modification could alter its conformation leading to

misfolding and/or reduced stability. Notably, THP1-derived macrophages harboring CRISPR/Cas9-modified *REVERBα* revealed a “loss-of-function” phenotype upon REVERBα ligand treatment. As illustrated by Fig.23, all CRISPR/Cas9-modified THP1-derived macrophages showed little to no effect on the expression of the *PVR* promoter upon REVERBα ligand treatment. Hence, these findings indicate a loss of ligand sensitivity, rather than the anticipated de-repression of the *PVR* promoter activity by the SR8278 antagonist or the expected super-repression by the SR9009 agonist in the empty vector control. Consequently, this loss of ligand sensitivity underlines the fact that CRISPR/Cas9 modification of *REVERBα* gene had an actual impact on its function, making a misfunctioning REVERBα possible. This misfunction could be caused due to misfolded tertiary structure after translation of REVERBα mRNA. Taken together, future whole genome sequencing and mass spectroscopy studies shall elucidate the exact modifications in the respective clones.

Building on the data regarding the characterization of *REVERBα* gene expression in macrophages and CRISPR/Cas9 THP1 clones, it was important to consider its well-documented role as a core circadian rhythm regulator. *REVERBα* mRNA expression is known to oscillate in a circadian manner as stated by Ikeda et. al., 2019. The cyclic expression of *REVERBα* mRNA was evident in PBMC-derived primary macrophages and THP1-derived macrophages as illustrated in Fig.11. Both cell types, parental THP1 and PBMC-derived primary macrophages, exhibited an oscillating expression pattern of *REVERBα* mRNA over 24h. During daytime a lower expression of *REVERBα* was observed compared to nighttime expression of *REVERBα* (Fig.11), underscoring the periodic expression pattern of the *REVERBα* gene. The *PVR* mRNA was also shown to be cyclically expressed over a time span of 24h. This cyclic expression pattern may influence REVERBα´s function as a transcriptional repressor, coordinating the timing of downstream gene regulation (Gibbs et. al., 2012), (Sulli et. al., 2018). Further on, the rhythmicity of its expression and activity is suggested to be critical in the modulation of immune responses and tumor interaction (Zhang et. al., 2023). More in depth investigation is required to elucidate how *REVERBα* oscillation impacts macrophage function within the colorectal cancer tumor-microenvironment. Single-cell RNA sequencing of CRISPR/Cas9-modified macrophages would give deeper insights about the functional impairment of REVERBα.

4.2 Regulatory interaction of REVERBα and the human *PVR* promoter

The poliovirus receptor (CD155/PVR) has emerged as a novel immune checkpoint molecule within CRC (Liu et. al., 2023). As outlined in the introductory section PVR is expressed on antigen-presenting cells (APCs), tumor cells and various other cells. It can bind several ligands and receptors, generating heterotypic interactions between adjacent cells (Wu et. al., 2024). Moreover, PVR binds to TIGIT on immune cells like T-cells, NK cells, monocytes and macrophages, triggering immunosuppressive signalling pathways which dampen anti-tumor immunity. Notably, high levels of PVR are correlated with reduced CD8+ T-cell infiltration and poor prognosis in CRC (Liang et. al., 2025). Further, PVR expression in macrophages and CRC cells is known to be regulated by ADAR-mediated RNA editing of the 3′-UTR of *PVR* mRNA, increasing its stability and expression. The manipulation of ADAR levels was shown to alter both *PVR* mRNA editing and expression which suggests post-transcriptional mechanisms contributing to immune evasion and tumor progression (Qian et. al., 2023).

It is known that REVERBα primarily acts as a transcriptional repressor of genes upon binding to DNA elements. To exert its repressive functions, REVERBα has to recruit the nuclear receptor co-repressor (NCoR) and histone deacetylase 3 (HDAC3) complex. This whole complex leads to chromatin condensation and therefore suppression of gene transcription. In addition to the direct binding of REVERBα to promoter elements, it can also repress gene expression by inhibiting the activity of distal enhancers. This is done by blocking transcription of enhancer RNAs (eRNAs) which are crucial for optimal enhancer function and activation of nearby genes (Lam et. al., 2013). The dual ability of REVERBα occupying retinoid-orphan receptor (ROR) responsive element (RORE) motifs in promoters while simultaneously engaging in enhance function underscores its broader influence over chromatin accessibility and transcriptional timing. ROREs typically consist of a 6 bp AT-rich sequence directly followed by a conserved AGGTCA motif, serving as binding sites for both REVERBα and activating receptor tyrosine kinase-like orphan receptors (RORs). This creates a competitive regulatory system maintaining the circadian oscillation of gene expression (Preitner et. al., 2002), (Jetten et. al., 2009). Given that REVERBα typically binds RORE motifs, the probability is high that similar elements are present in the *PVR* promoter, underlying the direct binding of REVERBα observed in the shown ChIP data.

This potential RORE-mediated control of the *PVR* gene highlights that REVERBα may act alongside other cytokine-driven pathways, creating a complex balance of regulation in macrophages within the CRC microenvironment.

While REVERBα exerts oscillative repression, tumor-derived signals and other alternative transcription factors can actively induce *PVR* expression (Molfetta et. al., 2020). Other studies revealed that the secretion of IL-4 by CRC cells trigger the expression of PVR in macrophages promoting their transition into an anti-inflammatory or immunosuppressive M2-like phenotype (van Dyken and Locksley ,2013), (Wang et. al., 2018). Further, the persistent activation of aryl-hydrocarbon receptor (AhR) in macrophages via IL-4 and lipopolysaccharide (LPS) leads to an upregulation of PVR transcription which is often co-expressed with PD-L1 on TAMs suggesting a shared regulatory mechanisms and roles in immune evasion (McKay et. al., 2021). These mechanisms drive immunosuppression and tumor progression, making PVR a promising target in CRC. In this context, investigating whether REVERBα regulates the *PVR* gene expression in a direct or indirect way is essential to unravel how metabolic and circadian signals influence the immune checkpoint dynamics in CRC. Moreover, the findings depicted in Fig.13 demonstrated for the first time that REVERBα directly binds to the human *PVR* gene promoter region in macrophages indicating possible regulatory functions.

4.3 Ligand-mediated modulation of REVERBα activity

REVERBα is a ligand-dependent nuclear receptor whose transcriptional activity can be modulated by both endogenous ligands like heme and also synthetic small molecules (Raghuram et. al., 2007). Heme for instance is the best characterized physiological ligand of REVERBα, binding directly to REVERBα´s ligand-binding domain (LBD) (Yin et. al., 2007). This ligand binding to the LBD stabilizes the interaction of the NCoR-HDAC3 co-repressor complex promoting transcriptional repression (Yin et. al., 2007). In turn, this allows REVERBα to act as a metabolic sensor, linking the timing of circadian rhythm, nutrient status and immune function. Not only acts REVERBα as a gatekeeper in circadian rhythm by repressing genes like *BMAL1* (Yin and Lazar, 2005) and many more, but it also controls genes involved lipid and glucose metabolism acting as a sensor of nutrient availability (Zhang et. al., 2015), (Delezie et. al., 2012). Consequently, REVERBα can be modulated in its function by

physiological or synthetic ligands. Among synthetic modulators, SR9009 and SR9011 represent widely used REVERBα agonists (Kojetin and Burris, 2014). These agonists enhance the recruitment of NCoR-HDAC3 to target genes, suppressing the transcription of genes involved in mitochondrial function, lipid metabolism and inflammatory signaling (Solt et. al., 2012). As suggested by Sulli et. al., 2018, the pharmacological activation of REVERBα represents a promising anti-cancer strategy. Both REVERBα agonists SR9009 and SR9011 exert anti-tumor effects by affecting a number of oncogenic drivers, such as HRAS, BRAF and PIK3CA with efficacy sustained even in p53-deficient or hypoxic conditions. Moreover, REVERBα has been implicated in limiting cancer progression through the suppression of cell proliferation, *de novo* lipogenesis and autophagy, alongside the induction of apoptosis in malignant cells (Wang et. al., 2020). Conversely, REVERBβ, displays an opposing pattern with elevated expression reported in breast cancer, suggesting potential or distinct roles of REVERBs in tumor biology (Sulli et. al., 2018).

Furthermore, the identification of heme as natural ligand of REVERB has facilitated the development of novel synthetic modulators, such as GSK4112 (SR6472) (Grant t. al., 2010). Although GSK4112 has poor pharmacokinetics limiting *in vivo* use, this agonist proved to be a valuable *in vitro* tool, demonstrating that REVERBα activation can suppress NF-κB signaling, inhibit NLRP3 inflammasome activity and is capable to reduce pro-inflammatory cytokine production (Wang et. al., 2018), (Guo et. al., 2019). In addition, GSK4112 has been shown to impair cancer cell proliferation, promote apoptosis and decrease glycolysis in cancer cells by downregulating key metabolic and cell cycle genes (Morioka et. al., 2016). Further, SR9009 treatment in macrophages decreased pro-inflammatory M1-like macrophages polarization and resulted in reduced expression of cytokines such as IL-6 and TNFα (Gibbs et al., 2012). On the other side, the REVERB-modulating ligand SR8278 resembles a competitive antagonist of REVERBα which prevents the recruitment of NCoR and HDAC3 co-repressors, thereby relieving transcriptional repression (Kojetin et. al., 2011). Despite its poor pharmacokinetic properties and a short half-life, SR8278 treatment of mice resulted in decreased plasma levels and hepatic homocysteine, indicating that REVERBα antagonism may exert protective effects against hyperhomocysteinemia (Zhang et. al., 2019). Additionally, SR8278 has been reported to enhance lean body mass and improve muscle function dystrophic *in vivo* models. This effect can be linked to the activation of Wnt signaling pathway (Tao et. al., 2019). Further on, SR8278

treatment in macrophages has been associated with increased expression levels of REVERBα target genes, enhanced pro-inflammatory responses and an altered circadian rhythm in immune gene expression. For instance, inhibiting of REVERBα-mediated repression of *Ccl2* before an active cycle of vesicular stomatitis virus infection showed to decrease survivability of mice. This suggests REVERBα-mediated suppression of *Ccl2* exerts protective effects against encephalitis and neuroinflammation (Gagnidze et. al.,2016). Another study showed that blocking REVERBα function via SR8278 antagonist resulted in a resistance of elderly mice to pneumococcal infection. In particular, pneumococcal infection has been associated with aging, likely due to changes in daily oscillations in gene expression and pathways. Rhythmic profiles were shown to be evident in young mice while profiles where non-rhythmic or time shifted in elderly mice. Moreover, REVERBα plays an essential role in modulating bacterial clearance by regulating. macrophage phagocytosis in a circadian manner (Angulo et. al., 2025). Several small-molecule ligands have been developed to modulate REVERBα function and activity, with many varying in specificity and pharmacokinetic properties (Kojetin and Burris, 2014). Natural compounds like berberine and puerarin provide structurally distinct scaffolds mimicking REVERBα agonists and antagonists, but their selectivity remains insufficiently validated (Zhou et. al., 2020), (Chen et. al., 2020). Overall, these ligands highlight the pharmacological versatility of REVERBα targeting, also underscoring the importance of evaluating off-target effects (Wang et. al., 2020).

While the direct effects of REVERBα SR9009 agonist or SR8278 antagonist have not yet been explored in CRC, their ability to alter the expression of genes such as *PVR* points out potential roles in modulating immune checkpoint pathways and consequently tumor-immune interactions. As shown here, the ChIP experiments confirmed the direct binding of REVERBα protein to the human *PVR* promotor (Fig.13). We predicted a putative RORE or REVERBα responsive element (RevRE) DNA motif using Alibaba software (Grabe, 2002) as a potential binding site for REVERBα in the proximal human *PVR* gene promotor. Classic RORE binding motifs have the following sequence: AA/TNTAGGTCA (Preitner et. al.,2002). However, future mutagenesis studies need to finally prove if this DNA motif is the only target site or other element are involved in addition. In line with these results, our ChIP and luciferase assays confirmed that SR9009 agonist and SR8278 antagonist directly modulate REVERBα-*PVR* interactions. Our findings support the fact that REVERBα act as a transcriptional

repressor of the *PVR* gene in THP-derived macrophages and cancer cells, showing that its activity can be modulated pharmacologically. The activation via the SR9009 agonist consistently reduced REVERBα binding to the human *PVR* promoter and downregulated its expression, whereas the SR8278 antagonist evoked the opposite effect, causing a de-repression (Fig. 20). These ligand-dependent effects were observed in THP1-derived as well as in reporter assays with human cancer cells, underscoring the robustness of this regulatory mechanism (Fig. 21). Together, these results highlight REVERBα as a crucial regulator of human *PVR* gene transcription, suggesting that pharmacological modulation of REVERBα activity could represent a strategy to influence macrophage immunoregulatory functions and potentially reshaping the tumor immune microenvironment.

Consistently, studies showed that REVERBα binds to glucocorticoid and hepatocyte nuclear factors at promoters and enhancers of genes which are involved in carbohydrate and lipid metabolism. Some examples of such genes in mice are *Irs1* (insulin receptor substrate 1), *Gck* (glucokinase), *Dgat2* (diacylglycerol O-acyltransferase 2) and *Lpin2* (Lipid phosphate phosphatase 2) which are all expressed in a circadian manner (Carrati et. al., 2018). Moreover, REVERBα is able to bind to its own promoter via the REVERBα-responsive element (RevRE) repressing its own transcription through a negative feedback loop. This autoregulatory binding of REVERBα protein to its own promoter is essential for maintaining the rhythmic circadian oscillation and stability of not only REVERBα mRNA and protein itself, but also of other genes regulated by REVERBα (Adelmant et. al., 1996), (Bugge et. al., 2012). In line with this, bioinformatic and experimental studies confirmed that REVERBα targets a wide set of promoters containing RevRE motifs especially in genes which are involved in circadian regulation and metabolism (Kumaki et. al., 2008). These findings highlight that the regulatory role of REVERBα extends beyond metabolic and circadian genes to immune checkpoint genes, as exemplified here for the *PVR* gene.

Considering that REVERBα act as a metabolic and transcriptional regulator in macrophages, its modulation via SR9009 agonist and SR8278 antagonist may be extended beyond checkpoint regulation and directly influence efferocytosis. It is well known that efferocytosis represents a key function of macrophages, maintaining tissue homeostasis and anti-tumor immunity by clearing apoptotic malignant cells (Werfel & Cook, 2018). Efferocytosis assays with PBMC-derived primary macrophages treated

with SR9009 agonist or SR8278 antagonist demonstrated an altered macrophage behaviour regarding the efferocytosis of tumor cells (Fig.28). A higher efferocytosis rate was observed in pro-inflammatory M(LPS/IFNγ) macrophages, when compared to macrophages with an anti-inflammatory M(IL4/IL13) phenotype. The higher efferocytosis in pro-inflammatory macrophages might be induced due to the applied treatments, but there was no clear evidence if REVERBα ligands directly alter efferocytosis. Furthermore, it is well-known that anti-inflammatory “M2-like” macrophages exert a higher efferocytotic activity than pro-inflammatory “M1-like” macrophages (Yurdagul et. al., 2017). Additionally, this higher efferocytosis of M2-like macrophages drives immunosuppressive responses leading to the secretion of IL-10, TGF-β and VEGFA supporting tissue repair, angiogenesis and tumor progression (Yurdagul et. al., 2017).

As discussed above, the CRISPR/Cas9 modification of *REVERBα* gene not only impacted REVERBα function itself, but also altered the function of THP1-derived macrophages. For example, a significant higher tumor cell efferocytosis was observed in all CRISPR/Cas9-modified THP1-derived macrophages when compared to the empty vector control (Fig.27). Moreover, a similar effect trending to higher phagocytosis was evident in all CRISPR/Cas9-modified macrophages (Fig.26).

It is known that REVERBα represses the expression of several cytokines and immune relevant factors including IL-10 (Chandra et. al., 2013). In general, IL-10 plays a crucial role in the modulation of inflammation, immune response and homeostasis. Specifically, IL-10 acts as an anti-inflammatory or immunosuppressive cytokine, downregulating the function of dendritic cells, monocytes and macrophages. On the other hand, IL-10 is also able to exerts immunostimulatory effects on NK cells, T-cells and B-cells (Carlini et. al., 2023), (Iyer and Cheng, 2012). Moreover, recent studies revealed that IL-10 and its associated signaling molecules increased CRC progression, suggesting potential oncogenic roles and prognostic relevance (Aslam et. al., 2025). A significant higher expression of IL-10 was evident in CRISPR/Cas9- modified THP1-derived macrophages having dysfunctional REVERBα protein (Fig.22 (B)). This finding highlights that IL-10 may not only be directly regulated by REVERBα, but may also act as a downstream target, similar to the PVR, thereby possibly contributing to altered cancer cell survival in the tumor tissue microenvironment of CRC.

Taken together, these data emphasize the multifaceted role of REVERBα in regulating and modifying macrophage effector phenotypes. The modification of REVERBα

function, either through CRISPR/Cas9 or ligand treatment, was found to alter macrophage functions, resulting in elevated effero- and phagocytosis rates in both THP1- and PBMC-derived primary macrophages. Not only did CRISPR/Cas9-modification of the *REVERBα* gene impact its function, but REVERBα ligand treatment also altered *PVR* expression, suggesting that targeting of REVERBα could open new possibilities for immune-related therapeutic options in CRC.

Despite these insights, the mechanisms of macrophage modulation by REVERBα still remains to be fully deciphered. The final question arising is whether pharmacological or genetic targeting of REVERBα could be exploited therapeutically, to enhance anti-cancer properties of macrophages within the TME of colorectal cancer cells *in vitro* and *in vivo*. In particular, it remains to be determined how the modulation of REVERBα might act synergistically together with PVR blocking antibodies, an aspect which will be discussed in the following section.

4.4 Impact of REVERBα modulation and immune checkpoint blockade on macrophage-tumor cell interactions

Macrophages play a dualistic role in the CRC microenvironment functioning either as tumor-promoting or tumor-suppressing immune cells, dependent on their polarization state and expression profile of immune checkpoints (Pathria et. al., 2019). As mentioned earlier, the PVR-TIGIT axis emerged as a central mechanism through which TAMs promote immune evasion, highlighting its relevance as an immune checkpoint system (Hou et. al., 2024). As mentioned in the introduction, the PVR is a central ligand of TIGIT which makes it a key immunosuppressor across cancers. For example, studies on CRC linked higher PVR-TIGIT signaling to worse outcomes and immune evasion which underscores PVR as checkpoint for immunotherapies (Cao et. al., 2025), (Liang et. al., 2025). In CRC, TAMs are known for shaping immune escape and therapeutic responses, making them promising targets for CRC therapy (Hou et. al., 2024). Moreover, the nuclear receptor REVERBα has gained attention as an immune metabolic checkpoint in macrophages. As outline before, REVERBα represses gene expression by recruiting NCoR and HDAC3 to promoter or enhancer regions (Wang et. al., 2020). Furthermore, SR9009 agonist and SR8278 antagonist are examples of widely used tools to modulate REVERBα function (Solt et. al., 2014), (Kojetin et. al., 2011).

The circadian control of genes is increasingly tied to immune checkpoint inhibitor efficacy. For instance, clinical and pre-clinical work indicate that the CLOCK status and time of dose can modulate immune checkpoint inhibitor outcomes, providing mechanistic insights to test CLOCK-guided or REVERBα-guided strategies together with PVR-TIGIT and other immune checkpoint blockade (Karaboué et. al., 2024), (Nagy et. al., 2025). Together the pharmacological activation of REVERBα via SR9009 agonist in macrophages may lower PVR expression or alter its dynamics, reducing the inhibitory input to TIGIT, thus sensitizing the microenvironment to TIGIT blockade, whereas SR8278 antagonism could exert opposite effects. To date, no direct regulation of *PVR* gene expression by REVERBα has been demonstrated, nor has its effect on macrophages within the TME been explored or described in the literature.

Macrophages play a central regulatory role in progression of CRC, either supporting tumor growth through immunosuppressive polarization or by contributing to anti-tumor activity upon activation (Edin et. al., 2012). To elucidate the role of REVERBα, CRISPR/Cas9-modified THP1-derived macrophages harbouring unmodified ("wildtype") or dysfunctional REVERBα were co-cultivated with CRC cells in direct physical contact. This allowed to understand how the genetic disruption of the *REVERBα* gene affects the ability of macrophages to modulate tumor cell survival. By further introducing REVERBα ligands, pharmacological modulation of REVERBα offers a double tracked impact. For instance, REVERBα ligands may alter cancer cell metabolism directly, while simultaneously reprogramming macrophage function within the TME. The use of CRISPR/Cas9-modified THP1-derived macrophages in co-cultures with HT29 cancer cells provided a framework to dissect these direct and indirect effects, and to finally evaluate whether ligand-mediated modulation of REVERBα impacts the macrophage-tumor crosstalk and its interactions towards a tumoricidal outcome. In the 3D co-cultures (Fig.29/30), THP1-derived macrophages with dysfunctional REVERBα significantly increased CRC cell death when compared to the empty vector control. SR9009 agonist had no effect on the viability of the HT29 cancer cells. One noteworthy observation found in Fig.30 (A) revealed the de-stabilization of HT29 cancer cell viability upon SR8278 antagonist treatment in co-culture.

REVERBα is known to directly repress murine CCL2 and IL6 expression in macrophages, and loss of REVERBα results in elevated expression levels of these cytokines (Sato et. al., 2014). The fact that CCL2 and IL6 represent two cytokines

which are crucial for shaping macrophage behaviour, modulation of REVERBα within the TME marks an important regulatory mechanism in controlling macrophage function and immune response in CRC. For example, the CCL2 pathway has been shown to drive TAM recruitment and anti-inflammatory “M2-like” macrophage polarization, fostering a pro-tumorigenic microenvironment, further promoting liver metastasis in CRC (Grossman et. al., 2018). In addition, IL6 exerted from macrophages drives STAT3 activation in neighbouring CRC cells, altering their phenotype and potentially increasing tumor cell survival (Kawamura et. al., 2024). Taken together, the effects of CCL2 and IL6 exerted on macrophage function and tumor cell viability underscore the importance of cytokine-directed reshaping of TME. Thus, REVERBα may act as a critical regulatory factor which is capable of restraining this inflammatory axis within the TME. This may explain the cause why SR8278 antagonist treatment (Fig.30 A) significantly decreased HT29 cancer cell survival. Furthermore, REVERBα is also known to repress NFκB and NLRP3 signaling, which are known to be negative regulators of inflammation. Wang et. al. 2018 showed that missing or dysfunctional REVERBα causes activation of NLRP3 inflammasome, thus promoting ulcerative colitis in mice. In general, REVERBα represses NFκB and NLRP3 targeted genes. Therefore, genetic loss or antagonism via SR8278 treatment shall de-repress this pathway, increasing pro-inflammatory cytokines and inflammasome activation (Pourcet et. al., 2018). Thus, reprogramming TAMs from immunosuppressive M2-like state towards a pro-inflammatory M1-like phenotype may reduce cancer cell viability by shifting the TME into an active tumoricidal niche, driven by macrophages.

Moreover, it is a well-known fact that PVR is highly expressed in CRC contributing to immune cell escape. Recent studies showed that high PVR expression negatively correlated with poor prognosis in CRC patients (Murakami et. al., 2022). Furthermore, PVR is regulated by the PI3K/Akt/NFκB pathway, which contributes to the depletion of cytotoxic CD8+ T-cells and the reduction on their effector activity (Liang et. al., 2025). Studies with specimens from human CRC patients evinced robust expression of PVR promoting polarization towards anti-inflammatory “M2-like” macrophages and CRC progression (Zhu et. al., 2022). To date, latest findings on targeting PVR-TIGIT checkpoint axis revealed the effective blocking of PVR-related immune globulin domain (PVRIG) with a bi-specific antibody, co-targeting both PVR and TIGIT. Enhanced anti-tumor immunity was evident making this a promising approach for further investigation in clinical trials (Lin et. al., 2025).

Co-culturing PBMC-derived macrophages with HT29 cancer cells revealed an impact on cancer cell viability upon PVR and CD47 blocking antibodies and REVERBα ligand treatment. A significant reduction of HT29 viability was evident in all treatment conditions when compared with the control (Fig. 31). Comparing the results of Fig.31 with Fig.32, neither the blocking antibodies nor the REVERBα ligands had a significant effect on reducing the viability of PBMC-derived macrophages. These results are consistent with the findings shown in Fig.34, which similarly demonstrated no impact on macrophage viability by any of the tested antibodies. According to data presented in Fig.33 significant higher levels of necrosis were evident in all pro-inflammatory macrophages and macrophages treated with anti-PVR and anti-CD47 antibodies, suggesting the following two conclusions. First, macrophages polarized to pro-inflammatory phenotype are known to suppress proliferation of CRC cells (Chiang et. al., 2023) and to induce necrosis in cancer cells via the release of pro-inflammatory cytokines as TNFα or reactive oxygen species (Pan et. al., 2020). Second, the increase upon treatment with PVR and CD47 blocking antibodies in the number of necrotic CRC cells in co-cultures with anti-inflammatory M(IL4/IL13) macrophages gave a hint of a possible re-polarization of macrophages towards a pro-inflammatory state exerting anti-tumor properties. Furthermore, co-cultures with organoids from patient no.22 (Fig.35) harbouring *TP53*, *KRAS* and *APC* mutations, demonstrated a significant reduction in CRC cell viability following PVR antibody treatment, consistent with the results shown by Fig.31. In addition, subsequent co-cultures with organoids from patient no.7 (Fig.41) carrying *KRAS* and *APC* mutations, showed a similar decrease in CRC cell viability as those PDOs from patient no.22 (Fig.35), indicating that PVR blockade may contribute to higher CRC cell death. These findings raise the possibility that PVR blockade may restore or enhance macrophage functions within the CRC microenvironment, shifting them towards a more anti-tumor, pro-inflammatory phenotype. As mentioned above, related studies demonstrated that PVR expression on tumor-associated macrophages promote a more “M2-like” immunosuppressive phenotype facilitating CRC progression (Zhu et. al.,2022). Thus, disrupting the PVR-TIGIT axis could relive immune checkpoint suppression of macrophages and foster their anti-tumor properties. In contrast to the observed antagonist-induced necrosis phenotype (Fig.37 B), neither the REVERBα agonist nor the antagonist significantly impacted the viability and apoptotic death types in co-cultures with PDO22, consistent

with the concept that a “lytic” cell death increases host inflammation response to improve response to ICI therapies (Huang et. al., 2025).

Moreover, no direct effect of REVERBα ligands could be linked to the decreased viabilities of PDOs in all co-cultures (Fig.35/40), suggesting an a priori drug resistance of the PDOs (Betge et. al., 2022). Turning to another important aspect, it should be noted that all co-culture experiments and most readouts were performed at daytime. Given the circadian nature of REVERBα, which expression is lower at daytime (Fig.11), the expression level at the time the experiments were performed may have influenced the actual observations. Alongside this, the high PDO viability in untreated co-cultures with anti-inflammatory M(IL4/IL13) PBMC-derived primary macrophages underscore the typical characteristics of tumor-associated macrophages, stabilizing and fostering tumor growth (Fig.35). In line with the findings in Fig.32, PBMC-derived primary macrophages maintained high viability under all co-culture and treatment conditions (Fig.36). Overall, these findings demonstrate that functional PVR-blocking antibodies displayed no direct cytotoxic effects on macrophages or HT29 cancer cells alone (Fig.34), but enhanced CRC cell killing when combined with macrophages emphasizing their potential as an effective strategy to boost macrophage-mediated anti-tumor responses against CRC.

Despite the mechanistic insights gained through *in vitro* co-culture systems, several limitations must be considered. Firstly, these models lack the of full immune complexity and key physiological features such as hypoxia, microbiota-derived metabolites and a full cytokine milieu, each of which significantly impacts macrophage behaviour and PVR expression. Additionally, gut microbiota metabolites such as butyrate and succinate have been shown to modulate macrophage function with succinate impairing phagocytosis, while butyrate and other similar short-chain fatty acids enhance macrophage phagocytosis activity (O'Callaghan et. al., 2021), (Garavaglia et. al., 2025). Furthermore, different cytokine-driven artificial activation states of macrophages *in vitro* may also alter PVR expression and macrophage function, reflecting the limitations of a simplified environment. In addition, several cross-talk signals are missed, for example TIGIT T-cell suppression or NK-cell cytotoxicity, which are major targets of PVR. Further on, macrophage heterogeneity plays also a crucial role, like the fact that PBMC-derived macrophages are not the same as TAMs resident in CRC tissue. These TAMs from CRC tissue are shaped by the environment of chronic hypoxia, metabolic gradients and cytokine-rich TME. For instance, it is known that

hypoxic conditions within the TME drive macrophage polarization towards an anti-inflammatory M2-like phenotype and enhance immune suppression (He and Zhang, 2021), (Bai et. al., 2022). While 2D co-cultures cannot recapitulate stromal and endothelial components, PDO cultures with extracellular matrices such as Matrigel® for instance, create an 3D microenvironment closer to the physiological conditions (Kim et. al., 2022). Secondly, translational limitations must be considered like the pharmacokinetics of REVERBα ligands may act differently under physiological conditions due to metabolism and drug clearance (Solt et. al., 2012), (Rahman and Hegazy, 2024). Finally, while *in vitro* assays are invaluable for uncovering potential mechanistic insights, they do not reliably predict the efficiency of PVR blockade *in vivo*, especially in context of immune exhaustion, tumor heterogeneity and adaptive resistance pathways.

Moreover, similar studies revealed that dual blocking of CD47/SIRPα and PVR/TIGIT pathways, together with azelnidipine, promotes macrophage-mediated phagocytosis of tumor cells *in vitro* and suppresses tumor growth *in vivo*, at least in part by augmenting both innate and adaptive immune responses (Zhou et. al., 2021). While most studies focus on T-cells and NK cells, evidence suggests that blocking PVR can support the reprogramming of TAMs from pro-tumor to an anti-tumor phenotype, enhancing their ability to attack colorectal cancer cells (Mantovani et. al., 2017). Finally, these findings suggest that PVR blockade represents a promising strategy to enhance macrophage-mediated tumor cytotoxicity, especially when combined with other immune checkpoint inhibitors.

4.5 Conclusion and future perspectives

This doctoral thesis provides novel insights into the role of REVERBα in macrophage-mediated anti-tumor immunity in colorectal cancer, with specific focus on the regulation of the PVR-TIGIT immune checkpoint axis. Through genetic modification of *REVERBα* via CRISPR/Cas9 and its pharmacological modulation using synthetic ligands, the results presented here revealed that REVERBα functions not only as a circadian and metabolic regulator, but also as a transcriptional modulator of immune checkpoint expression. The experiments conducted demonstrated that REVERBα directly binds the *PVR* gene promoter and that ligand treatment fine-tunes this regulatory capacity, leading to significant changes in *PVR* gene expression and macrophage function. As illustrated in concluding Fig.42, the SR90909 agonist treatment lowered the *PVR* expression and promoter activity, whereas antagonism by SR8278 increased both.

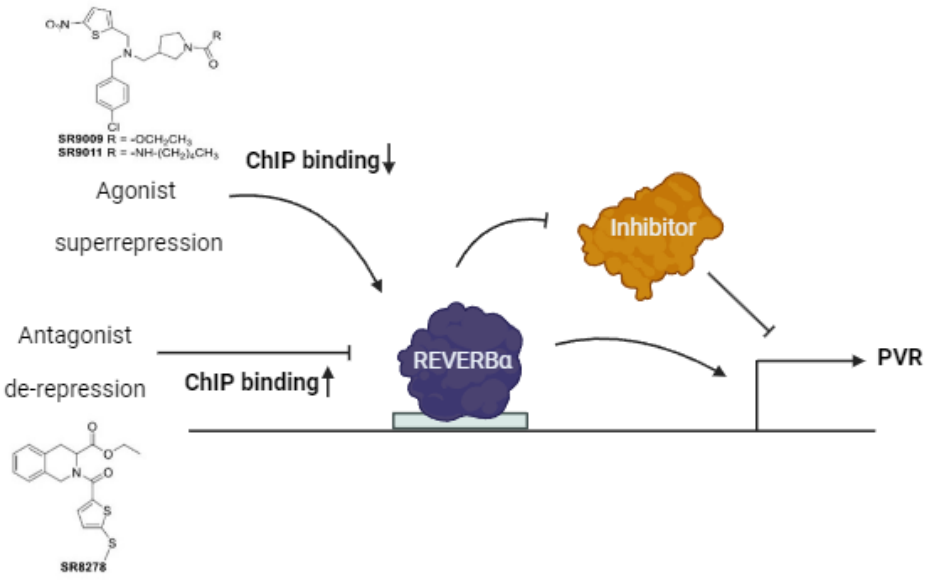

Fig.42 Model of regulation of PVR by REVERBα For gene repression, REVERBα recruits NCOR1 (nuclear receptor corepressor 1) and HDAC3 (histone deacetylase complex 3) to act as a transcriptional repressor. The small molecule drug-like SR9009 agonist reduced binding of REVERBα to the *PVR* gene promotor leading to *super-repression* of the gene (thus less *PVR* mRNA). In contrast, the SR8278 antagonist enhanced binding of REVERBα to the *PVR* gene promotor resulting in *de-repression* of *PVR* gene expression (thus more *PVR* mRNA). REVERBα may thus act as an indirect positive modulator of *PVR* expression suggesting the therapeutic use of REVERBα agonists against CRC. This model is consistent with “Pharmacological activation of REV-ERBs is lethal in cancer and oncogene-induced senescence” by Sulli et al. (*Nature. 2018;553(7688):351*) and may involve an additional inhibitor or trans-repressor complex yet to be identified.

In line with this, changes coincide with altered macrophage behaviour e.g., effero- and phagocytosis. Importantly, this work uncovers the first evidence of a mechanistic link between REVERBα and the PVR-TIGIT pathway in macrophages, thereby expanding the understanding of transcriptional regulation of immune checkpoints, in this case PVR. However, whether these effects translate into clinically relevant outcomes is still an open question.

Functionally, the CRISPR/Cas9-mediated modification of REVERBα revealed an altered ligand sensitivity and changes in macrophage behaviour, including enhanced effero- and phagocytosis as well as altered cytokine expression, underlining the importance of REVERBα integrity for macrophage function. Furthermore, co-culture experiments with HT29 colorectal cancer cells and PDOs highlighted that blocking PVR significantly influenced tumor cell viability through macrophage effector functions, underscoring their central role in shaping anti-tumor immunity. Nonetheless, several limitations must be considered. The used *in vitro* systems provide valuable mechanistic insights, but do not fully recapitulate the complexity of a tumor-microenvironment and the diversity of several immune cell subsets. Moreover, REVERBα ligands like SR9009 and SR8278 are limited by their poor pharmacokinetics and potential off-target effects. Further studies should therefore validate these findings in *in vivo* colorectal cancer cell models, ideally by combining REVERBα targeting and immune checkpoint blockade. Looking forward, for future studies three promising avenues emerge from this work. First, *in vivo* validation of REVERBα modulation in mouse CRC models, tracking *PVR* gene expression, macrophage status and synergistic effects with blocking PVR or PD-L1 for instance, will give more in-depth insight into how REVERBα shapes immune checkpoint regulation and macrophage function within a complex TME. This *in vivo* validation has already started by treating gastrointestinal tumor mouse models with REVERBα ligands in our research group (D. Kato et al. unpublished). Second, a mechanistic mapping of REVERBα target gene interactions is required, including defining the REVERBα co-repressor/co-factor complex at the *PVR* gene promoter, investigating the loss of ligand sensitivity observed in CRISPR/Cas9-modified cell clones. This unravelling of REVERBα target interactions could identify novel intervention points for enhancing the efficacy of macrophage-based immunotherapies. Third, applying chrono-translation to REVERBα by integrating its rhythmic activity, immunometabolic functions, co-regulatory complexes as well as circadian oscillations

could identify novel therapeutic targets and provide insights into how chronobiology can be exploited to enhance immunotherapeutic effects in a time-of-day dependent manner.

To conclude, this PhD thesis uncovered REVERBα as a novel immune checkpoint modulator in macrophages and colorectal cancer, underscoring the importance of integrating circadian biology into cancer immunotherapy. Exploiting metabolic and transcriptional timing, these strategies may help to overcome immune suppression and ultimately improve outcomes for colorectal cancer patients. Altogether, these findings identify REVERBα as novel regulator of immune checkpoint dynamics, underscoring the potential of unexplored opportunities for integrating circadian biology into immunotherapy against colorectal cancer.

5. References

Adelmant, G., Begue, A., Stehelin, D., and Laudet, V. (1996). A functional Rev-erb alpha responsive element located in the human Rev-erb alpha promoter mediates a repressing activity. Proc Natl Acad Sci U S A 93, 3553-3558. 10.1073/pnas.93.8.3553.
Aisenbrey, E.A., and Murphy, W.L. (2020). Synthetic alternatives to Matrigel. Nat Rev Mater 5, 539-551.

Ali, S., Saik, J.E., Gould, D.J., Dickinson, M.E., and West, J.L. (2013). Immobilization of Cell-Adhesive Laminin Peptides in Degradable PEGDA Hydrogels Influences Endothelial Cell Tubulogenesis. Biores Open Access 2, 241-249.

Amin, M.B., Greene, F.L., Edge, S.B., Compton, C.C., Gershenwald, J.E., Brookland, R.K., Meyer, L., Gress, D.M., Byrd, D.R., and Winchester, D.P. (2017). The Eighth Edition AJCC Cancer Staging Manual: Continuing to build a bridge from a population-based to a more "personalized" approach to cancer staging. CA Cancer J Clin 67, 93-99.

Andre, T., Elez, E., Lenz, H.J., Jensen, L.H., Touchefeu, Y., Van Cutsem, E., Garcia-Carbonero, R., Tougeron, D., Mendez, G.A., Schenker, M., et al. (2025). Nivolumab plus ipilimumab versus nivolumab in microsatellite instability-high metastatic colorectal cancer (CheckMate 8HW): a randomised, open-label, phase 3 trial. Lancet *405*, 383-395. 10.1016/S0140-6736(24)02848-4.

Andre, T., Shiu, K.K., Kim, T.W., Jensen, B.V., Jensen, L.H., Punt, C., Smith, D., Garcia-Carbonero, R., Benavides, M., Gibbs, P., et al. (2020). Pembrolizumab in Microsatellite-Instability-High Advanced Colorectal Cancer. N Engl J Med *383*, 2207-2218. 10.1056/NEJMoa2017699.

Angulo, F.S., Trottein, F., Pourcet, B., et al. (2025). Rev-erb-α antagonism in alveolar macrophages protects against pneumococcal infection by reversing age-related decline in host defense. *Cell Rep.* 44, 115273.

References

Archilla-Ortega, A., Domuro, C., Martin-Liberal, J., and Munoz, P. (2022). Blockade of novel immune checkpoints and new therapeutic combinations to boost antitumor immunity. J Exp Clin Cancer Res *41*, 62. 10.1186/s13046-022-02264-x.

Aroca-Siendones, M. I., et al. (2021). "Core Circadian Clock Proteins as Biomarkers of Progression in Colorectal Cancer." Biomedicines 9(8).
Bateman, A.C. (2014). Pathology of serrated colorectal lesions. J Clin Pathol 67, 865-874.

Aslam, A., Refaat, B., Almaimani, R.A., Obaid, A.A., Mujalli, A., Farrash, W.F., Elzubier, M.E., Idris, S., Salaka, A., Almalki, A.H., et al. (2025). Increased protein expression of interleukin-10 and its signalling molecules in colon cancer progression: potential prognostic and therapeutic targets. Discov Oncol *16*, 637. 10.1007/s12672-025-02452-z.

Bai, R., Li, Y., Jian, L., Yang, Y., Zhao, L., and Wei, M. (2022). The hypoxia-driven crosstalk between tumor and tumor-associated macrophages: mechanisms and clinical treatment strategies. Mol Cancer *21*, 177. 10.1186/s12943-022-01645-2.

Balata, G.F., Azzam, H.N. (2025) Synopsis of colorectal cancer: prevalence, symptoms, screening, staging, risk factors, and treatment. *Egypt J Intern Med* **37**, 4.

Benson, A.B., Venook, A.P., Adam, M., Chang, G., Chen, Y.J., Ciombor, K.K., Cohen, S.A., Cooper, H.S., Deming, D., Garrido-Laguna, I., et al. (2024). Colon Cancer, Version 3.2024, NCCN Clinical Practice Guidelines in Oncology. J Natl Compr Canc Netw *22*. 10.6004/jnccn.2024.0029.

Betge, J., Rindtorff, N., Sauer, J., Rauscher, B., Dingert, C., Gaitantzi, H., Herweck, F., Srour-Mhanna, K., Miersch, T., Valentini, E., Boonekamp, K. E., Hauber, V., Gutting, T., Frank, L., Belle, S., Gaiser, T., Buchholz, I., Jesenofsky, R., Härtel, N., Zhan, T., … Boutros, M. (2022). The drug-induced phenotypic landscape of colorectal cancer organoids. *Nature communications*, *13*(1), 3135.

Boland, C.R., and Goel, A. (2010). Microsatellite instability in colorectal cancer. Gastroenterology 138, 2073-2087 e2073.

Brenner, H., Kloor, M., and Pox, C.P. (2014). Colorectal cancer. *Lancet* 383, 1490–1502.

Bugge, A., Feng, D., Everett, L.J., Briggs, E.R., Mullican, S.E., Wang, F., Jager, J., and Lazar, M.A. (2012). Rev-erbalpha and Rev-erbbeta coordinately protect the circadian clock and normal metabolic function. Genes Dev *26*, 657-667. 10.1101/gad.186858.112.

Buikhuisen, J.Y., Torang, A., and Medema, J.P. (2020). Exploring and modelling colon cancer inter-tumour heterogeneity: opportunities and challenges. Oncogenesis 9, 66.

Burris, T.P. (2008). Nuclear hormone receptors for heme: REV-ERBalpha and REV-ERBbeta are ligand-regulated components of the mammalian clock. Mol Endocrinol *22*, 1509-1520. 10.1210/me.2007-0519.

Burgermeister, E., et al. (2019). "Aryl hydrocarbon receptor nuclear translocator-like (ARNTL/BMAL1) is associated with bevacizumab resistance in colorectal cancer via regulation of vascular endothelial growth factor A." EBioMedicine 45: 139-154.

Caceres-Matos, R., Castro-Méndez, A., Domínguez, M. G., Pabón-Carrasco, D., & Pabón-Carrasco, M. (2024). The Influence of Ultra-Processed Food on Colorectal Cancer: A Systematic Review. *Gastrointestinal Disorders*, *6*(1), 164-179.

Cao, S., Wang, M., Sun, W., Ma, Z., Yang, K., Li, T., Zhu, X., Pei, Y., Pan, M., Wang, L., and Ding, H. (2025). Identification of a TIGIT-expressing CD8(+) T cell subset as a potential prognostic biomarker in colorectal cancer. Front Immunol *16*, 1626367. 10.3389/fimmu.2025.1626367.

Caratti, G., Iqbal, M., Hunter, L., Kim, D., Wang, P., Vonslow, R.M., Begley, N., Tetley, A.J., Woodburn, J.L., Pariollaud, M., et al. (2018). REVERBa couples the circadian

clock to hepatic glucocorticoid action. J Clin Invest *128*, 4454-4471. 10.1172/JCI96138.

Carlini, V., Noonan, D.M., Abdalalem, E., Goletti, D., Sansone, C., Calabrone, L., and Albini, A. (2023). The multifaceted nature of IL-10: regulation, role in immunological homeostasis and its relevance to cancer, COVID-19 and post-COVID conditions. Front Immunol *14*, 1161067. 10.3389/fimmu.2023.1161067.

Cassetta, L. and J. W. Pollard (2018). "Targeting macrophages: therapeutic approaches in cancer." Nat Rev Drug Discov 17(12): 887-904.

Cen, B., Wei, J., Wang, D., Xiong, Y., Shay, J.W., and DuBois, R.N. (2021). Mutant APC promotes tumor immune evasion via PD-L1 in colorectal cancer. Oncogene.

Cha, Y., Cho, S.H., Park, E.Y., Lee, D.E., Park, T., Choi, M.K., Hwang, I.G., Beom, S.H., Kang, B.W., Kim, J.S., et al. (2025). Platform study of circulating tumor DNA directed adjuvant chemotherapy in colon cancer (CLAUDIA colon cancer, KCSG CO22-12). BMC Cancer *25*, 1373. 10.1186/s12885-025-14746-0.

Chandra, V., Mahajan, S., Saini, A., Dkhar, H.K., Nanduri, R., Raj, E.B., Kumar, A., and Gupta, P. (2013). Human IL10 gene repression by Rev-erbalpha ameliorates Mycobacterium tuberculosis clearance. J Biol Chem *288*, 10692-10702. 10.1074/jbc.M113.455915.

Chauvin, J.M., and Zarour, H.M. (2020). TIGIT in cancer immunotherapy. J Immunother Cancer 8.

Chauvin, J.M., Pagliano, O., Fourcade, J., Sun, Z., Wang, H., Sander, C., Kirkwood, J.M., Chen, T.H., Maurer, M., Korman, A.J., et al. (2015). TIGIT and PD-1 impair tumor antigen-specific CD8(+) T cells in melanoma patients. J Clin Invest 125, 2046-2058.

Della-Morte, D. (2019). "Deregulation of the circadian clock machinery: A novel biomarker for anti-angiogenic drug resistance in colorectal cancer." EBioMedicine 46: 17-18.

Chen, M., Zhou, C., Xu, H., Zhang, T., and Wu, B. (2020). Chronopharmacological targeting of Rev-erbalpha by puerarin alleviates hyperhomocysteinemia in mice. Biomed Pharmacother *125*, 109936. 10.1016/j.biopha.2020.109936.

Chen, X., Dong, X., Zheng, Y., Wang, C., Luo, Z., Xie, J., Guo, Z., Shi, X., Zhu, X., Xu, Y., et al. (2025). Global Trajectories of Colorectal Cancer Burden From 1990 to 2021 and Projection to 2040. Cancer Innov *4*, e70020. 10.1002/cai2.70020.

Chiang, E.Y., and Mellman, I. (2022). TIGIT-CD226-PVR axis: advancing immune checkpoint blockade for cancer immunotherapy. J Immunother Cancer *10*. 10.1136/jitc-2022-004711.

Chiang, C., Hixon, D., Mooradian, N., Kshetri, P., Valena, S., Lau, R., Ambrose, C., Doche, M., Hill, R., and Mumenthaler, S. (2023). Exploring the interplay between macrophage subtypes and colorectal cancer cell growth. *Cancer Immunol. Res.* 11 (Suppl. 1), A017.

Cho, H., Zhao, X., Hatori, M., Yu, R.T., Barish, G.D., Lam, M.T., Chong, L.W., DiTacchio, L., Atkins, A.R., Glass, C.K., et al. (2012). Regulation of circadian behaviour and metabolism by REV-ERB-alpha and REV-ERB-beta. Nature *485*, 123-127. 10.1038/nature11048.

Cui, H., Hamad, M., and Elkord, E. (2025). TIGIT in cancer: from mechanism of action to promising immunotherapeutic strategies. Cell Death Dis *16*, 664. 10.1038/s41419-025-07984-4.

Dekker, E., Tanis, P.J., Vleugels, J.L.A., Kasi, P.M., and Wallace, M.B. (2019). Colorectal cancer. Lancet *394*, 1467-1480. 10.1016/S0140-6736(19)32319-0.

Della-Morte, D. (2019). Deregulation of the circadian clock machinery: A novel biomarker for anti-angiogenic drug resistance in colorectal cancer. EBioMedicine *46*, 17-18. 10.1016/j.ebiom.2019.08.003.

References

Delezie, J., Dumont, S., Dardente, H., Oudart, H., Gréchez-Cassiau, A., Klosen, P., Teboul, M., Delaunay, F., Pévet, P., and Challet, E. (2012). The nuclear receptor REV-ERBα is required for the daily balance of carbohydrate and lipid metabolism. *FASEB J.* 26, 3321–3335.

Dos Santos, I.B., da Costa, A.C.A., Gellen, L.P.A., Sales, L.L.S., Monte, N., de Moraes, F.C.A., Santo, M.O.M., Rodrigues, J.C.G., de Assumpcao, P.P., Guerreiro, J.F., et al. (2025). Identification of genomic variants associated with colorectal cancer heredity in indigenous populations of the Amazon. Sci Rep *15*, 14616. 10.1038/s41598-025-87401-0.

Dougall, W.C., Kurtulus, S., Smyth, M.J., and Anderson, A.C. (2017). TIGIT and CD96: new checkpoint receptor targets for cancer immunotherapy. Immunol Rev *276*, 112-120. 10.1111/imr.12518.

Drost, J., and Clevers, H. (2018). Organoids in cancer research. Nat Rev Cancer *18*, 407-418. 10.1038/s41568-018-0007-6.

Dunne, P.D., and Arends, M.J. (2024). Correction to: Molecular pathological classification of colorectal cancer-an update. Virchows Arch *484*, 287. 10.1007/s00428-024-03773-0.

Dunn, G.P., Old, L.J., and Schreiber, R.D. (2004). The immunobiology of cancer immunoediting and immunosurveillance. *Immunity* 21, 137–148.

Edin, S., Wikberg, M.L., Dahlin, A.M., Rutegard, J., Oberg, A., Oldenborg, P.A., and Palmqvist, R. (2012). The distribution of macrophages with a M1 or M2 phenotype in relation to prognosis and the molecular characteristics of colorectal cancer. PLoS One 7, e47045.

Everett, L.J., and Lazar, M.A. (2014). Nuclear receptor Rev-erbalpha: up, down, and all around. Trends Endocrinol Metab *25*, 586-592. 10.1016/j.tem.2014.06.011.

Fearon, E.R., and Vogelstein, B. (1990). A genetic model for colorectal tumorigenesis. Cell *61*, 759-767. 10.1016/0092-8674(90)90186-i.

Fleming, M., Ravula, S., Tatishchev, S.F., and Wang, H.L. (2012). Colorectal carcinoma: Pathologic aspects. J Gastrointest Oncol 3, 153-173.

Fortin, B. M., et al. (2024). "Circadian control of tumor immunosuppression affects efficacy of immune checkpoint blockade." Nat Immunol 25(7): 1257-1269.

Fujii, M., Clevers, H., and Sato, T. (2019). Modeling Human Digestive Diseases With CRISPR-Cas9-Modified Organoids. Gastroenterology 156, 562-576.

Gagnidze, K., Hajdarovic, K.H., Moskalenko, M., Karatsoreos, I.N., McEwen, B.S., and Bulloch, K. (2016). Nuclear receptor REV-ERBalpha mediates circadian sensitivity to mortality in murine vesicular stomatitis virus-induced encephalitis. Proc Natl Acad Sci U S A *113*, 5730-5735. 10.1073/pnas.1520489113.

Galassi, C., Chan, T.A., Vitale, I., and Galluzzi, L. (2024). The hallmarks of cancer immune evasion. Cancer Cell *42*, 1825-1863. 10.1016/j.ccell.2024.09.010.

Ganesh, K., Stadler, Z.K., Cercek, A., Mendelsohn, R.B., Shia, J., Segal, N.H., and Diaz, L.A., Jr. (2019). Immunotherapy in colorectal cancer: rationale, challenges and potential. Nat Rev Gastroenterol Hepatol *16*, 361-375. 10.1038/s41575-019-0126-x.

Garavaglia, B., Vallino, L., Ferraresi, A., Amoruso, A., Pane, M., and Isidoro, C. (2025). Probiotic-Derived Metabolites from Lactiplantibacillus plantarum OC01 Reprogram Tumor-Associated Macrophages to an Inflammatory Anti-Tumoral Phenotype: Impact on Colorectal Cancer Cell Proliferation and Migration. Biomedicines *13*. 10.3390/biomedicines13020339.

Gomatou, G., Karachaliou, A., Veloudiou, O.Z., Karvela, A., Syrigos, N., and Kotteas, E. (2023). The Role of REV-ERB Receptors in Cancer Pathogenesis. Int J Mol Sci *24*. 10.3390/ijms24108980.

Giacchetti, S. (2002). "Chronotherapy of colorectal cancer." Chronobiol Int 19(1): 207-219.

Gibbs, J.E., Blaikley, J., Beesley, S., Matthews, L., Simpson, K.D., Boyce, S.H., Farrow, S.N., Else, K.J., Singh, D., Ray, D.W., and Loudon, A.S. (2012). The nuclear receptor REV-ERBalpha mediates circadian regulation of innate immunity through selective regulation of inflammatory cytokines. Proc Natl Acad Sci U S A *109*, 582-587. 10.1073/pnas.1106750109.

Grabe, N. (2002). AliBaba2: context specific identification of transcription factor binding sites. In Silico Biol *2*, S1-15.

Grant, D., Yin, L., Collins, J.L., Parks, D.J., Orband-Miller, L.A., Wisely, G.B., Joshi, S., Lazar, M.A., Willson, T.M., and Zuercher, W.J. (2010). GSK4112, a small molecule chemical probe for the cell biology of the nuclear heme receptor Rev-erbalpha. ACS Chem Biol *5*, 925-932. 10.1021/cb100141y.

Graff, R.E., Moller, S., Passarelli, M.N., Witte, J.S., Skytthe, A., Christensen, K., Tan, Q., Adami, H.O., Czene, K., Harris, J.R., et al. (2017). Familial Risk and Heritability of Colorectal Cancer in the Nordic Twin Study of Cancer. Clin Gastroenterol Hepatol 15, 1256-1264.

Grossman, J.G., Nywening, T.M., Belt, B.A., Panni, R.Z., Krasnick, B.A., DeNardo, D.G., Hawkins, W.G., Goedegebuure, S.P., Linehan, D.C., and Fields, R.C. (2018). Recruitment of CCR2(+) tumor associated macrophage to sites of liver metastasis confers a poor prognosis in human colorectal cancer. Oncoimmunology *7*, e1470729. 10.1080/2162402X.2018.1470729.

Guo, D.K., Zhu, Y., Sun, H.Y., Xu, X.Y., Zhang, S., Hao, Z.B., Wang, G.H., Mu, C.C., and Ren, H.G. (2019). Pharmacological activation of REV-ERBalpha represses LPS-induced microglial activation through the NF-kappaB pathway. Acta Pharmacol Sin *40*, 26-34. 10.1038/s41401-018-0064-0.

Guo, L., Tang, X., Wong, S.W., Guo, A., Lin, Y., and Kwok, H.F. (2022). Regulation of IFN-gamma-mediated PD-L1 expression by MYC in colorectal cancer with wild-type KRAS and TP53 and its clinical implications. Front Pharmacol *13*, 1022129. 10.3389/fphar.2022.1022129.

Gur, C., Ibrahim, Y., Isaacson, B., Yamin, R., Abed, J., Gamliel, M., Enk, J., Bar-On, Y., Stanietsky-Kaynan, N., Coppenhagen-Glazer, S., et al. (2015). Binding of the Fap2 protein of Fusobacterium nucleatum to human inhibitory receptor TIGIT protects tumors from immune cell attack. Immunity 42, 344-355.

Gutting, T., Hauber, V., Pahl, J., Klapproth, K., Wu, W., Dobrota, I., Herweck, F., Reichling, J., Helm, L., Schroeder, T., et al. (2021). PPARgamma induces PD-L1 expression in MSS+ colorectal cancer cells. Oncoimmunology 10, 1906500.

Harjunpaa, H., and Guillerey, C. (2020). TIGIT as an emerging immune checkpoint. Clin Exp Immunol 200, 108-119.

He, Z., and Zhang, S. (2021). Tumor-Associated Macrophages and Their Functional Transformation in the Hypoxic Tumor Microenvironment. Front Immunol *12*, 741305. 10.3389/fimmu.2021.741305.

Hegde, P.S., and Chen, D.S. (2020). Top 10 Challenges in Cancer Immunotherapy. Immunity 52, 17-35.

Hirota, T., Irie, K., Okamoto, R., Ikeda, W., and Takai, Y. (2005). Transcriptional activation of the mouse Necl-5/Tage4/PVR/CD155 gene by fibroblast growth factor or oncogenic Ras through the Raf-MEK-ERK-AP-1 pathway. Oncogene 24, 2229-2235.

Ho, V.W., Hofs, E., Elisia, I., Lam, V., Hsu, B.E., Lai, J., Luk, B., Samudio, I., and Krystal, G. (2016). All Trans Retinoic Acid, Transforming Growth Factor beta and Prostaglandin E2 in Mouse Plasma Synergize with Basophil-Secreted Interleukin-4 to M2 Polarize Murine Macrophages. PLoS One 11, e0168072.

References

Hodi, F.S., Chiarion-Sileni, V., Gonzalez, R., Grob, J.J., Rutkowski, P., Cowey, C.L., Lao, C.D., Schadendorf, D., Wagstaff, J., Dummer, R., et al. (2018). Nivolumab plus ipilimumab or nivolumab alone versus ipilimumab alone in advanced melanoma (CheckMate 067): 4-year outcomes of a multicentre, randomised, phase 3 trial. Lancet Oncol 19, 1480-1492.

Hou, S., Zhao, Y., Chen, J., Lin, Y., and Qi, X. (2024). Tumor-associated macrophages in colorectal cancer metastasis: molecular insights and translational perspectives. J Transl Med *22*, 62. 10.1186/s12967-024-04856-x.

Huang, C., Li, J., Wu, R., Li, Y., and Zhang, C. (2025). Targeting pyroptosis for cancer immunotherapy: mechanistic insights and clinical perspectives. Mol Cancer *24*, 131. 10.1186/s12943-025-02344-4.

Ikeda, R., Tsuchiya, Y., Koike, N., Umemura, Y., Inokawa, H., Ono, R., Inoue, M., Sasawaki, Y., Grieten, T., Okubo, N., et al. (2019). REV-ERBalpha and REV-ERBbeta function as key factors regulating Mammalian Circadian Output. Sci Rep *9*, 10171. 10.1038/s41598-019-46656-0.

Inozume, T., Yaguchi, T., Furuta, J., Harada, K., Kawakami, Y., and Shimada, S. (2016). Melanoma Cells Control Antimelanoma CTL Responses via Interaction between TIGIT and CD155 in the Effector Phase. J Invest Dermatol 136, 255-263.

Iyer, S.S., and Cheng, G. (2012). Role of interleukin 10 transcriptional regulation in inflammation and autoimmune disease. Crit Rev Immunol *32*, 23-63. 10.1615/critrevimmunol.v32.i1.30.

Jasperson, K.W., Tuohy, T.M., Neklason, D.W., and Burt, R.W. (2010). Hereditary and familial colon cancer. Gastroenterology 138, 2044-2058.

Jetten, A.M. (2009). Retinoid-related orphan receptors (RORs): critical roles in development, immunity, circadian rhythm, and cellular metabolism. Nucl Recept Signal *7*, e003. 10.1621/nrs.07003.

Jiang, K., Zhong, B., Gilvary, D.L., Corliss, B.C., Hong-Geller, E., Wei, S., and Djeu, J.Y. (2000). Pivotal role of phosphoinositide-3 kinase in regulation of cytotoxicity in natural killer cells. Nat Immunol 1, 419-425.

Jiao, S., Peters, U., Berndt, S., Brenner, H., Butterbach, K., Caan, B.J., Carlson, C.S., Chan, A.T., Chang-Claude, J., Chanock, S., et al. (2014). Estimating the heritability of colorectal cancer. Hum Mol Genet 23, 3898-3905.

Jin, W. (2020). Regulation of Src Family Kinases during Colorectal Cancer Development and Its Clinical Implications. Cancers (Basel) 12.

Joanito, I., et al. (2022). "Single-cell and bulk transcriptome sequencing identifies two epithelial tumor cell states and refines the consensus molecular classification of colorectal cancer." Nat Genet 54(7): 963-975.

Joller, N., Lozano, E., Burkett, P.R., Patel, B., Xiao, S., Zhu, C., Xia, J., Tan, T.G., Sefik, E., Yajnik, V., et al. (2014). Treg cells expressing the coinhibitory molecule TIGIT selectively inhibit proinflammatory Th1 and Th17 cell responses. Immunity *40*, 569-581. 10.1016/j.immuni.2014.02.012.

Johnston, R.J., Comps-Agrar, L., Hackney, J., Yu, X., Huseni, M., Yang, Y., Park, S., Javinal, V., Chiu, H., Irving, B., et al. (2014). The immunoreceptor TIGIT regulates antitumor and antiviral CD8(+) T cell effector function. Cancer Cell 26, 923-937.

Kang, G.H. (2011). Four molecular subtypes of colorectal cancer and their precursor lesions. Arch Pathol Lab Med 135, 698-703.

Karaboue, A., Innominato, P.F., Wreglesworth, N.I., Duchemann, B., Adam, R., and Levi, F.A. (2024). Why does circadian timing of administration matter for immune checkpoint inhibitors' efficacy? Br J Cancer *131*, 783-796. 10.1038/s41416-024-02704-9.

Kawamura, I., Ohe, R., Suzuki, K., Kabasawa, T., Kitaoka, T., Takahara, D., Kono, M., Uchiyama, N., Musha, H., Futakuchi, M., and Motoi, F. (2024). Neighboring

macrophage-induced alteration in the phenotype of colorectal cancer cells in the tumor budding area. Cancer Cell Int *24*, 107. 10.1186/s12935-024-03292-7.

Kciuk, M., Wanke, K., Kruczkowska, W., Marciniak, B., and Kontek, R. (2025). Focus on PD-1/PD-L1-Targeting Antibodies in Colorectal Cancer: Are There Options Beyond Dostarlimab, Nivolumab, and Pembrolizumab? A Comprehensive Review. Molecules *30*. 10.3390/molecules30132686.

Keum, N., and Giovannucci, E. (2019). Global burden of colorectal cancer: emerging trends, risk factors and prevention strategies. Nat Rev Gastroenterol Hepatol 16, 713-732.

Kikkawa, Y., Hozumi, K., Katagiri, F., Nomizu, M., Kleinman, H.K., and Koblinski, J.E. (2013). Laminin-111-derived peptides and cancer. Cell Adh Migr 7, 150-256.

Kim, S., Min, S., Choi, Y.S., Jo, S.H., Jung, J.H., Han, K., Kim, J., An, S., Ji, Y.W., Kim, Y.G., and Cho, S.W. (2022). Tissue extracellular matrix hydrogels as alternatives to Matrigel for culturing gastrointestinal organoids. Nat Commun *13*, 1692. 10.1038/s41467-022-29279-4.

Kinzler, K.W., and Vogelstein, B. (1996). Lessons from hereditary colorectal cancer. Cell 87, 159-170.

Knudsen-Clark, A.M., Mwangi, D., Cazarin, J., Morris, K., Baker, C., Hablitz, L.M., McCall, M.N., Kim, M., and Altman, B.J. (2024). Circadian rhythms of macrophages are altered by the acidic tumor microenvironment. EMBO Rep *25*, 5080-5112. 10.1038/s44319-024-00288-2.

Kojetin, D.J., and Burris, T.P. (2014). REV-ERB and ROR nuclear receptors as drug targets. Nat Rev Drug Discov *13*, 197-216. 10.1038/nrd4100.

Kojetin, D., Wang, Y., Kamenecka, T.M., and Burris, T.P. (2011). Identification of SR8278, a synthetic antagonist of the nuclear heme receptor REV-ERB. ACS Chem Biol *6*, 131-134. 10.1021/cb1002575.

Kong, Y., Zhu, L., Schell, T.D., Zhang, J., Claxton, D.F., Ehmann, W.C., Rybka, W.B., George, M.R., Zeng, H., and Zheng, H. (2016). T-Cell Immunoglobulin and ITIM Domain (TIGIT) Associates with CD8+ T-Cell Exhaustion and Poor Clinical Outcome in AML Patients. Clin Cancer Res 22, 3057-3066.

Kuipers, E.J., Grady, W.M., Lieberman, D., Seufferlein, T., Sung, J.J., Boelens, P.G., van de Velde, C.J., and Watanabe, T. (2015). Colorectal cancer. Nat Rev Dis Primers 1, 15065.

Kumaki, Y., Ukai-Tadenuma, M., Uno, K.D., Nishio, J., Masumoto, K.H., Nagano, M., Komori, T., Shigeyoshi, Y., Hogenesch, J.B., and Ueda, H.R. (2008). Analysis and synthesis of high-amplitude Cis-elements in the mammalian circadian clock. Proc Natl Acad Sci U S A *105*, 14946-14951. 10.1073/pnas.0802636105.

Kurtulus, S., Sakuishi, K., Ngiow, S.F., Joller, N., Tan, D.J., Teng, M.W., Smyth, M.J., Kuchroo, V.K., and Anderson, A.C. (2015). TIGIT predominantly regulates the immune response via regulatory T cells. J Clin Invest *125*, 4053-4062. 10.1172/JCI81187.

Kwong, L.N., and Dove, W.F. (2009). APC and its modifiers in colon cancer. Adv Exp Med Biol 656, 85-106.

Lam, M. T., et al. (2013). "Rev-Erbs repress macrophage gene expression by inhibiting enhancer-directed transcription." Nature 498(7455): 511-515.

Lee, Y. (2021). "Roles of circadian clocks in cancer pathogenesis and treatment." Exp Mol Med 53(10): 1529-1538.

Levine, J.S., and Ahnen, D.J. (2006). Clinical practice. Adenomatous polyps of the colon. N Engl J Med 355, 2551-2557.

Li, X., Chang, Z., Wang, J., Ding, K., Pan, S., Hu, H., and Tang, Q. (2024). Unhealthy lifestyle factors and the risk of colorectal cancer: a Mendelian randomization study. Sci Rep *14*, 13825. 10.1038/s41598-024-64813-y.

Liang, R., Liu, L., Ding, D., Li, Y., Ren, J., and Wei, B. (2025). CD155 promotes the progression of colorectal cancer by restraining CD8(+) T cells via the PI3K/AKT/NF-kappaB pathway. Cancer Immunol Immunother *74*, 94. 10.1007/s00262-025-03947-y.

Li, H.S., and Watowich, S.S. (2014). Innate immune regulation by STAT-mediated transcriptional mechanisms. Immunol Rev 261, 84-101.

Li, M., Xia, P., Du, Y., Liu, S., Huang, G., Chen, J., Zhang, H., Hou, N., Cheng, X., Zhou, L., et al. (2014). T-cell immunoglobulin and ITIM domain (TIGIT) receptor/poliovirus receptor (PVR) ligand engagement suppresses interferon-gamma production of natural killer cells via beta-arrestin 2-mediated negative signaling. J Biol Chem 289, 17647-17657.

Li, W., Tan, D., Zhang, Z., Liang, J.J., and Brown, R.E. (2008). Activation of Akt-mTOR-p70S6K pathway in angiogenesis in hepatocellular carcinoma. Oncol Rep 20, 713-719.

Lin, Y., Zhao, J.L., Zheng, Q.J., Jiang, X., Tian, J., Liang, S.Q., Guo, H.W., Qin, H.Y., Liang, Y.M., and Han, H. (2018). Notch Signaling Modulates Macrophage Polarization and Phagocytosis Through Direct Suppression of Signal Regulatory Protein alpha Expression. Front Immunol 9, 1744.

Lin, Y., Lin, K., Fu, Q., Sun, X., Wang, H., Su, L., Xu, Y., and Liao, C. (2025). Co-blocking TIGIT and PVRIG Using a Novel Bispecific Antibody Enhances Antitumor Immunity. Mol Cancer Ther *24*, 664-677. 10.1158/1535-7163.MCT-23-0614.

Liu, L., You, X., Han, S., Sun, Y., Zhang, J., and Zhang, Y. (2021). CD155/TIGIT, a novel immune checkpoint in human cancers (Review). Oncol Rep 45, 835-845.

Liu, L., Yu, L., Li, Z., Li, W., and Huang, W. (2021). Patient-derived organoid (PDO) platforms to facilitate clinical decision making. J Transl Med 19, 40.

Lozano, E., Dominguez-Villar, M., Kuchroo, V., and Hafler, D.A. (2012). The TIGIT/CD226 axis regulates human T cell function. J Immunol 188, 3869-3875.

Lu, B., Li, N., Luo, C.Y., Cai, J., Lu, M., Zhang, Y.H., Chen, H.D., and Dai, M. (2021). Colorectal cancer incidence and mortality: the current status, temporal trends and their attributable risk factors in 60 countries in 2000-2019. Chin Med J (Engl) *134*, 1941-1951. 10.1097/CM9.0000000000001619.

Lun, H., Li, P., Li, J., and Liu, F. (2024). The effect of intestinal flora metabolites on macrophage polarization. Heliyon *10*, e35755. 10.1016/j.heliyon.2024.e35755.

Ma, R.Y., Black, A., and Qian, B.Z. (2022). Macrophage diversity in cancer revisited in the era of single-cell omics. Trends Immunol *43*, 546-563. 10.1016/j.it.2022.04.008.

Maas, R.J., Hoogstad-van Evert, J.S., Van der Meer, J.M., Mekers, V., Rezaeifard, S., Korman, A.J., de Jonge, P.K., Cany, J., Woestenenk, R., Schaap, N.P., et al. (2020). TIGIT blockade enhances functionality of peritoneal NK cells with altered expression of DNAM-1/TIGIT/CD96 checkpoint molecules in ovarian cancer. Oncoimmunology 9, 1843247.

Malilas, W., Koh, S.S., Kim, S., Srisuttee, R., Cho, I.R., Moon, J., Yoo, H.S., Oh, S., Johnston, R.N., and Chung, Y.H. (2013). Cancer upregulated gene 2, a novel oncogene, enhances migration and drug resistance of colon cancer cells via STAT1 activation. Int J Oncol 43, 1111-1116.

Mantovani, A., Marchesi, F., Malesci, A., Laghi, L., and Allavena, P. (2017). Tumour-associated macrophages as treatment targets in oncology. Nat Rev Clin Oncol *14*, 399-416. 10.1038/nrclinonc.2016.217.

Markowitz, S.D., and Bertagnolli, M.M. (2009). Molecular origins of cancer: Molecular basis of colorectal cancer. N Engl J Med *361*, 2449-2460. 10.1056/NEJMra0804588.

Martinez, F.O., and Gordon, S. (2014). The M1 and M2 paradigm of macrophage activation: time for reassessment. F1000Prime Rep *6*, 13. 10.12703/P6-13.

References

Masri, S., and Sassone-Corsi, P. (2018). The emerging link between cancer, metabolism, and circadian rhythms. Nat Med *24*, 1795-1803. 10.1038/s41591-018-0271-8.

Matsuda, T., Fujimoto, A., and Igarashi, Y. (2025). Colorectal Cancer: Epidemiology, Risk Factors, and Public Health Strategies. Digestion *106*, 91-99. 10.1159/000543921.

Mazzoccoli, G., Panza, A., Valvano, M.R., Palumbo, O., Carella, M., Pazienza, V., Biscaglia, G., Tavano, F., Di Sebastiano, P., Andriulli, A., and Piepoli, A. (2011). Clock gene expression levels and relationship with clinical and pathological features in colorectal cancer patients. Chronobiol Int *28*, 841-851. 10.3109/07420528.2011.615182.

McNabb, S., Harrison, T.A., Albanes, D., Berndt, S.I., Brenner, H., Caan, B.J., Campbell, P.T., Cao, Y., Chang-Claude, J., Chan, A., et al. (2020). Meta-analysis of 16 studies of the association of alcohol with colorectal cancer. Int J Cancer *146*, 861-873. 10.1002/ijc.32377.

McKay, Z.P., Brown, M.C., and Gromeier, M. (2021). Aryl Hydrocarbon Receptor Signaling Controls CD155 Expression on Macrophages and Mediates Tumor Immunosuppression. J Immunol 206, 1385-1394.

McQuade, R.M., Stojanovska, V., Bornstein, J.C., and Nurgali, K. (2017). Colorectal Cancer Chemotherapy: The Evolution of Treatment and New Approaches. Curr Med Chem 24, 1537-1557.

Messersmith, W.A. (2019). NCCN Guidelines Updates: Management of Metastatic Colorectal Cancer. J Natl Compr Canc Netw 17, 599-601.

Mezzapesa, M., Losurdo, G., Celiberto, F., Rizzi, S., d'Amati, A., Piscitelli, D., Ierardi, E., and Di Leo, A. (2022). Serrated Colorectal Lesions: An Up-to-Date Review from Histological Pattern to Molecular Pathogenesis. Int J Mol Sci *23*. 10.3390/ijms23084461.

Mills, C. D., et al. (2000). "M-1/M-2 macrophages and the Th1/Th2 paradigm." J Immunol 164(12): 6166-6173.

Mola, S., Pandolfo, C., Sica, A., and Porta, C. (2020). The Macrophages-Microbiota Interplay in Colorectal Cancer (CRC)-Related Inflammation: Prognostic and Therapeutic Significance. Int J Mol Sci 21.

Molfetta, R., Zitti, B., Lecce, M., Milito, N.D., Stabile, H., Fionda, C., Cippitelli, M., Gismondi, A., Santoni, A., and Paolini, R. (2020). CD155: A Multi-Functional Molecule in Tumor Progression. Int J Mol Sci *21*. 10.3390/ijms21030922.

Morioka, N., Tomori, M., Zhang, F.F., Saeki, M., Hisaoka-Nakashima, K., and Nakata, Y. (2016). Stimulation of nuclear receptor REV-ERBs regulates tumor necrosis factor-induced expression of proinflammatory molecules in C6 astroglial cells. Biochem Biophys Res Commun *469*, 151-157. 10.1016/j.bbrc.2015.11.086.

Mulder, K., Patel, A.A., Kong, W.T., Piot, C., Halitzki, E., Dunsmore, G., Khalilnezhad, S., Irac, S.E., Dubuisson, A., Chevrier, M., et al. (2021). Cross-tissue single-cell landscape of human monocytes and macrophages in health and disease. Immunity *54*, 1883-1900 e1885. 10.1016/j.immuni.2021.07.007.

Mundade, R., Imperiale, T.F., Prabhu, L., Loehrer, P.J., and Lu, T. (2014). Genetic pathways, prevention, and treatment of sporadic colorectal cancer. Oncoscience 1, 400-406.

Murakami, K., and Ganguly, S. (2024). The Nectin family ligands, PVRL2 and PVR, in cancer immunology and immunotherapy. Front Immunol *15*, 1441730. 10.3389/fimmu.2024.1441730.

Murakami, D., Matsuda, K., Iwamoto, H., Mitani, Y., Mizumoto, Y., Nakamura, Y., Matsuzaki, I., Iwamoto, R., Takahashi, Y., Kojima, F., et al. (2022). Prognostic value of CD155/TIGIT expression in patients with colorectal cancer. PLoS One *17*, e0265908. 10.1371/journal.pone.0265908.

Murray, P.J. (2017). Macrophage Polarization. Annu Rev Physiol *79*, 541-566. 10.1146/annurev-physiol-022516-034339.

Nagtegaal, I.D., Odze, R.D., Klimstra, D., Paradis, V., Rugge, M., Schirmacher, P., Washington, K.M., Carneiro, F., Cree, I.A., and Board, W.H.O.C.o.T.E. (2020). The 2019 WHO classification of tumours of the digestive system. Histopathology *76*, 182-188. 10.1111/his.13975.

Nagy, J.A., Chang, S.H., Dvorak, A.M., and Dvorak, H.F. (2009). Why are tumour blood vessels abnormal and why is it important to know? Br J Cancer 100, 865-869.

O'Callaghan, A.A., Dempsey, E., Iyer, N., Stiegeler, S., Mercurio, K., and Corr, S.C. (2021). Intestinal Metabolites Influence Macrophage Phagocytosis and Clearance of Bacterial Infection. Front Cell Infect Microbiol *11*, 622491. 10.3389/fcimb.2021.622491.

Pan, Y., Yu, Y., Wang, X., and Zhang, T. (2020). Tumor-Associated Macrophages in Tumor Immunity. Front Immunol *11*, 583084. 10.3389/fimmu.2020.583084.

Pariollaud, M., Gibbs, J.E., Hopwood, T.W., Brown, S., Begley, N., Vonslow, R., Poolman, T., Guo, B., Saer, B., Jones, D.H., et al. (2018). Circadian clock component REV-ERBalpha controls homeostatic regulation of pulmonary inflammation. J Clin Invest *128*, 2281-2296. 10.1172/JCI93910.

Pathria, P., Louis, T.L., and Varner, J.A. (2019). Targeting Tumor-Associated Macrophages in Cancer. Trends Immunol *40*, 310-327. 10.1016/j.it.2019.02.003.

Peruzzi, P., and Chiocca, E.A. (2018). Viruses in cancer therapy - from benchwarmers to quarterbacks. Nat Rev Clin Oncol 15, 657-658.

Pino, M.S., and Chung, D.C. (2010). The chromosomal instability pathway in colon cancer. Gastroenterology 138, 2059-2072.

Pourcet, B., Zecchin, M., Ferri, L., Beauchamp, J., Sitaula, S., Billon, C., Delhaye, S., Vanhoutte, J., Mayeuf-Louchart, A., Thorel, Q., et al. (2018). Nuclear Receptor Subfamily 1 Group D Member 1 Regulates Circadian Activity of NLRP3 Inflammasome to Reduce the Severity of Fulminant Hepatitis in Mice. Gastroenterology *154*, 1449-1464 e1420. 10.1053/j.gastro.2017.12.019.

Preitner, N., Damiola, F., Lopez-Molina, L., Zakany, J., Duboule, D., Albrecht, U., and Schibler, U. (2002). The orphan nuclear receptor REV-ERBalpha controls circadian transcription within the positive limb of the mammalian circadian oscillator. Cell *110*, 251-260. 10.1016/s0092-8674(02)00825-5.

Punt, C.J., Koopman, M., and Vermeulen, L. (2017). From tumour heterogeneity to advances in precision treatment of colorectal cancer. Nat Rev Clin Oncol 14, 235-246.
Ramesh, A., Kumar, S., Brouillard, A., Nandi, D., and Kulkarni, A. (2020). A Nitric Oxide (NO) Nanoreporter for Noninvasive Real-Time Imaging of Macrophage Immunotherapy. Adv Mater 32, e2000648.

Qian, C.J., He, Y.S., Guo, T., Tao, J., Wei, Z.Y., Zhang, J.L., Bao, C., and Chen, J.H. (2024). ADAR-mediated RNA editing regulates PVR immune checkpoint in colorectal cancer. Biochem Biophys Res Commun *695*, 149373. 10.1016/j.bbrc.2023.149373.

Raghuram, S., Stayrook, K.R., Huang, P., Rogers, P.M., Nosie, A.K., McClure, D.B., Burris, L.L., Khorasanizadeh, S., Burris, T.P., and Rastinejad, F. (2007). Identification of heme as the ligand for the orphan nuclear receptors REV-ERBalpha and REV-ERBbeta. Nat Struct Mol Biol *14*, 1207-1213. 10.1038/nsmb1344.

Rahman, M.H., and Hegazy, L. (2024). Mechanism of antagonist ligand binding to REV-ERBalpha. Sci Rep *14*, 8401. 10.1038/s41598-024-58945-4.

Rakina, M., Larionova, I., and Kzhyshkowska, J. (2024). Macrophage diversity in human cancers: New insight provided by single-cell resolution and spatial context. Heliyon *10*, e28332. 10.1016/j.heliyon.2024.e28332.

Rao, X. and L. Lin (2022). "Circadian clock as a possible control point in colorectal cancer progression (Review)." Int J Oncol 61(6).

Rodriguez-Abreu, D., Johnson, M.L., Hussein, M.A., Cobo, M., Patel, A.J., Secen, N.M., Lee, K.H., Massuti, B., Hiret, S., Yang, J.C.-H., et al. (2020). Primary analysis of a randomized, double-blind, phase II study of the anti-TIGIT antibody tiragolumab (tira) plus atezolizumab (atezo) versus placebo plus atezo as first-line (1L) treatment in patients with PD-L1-selected NSCLC (CITYSCAPE). Journal of Clinical Oncology 38, 9503-9503.

Rotte, A. (2019). Combination of CTLA-4 and PD-1 blockers for treatment of cancer. J Exp Clin Cancer Res 38, 255.

Sakatani, A., et al. (2019). "Melatonin-mediated downregulation of thymidylate synthase as a novel mechanism for overcoming 5-fluorouracil associated chemoresistance in colorectal cancer cells." Carcinogenesis 40(3): 422-431.

Samadder, N.J., and Curtin, K. (2017). The Impact of Family History on the Risk of Colorectal Neoplasia and Screening Practices. Clin Gastroenterol Hepatol *15*, 1204-1206. 10.1016/j.cgh.2017.04.022.

Sanderson, E., Gibbs, P., and Tie, J. (2025). The emerging clinical utility of ctDNA to guide adjuvant treatment in cancer. Lancet Reg Health West Pac *59*, 101595. 10.1016/j.lanwpc.2025.101595.

Sato, E., Suzuki, T., Hoshi, N., Sugino, T., and Hasegawa, H. (2008). Sodium azide induces necrotic cell death in rat squamous cell carcinoma SCC131. Med Mol Morphol 41, 211-220.

Sato, S., Sakurai, T., Ogasawara, J., Takahashi, M., Izawa, T., Imaizumi, K., Taniguchi, N., Ohno, H., and Kizaki, T. (2014). A circadian clock gene, Rev-erbalpha, modulates the inflammatory function of macrophages through the negative regulation of Ccl2 expression. J Immunol *192*, 407-417. 10.4049/jimmunol.1301982.

Shaw, E., Farris, M.S., Stone, C.R., Derksen, J.W.G., Johnson, R., Hilsden, R.J., Friedenreich, C.M., and Brenner, D.R. (2018). Effects of physical activity on colorectal cancer risk among family history and body mass index subgroups: a systematic review and meta-analysis. BMC Cancer *18*, 71. 10.1186/s12885-017-3970-5.

Simon, K. (2016). Colorectal cancer development and advances in screening. Clin Interv Aging 11, 967-976.

Singh, M.P., Rai, S., Pandey, A., Singh, N.K., and Srivastava, S. (2021). Molecular subtypes of colorectal cancer: An emerging therapeutic opportunity for personalized medicine. Genes Dis 8, 133-145.

Smits, A.H., Ziebell, F., Joberty, G., Zinn, N., Mueller, W.F., Clauder-Munster, S., Eberhard, D., Falth Savitski, M., Grandi, P., Jakob, P., et al. (2019). Biological plasticity rescues target activity in CRISPR knock outs. Nat Methods *16*, 1087-1093. 10.1038/s41592-019-0614-5.

Stamm, H., Wellbrock, J., and Fiedler, W. (2018). Interaction of PVR/PVRL2 with TIGIT/DNAM-1 as a novel immune checkpoint axis and therapeutic target in cancer. Mamm Genome 29, 694-702.

Solt, L.A., Wang, Y., Banerjee, S., Hughes, T., Kojetin, D.J., Lundasen, T., Shin, Y., Liu, J., Cameron, M.D, Noel, R., et al. (2012). Regulation of circadian behaviour and metabolism by synthetic REV-ERB agonists. Nature *485*, 62-68. 10.1038/nature11030.

Stanietsky, N., Simic, H., Arapovic, J., Toporik, A., Levy, O., Novik, A., Levine, Z., Beiman, M., Dassa, L., Achdout, H., et al. (2009). The interaction of TIGIT with PVR and PVRL2 inhibits human NK cell cytotoxicity. Proc Natl Acad Sci U S A 106, 17858-17863.

Stracci, F., Zorzi, M., and Grazzini, G. (2014). Colorectal cancer screening: tests, strategies, and perspectives. Front Public Health 2, 210.

Su, Z., Zhang, P., Yu, Y., Lu, H., Liu, Y., Ni, P., Su, X., Wang, D., Liu, Y., Wang, J., et al. (2016). HMGB1 Facilitated Macrophage Reprogramming towards a Proinflammatory M1-like Phenotype in Experimental Autoimmune Myocarditis Development. Sci Rep 6, 21884.

Sulli, G., Rommel, A., Wang, X., Kolar, M.J., Puca, F., Saghatelian, A., Plikus, M.V., Verma, I.M., and Panda, S. (2018). Pharmacological activation of REV-ERBs is lethal in cancer and oncogene-induced senescence. Nature *553*, 351-355. 10.1038/nature25170.

Sulli, G., Lam, M. T. Y., & Panda, S. (2019). Interplay between Circadian Clock and Cancer: New Frontiers for Cancer Treatment. *Trends in cancer*, *5*(8), 475–494. https://doi.org/10.1016/j.trecan.2019.07.002

Sultan, M., Coyle, K.M., Vidovic, D., Thomas, M.L., Gujar, S., and Marcato, P. (2017). Hide-and-seek: the interplay between cancer stem cells and the immune system. Carcinogenesis 38, 107-118.

Sun, L., and Yu, S. (2012). Diabetes mellitus is an independent risk factor for colorectal cancer. Dig Dis Sci 57, 1586-1597.

Sung, H., Siegel, R.L., Laversanne, M., Jiang, C., Morgan, E., Zahwe, M., Cao, Y., Bray, F., and Jemal, A. (2025). Colorectal cancer incidence trends in younger versus older adults: an analysis of population-based cancer registry data. Lancet Oncol *26*, 51-63. 10.1016/S1470-2045(24)00600-4.

Taieb, J., and Gallois, C. (2020). Adjuvant Chemotherapy for Stage III Colon Cancer. Cancers (Basel) *12*. 10.3390/cancers12092679.

Tao L, Yu H, Liang R, et al. (2019). Rev-erbα inhibits proliferation by reducing glycolytic flux and pentose phosphate pathway in human gastric cancer cells. *Oncogenesis* **8**, 57.

Tugal, D., Liao, X., and Jain, M.K. (2013). Transcriptional control of macrophage polarization. Arterioscler Thromb Vasc Biol 33, 1135-1144.

Uriz-Huarte, A., et al. (2020). "The transcriptional repressor REV-ERB as a novel target for disease." Bioorg Med Chem Lett 30(17): 127395.

Van Dyken, S.J., and Locksley, R.M. (2013). Interleukin-4- and interleukin-13-mediated alternatively activated macrophages: roles in homeostasis and disease. *Annu. Rev. Immunol.* 31, 317–343.

Verlande, A. and S. Masri (2019). "Circadian Clocks and Cancer: Timekeeping Governs Cellular Metabolism." Trends Endocrinol Metab 30(7): 445-458.

Vesely, M.D., Kershaw, M.H., Schreiber, R.D., and Smyth, M.J. (2011). Natural innate and adaptive immunity to cancer. *Annu. Rev. Immunol.* 29, 235–271.

Wang, C., Yang, J., Yuan, J., Wang, X., Li, Q., Ren, C., Zhi, X., Lv, X., Liu, K., Zhao, X., and Li, Y. (2025). Role of circadian transcription factor REV-ERB in cardiovascular diseases: a review. Front Cardiovasc Med *12*, 1516279. 10.3389/fcvm.2025.1516279.

Wang, J.D., Xu, G.S., Hu, X.L., Li, W.Q., Yao, N., Han, F.Z., Zhang, Y., and Qu, J. (2024). The histologic features, molecular features, detection and management of serrated polyps: a review. Front Oncol *14*, 1356250. 10.3389/fonc.2024.1356250.

Wang, Q., Yu, M., and Zhang, S. (2024). The characteristics of the tumor immune microenvironment in colorectal cancer with different MSI status and current therapeutic strategies. Front Immunol *15*, 1440830. 10.3389/fimmu.2024.1440830.

Wang, R., Liu, S.L., Guo, Q.Q., Shi, X.H., and Ma, M.M. (2023). Circadian Clock REV-ERBs Agonist SR9009 Induces Synergistic Antitumor Activity in Multiple Myeloma by Suppressing Glucose-Regulated Protein 78-Dependent Autophagy and Lipogenesis. World J Oncol *14*, 464-475. 10.14740/wjon1681.

Wang, S., Li, F., Lin, Y., and Wu, B. (2020). Targeting REV-ERBalpha for therapeutic purposes: promises and challenges. Theranostics *10*, 4168-4182. 10.7150/thno.43834.

Wang, S., Lin, Y., Yuan, X., Li, F., Guo, L., and Wu, B. (2018). REV-ERBalpha integrates colon clock with experimental colitis through regulation of NF-kappaB/NLRP3 axis. Nat Commun *9*, 4246. 10.1038/s41467-018-06568-5.

Wang, Y., et al. (2017). Upregulation of circadian gene hClock contributes to metastasis of colorectal cancer. *Int. J. Oncol.*50, 2191–2199.

Werfel, T.A., and Cook, R.S. (2018). Efferocytosis in the tumor microenvironment. Semin Immunopathol *40*, 545-554. 10.1007/s00281-018-0698-5.

Whelan, S., Ophir, E., Kotturi, M.F., Levy, O., Ganguly, S., Leung, L., Vaknin, I., Kumar, S., Dassa, L., Hansen, K., et al. (2019). PVRIG and PVRL2 Are Induced in Cancer and Inhibit CD8(+) T-cell Function. Cancer Immunol Res 7, 257-268.

Whiteside, T.L. (1993). Correspondence re: J. P. Alexander et al., T-cells infiltrating renal cell carcinoma display a poor proliferative response even though they can produce interleukin 2 and express interleukin 2 receptors. Cancer Res., 53: 1380-1387, 1993. Cancer Res 53, 5828.

Whiteside, T.L. (2006). The role of immune cells in the tumor microenvironment. Cancer Treat Res 130, 103-124.

Wu, W. (2021). Expression and function of blood receptors RORα, REVERBα and BMAL1 in human colorectal cancer. Doctoral thesis, Heidelberg University.

Wu, J.W., Liu, Y., Dai, X.J., Liu, H.M., Zheng, Y.C., and Liu, H.M. (2024). CD155 as an emerging target in tumor immunotherapy. Int Immunopharmacol *131*, 111896. 10.1016/j.intimp.2024.111896.

Xiang, B., Snook, A.E., Magee, M.S., and Waldman, S.A. (2013). Colorectal cancer immunotherapy. Discov Med 15, 301-308.

Xie, Y.H., Chen, Y.X., and Fang, J.Y. (2020). Comprehensive review of targeted therapy for colorectal cancer. Signal Transduct Target Ther 5, 22.

Xie, Z., Qu, X., Zhang, J., Huang, Y., Runhan, Z., Tang, D., Li, N., Wang, Z., and Luo, X. (2025). Integrative single-cell and bulk RNA-seq analysis identifies lactylation-related signature in osteosarcoma. Funct Integr Genomics *25*, 60. 10.1007/s10142-025-01559-4.

Xue, J., Schmidt, S.V., Sander, J., Draffehn, A., Krebs, W., Quester, I., De Nardo, D., Gohel, T.D., Emde, M., Schmidleithner, L., et al. (2014). Transcriptome-based network analysis reveals a spectrum model of human macrophage activation. Immunity *40*, 274-288. 10.1016/j.immuni.2014.01.006.

Yamane, L., Scapulatempo-Neto, C., Reis, R.M., and Guimaraes, D.P. (2014). Serrated pathway in colorectal carcinogenesis. World J Gastroenterol 20, 2634-2640.

Yang, C., Fu, J., Zheng, F., Fu, Y., Duan, X., Zuo, R., and Zhu, J. (2024). Aconitine promotes ROS-activated P38/MAPK/Nrf2 pathway to inhibit autophagy and promote myocardial injury. J Cardiothorac Surg *19*, 665. 10.1186/s13019-024-03149-0.

Yin, L., Wu, N., Curtin, J.C., Qatanani, M., Szwergold, N.R., Reid, R.A., Waitt, G.M., Parks, D.J., Pearce, K.H., Wisely, G.B., and Lazar, M.A. (2007). Rev-erbalpha, a heme sensor that coordinates metabolic and circadian pathways. Science *318*, 1786-1789. 10.1126/science.1150179.

Yin, L., and Lazar, M.A. (2005). The orphan nuclear receptor Rev-erbalpha recruits the N-CoR/histone deacetylase 3 corepressor to regulate the circadian Bmal1 gene. Mol Endocrinol *19*, 1452-1459. 10.1210/me.2005-0057.

Yu, X., Harden, K., Gonzalez, L.C., Francesco, M., Chiang, E., Irving, B., Tom, I., Ivelja, S., Refino, C.J., Clark, H., et al. (2009). The surface protein TIGIT suppresses T cell

activation by promoting the generation of mature immunoregulatory dendritic cells. Nat Immunol 10, 48-57.

Yuki, K., Cheng, N., Nakano, M., and Kuo, C.J. (2020). Organoid Models of Tumor Immunology. Trends Immunol 41, 652-664.

Yurdagul, A., Jr., Doran, A.C., Cai, B., Fredman, G., and Tabas, I.A. (2017). Mechanisms and Consequences of Defective Efferocytosis in Atherosclerosis. Front Cardiovasc Med *4*, 86. 10.3389/fcvm.2017.00086.

Zhang, T., Chen, M., Guo, L., Yu, F., Zhou, C., Xu, H., and Wu, B. (2019). Reverse Erythroblastosis Virus alpha Antagonism Promotes Homocysteine Catabolism and Ammonia Clearance. Hepatology *70*, 1770-1784. 10.1002/hep.30675.

Zhang, C., Wang, Y., Xun, X., Wang, S., Xiang, X., Hu, S., Cheng, Q., Guo, J., Li, Z., and Zhu, J. (2020). TIGIT Can Exert Immunosuppressive Effects on CD8+ T Cells by the CD155/TIGIT Signaling Pathway for Hepatocellular Carcinoma In Vitro. J Immunother 43, 236-243.

Zhang, Z., et al. (2021). "Circadian clock: a regulator of the immunity in cancer." Cell Commun Signal 19(1): 37.

Zhang, L., Wang, X., Song, Q., & Jiang, C. (2023). The circadian clock gene REV-ERBα: a novel therapeutic target in cancer immunology. *Frontiers in Immunology*, 14, 112233.

Zhou, Z., Lin, Y., Gao, L., Yang, Z., Wang, S., and Wu, B. (2020). Circadian pharmacological effects of berberine on chronic colitis in mice: Role of the clock component Rev-erbalpha. Biochem Pharmacol *172*, 113773. 10.1016/j.bcp.2019.113773.

Zhou, X., Jiao, L., Qian, Y., Dong, Q., Sun, Y., Zheng, W.V., Zhao, W., Zhai, W., Qiu, L., Wu, Y., et al. (2021). Repositioning Azelnidipine as a Dual Inhibitor Targeting

CD47/SIRPalpha and TIGIT/PVR Pathways for Cancer Immuno-Therapy. Biomolecules *11*. 10.3390/biom11050706.

Zorzi, M., and Urso, E.D.L. (2023). Impact of colorectal cancer screening on incidence, mortality and surgery rates: Evidences from programs based on the fecal immunochemical test in Italy. Dig Liver Dis *55*, 336-341. 10.1016/j.dld.2022.08.013.

Zhu, X., Liang, R., Lan, T., Ding, D., Huang, S., Shao, J., Zheng, Z., Chen, T., Huang, Y., Liu, J., et al. (2022). Tumor-associated macrophage-specific CD155 contributes to M2-phenotype transition, immunosuppression, and tumor progression in colorectal cancer. J Immunother Cancer *10*. 10.1136/jitc-2021-004219.

Zhu, Y. J., Li, X., Chen, T. T., Wang, J. X., Zhou, Y. X., Mu, X. L., Du, Y., Wang, J. L., Tang, J., & Liu, J. Y. (2023). Personalised neoantigen-based therapy in colorectal cancer. *Clinical and translational medicine*, *13*(11), e1461. https://doi.org/10.1002/ctm2.1461

6. Supplementary Data

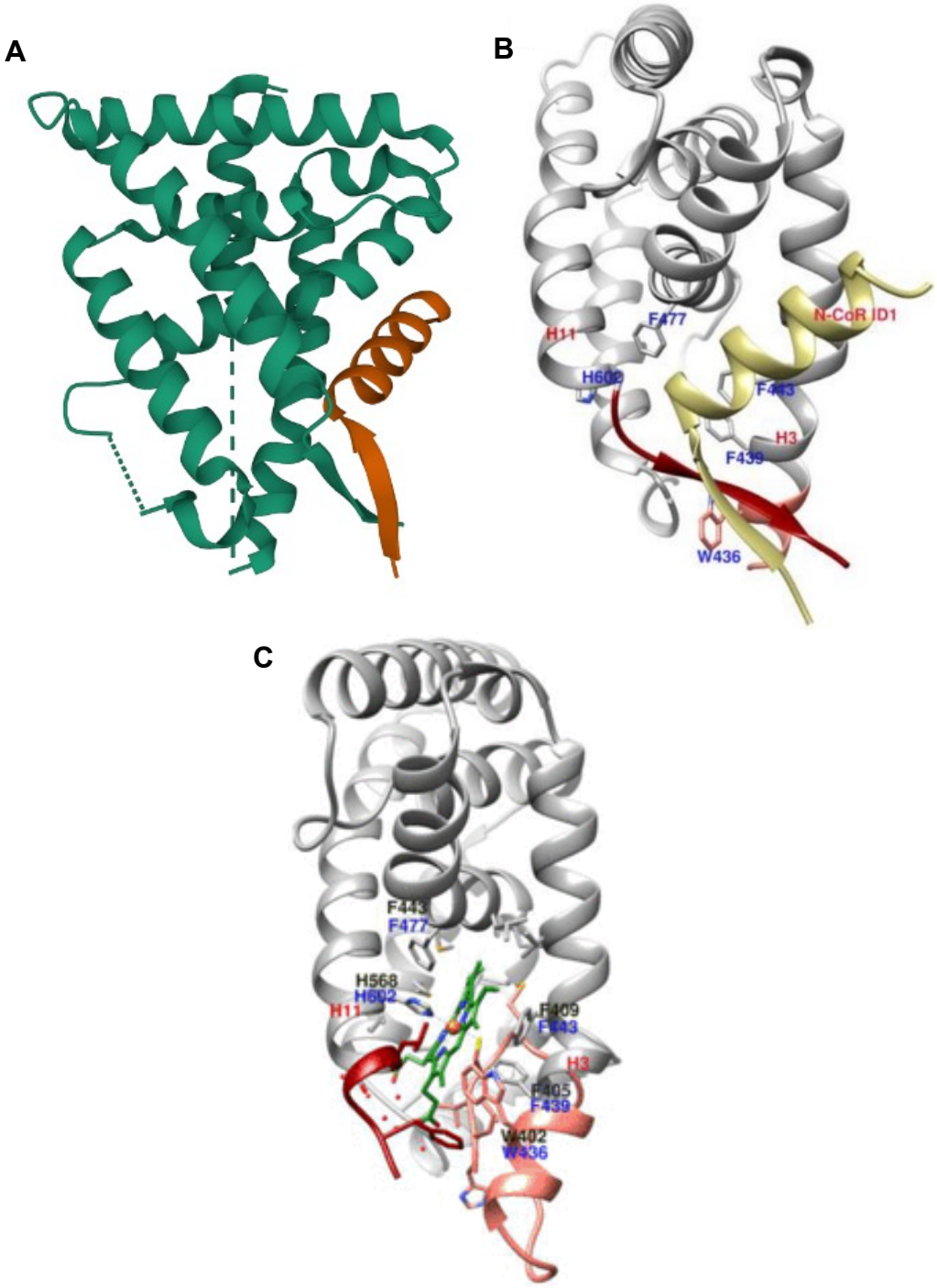

S1. 3D Structures of REVERBα. (A) X-ray crystallography of a truncation mutant of the human REVERBα ligand-binding domain (LBD) bound with the corepressor NCoR ID1 peptide (orange) determined to 2.60A resolution. The protein was expressed in *E. coli* BL21(DE3) and has no indicated sequence mutations. This structure has a total molecular weight of 30.08 kDa, an atom count of 1,611, a modeled residue count of 205 and a deposited residue count of 266. The structure of this REVERBα protein was determined via x-ray diffraction by Gampe, R. and Nolte, R. (03.06.2010) (3N00 https://doi.org/10.2210/pdb3N00/pdb). (B)/(C) X-ray crystallography of the REVERBα LBD bound with (B) corepressor NCoR-ID1 (3N00) and (C) Heme (PDB: 3CQV). Structural differences in the conformations of REVERBα LBD between (B) and (C) suggest that the ligand binding pocket (LBP) of REVERBα has a degree of flexibility, offering the accommodation of various ligand scaffolds (Hegazy et. al., 2021).

Confidence	% i.d.	Template Information
100.0	100	**PDB header:**transcription regulator **Chain:** A: **PDB Molecule:**rev-erba-alpha; **PDBTitle:** crystal structure of a deletion mutant of human reverba ligand binding2 domain bound with an ncor id1 peptide determined to 2.60a **PDB Entry:** PDBe RCSB PDBj

S.2 Computational 3D structure modelling of REVERBα by Phyre2 software. (A) Alignment of query and template protein sequence of REVERBα showing predicted secondary structure elements of the wildtype (WT) REVERBα peptide sequence (NP_068370.1; P20393_HUMAN). (B) 3D structure of REVERBα modelled by Phyre 2 using a query protein sequence of human "*nuclear receptor subfamily 1 group D member 1"* (NR1D1) from the "National Center for Biotechnology" (NCBI). The modeling of REVERBα/NR1D1 C-terminal domain (434-611 aa) resulted in a full match of c3n00A showing Confidence 100% | Identity 100% with the x-ray structure deposited in the RCSB Protein Data Bank (PDB; https://www.rcsb.org/). Based on PDB data, best fit models (N=20) were generated.

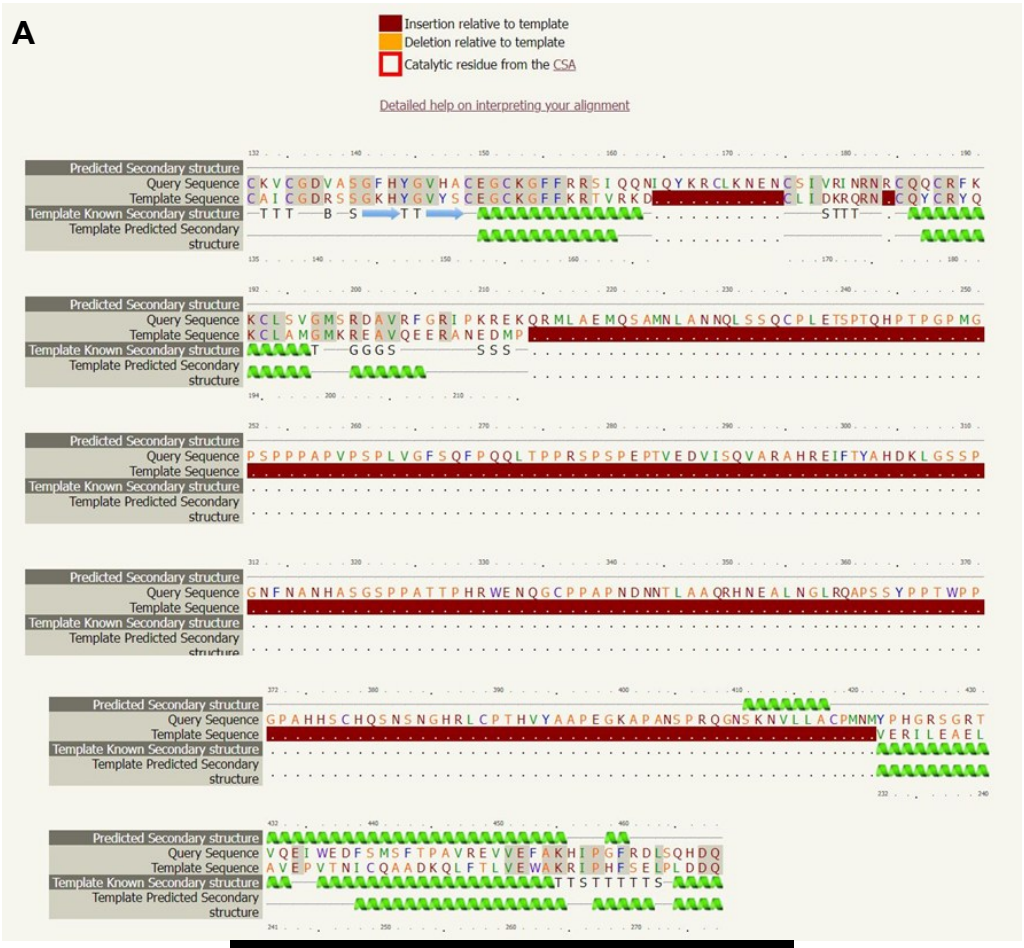

Confidence	% i.d.	Template Information
99.8	72	**PDB header:**transcription/dna **Chain:** A: **PDB Molecule:**retinoic acid receptor rxr-alpha; **PDBTitle:** crystal structure of multi-domain rar-beta-rxr-alpha heterodimer on2 dna **PDB Entry:** PDBe RCSB PDBj

S.3 Computational 3D structure modelling structure prediction of the C-Terminal CRISPR/Cas9-modified REVERBα by Phyre2 software. (A) Alignment showing predicted secondary structure elements of the C-terminal peptide sequence of the CRISPR/Cas9-modified REVERBα harbouring the C-terminal sgRNA. The peptide sequence depicts missing secondary structure elements of the modified ΔC-Terminus (aa 132-468) domain, suggesting a distorted folding of the C-terminal ligand binding domain (LBD). (B) 3D modelled structure of the CRISPR/Cas9-modified C-terminal region of REVERBα revealing disordered folding. The alignment and length coverage for the modified LBD were the highest for the human “retinoic acid receptor rxr-alpha” with c5uanA giving a Confidence 99.8% | Identity 72%. Based on PDB data, best fit models (N=20) were generated.

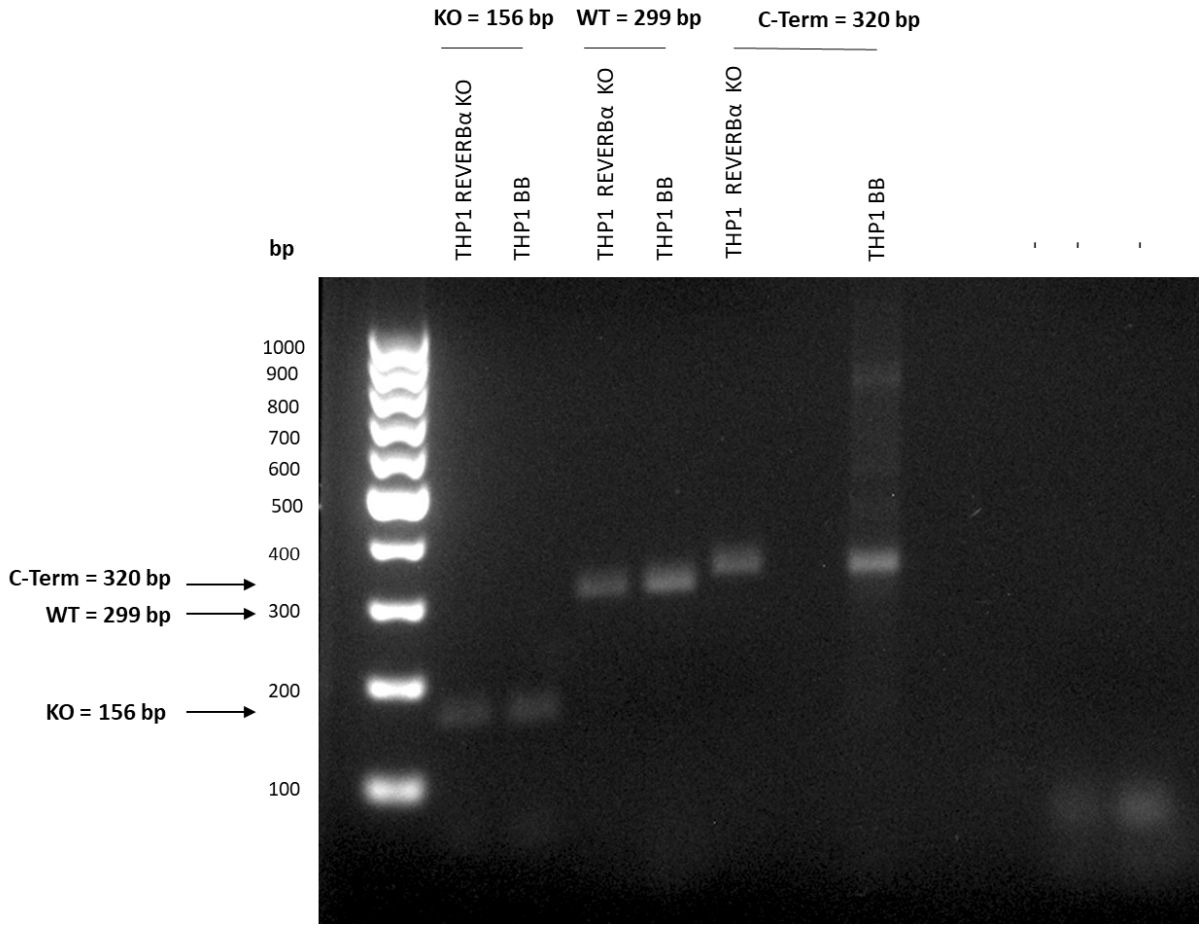

S.4 PCR amplification of genomic DNA from THP1-derived macrophages with CRISPR/Cas9-modifed REVERBα. Agarose gel analysis of CRISPR/Cas9-modification of the *REVERBα / NR1D1* gene in THP1-derived macrophages. The gDNA was isolated from CRISPR/Cas9-modified THP1 clones and subjected to PCR amplification using primers flanking the C-terminal sgRNA target insertion region (Exon 6) of the *REVERBα* / *NR1D1* coding sequence (CDS). Knock-out (KO) and backbone vector (BB) bands are visualized. PCR analysis was performed with 30x cycles, 94°C melting temp., 60°C annealing temp. and 72°C extension temp. The DNA was separated on a 2% agarose gel and a 1 kbp DNA ladder was used as size reference.

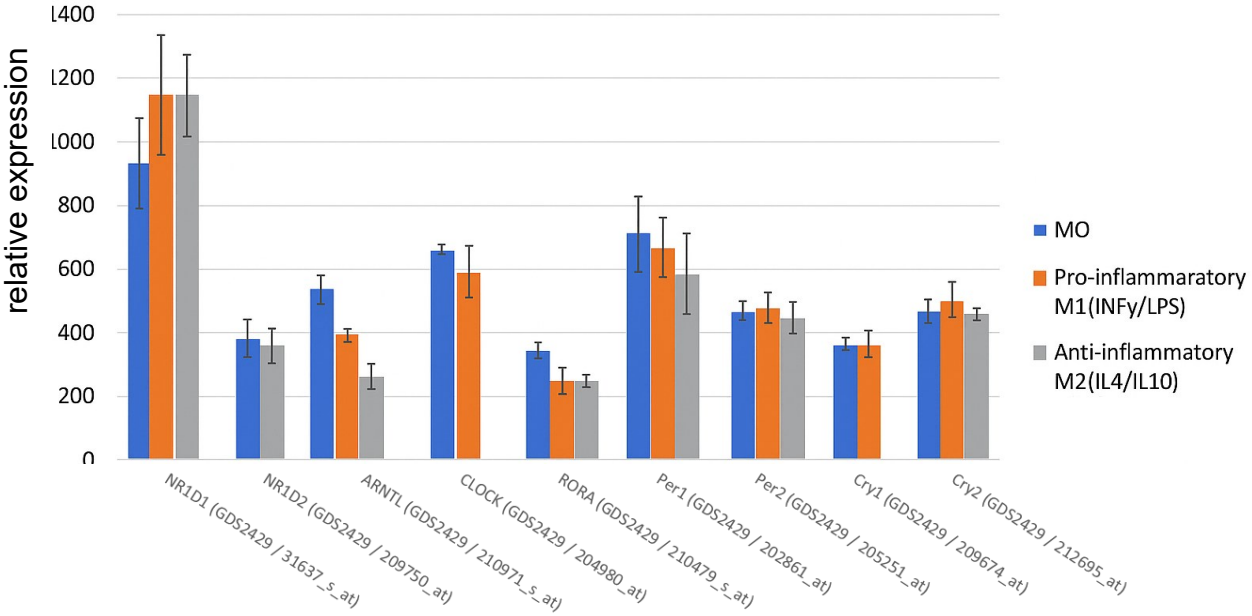

S5. NCBI Geoprofile Data of CLOCK gene expression. NCBI Geoprofile Data HG-U133A (GDS2429) representing the expression of circadian rhythm genes (NR1D1 (REVERBα), NR1D2 (REVERBβ), ARNTL, CLOCK, PER1, PER2, CRY1) in unpolarized macrophages (M0, blue), pro-inflammatory macrophages (M1, IFNγ/LPS, orange), and anti-inflammatory macrophages (M2, IL4/IL10, gray). The data depicts the relative expression by the number of counts generated via *in situ* hybridization.

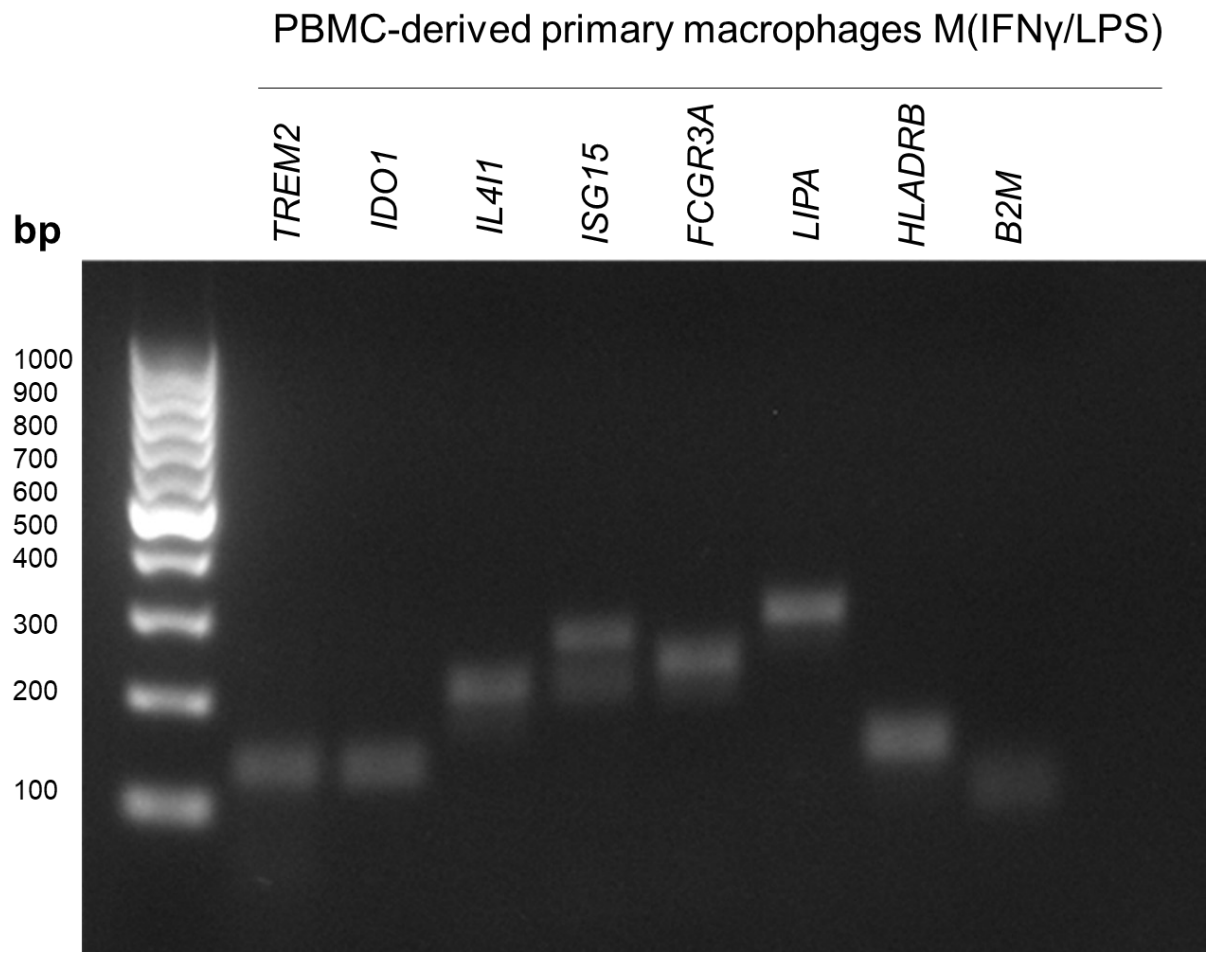

S.6 PCR amplification of cDNA encoding macrophage subset markers in differentiated, polarized PBMC-derived primary M(IFNγ/LPS) macrophages. Agarose gel analysis depicting *TREM2, IDO1, IL4I1, ISG15, FCGR3A, LIPA* and *HLADRB* macrophage subset marker expression. As shown, all subset markers are expressed. cDNA was synthesized from mRNA isolated from PBMC-derived primary macrophages polarized with IFNγ/LPS. RT-PCR analysis was performed with 40x cycles, 92°C melting temp., 60°C annealing temp. and 75°C extension temp. The DNA was separated on a 2% agarose gel, for size reference a 1 kbp DNA ladder was used.

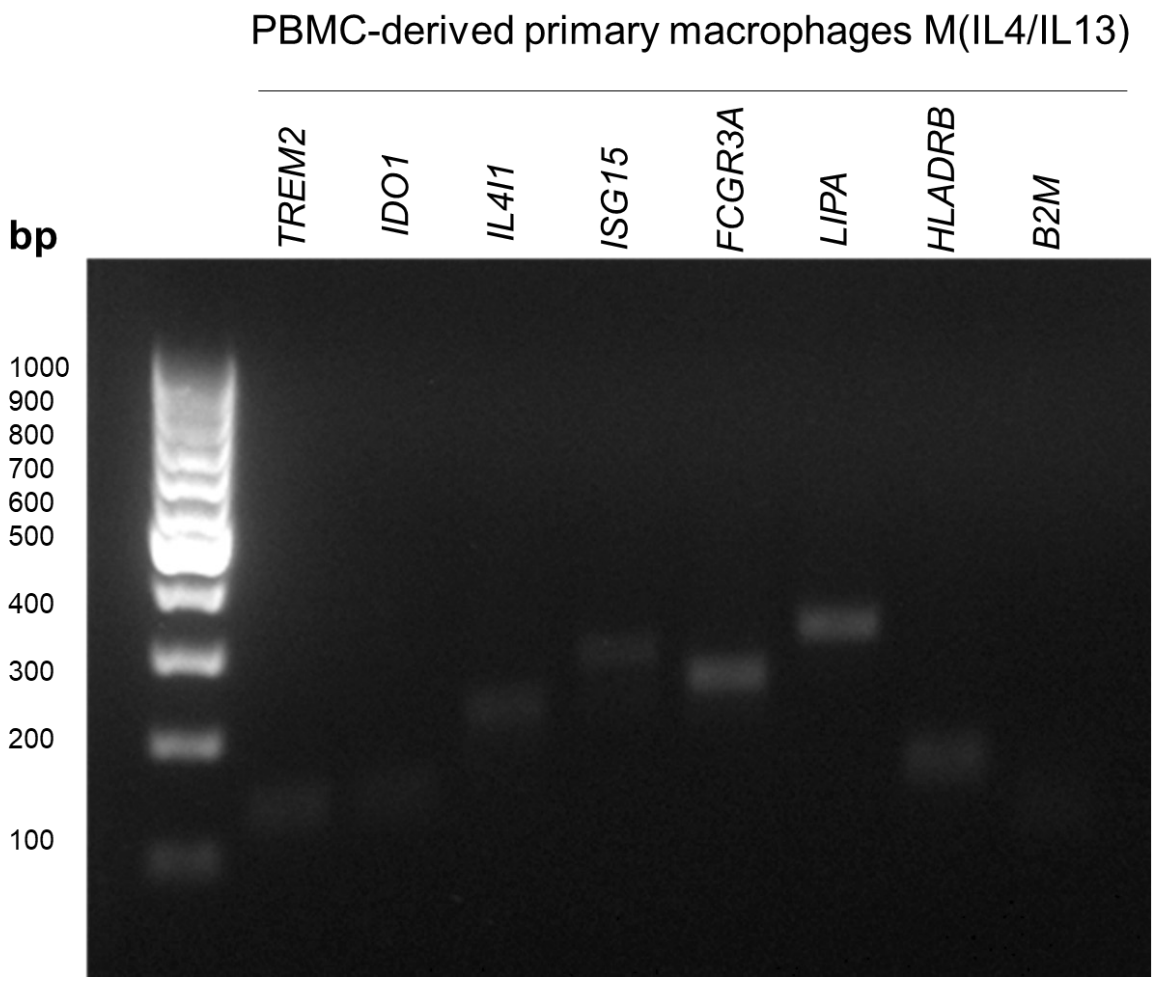

S.7 PCR amplification of cDNA encoding macrophage subset markers in differentiated, polarized PBMC-derived primary M(IL4/IL13) macrophages. Agarose gel analysis depicting the expression of *LIPA* and *HLADRB*. The cDNA was synthesized from mRNA isolated from PBMC-derived primary macrophages polarized with IL4/IL13. RT-PCR analysis was performed with 40x cycles, 92°C melting temp., 60°C annealing temp. and 75°C extension temp. The DNA separated on a 2% agarose gel. For size reference a 1 kbp DNA ladder was used.

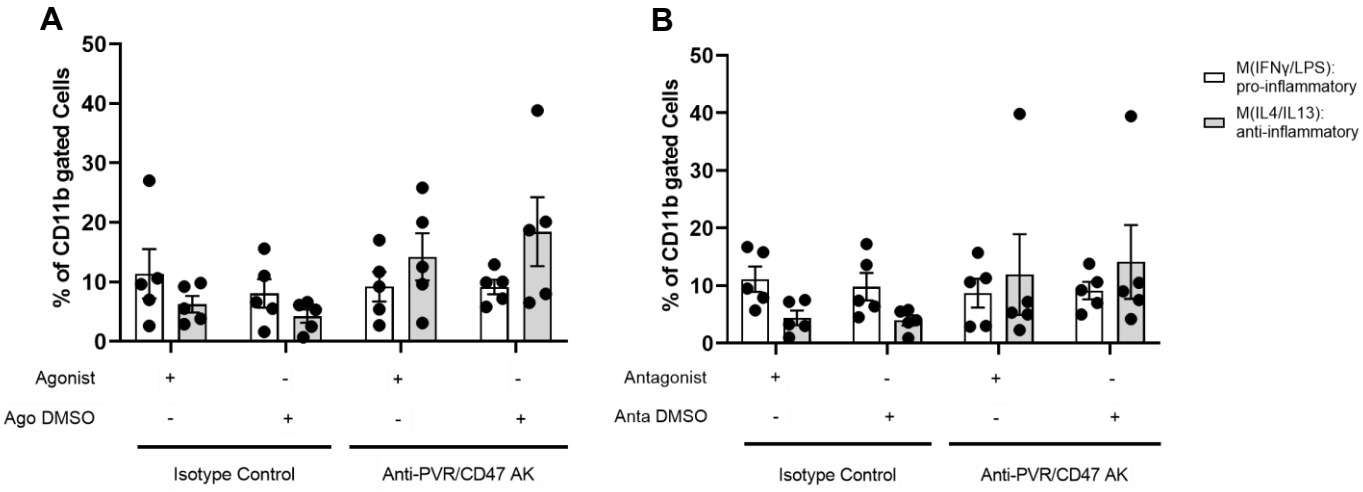

S.8 Necrotic differentiated, polarized PBMC-derived human primary macrophages (M(IFNγ/LPS) & M(IL4/IL13)) in co-culture with HT29 CRC cells. The co-cultures were treated with vehicle (DMSO), REVERBα (A) 10 µM SR9009 Agonist or (B) 6.7 µM SR 8275 Antagonist together with 5 µg/ml PVR and 10 µg/ml CD47 blocking Abs vs. isotype control for 5 days. Flow cytometry (FC) was performed to investigate the viability and death types of CD11b+ macrophages using annexin & SYTOX™ dye. Respective percentages of gated CD11b+ cells are shown. The number of macrophages undergoing necrosis remained under 20% in all conditions. Necrosis rates were slightly elevated in anti-inflammatory M(IL4/IL13) macrophages treated with PVR/CD47 Abs as shown in (A) and (B), without reaching statistical significance. Significances were calculated using two-way ANOVA with Tukey´s multiple comparisons test (n.s.; N=5 independent experiments, mean ± SEM). Cells were analyzed on a BD Canto FC device (Flow Core UMM).

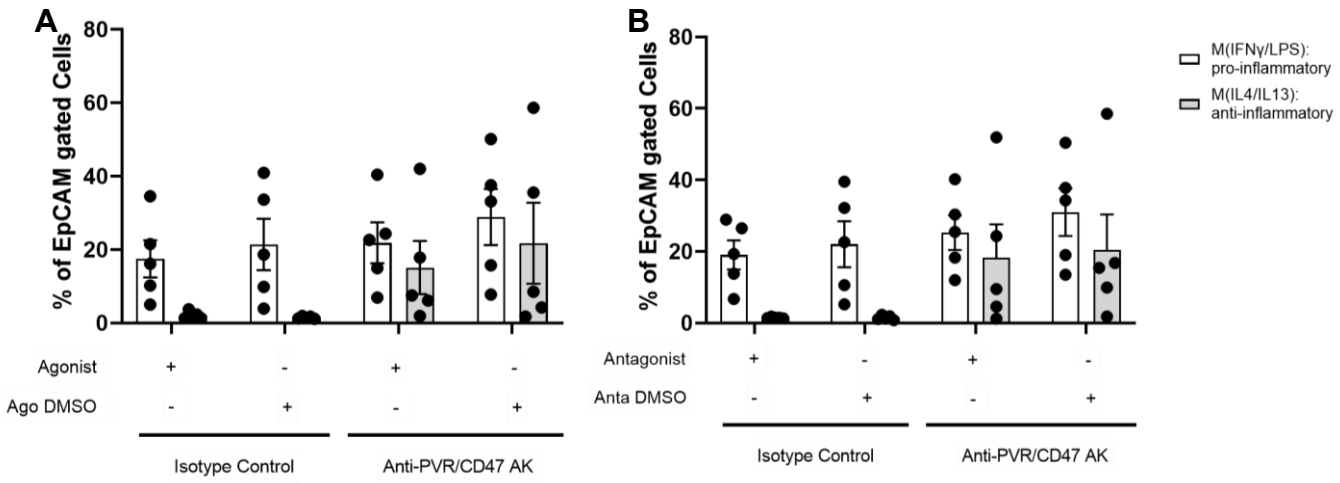

S.9 Early apoptotic HT29 CRC cells after co-culture with differentiated, polarized PBMC-derived human primary macrophages (M(IFNγ/LPS) & M(IL4/IL13)). The co-cultures were treated with vehicle (DMSO), REVERBα (A) 10 µM SR9009 Agonist or (B) 6.7 µM SR 8275 Antagonist together with 5 µg/ml PVR and 10 µg/ml CD47 blocking Abs vs. isotype control for 5 days. Flow cytometry (FC) was performed to investigate the viability and death types of EpCAM+ tumor cells using annexin & SYTOX™ dye. Respective percentages of gated EpCAM+ cells are shown. Higher numbers of cancer cells in early apoptosis stage were evident in all co-cultures with pro-inflammatory M(LPS/IFNγ) macrophages in (A) and (B). Numbers of early apoptotic EpCAM+ tumor cells increased in co-cultures of anti-inflammatory M(IL4/IL13) macrophages treated with PVR and CD47 Abs as depicted in (A) and (B), however without reaching statistical significance. Significances were calculated using two-way ANOVA with Tukey´s multiple comparisons test (n.s.; N=5 independent experiments, mean ± SEM). Cells were analyzed on a BD Canto FC device (Flow Core UMM).

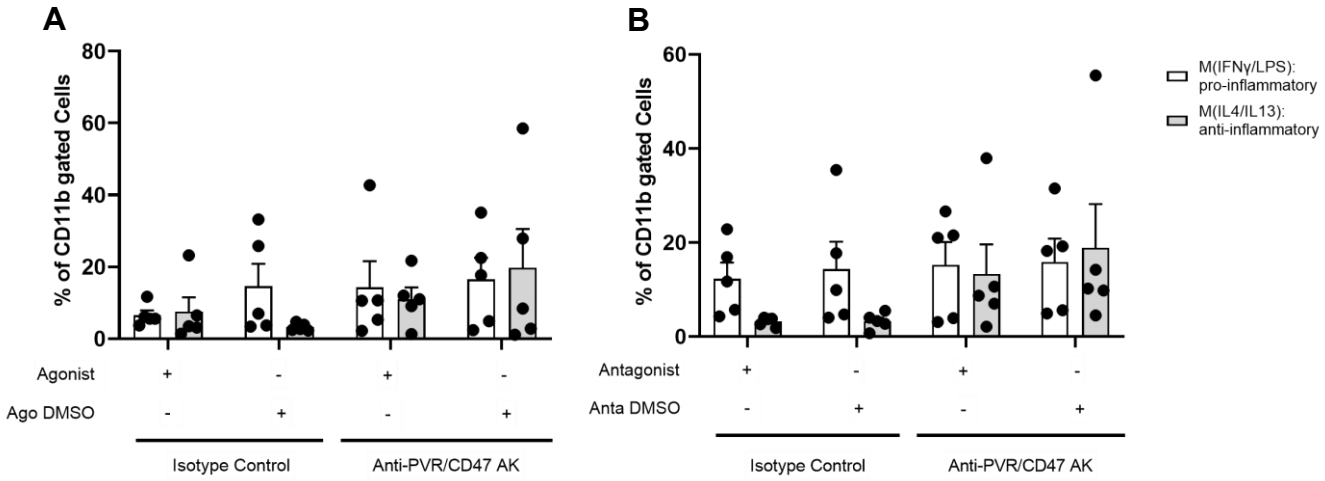

S.10 Early apoptotic differentiated, polarized PBMC-derived human primary macrophages (M(IFNγ/LPS) & M(IL4/IL13)) in co-culture with HT29 CRC cells. The co-cultures were treated with vehicle (DMSO), REVERBα (A) 10 µM SR9009 Agonist or (B) 6.7 µM SR 8275 Antagonist together with 5 µg/ml PVR and 10 µg/ml CD47 blocking Abs vs. isotype control for 5 days. Flow cytometry (FC) was performed to investigate the viability and death types of CD11b+ macrophages using annexin & SYTOX™ dye. Respective percentages of gated CD11b+ cells are shown. The number of macrophages in early apoptotic stage remained under 20% in all conditions. Numbers of early apoptotic macrophages were slightly increased in co-cultures harboring pro-inflammatory M(LPS/IFNγ) macrophages in combination with PVR and CD47 Abs as shown in (A) and (B), without reaching statistical significance. Significances were calculated using two-way ANOVA with Tukey´s multiple comparisons test (n.s.; N=5 independent experiments, mean ± SEM). Cells were analyzed on a BD Canto FC device (Flow Core UMM).

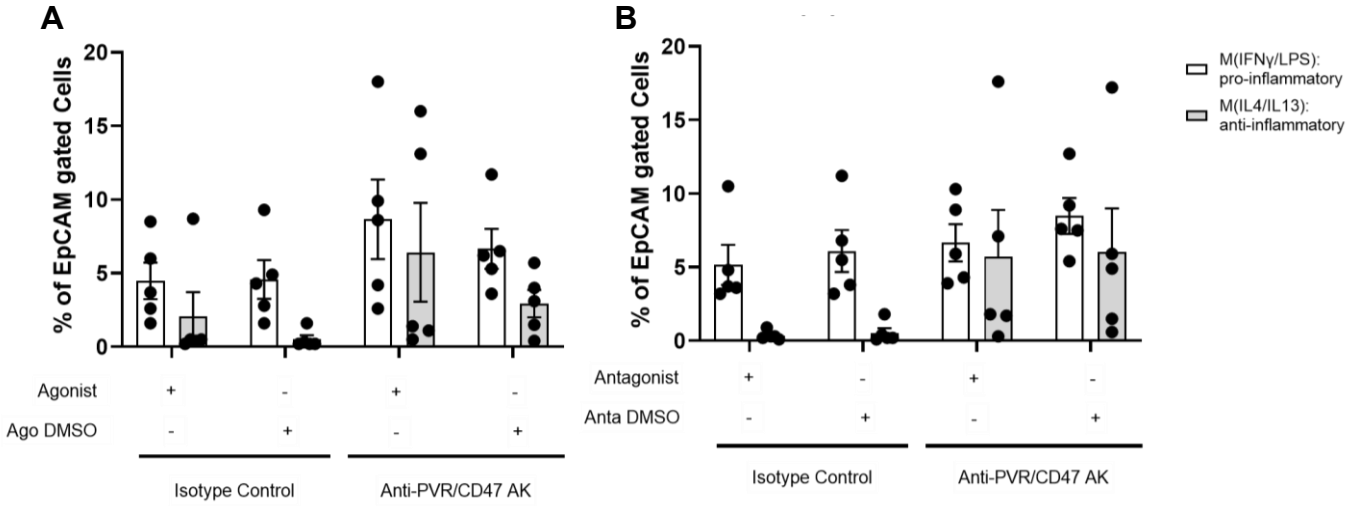

S.11 Late apoptotic HT29 CRC cells after co-culture with differentiated, polarized PBMC-derived human primary macrophages (M(IFNγ/LPS) & M(IL4/IL13)). The co-culture was treated with vehicle (DMSO), REVERBα (A) 10 µM SR9009 Agonist or (B) 6.7 µM SR 8275 Antagonist together with 5 µg/ml PVR and 10 µg/ml CD47 blocking Abs vs. isotype control for 5 days. Flow cytometry (FC) was used to investigate the viability and death types of EpCAM+ tumor cells using annexin & SYTOX™ dye. Respective percentages of gated EpCAM+ cells are shown. Higher numbers of late apoptotic HT29 cancer cells were observed in co-cultures harboring pro-inflammatory M(LPS/IFNγ) macrophages in combination with PVR and CD47 Abs as shown in (A) and (B), however without reaching statistical significance. Significances were calculated using two-way ANOVA with Tukey´s multiple comparisons test (n.s.; N=5 independent experiments, mean ± SEM). Cells were analyzed on a BD Canto FC device (Flow Core UMM).

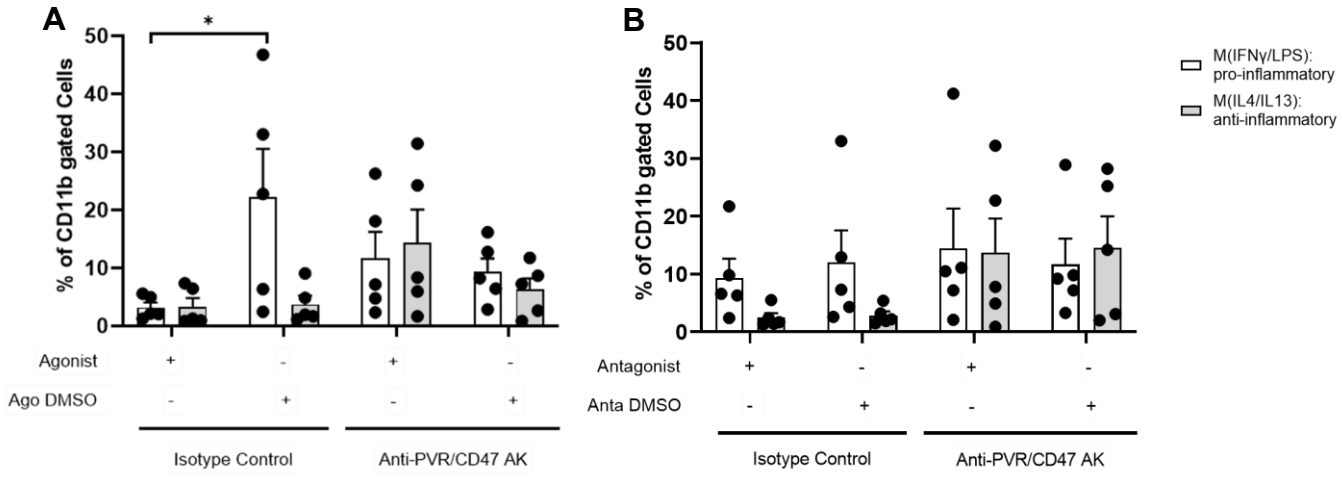

S.12 Late apoptotic differentiated, polarized PBMC-derived human primary macrophages (M(IFNγ/LPS) & M(IL4/IL13)) in co-culture with HT29 CRC cells. The co-culture was treated with vehicle (DMSO), REVERBα (A) 10 µM SR9009 Agonist or (B) 6.7 µM SR 8275 Antagonist together with 5 µg/ml PVR and 10 µg/ml CD47 blocking Abs vs. isotype control for 5 days. Flow cytometry (FC) was used to investigate the viability and death types of CD11b+ macrophages using annexin & SYTOX™ dye. Respective percentages of gated CD11b+ cells are shown. Numbers of late apoptotic anti-inflammatory M(IL4/IL13) macrophages were slightly elevated in co-cultures treated with PVR and CD47 Abs as shown in (A) and (B), however without reaching statistical significance. The lowest number of late apoptotic macrophages was observed upon treatment with REVERBα agonist vs. the DMSO control as shown in (A). Significances were calculated using two-way ANOVA with Tukey´s multiple comparisons test (*p<0.05; N=5 independent experiments, mean ± SEM). Cells were analyzed on a BD Canto FC device (Flow Core UMM).

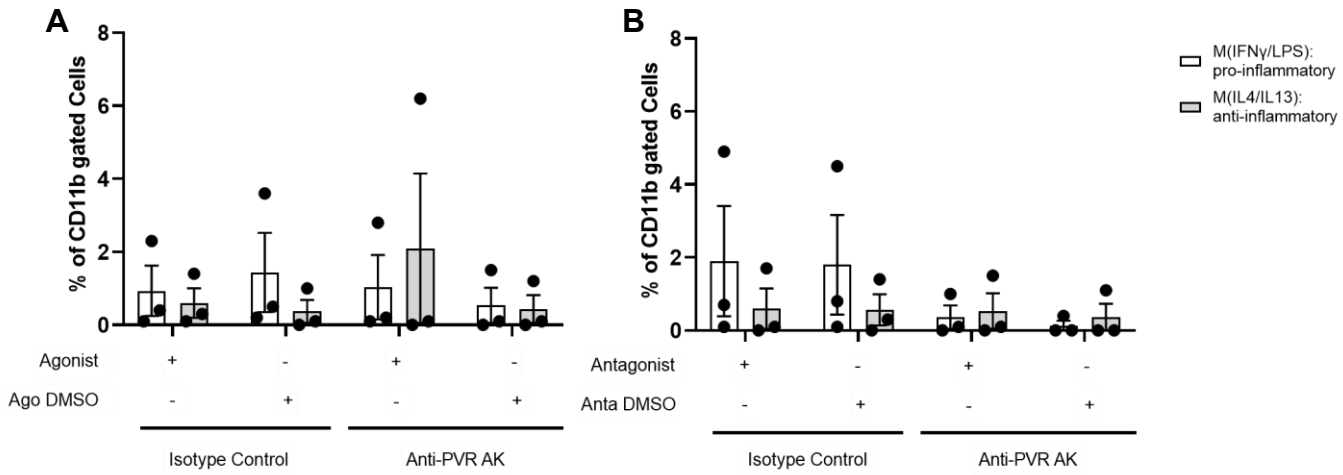

S.13 Necrotic differentiated, polarized PBMC-derived human primary macrophages (M(IFNγ/LPS) & M(IL4/IL13)) in co-culture with PDO P022 CRC cells. The co-culture was treated with vehicle (DMSO), REVERBα (A) 10 µM SR9009 Agonist or (B) 6.7 µM SR 8275 Antagonist together with 5 µg/ml PVR blocking Ab vs. isotype control for 5 days. Flow cytometry (FC) was used to investigate the viability and death types of CD11b+ macrophages using annexin & SYTOX™ dye. Respective percentages of gated CD11b+ cells are shown. The number of macrophages undergoing necrosis remained under 4% in all conditions. Elevated number of necrotic macrophages were observed in conditions harboring pro-inflammatory M(LPS/IFNγ) macrophages as shown in (A) and (B). Ab treatment slightly augmented necrosis in anti-inflammatory M(IL4/IL13) macrophages as seen in (A). Neither data from (A) nor (B) reached statistical significance. Significances were calculated using two-way ANOVA with Tukey´s multiple comparisons test (n.s.; N=3 independent experiments, mean ± SEM). Cells were analyzed on a BD Canto FC device (Flow Core UMM).

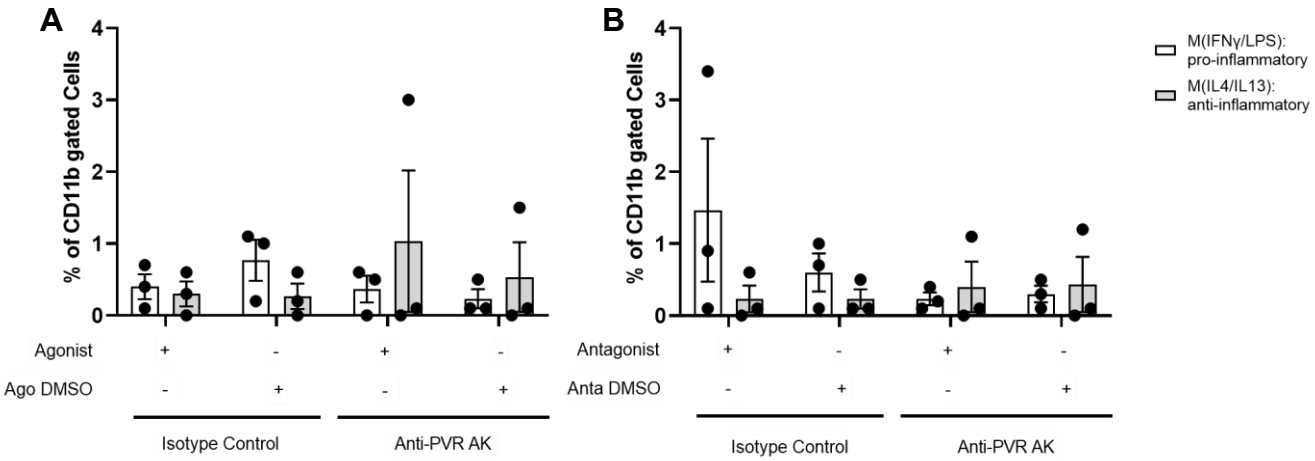

S.14 Early apoptotic differentiated, polarized PBMC-derived human primary macrophages (M(IFNγ/LPS) & M(IL4/IL13)) in co-culture with PDO P022 CRC cells. The co-cultures were treated with vehicle (DMSO), REVERBα (A) 10 µM SR9009 Agonist or (B) 6.7 µM SR 8275 Antagonist together with 5 µg/ml PVR blocking Ab vs. isotype control for 5 days. Flow cytometry (FC) was used to investigate the viability and death types of CD11b+ macrophages using annexin & SYTOX™ dye. Respective percentages of gated CD11b+ cells are shown. The number of macrophages in early apoptotic stage remained under 2% in all conditions. No significant changes in the numbers of early apoptotic macrophages were observed as shown in (A) and (B). Significances were calculated using two-way ANOVA with Tukey´s multiple comparisons test (n.s.; N=3 independent experiments, mean ± SEM). Cells were analyzed on a BD Canto FC device (Flow Core UMM).

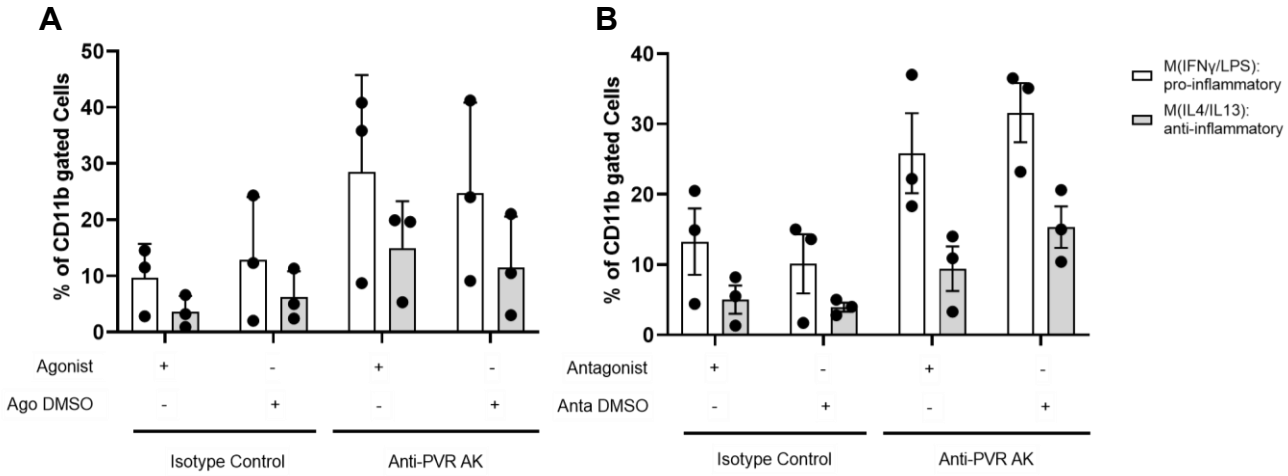

S.15 Late apoptotic differentiated, polarized PBMC-derived human primary macrophages (M(IFNγ/LPS) & M(IL4/IL13)) in co-culture with PDO P022 CRC cells. The co-cultures were treated with vehicle (DMSO), REVERBα (A) 10 µM SR9009 Agonist or (B) 6.7 µM SR 8275 Antagonist together with 5 µg/ml PVR blocking Ab vs. isotype control for 5 days. Flow cytometry (FC) was used to investigate the viability and death types of CD11b+ macrophages using annexin & SYTOX™ dye. Respective percentages of gated CD11b+ cells are shown. The number of late apoptotic macrophages was higher in co-cultures with pro-inflammatory M(LPS/IFNγ) macrophages and PVR Ab as depicted in (A) and (B). No significant effect was observed in the numbers of late apoptotic macrophages as shown in (A) and (B). Significances were calculated using two-way ANOVA with Tukey´s multiple comparisons test (n.s.; N=3 independent experiments, mean ± SEM). Cells were analyzed on a BD Canto FC device (Flow Core UMM).

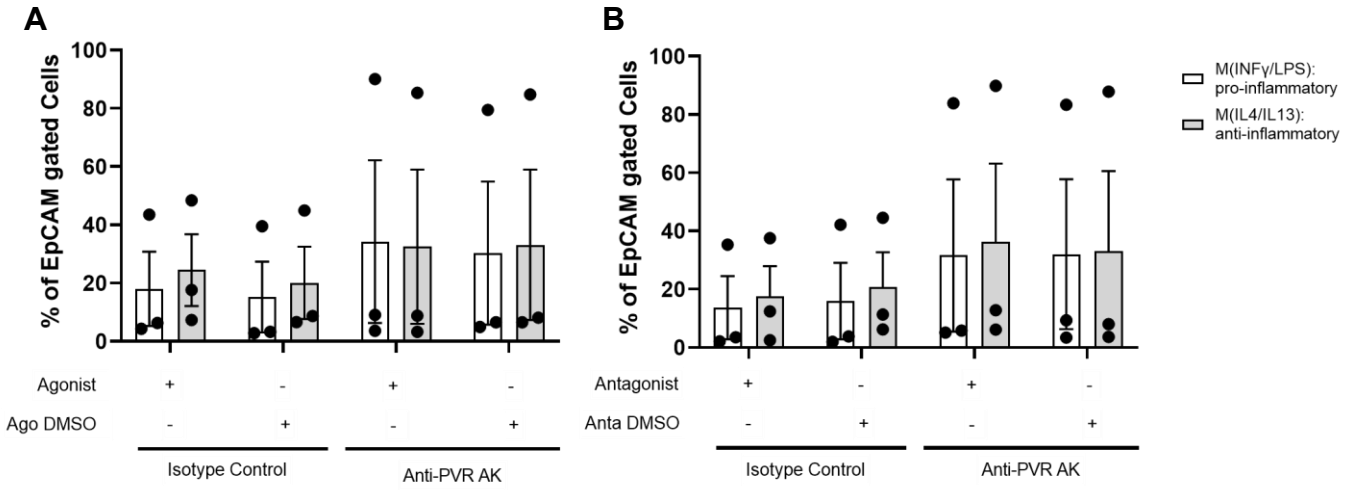

S.16 Necrotic PDO P007 CRC cells after co-culture with differentiated, polarized PBMC-derived human primary macrophages (M(IFNγ/LPS) & M(IL4/IL13)) The co-cultures were treated with vehicle (DMSO), REVERBα (A) 10 µM SR9009 Agonist or (B) 6.7 µM SR 8275 Antagonist together with 5 µg/ml PVR blocking Ab vs. isotype control for 5 days. Flow cytometry (FC) was used to investigate the viability and death types of EpCAM+ tumor cells using annexin & SYTOX™ dye. Respective percentages of gated EpCAM+ cells are shown. The amount of necrotic PDO tumor stem cells undergoing necrosis after PVR Ab treatment is depicted in both (A) and (B). Necrosis of PDO P007 cancer cells was shown to be below 40% in all conditions. No significant changes in the numbers of necrotic PDOs were observed as depicted in (A) and (B). Significances were calculated using two-way ANOVA with Tukey´s multiple comparisons test (n.s.; N=3 independent experiments, mean ± SEM). Cells were analyzed on a BD Canto FC device (Flow Core UMM).

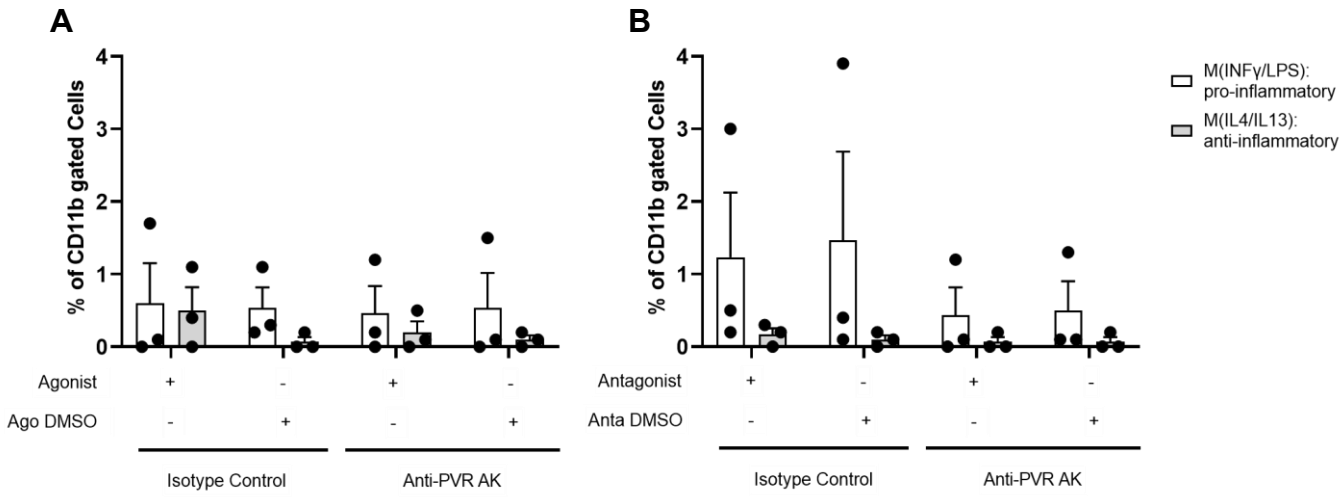

S.17 Necrotic differentiated, polarized PBMC-derived human primary macrophages (M(IFNγ/LPS) & M(IL4/IL13)) in co-culture with PDO P007 CRC cells. The co-cultures were treated with vehicle (DMSO), REVERBα (A) 10 µM SR9009 Agonist or (B) 6.7 µM SR 8275 Antagonist together with 5 µg/ml PVR blocking Ab vs. isotype control for 5 days. Flow cytometry (FC) was utilized to investigate the viability and death types of CD11b+ macrophages using annexin & SYTOX™ dye. Respective percentages of gated CD11b+ cells are shown. The number of macrophages undergoing necrosis remained under 4% in all conditions. Elevated number of necrotic macrophages were observed in conditions harboring pro-inflammatory M(LPS/IFNγ) macrophages as shown in (A) and (B), however without reaching statistical significance. Significances were calculated using two-way ANOVA with Tukey´s multiple comparisons test (n.s.; N=3 independent experiments, mean ± SEM). Cells were analyzed on a BD Canto FC device (Flow Core UMM).

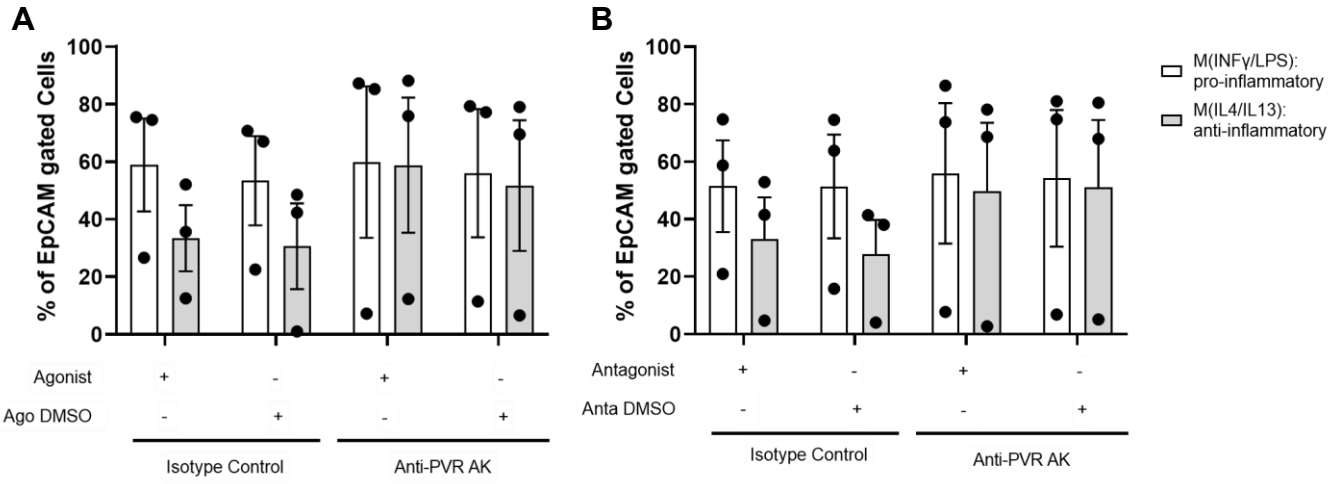

S.18 Early apoptotic PDO P007 CRC cells after co-culture with differentiated, polarized PBMC-derived human primary macrophages (M(IFNγ/LPS) & M(IL4/IL13)). The co-cultures were treated with vehicle (DMSO), REVERBα (A) 10 µM SR9009 Agonist or (B) 6.7 µM SR 8275 Antagonist together with 5 µg/ml PVR blocking Ab vs. isotype control for 5 days. Flow cytometry (FC) was used to investigate the viability and death types of EpCAM+ tumor cells using annexin & SYOX™ dye. Respective percentages of gated EpCAM+ cells are shown. Higher numbers of PDO cancer cells undergoing early phase apoptosis were evident in all co-cultures. Additionally, co-cultures harboring pro-inflammatory M(LPS/IFNγ) macrophages revealed higher amounts of early apoptotic PDOs in conditions without PVR Ab as depicted in (A) and (B). However, no significant changes in the numbers of early apoptotic PDOs were observed. Significances were calculated using two-way ANOVA with Tukey´s multiple comparisons test (n.s.; N=3 independent experiments, mean ± SEM). Cells were analyzed on a BD Canto FC device (Flow Core UMM).

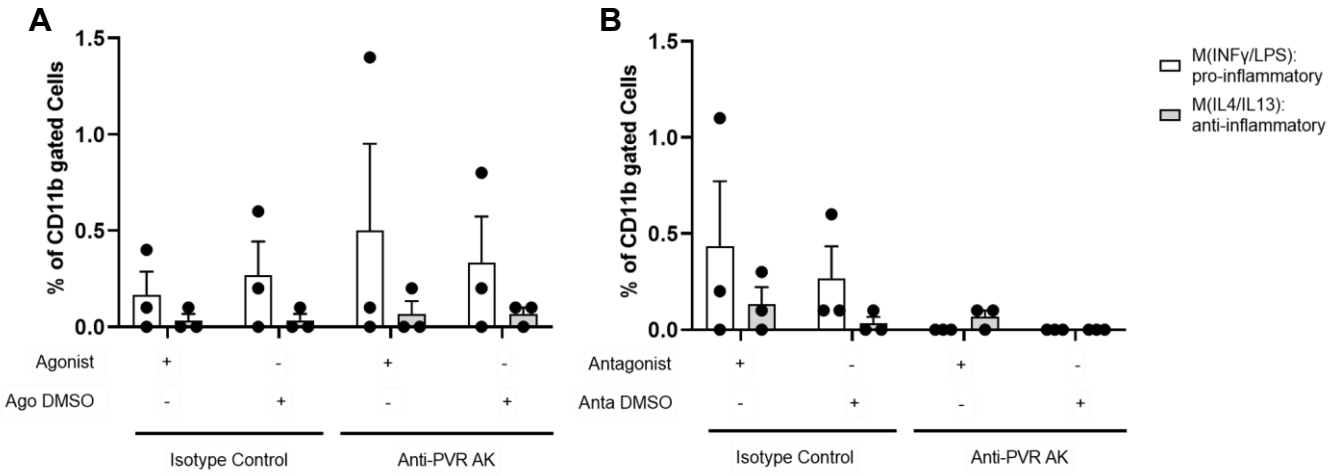

S.19 Early apoptotic differentiated, polarized PBMC-derived human primary macrophages (M(IFNγ/LPS) & M(IL4/IL13)) in co-culture with PDO P007 CRC cells. The co-cultures were treated with vehicle (DMSO), REVERBα (A) 10 µM SR9009 Agonist or (B) 6.7 µM SR 8275 Antagonist together with 5 µg/ml PVR blocking Ab vs. isotype control for 5 days. Flow cytometry (FC) was used to investigate the viability and death types of CD11b+ macrophages using annexin & SYOX™ dye. Respective percentages of gated CD11b+ cells are shown. The number of macrophages in early apoptotic phase remained under 2% in all conditions. No significant changes in the number of early apoptotic macrophages were observed as shown in (A) and (B). Significances were calculated using two-way ANOVA with Tukey´s multiple comparisons test (n.s.; N=3 independent experiments, mean ± SEM). Cells were analyzed on a BD Canto FC device (Flow Core UMM).

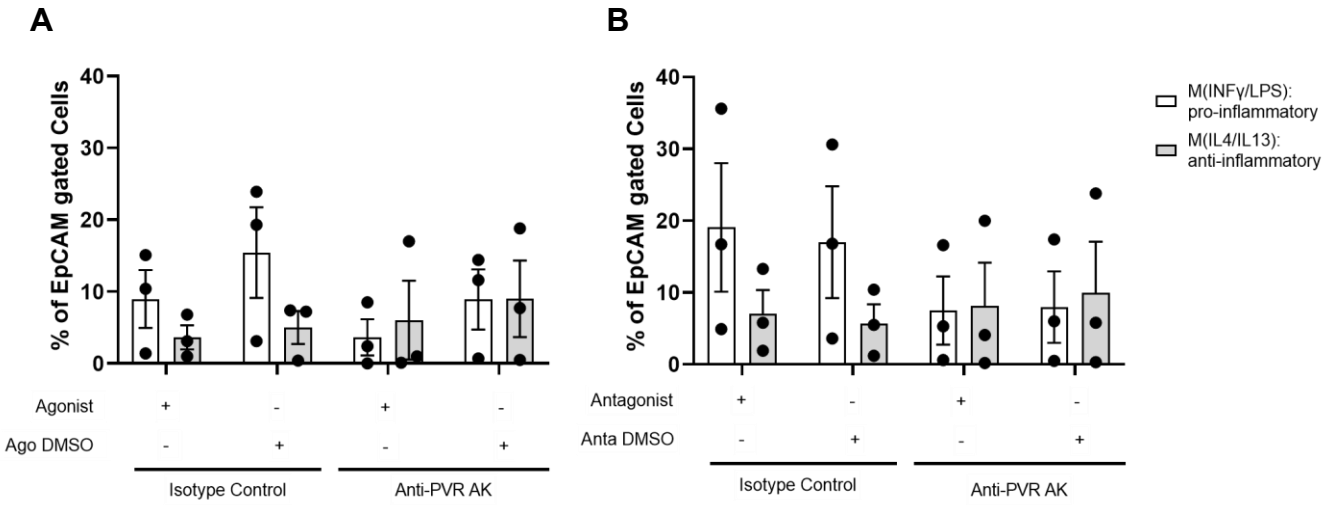

S.20 Late apoptotic PDO P007 CRC cells after co-culture with differentiated, polarized PBMC-derived human primary macrophages (M(IFNγ/LPS) & M(IL4/IL13)). The co-cultures were treated with vehicle (DMSO), REVERBα (A) 10 µM SR9009 Agonist or (B) 6.7 µM SR 8275 Antagonist together with 5 µg/ml PVR blocking Ab vs. isotype control for 5 days. Flow cytometry (FC) was utilized to investigate the viability and death types of EpCAM+ tumor cells using annexin & SYTOX™ dye. Respective percentages of gated EpCAM+ cells are shown. Numbers of late apoptotic PDOs remained below 40%. An elevation of late apoptotic PDOs was observed in conditions harboring pro-inflammatory M(LPS/IFNγ) macrophages as shown in (A) and (B), however not reaching statistical significance. Significances were calculated using two-way ANOVA with Tukey´s multiple comparisons test (n.s.; N=3 independent experiments, mean ± SEM). Cells were analyzed on a BD Canto FC device (Flow Core UMM).

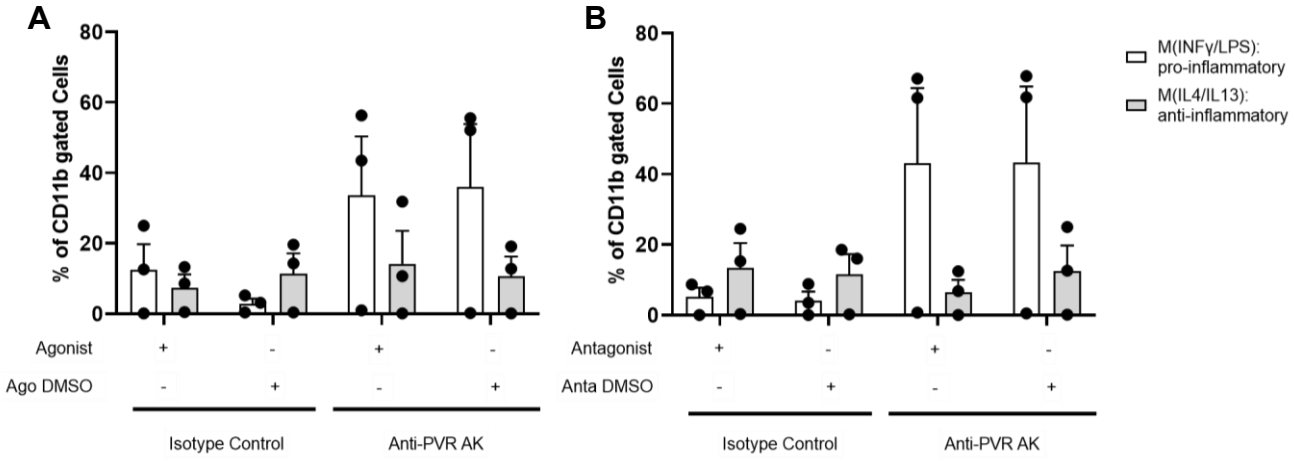

S.21 Late apoptotic differentiated, polarized PBMC-derived human primary macrophages (M(IFNγ/LPS) & M(IL4/IL13)) in co-culture with PDO P007 CRC cells. The co-cultures were treated with vehicle (DMSO), REVERBα (A) 10 µM SR9009 Agonist or (B) 6.7 µM SR 8275 Antagonist together with 5 µg/ml PVR blocking Ab vs. isotype control for 5 days. Flow cytometry (FC) was used to investigate the viability and death types of CD11b+ macrophages using annexin & SYTOX™ dye. Respective percentages of gated CD11b+ cells are shown. Elevated numbers of late apoptotic macrophages were evident in co-cultures containing pro-inflammatory M(LPS/IFNγ) macrophages and PVR Ab as depicted in (A) and (B). No significant difference in the number of late apoptotic macrophages was observed as shown in (A) and (B). Significances were calculated using two-way ANOVA with Tukey´s multiple comparisons test (n.s.; N=3 independent experiments, mean ± SEM). Cells were analyzed on a BD Canto FC device (Flow Core UMM).

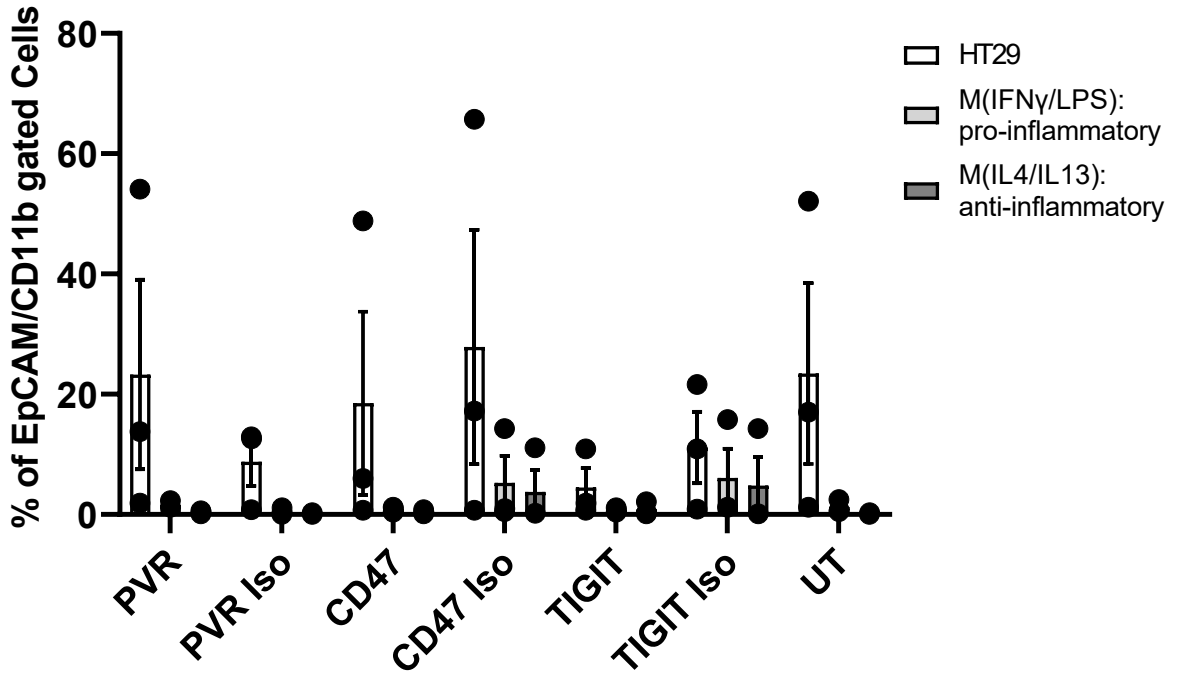

S.22 Necrosis upon functional grade blocking Ab treatment in single cultures of HT29 CRC cells and differentiated, polarized PBMC-derived human primary macrophages (M(IFNγ/LPS) & M(IL4/IL13)) The single cultures were treated with 5 µg/ml PVR, 10 µg/ml CD47 or 5 µg/ml TIGIT blocking Ab vs. isotype controls for 3 days. Flow cytometry (FC) was used to detect the viability and death types of EpCAM+ tumor cells and CD11b+ macrophages using annexin & SYTOX™ dye. Respective percentages of gated cells are shown. The highest amounts of cells undergoing necrosis were found to be in HT29 cancer cells across different treatment conditions. Furthermore, the treatment with functional grade blocking Abs did not significantly increase necrosis events. Significances were calculated using two-way ANOVA with Tukey´s multiple comparisons test (n.s.; N=3 independent experiments, mean ± SEM). Cells were analyzed on a BD Canto FC device (Flow Core UMM). UT = untreated; Iso = Isotype control.

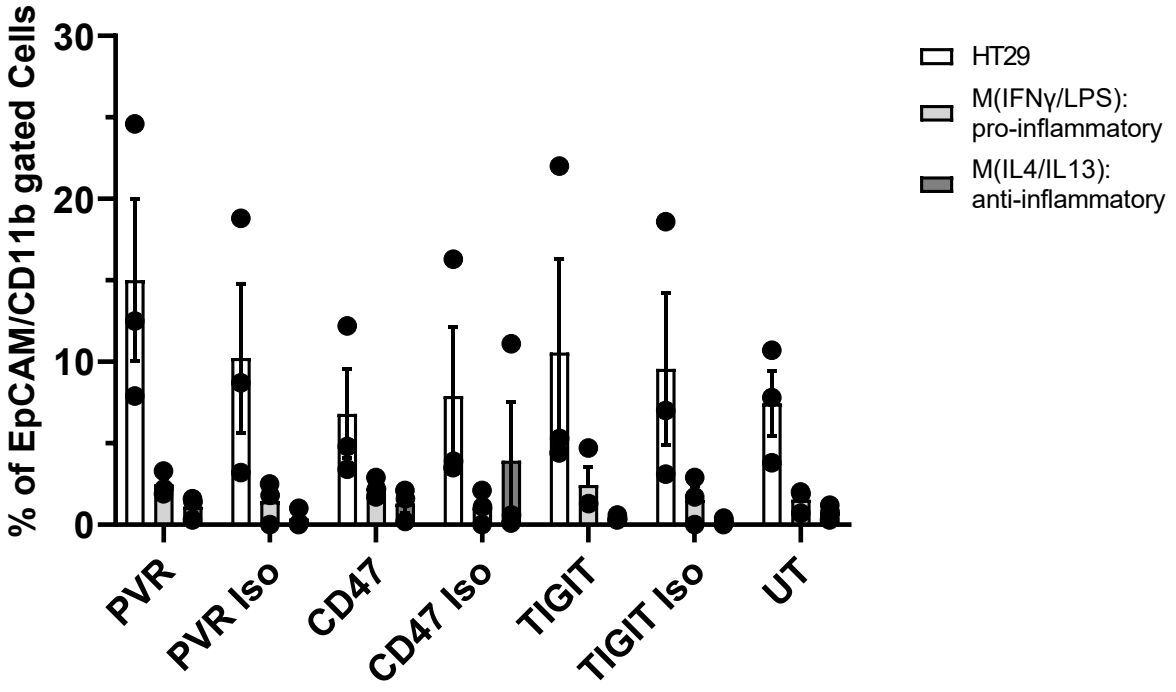

S.23 Early apoptosis upon functional grade blocking Ab treatment in single cultures of HT29 CRC cells and differentiated, polarized PBMC-derived human primary macrophages (M(IFNγ/LPS) & M(IL4/IL13)). The single cultures were treated with 5 µg/ml PVR, 10 µg/ml CD47 or 5 µg/ml TIGIT blocking Ab vs. isotype controls for 3 days. Flow cytometry (FC) was used to detect the viability and death types of EpCAM+ tumor cells and CD11b+ macrophages using annexin & SYTOX™ dye. Respective percentages of gated cells are shown. Early apoptosis was detected to be below 20% in all conditions. Treated HT29 cancer cells had the highest amounts of cells undergoing early apoptosis among all cells. Furthermore, no significant difference in the number of early apoptotic cells in all treatment conditions was observed. Significances were calculated using two-way ANOVA with Tukey´s multiple comparisons test (n.s.; N=3 independent experiments, mean ± SEM). Cells were analyzed on a BD Canto FC device (Flow Core UMM). UT = untreated; Iso = Isotype control.

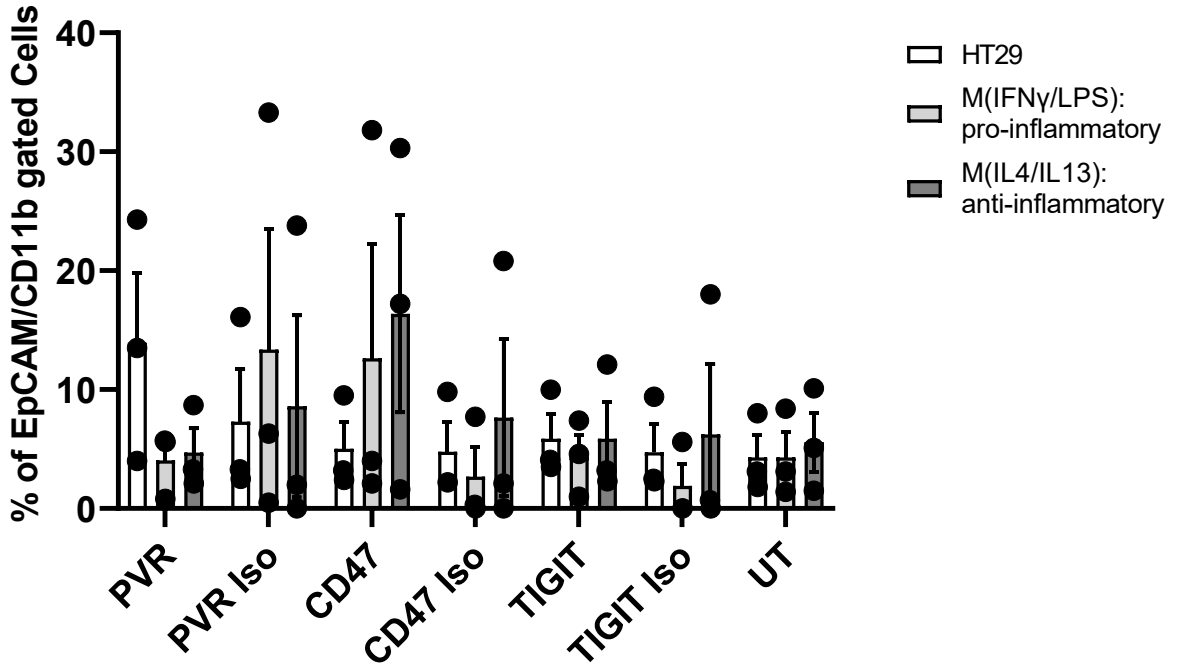

S.24 Late apoptosis upon functional grade blocking Ab treatment in single cultures of HT29 CRC cells and differentiated, polarized PBMC-derived human primary macrophages (M(IFNγ/LPS) & M(IL4/IL13)). The single cultures were treated with 5 µg/ml PVR, 10 µg/ml CD47 or 5 µg/ml TIGIT blocking Ab vs. isotype controls for 3 days. Flow cytometry (FC) was used to detect the viability and death types of EpCAM+ tumor cells and CD11b+ macrophages using annexin & SYTOX™ dye. Respective percentages of gated cells are shown. The treatment with CD47 Ab revealed higher numbers of macrophages undergoing late-stage apoptosis compared to other treatment conditions. No significant difference in the number of cells undergoing late-stage apoptosis was observed in all treatment conditions. Significances were calculated using two-way ANOVA with Tukey´s multiple comparisons test (n.s.; N=3 independent experiments, mean ± SEM). Cells were analyzed on a BD Canto FC device (Flow Core UMM). UT = untreated; Iso = Isotype control.

7. Acknowledgment

First and foremost, I would like to thank Prof. Matthias Ebert for giving me the opportunity to do my research and thesis at the II. Medical Department, Medical Faculty Mannheim of the University Heidelberg in Mannheim, Germany. My deepest gratitude goes to my supervisor, mentor and head of the laboratory Prof. Elke Burgermeister. Your support and guidance have shaped both this thesis and myself as a researcher, and I am very thankful for your support, scientific mentorship and trust.

Further on, I would like to thank my supervisors Prof. Viktor Umansky, Prof. Gert Fricker and Prof. Stefan Wölfl for their scientific guidance and support. I also wish to thank Prof. Mathias Müller from the VetMed Uni Wien, for generously hosting me in his laboratory during my stay in Vienna and for supporting me in part of this work.

I am also grateful to Prof. Adelheid Cerwenka and Martin Schneider for welcoming and supporting me within the graduate school GRK 2727 - InCheck „Innate Immune Checkpoints in Cancer and Tissue Damage" and for their kind support. I gratefully acknowledge the financial support of the Deutsche Forschungsgemeinschaft (DFG) (GRK2727). I also thank the Heidelberg Biosciences International Graduate School (HBIGS) and the Faculty of Biosciences of the University of Heidelberg for giving me the honor and privilege to conduct my studies.

I would like to extend special thanks to Stefanie Uhlig from FlowCore Mannheim for her expert assistance with FACS experiments. My gratitude goes as well to my past and present colleagues in Mannheim. Thank you for your constant help and for creating a great working environment during the last past years. Especially I want to thank Frank Herweck and Alexandra Kerner for excellent outstanding technical assistance.

Finally, I owe my deepest gratitude to my parents Tiberiu-Mihai and Mikaela Kato, my grandma Magdalena Kato and all my family members for their unwavering love, support and encouragement. I am equally thankful to my dear friends Steffen, Elisa, Felix, Johannes, Linda and Pol as well as to my university collogues Malte, Julian and Antós, whose friendship and support carried me through this journey.

Last but not least, I want to thank you, Ronja, for your love, patience and trust in me. Having you in my life gave me the greatest source of strength and joy.